Skolkovo Institute of Science and Technology

ACCURATE AB INITIO EVALUATION OF THE INTERATOMIC POTENTIALS AND LONG-RANGE COEFFICIENTS

Doctoral Thesis

by

GIORGIO VISENTIN

DOCTORAL PROGRAM IN MATERIALS SCIENCE AND ENGINEERING

Supervisor

Professor Alexei A. Buchachenko

Moscow – 2021

© Giorgio Visentin 2021

“Enthusiasm and diligence can find ways, be they ever so snowed under”

(Georg Philipp Telemann)

I hereby declare that the work presented in this thesis was carried out by myself at Skolkovo Institute of Science and Technology, Moscow, except where due acknowledgement is made, and has not been submitted for any other degree.

Candidate, Giorgio Visentin

Supervisor, Prof. Alexei A. Buchachenko

Table of contents

List of figures

List of tables

Abstract

Despite the maturity of intermolecular interaction theory and the progress in modern computational quantum chemistry methods, improvement of ab initio interaction potentials still remains challenging, being heated up by constantly growing accuracy demands from various fields, ranging from diatomic interactions explored in ultracold atomic physics to modeling huge and complex atomistic systems in materials chemistry. In the field of the weak van der Waals interactions, two possibilities coexist. The dimeric (molecular) approach targets global potentials, but experience inherent limitations at long range. Monomeric (atomic) approach cover specifically the latter, using long-range coefficients expressed through the electric properties of the monomers. An opportunity to improve the overall theoretical accuracy lies in more thorough bridging and balancing of these two alternatives. In this work, the performance of molecular approaches in the long-range region is assessed throughout four test cases, which, in turn, represent exemplary situations where both the global potential and its long-range wedge should be known consistently. More precisely, the cases address 1) the performance of molecular approaches in modelling the long-range potential of alkaline-earth atoms and Yb, 2) the possibility of matching atomic and molecular approaches for the benchmark description of the interaction potential of the Yb dimer, 3) combination of molecular and atomic approaches for dispersion interactions of open-shell systems, which, exploring the transferability of atomic properties, eventually results in the new combining rule for dispersion coefficients, and 4) the performance of molecular approaches in the investigation of interactions and gas-phase mobility of heavy ions with rare gases. In all cases, the results reveal that the choice of an adequate ab initio method, electron core description and basis set customization strongly improves the ability of molecular approaches in dealing with long-range interaction terms and, thus, provides a useful means to improve consistency and accuracy of ab initio interaction potentials.

Publications (thesis related)

1) **G. Visentin** and A.A. Buchachenko, *Polarizabilities, dispersion coefficients and retardation functions at the complete basis set CCSD limit: Be-Ba and Yb,* J. Chem. Phys. **151**, 214302 (2019); doi: 10.1063/1.5129583;
2) **G. Visentin**, M. Laatiaoui, L.A. Viehland, and A.A. Buchachenko, *Mobility of the Singly-Charged Lanthanide and Actinide Cations: Trends and Perspectives,* Front. Chem. **8**, 438 (2020); doi: 10.3389/fchem.2020.00438;
3) **G. Visentin,** I.S. Kalinina and A.A. Buchachenko, *Extended combination rule for like-atom dipole dispersion coefficients*, J. Chem. Phys. **153**, 064110 (2020); doi: 10.1063/5.0019010;
4) **G. Visentin**, A.A. Buchachenko and Paweł Tecmer, *Ab intio Yb_2 ground state potential revisited* (submitted to Phys. Rev. A, arXiv:2107.10353 preprint available at https://arxiv.org/abs/2107.10353).

Conference presentations (thesis related)

Presenter

1) TASQ- Torun Astrophysics, Spectroscopy and Quantum Chemistry School, Torun, Poland, 01-12 July 2019

Presenting (**poster**): *Polarizabilities, dispersion coefficients and retardation functions at the complete basis set CCSD limit: Be-Ba and Yb.*

Organizer: A. Jablonski Foundation, Nicolaus Copernicus University of Torun.

Financial Support (Grant): Skoltech CEST student's mobility program

Website: http://tasq.fizyka.umk.pl/

Status: completed.

2) 27th International Scientific Conference for Undergraduate and Postgraduate Students and Young Scientists "Lomonosov", Moscow, Russia, 12-23 April 2021.

Presenting (**oral presentation**): *Gas-phase mobility of the singly-charged actinide cations.*

Organizer: M. V. Lomonosov Moscow State University.

Website: https://lomonosov-msu.ru/eng/event/7000/

Status: completed. Best oral presentation diploma awarded.

3) Virtual International Conference on Photonic, Electronic and Atomic Collisions (ViCPEAC 2021), 20-23 July 2021.

Presenting: *Accurate binding energy of Yb dimer (Yb_2) from ab initio calculations and ultracold photoassociation spectroscopy.*

Organizer: IUPAP – International Union of Pure and Applied Physics.

Financial Support (Grant): Russian Science Foundation, project No. 17-13-01466.

Website: https://www.icpeac2021.ca/

Status: completed.

Contributor

1) Virtual workshop on the "Atomic Structure of Actinides & Related Topics", 26-28 May 2021.

Contribution: *Laser resonance chromatography: theoretical assessment for lanthanide and actinide ions.*

Organizer: Helmoltz Institut, Mainz (HIM); GSI; Johannes Gutenberg Universität, Mainz.

Website: https://indico.him.uni-mainz.de/event/78/

Status: completed.

1. Introduction

Though writing on intermolecular forces may appear as something technical and far from common knowledge, really they are more rooted in common culture than one may think. In a paradoxical manner, it may be said that humans knew about intermolecular forces before discovering them, or, better, that they knew about them, but without being conscious of their nature and origin. The first person to write on them was also the first historical person interested in nature: Thales, living between the 7^{th} and the 6^{th} century b. C. This "naturalist philosopher", as people interested in science were called at that time, wrote on the attraction that amber exerted on small light objects upon scratching it. This is the first documented historical mention of intermolecular forces, albeit he thought that it was an intrinsic property of amber, rather than a force affecting matter. For more than 1500 years, none dared to confute the theses adduced by the Greeks, until Scholastic philosophy left the place to experimental method, at the dawn of the so called Scientific Revolution. The first steps were still irresolute and still tied to refusing the concept of forces acting from a distance: in 1600, William Gilbert hypothesized that electric and magnetic forces should be originated by unperceivable effluvia. However, his nowadays obsolescent theories hid even some hints to modern theories on interactions, such as the role of temperature in encouraging interactions in matter [1]. A powerful voice in favor of the model of forces acting from a distance came from Newton's and Leibniz's works, stating that forces acting on gas particles should follow an inverse distance-dependence relation [1]. However, doubts still arose: how can the inverse distance dependence of forces explain the incompressibility of matter? It was clear that an equilibrium distance should exist, beyond which two bodies can hardly be pushed closer to each other: Roger Boscovich (1711-1787) proposed that forces among atoms should have an oscillatory nature. Indeed, resembling intermolecular forces to a spring would have solved the problem of incompressibility of bodies. However, Boscovich attributed repulsive effects to heat, rather than to the finite size of atoms and, like Newton, supposed gas particles to be static [1]. It was only with Daniel Bernoulli, in 1738, that the first kinetic theory of gases was proposed, where it was clearly stated that particles in gases move and collide [1]. Linking the concept of an intermolecular force with that of collision and potential repulsion was particularly fruitful for further advancements in this study: the electrostatic law by Charles-Augustin de Coulomb, first proposed in 1785 [1], was soon extended to atoms and, later, molecules, while, in the next century, Jan Diderik van der Waals formulated his famous equation of

state, where both the finite size of molecules and the attractive intermolecular forces between them were quantitatively accounted for [1].

The evolution of scientific research throughout history has shed light on the nature of intermolecular forces. Nowadays, their ubiquitous role in nature is well known. For instance, they are responsible for the states of matter: the definite density of liquid water and its incompressibility to smaller volumes witness the existence of intermolecular forces keeping the constituent molecules together and the rise of repulsive forces when one tries to push them closer to each other [2]. However, intermolecular forces can even lead molecules to arrange into solids: molecular solids are defined as a state of matter where a theoretically infinite number of molecules is kept together in a periodic lattice by intermolecular forces [3]. Such forces can even drive the displacement of such molecules towards different configurations in the lattice, as a phenomenon called polymorphism [4]. Interactions between atoms (or molecules) and surfaces represent another scenario where intermolecular forces play a determinant role, which, in turn, is commonly exploited by experimental techniques such as Electrophoretic Deposition (EPD) [5] and Atomic Force Microscopy (AFM) [6]. Furthermore, recently, nanotechnology has focused on those processes where molecular components organize themselves into more complex patterns or structures without human intervention: this bottom-up supramolecular arrangement, called self-assembly, is mediated by intermolecular forces [7] and has been proposed as a mechanism driving the origin of life [8].

Accordingly, our knowledge of intermolecular forces is much more complete and systematic than in van der Waals time: intermolecular interaction is defined as a physical phenomenon responsible for the attraction or the repulsion between two charge distributions (atoms, molecules, ions…) [2,9]. In particular, intermolecular forces are classified into two branches, depending on the internuclear distance at which they are effective: short-range forces and long-range forces. The former accounts for "chemical" effects, such as exchange interaction and covalent or ionic bond formation [10]. Definition of the long-range forces excludes the latter effects [11]. They are regarded as *weak* and grouped under the name of *van der Waals forces* [11]. This definition implies that the long-range forces can be described perturbatively, by considering interaction of two independent charge distributions created by electrons and nuclei of each monomer. The well-known intermolecular perturbation theory [12-16] provides general and transparent expression of intermolecular potential

creating these forces. The potential of interacting monomers A and B has the generic asymptotic form of an inverse power series in the internuclear distance *R*, in the simplest exemplary case,

$$U^{\mathrm{AB}}(R) \underset{R\to\infty}{\longrightarrow} -\sum_n \frac{C_n^{\mathrm{AB}}}{R^n} \tag{1.1}$$

with the *long-range coefficients* C_n^{AB} [9,10]. The latter depend on the *static moments* and/or *response properties* that characterize the charge distribution of the *free* monomers [2,9,10]. In a potential energy curve, the long-range region described by the form (1.1) correspond to the asymptote of the curve

In particular, the interaction potential (1.1) can be split into several contributions, each one creating a different force: the *electrostatic* contribution accounts for the interaction of the permanent multipole moments of the monomers and, consequently, is zero for spherically symmetric overall neutral charge distributions [10]; the *induction* contribution, scaling with the fourth inverse power of *R* or higher, accounts for the polarization of the charge cloud of each monomer by the electrostatic field due to each other [10]; finally, the *dispersion* contribution, scaling with inverse power of *R* equal or larger than six, accounts for the interaction due to correlations of the fluctuating multipole moments of the two monomers [10].

The basic equation of intermolecular interaction theory (1.1) delineates two alternative, but complementary approaches. Long-range coefficients can be defined from the known (calculated or empirically reconstructed) *global* interaction potential of a dimer. This constitutes a *dimeric*, or, in the context of the present Thesis, *molecular* approach. In principle, it provides the complete description of the potential and all related phenomena, and can be realized with the help of sophisticated methods of *ab initio* electronic structure theory. Understandably, the cost of the molecular approach rapidly grows with the complexity of the monomers. In addition, precise definition of the long-range coefficients from the global potential suffers from numerical errors for very small asymptotic energies and poor and ambiguous fitting. The *monomeric* (or *atomic*) approach focuses on the electrostatic and response properties of the monomers to calculate long-range coefficients directly. Offering unambiguous definition of the whole set of the coefficients to a desirable order and their (partial) transferability, the monomeric approach is especially productive in the simplest cases of atomic monomers, when the special non-standard theoretical methods are applicable to account for the higher-order relativistic effects, non-Born-Oppenheimer terms,

quantum electrodynamic (QED) corrections, etc. Its computational cost exhibits slower growths with the monomer complexity than that of dimeric approach, but not without accuracy suffering, as the *ab initio* methods for response property calculations are usually less precise than that available for energy calculations required for a dimer. And evidently, the monomeric approach cannot provide the global potential; moreover, its applicability at any finite distance is formally questionable, both due to the convergence of the series (1.1) and omitted forces of the non-Coulomb origin (e.g. forces rising from the overlap of the electron clouds). Coupled Cluster level of theory (CC) [17-19], for instance, defines a family of ab initio methods often employed for accurate molecular approaches. Among these, in the framework of CC, the Coupled-Cluster Equation of Motion (CC-EOM) approach [19,20] and, in particular, the Polarization Propagator approach [21,22] were devised in order to determine response properties of atoms and molecules. However, in the ambit of atomic response properties, atomic approaches, such as that combining the Configuration Interaction method and Many-Body Perturbation Theory (CI-MBPT) [23] turned out to be more flexible and more easily customizable for specific systems, having the possibility even to embody empirical corrections (see Ref. [23]). Several ways have been tried in order to overcome this dichotomy between the accurate estimation of the global potential and the accurate unambiguous knowledge of the long-range coefficients. Symmetry-Adapted Perturbation Theory (SAPT) [24] represents the most theoretically consistent compromise between molecular and atomic approaches: at this level, antisymmetrized eigenfunctions from molecular *ab initio* methods are used to build up the unperturbed wave function [2,25-27], whereas electron correlation and the interaction potential are treated as a perturbation [2,25,26]. However, SAPT tends to lose accuracy at short ranges and higher-level corrections applied to increase its accuracy may dramatically increase the computational demands of the method, while higher accuracy comparable to the gold standard CCSD(T) method is not always ensured [27]. The most widely used SAPT correction to account for the breakdown in the short-range region, SAPTδMP2, does not unambiguously decompose the terms constituting the interaction energy, as δMP2 itself includes both dispersion and induction contributions [27]. Moreover, SAPT treatment of interaction is not really transferable to systems consisting of more than two interacting bodies. In the fields of molecular dynamics and molecular mechanics, synthetic potentials, also called *model potentials*, have proven to be a successful option. The scope of synthetic potentials is to propose a simplified but still effective description of the interaction potential by an approximate functional model decomposing the short- and long-

range contributions into a set of parameters [2,28,29]. Such parameters can be separately achieved and flexibly embodied into the model potential: they are usually phenomenological, retrieved from first-principles ab initio calculations or from experimental data [24,29]. Besides the lower computational effort, flexibility is another advantage of this approach: synthetic potentials can be customized for one system (see, for instance, Ref. [30]) or for a whole class of systems. In this latter case, parameters are often achieved from properties of a subset. In particular, geometrical or empirical relations are used to retrieve interaction parameters for two unlike partners A, B from the analogs for the pure phases [2,9]: such relations are called *combining rules* [31]. Combining rules address the transferability of approaches used to investigate intermolecular interactions: while rules for short-range parameters depend on the model potential parametrization [31-34], those for long-range coefficients respond to the inverse power series (1.1) [31] and are, thus, easily transferable to any kind of potential function. When matched with synthetic potentials, such rules are used to decrease the number of parameters employed and, thus, reduce the computational effort and increase the transferability of the model potential [28]. However, despite their flexibility and transferability, model potentials do not attain accuracies similar to those characterizing molecular and atomic approaches, due to the oversimplified formalism of the empirical parameters [35]. The same oversimplification affects many combining rules, whose theoretical basis is quite flimsy [2] and the success irregular [36].

Accuracy and consistency are particularly important when dealing with gaseous phases; here, long-range weak forces play a remarkable role and are protagonists in several applications of growing interest, where precise estimations are crucial: they govern scattering processes and phenomena occurring in the ultracold regime, such as photoassociation [37-43,30,44-46] and the Feshbach effect [23,24]. Intensive studies were also devoted to the long-range forces affecting ultracold alkaline earth atoms, such as Ca [23,47] and Sr [47,48], for several applications, among which the search for new frequency standards [23,47,48], that requires accuracy up to the eighteenth decimal place in frequency units [49,50]. In addition, very recently, weak interactions of ytterbium atoms at ultracold temperature have been investigated as sensors of short-range gravity-like forces [30,51]. Though counterintuitive in appearance, even the study of transport properties of ions in buffer gases offers the chance for the investigation of van der Waals forces: the relationship between gas-phase mobility of ions and their interaction potential with rare gases is well known and exploited in several experimental techniques, such as the so-called Electronic State Chromatography [52-54]

or the novel Laser Resonance Chromatography, to characterize heavy and superheavy elements [55-57]. Really, at the lowest order, intermolecular forces between ions and neutral buffer gases do not directly sense the electronic structure of the formers [55] and, therefore, such experimental techniques should be flanked by theoretical investigation of higher-order interactions, which, in turn, depend on response properties of the ion.

Many important and sensitive applications to few-body systems, such as mentioned above, require the accurate and consistent description of both the short- and long-range regions of the interaction potential. The way to address this requirement within the standard implementations of the high-level ab initio CC methods is to elucidate

1. How accurate are the methods approved for molecular approach when applied within the atomic approach? Do the recipes for improving molecular ab initio calculation work in the atomic limits and are they helpful for balancing the accuracy?

2. Can molecular and atomic approaches be directly combined at some point to provide a really global and consistent interaction potential?

At the other extreme of the current research agenda, approaches to molecular modeling of large and complex systems operate with simplified potentials, or additive force fields, containing a limited set of general parameters, frequently interconnected with the help of empirical relations, or combining rules. For the long-range part, the atomic approach is indispensable due to the transferability of underlying atomic properties. However, it becomes non-trivial for the most general case of dispersion interactions, for which the long-range coefficients are represented by convolutions of the response properties rather than by the product of the static ones. Further questions arise:

3. Can the link between the molecular and atomic approaches be explored to deduce the response properties hardly available from direct calculations (e.g., for open-shell systems)? Can it give relations between the dispersion coefficients useful as the combining rules?

Finally, the value of the global interaction potential, or, more generally, the potential energy surfaces, is determined by the amount and accuracy of information on the experimentally observable quantities to be extracted by solving suitable nuclear motion problem. At this level, the effects of short- and long-range forces cannot be strictly disentangled. One can only expect different sensitivity

and judge the balance and accuracy of their descriptions. Answers to the previous questions aim to improve both factors. But it remains to be proven if:

4. The carefully constructed interaction potentials are capable of interpreting and predicting the experimental results of, say, macroscopic transport properties?

The goal of the thesis is to address four questions raised above. Towards this goal, four relevant and practically interesting examples are considered in the Chapters 3 to 6. Chapter 2 is devoted to introduce the reader to the theoretical background behind the methods and approaches used. Finally, Chapter 7 summarizes the main conclusions of the work and highlights some prospects.

References

[1] J. Israelachvili and M. Ruths, *Brief History of Intermolecular and Intersurface Forces in Complex Fluid Systems*, Langmuir **29,** 31, 9605–9619 (2013); doi: 10.1021/la401002b.

[2] A. J. Stone, *The Theory of Intermolecular Forces* (Oxford University Press, Oxford, 2013).

[3] G. Hall, *Molecular Solid State Physics*, Springer-Verlag, Berlin, 1965.

[4] C. Tantardini, A.A.L. Michalchuk, A. Samtsevich, C. Rota, A. Kvashnin, *The Volumetric Source Function: Looking Inside van der Waals Interactions*, *Sci Rep* **10**, 7816 (2020); doi: 10.1038/s41598-020-64261-4.

[5] C. Randal, J. van Tassel in *Encyclopedia of Materials: Science and Technology*, Pergamon, 2001.

[6] D.J. Müller, A. Engel in *Methods in Cell Biology*, Elsevier Academic Press, 2002.

[7] G. M. Whitesides, B. Grzybowski, *Self-Assembly at All Scales*, *Science*, **295**, 5564, 2418-2421 (2002).

[8] W.M. Heckl, *Molecular Self-Assembly and the Origin of Life*. In: Horneck G., Baumstark-Khan C. (eds.), Astrobiology. Springer, Berlin, Heidelberg (2002); doi: 10.1007/978-3-642-59381-9_23.

[9] I.G. Kaplan, *Intermolecular Interactions: Physical Picture, Computational Methods and Model Potentials* (Wiley, New York, 2006).

[10] A.D. Buckingham, P.W. Fowler, J.M. Hutson, *Theoretical Studies of van der Waals Molecules and Intermolecular Forces*, Chem. Rev. **88**, 963-988 (1988); doi: 10.1021/cr00088a008;

[11] PAC, **66**, 1077 (1994). (*Glossary of terms used in physical organic chemistry (IUPAC Recommendations 1994)*) on page 1175.

[12] F. London, *Zur Theorie und Systematik der Molekularkräfte*, *Z. Phys.* **63**, 245–279. 57 (1930).

[13] F. London, *The general theory of molecular forces*, *Trans. Faraday Soc.* **33**, 8–26. 57, 64 (1937).

[14] A. D. Buckingham, *Permanent and induced molecular moments and long-range intermolecular forces*, *Adv. Chem. Phys.* **12**, 107–143. 39, 46, 57, 66, 241 (1967).

[15] H. C. Longuet-Higgins, *The electronic states of composite systems*, Proc. Roy. Soc. A **235**, 537–543. 57, 58 (1956).

[16] H. Margenau, *Van der Waals forces*, Rev. Mod. Phys. **11**, 1–35. 57 (1939).

[17] F. Coester, H. Kummel, *Short-range correlations in nuclear wave functions, Nucl. Phys.*, **17**, 477-485 (1960); doi: 10.1016/0029-5582(60)90140-1.

[18] P. von Ragu-Schleyer, *Encyclopedia of Computational Chemistry* (Wiley, Chichester, 1998).

[19] I. Shavitt, R. J. Bartlett, *Many-Body Methods in Chemistry and Physics* (Cambridge University Press, Cambridge, 2009).

[20] T. Korona, H. J. Werner, *Local treatment of electron excitations in the EOM-CCSD method*, J. Chem. Phys. **118**, 3006 (2003); doi: 10.1063/1.1537718.

[21] R. Moszinski, P.S. Żukovski, B. Jeziorski, *Time-Independent Coupled-Cluster Theory of the Polarization Propagator;* Collect. Czech. Chem. Commun. (Vol.**70**) (2005); doi: 10.1135/cccc20051109.

[22] T. Korona, M. Przybytek, and B. Jeziorski, *Time-independent coupled cluster theory of the polarization propagator. Implementation and application of the singles and doubles model to dynamic polarizabilities and van der Waals constants*, Mol. Phys. **104**, 2303 (2006); doi: 10.1080/00268970600673975.

[23] S.G. Porsev, A. Derevianko, *High-Accuracy Calculations of Dipole, Quadrupole, and Octupole Electric Dynamic Polarizabilities and van der Waals Coefficients C_6, C_8, and C_{10} for Alkaline-Earth Dimers*, JETP,**102**, 2 (2006); doi: 10.1134/S1063776106020014.

[24] G. Visentin and A.A. Buchachenko, *Polarizabilities, dispersion coefficients and retardation functions at the complete basis set CCSD limit: Be-Ba and Yb*, J. Chem. Phys. **151**, 214302 (2019); doi: 10.1063/1.5129583.

[25] B. Jeziorski, R. Moszynski, K. Szalewicz, *Perturbation Theory Approach to Intermolecular Potential Energy Surfaces of van der Waals Complexes*, Chem. Rev. **94**, 1 887-1 *930* (1994); doi: 10.1021/cr00031a008.

[26] K. Szalewicz, *Symmetry-adapted perturbation theory of intermolecular forces*, *WIREs Comput. Mol. Sci.* **2**: 254–272 (2012); doi: 10.1002/wcms.86.

[27] T. M. Parker, L. A. Burns, R. M. Parrish, A. G. Ryno, and C. D. Sherrill, *Levels of symmetry adapted perturbation theory (SAPT). I. Efficiency and performance for interaction energies*, J. Chem. Phys. **140**, 094106 (2014); doi: 10.1063/1.4867135.

[28] M. Waldman and A. T. Hagler, *New Combining Rules for Rare Gas van der Waals Parameters*, J. Comput. Chem. **14**, 1077 (1993); doi: 10.1002/jcc.540140909.

[29] K.T. Tang and J.P. Toennies, *An improved simple model for the van der Waals potential damping functions for the dispersion coefficients*, J. Chem. Phys. **80**, 3726 (1984); doi: 10.1063/1.447150.

[30] M. Borkowski, A. A. Buchachenko, R. Ciuryło, P. S. Julienne, H. Yamada, Y. Kikuchi, K. Takahashi, Y. Takasu, and Y. Takahashi, *Beyond-Born-Oppenheimer effects in sub-kHz-precision photoassociation spectroscopy of ytterbium atoms*, Phys. Rev. A **96**, 063405 (2017); doi: 10.1103/PhysRevA.96.063405.

[31] G. Visentin**,** I.S. Kalinina and A.A. Buchachenko, *Extended combination rule for like-atom dipole dispersion coefficients*, J. Chem. Phys. **153**, 064110 (2020); doi: 10.1063/5.0019010.

[32] H. Pauly and J. P. Toennies, *The Study of Intermolecular Potentials with Molecular Beams at Thermal Energies*, Adv. At. Mol. Phys. **1**, 195 (1965); doi: 10.1016/S0065-2199(08)60283-3.

[33] K. T. Tang and J. P. Toennies, *New Combining Rules for Well Parameters and Shapes of the van der Waals Potential of Mixed Rare Gas Systems*, Z. Phys. D: At., Mol. Clusters **1**, 91 (1986); doi: 10.1007/BF01384663.

[34] G. P. Yin, P. Li, and K. T. Tang, *The ground state van der Waals potentials of the strontium dimer and strontium rare-gas complexes*, J. Chem. Phys. **132**, 074303 (2010); doi: 10.1063/1.3317406.

[35] C.L. Kong, *Combining rules for intermolecular potential parameters. I. Rules for the Dymond-Alder potential*, J. Chem. Phys. 59, 1953 (1973); doi: 10.1063/1.1680281.

[36] H.L. Kramer and D.R. Herschbach, *Combination Rules for van der Waals Force Constants*, J. Chem. Phys. **53**, 2792 (1970); doi: 10.1063/1.1674404.

[37] S. Tojo, M. Kitagawa, K. Enomoto, Y. Kato, Y. Takasu, M. Kumakura, and Y. Takahashi, *High-Resolution Photoassociation Spectroscopy of Ultracold Ytterbium Atoms by Using the Intercombination Transition,* Phys. Rev. Lett. **96**, 153201 (2006); doi: 10.1103/PhysRevLett.96.153201.

[38] K. Enomoto, M. Kitagawa, S. Tojo, and Y. Takahashi, *Hyperfine-Structure-Induced Purely Long-Range Molecules,* Phys. Rev. Lett. **100**, 123001 (2008); doi: 10.1103/PhysRevLett.100.123001.

[39] M. Borkowski, R. Ciuryło, P.S. Julienne, S. Tojo, K. Enomoto, and Y. Takahashi, *Line shapes of optical Feshbach resonances near the intercombination transition of bosonic ytterbium*, Phys. Rev. A **80**, 012715 (2009); doi: 10.1103/PhysRevA.80.012715.

[40] Y. Takasu, Y. Saito, Y. Takahashi, M. Borkowski, R. Ciuryło, and P. S. Julienne, *Controlled Production of Subradiant States of a Diatomic Molecule in an Optical Lattice,* Phys. Rev. Lett. **108**, 173002 (2012).

[41] S. Kato, S. Sugawa, K. Shibata, R. Yamamoto, and Y. Takahashi, *Control of Resonant Interaction between Electronic Ground and Excited States*, Phys. Rev. Lett. **110**, 173201 (2013); doi: 10.1103/PhysRevLett.110.173201.

[42] D. G. Green, C. L. Vaillant, M. D. Frye, M. Morita, and J. M. Hutson, *Quantum chaos in ultracold collisions between Yb($^1S_0$) and Yb($^3P_2$)*, Phys. Rev. A **93**, 022703 (2016); doi: 10.1103/PhysRevA.93.022703.

[43] Y. Takasu, Y. Fukushima, Y. Nakamura, and Y. Takahashi, *Magnetoassociation of a Feshbach molecule and spin-orbit interaction between the ground and electronically excited states,* Phys. Rev. A **96**, 023602 (2017); doi: 10.1103/PhysRevA.96.023602.

[44] L. Franchi, L. F. Livi, G. Cappellini, G. Binella, M. Inguscio, J. Catani, and L. Fallani, *State-dependent interactions in ultracold ^{174}Yb probed by optical clock spectroscopy,* New J. Phys. **19**, 103037 (2017); doi: 10.1088/1367-2630/aa8fb4.

[45] R. Bouganne, M. B. Aguilera, A. Dareau, E. Soave, J. Beugnon, and F. Gerbier, *Clock spectroscopy of interacting bosons in deep optical lattices,* New J. Phys. **19**, 113006 (2017); doi: 10.1088/1367-2630/aa8c45.

[46] G. Cappellini, L. F. Livi, L. Franchi, D. Tusi, D. Benedicto Orenes, M. Inguscio, J. Catani, and L. Fallani, *Coherent Manipulation of Orbital Feshbach Molecules of Two-Electron Atoms*, Phys. Rev. X **9**, 011028 (2019); doi: 10.1103/PhysRevX.9.011028.

[47] J. Jiang, J. Mitroy, Y. Cheng, and M. W. J. Bromley, *Effective oscillator strength distributions of spherically symmetric atoms for calculating polarizabilities and long-range atom–atom interactions*, At. Data Nucl. Data Tables **101**, 158 (2015); doi: 10.1016/j.adt.2014.10.001.

[48] S.G. Porsev, M.S. Safronova and C.W. Clark, *Relativistic calculations of C6 and C8 coefficients for strontium dimers*, Phys. Rev. A **90**, 052715 (2014); doi: 10.1103/PhysRevA.90.052715.

[49] A. Derevianko, V.A. Dzuba, and V.V. Flambaum, *Highly Charged Ions as a Basis of Optical Atomic Clockwork of Exceptional Accuracy*, Phys. Rev. Lett. **109**, 180801 (2012); doi: 10.1103/PhysRevLett.109.180801.

[50] A. Derevianko, H. Katori, *Colloquium: Physics of optical lattice clocks*, Rev. Mod. Phys. **83**, 2 (2011).

[51] M. Borkowski, A. A. Buchachenko, R. Ciuryło, P. S. Julienne, H. Yamada, Y. Kikuchi, Y. Takasu, and Y. Takahashi, *Weakly bound molecules as sensors of new gravitylike forces*, Sci. Rep. **9**, 14807 (2019); doi: 10.1038/s41598-019-51346-y.

[52] P.R. Kemper, and M.T. Bowers, *Electronic-state chromatography: application to first-row transition-metal ions*, J. Phys. Chem. **95**, 5134-5146 (1991); doi: 10.1021/j100166a042.

[53] M.T. Bowers, P.R. Kemper, G. von Helden, and P.A.M. van Koppen, *Gas-phase ion chromatography: transition metal state selection and carbon cluster formation*, Science **260**, 1446-1451 (1993); doi: 10.1126/science.260.5113.1446.

[54] W.S. Taylor, E.M. Spicer, and D.F. Barnas, *Metastable metal ion production in sputtering DC glow discharge plasmas: characterization by electronic state chromatography*, J. Phys. Chem. A **103**, 643-650 (1999); doi: 10.1021/jp983887i.

[55] G. Visentin, M. Laatiaoui, L.A. Viehland, and A.A. Buchachenko, *Mobility of the Singly-Charged Lanthanide and Actinide Cations: Trends and Perspectives*, Front. Chem. **8**, 438 (2020); doi: 10.3389/fchem.2020.00438.

[56] M. Laatiaoui, A.A. Buchachenko and L.A. Viehland, *Laser Resonance Chromatography of Superheavy Elements*, Phys. Rev. Lett. **125**, 023002 (2020); doi: 10.1103/PhysRevLett.125.023002.

[57] M. Laatiaoui, *"Laser resonance chromatography (LRC): a new methodology in superheavy element research,"* in The 13th International Conference on Stopping and Manipulation of Ions and Related Topics (SMI-2019), Book of Abstracts, **8** (Montreal, QC, 2019).

2. Theoretical background

2.1. The theory of weak intermolecular forces

2.1.1. Introduction

The interaction of two atoms or molecules can be roughly compared to a conversation of two people: the main driving forces leading two people to sympathize with each other consist of either intrinsic factors of each person, such as their more or less marked extroversion, or induced factors, such as the interlocutor's ability of orienting his companion to sympathize with him. In other words, *intrinsic* or *induced* features may concur to raise a conversation. In a very similar manner, two atoms interact either by an intrinsic property or by an induced property. Examples of intrinsic properties in atoms and molecules are their *electric polarizabilities*, while their *induced electric multipole moments* are defined as the system's *induced* response to an electric external stimulus.

In this section the theory behind Van der Waals forces is explored, starting from the pristine model of a uniform distribution of charges in an electric field to the model of two atoms with an isotropic electron distribution. This model is particularly relevant, as the Thesis will mostly deal with interactions of closed-shell atoms, where no anisotropy in the charge distribution arises.

2.1.2. Electric multipole moments

Let us take a uniform distribution of charges. The simplest multipole moment is the total charge, q,

$$q = \Sigma_a e_a, \tag{2.1}$$

where e_a represents the charge owned by each particle composing the system. Upon placing the charge distribution into an electrostatic potential field $V(\boldsymbol{r})$, the energy of the charge distribution will be affected by such a potential field, thus generating a potential energy for the interaction with it, U:

$$U = \Sigma_a e_a V(\boldsymbol{a}), \tag{2.2}$$

where $\boldsymbol{a}$ defines the position vector of each charge composing the system. Throughout the Thesis, we will use equally *U* and *V* to refer to the potential energy, except in cases when potential energy

and electric field are considered simultaneously. In that specific case, such as in the present one, V will always refer to the electrostatic potential field.

A uniform electric field, $\boldsymbol{F}$, generates an electric potential field $V(\boldsymbol{r}) = V_0 - \boldsymbol{r} \cdot \boldsymbol{F}$ and thus the potential energy becomes

$$U = qV_0 - \Sigma_a e_a \boldsymbol{a} \cdot \boldsymbol{F} \tag{2.3}$$

In eq. (2.3), V_0 represents the potential at the origin and one can distinguish two contributions: the first is the potential energy at the origin, the second is the product of the electric field times an intrinsic property of the charge distribution, i.e. its *dipole moment*

$$\boldsymbol{\mu} = \Sigma_a e_a \boldsymbol{a} \tag{2.4}$$

Besides the dipole moment, other higher order multipole moments exist, such as the *quadrupole moment* and the *octupole moment*; the former is so called since a quadrupolar charge distribution using charges of equal magnitude needs four of them, two positive and two negative [1]; the latter is so called since eight charges of equal magnitude are needed for an octupolar charge distribution, four positive and four negative. In general, any electric multipole moment of rank *n* can be expressed in the following tensor notation [1]:

$$\zeta^{(n)}_{\alpha\beta} \dots \nu = \frac{(-1)^n}{n!} \Sigma_a e_a a^{2n+1} \partial_{a_\nu} \dots \partial_{a_\beta} \partial_{a_\alpha} \left(\frac{1}{\boldsymbol{a}}\right), \tag{2.5}$$

where the Greek letters $\alpha, \beta, \dots, \nu$ indicate the Cartesian components of the multipole moment tensor. The sum runs over the positions of each charge.

It is worthy of notice that the number of independent tensor components for the rank *n* multipole moment is equal to $2n+1$, corresponding to the number of spherical harmonics of that rank [1]. For many applications it is thus much more practical to use a polar coordinate system instead of a Cartesian one. In that case, one can describe multipole moment tensors Q by means of regular spherical harmonics R_{lk}:

$$Q_{lk} = \Sigma_a e_a R_{lk}(\boldsymbol{a}) \quad \text{or} \quad Q_{lk} = \int \rho(\boldsymbol{r}) R_{lk}(\boldsymbol{r}) d^3\boldsymbol{r}, \tag{2.6}$$

where ρ signifies the continuous charge density.

An atom or a molecule in a non-uniform electric field feels a potential $V(\boldsymbol{r})$. The related electric field is expressed as $F_a = \partial_{r_\alpha} V = V_\alpha$ and its gradient is $F_{\alpha\beta} = -\partial_{r_\alpha}\partial_{r_\beta} V = -V_{\alpha\beta}$. Upon choosing a proper coordinate origin, we can expand the potential in Taylor Series:

$$V(\boldsymbol{r}) = V(0) + r_\alpha V_\alpha|_0 + \frac{1}{2} r_\alpha r_\beta V_{\alpha\beta}|_0 + \frac{1}{3!} r_\alpha r_\beta r_\gamma V_{\alpha\beta\gamma}|_0 + \cdots \tag{2.7}$$

The Hamiltonian operator describing the energy for the interaction with the field, $\widehat{\mathcal{H}}'$, can be expressed in terms of all the charges of the atom or molecule in each position *a* times the potential:

$$\widehat{\mathcal{H}}' = \hat{V}(0)\Sigma_a e_a + \hat{V}_\alpha|_0 \Sigma_a e_a\, \hat{r}_\alpha + \frac{1}{2}\hat{V}_{\alpha\beta}|_0 \Sigma_a e_a\, \hat{r}_\alpha\, \hat{r}_\beta + \frac{1}{3!}\hat{V}_{\alpha\beta\gamma}|_0 \Sigma_a e_a\, \hat{r}_\alpha\, \hat{r}_\beta\, \hat{r}_\gamma + \ldots \tag{2.8}$$

Eq. (2.8), called the Multipole Expansion, leads, after tedious calculations, to the following result,

$$\widehat{\mathcal{H}}' = q\hat{V} + \hat{\mu}_\alpha \hat{V}_\alpha + \frac{1}{3}\widehat{\Theta}_{\alpha\beta}\hat{V}_{\alpha\beta} + \frac{1}{3.5}\widehat{\Omega}_{\alpha\beta\gamma}\hat{V}_{\alpha\beta\gamma} + \cdots + \frac{1}{(2n-1)!!}\hat{\zeta}^n_{\alpha\beta\ldots\nu}\hat{V}_{\alpha\beta\ldots\nu}\,, \tag{2.9}$$

i.e. an expansion in terms of the potential operator and its derivatives, containing the dipole moment operator along the α component, $\hat{\mu}_\alpha$, the quadrupole moment operator along the α, β components, $\widehat{\Theta}_{\alpha\beta}$, the octupole moment operator along the α, β, γ components and so forth. According to the previous analysis, the multipole moments can be expressed either in the Cartesian coordinate system or in the polar coordinate system.

2.1.3. Static Polarizabilities

The early result achieved in eq. (2.9) can be worked out with Perturbation Theory. Upon treating (2.9) perturbatively, one can get the expectation value for the ground state interaction at the first order, $E' = <0|\widehat{\mathcal{H}}'|0>$:

$$E' = <0|\widehat{\mathcal{H}}'|0> = qV + \mu_\alpha V_\alpha + \frac{1}{3}\Theta_{\alpha\beta}V_{\alpha\beta} + \frac{1}{(3)\cdot(5)}\Omega_{\alpha\beta\gamma}V_{\alpha\beta\gamma} + \cdots + \frac{1}{(2n-1)!!}\zeta^n_{\alpha\beta\ldots\nu}V_{\alpha\beta\ldots\nu} = \Sigma_{lk} Q_{lk} V_{lk}\,, \tag{2.10}$$

where, for short, for each intrinsic multipole moment we mean its ground state expectation value.

The second-order term of the interaction yields the Rayleigh-Schrödinger sum over states [1]:

$$E'' = -\frac{\Sigma_n'(<0|\hat{\mathcal{H}}'|n><n|\hat{\mathcal{H}}'|0>)}{E_n-E_0} = -V_\alpha V_{\alpha'}\Sigma_n' \frac{<0|\hat{\mu_\alpha}|n><n|\hat{\mu}_{\alpha'}|0>}{E_n-E_0} - \frac{1}{3}V_\alpha V_{\alpha'\beta'}\Sigma_n' \frac{<0|\hat{\mu}_\alpha|n><n|\hat{\Theta}_{\alpha'\beta'}|0>}{E_n-E_0} - \frac{1}{3}V_{\alpha\beta}V_\alpha'\Sigma'_n \frac{<0|\hat{\Theta}_{\alpha\beta}|n><n|\hat{\mu}'_\alpha|0>}{E_n-E_0} - \cdots \quad (2.11)$$

The prime upon the summation means that the state $|0>$ should be omitted. We can rewrite eq. (2.11) as follows:

$$E'' = -\frac{1}{2}\alpha_{\alpha\beta}V_\alpha V_\beta - \frac{1}{6}\alpha_{\alpha\beta\gamma}V_\alpha V_{\beta\gamma} - \cdots, \quad (2.12)$$

with

$$\begin{cases} \alpha_{\alpha\beta} = \Sigma_n' \frac{<0|\hat{\mu}_\alpha|n><n|\hat{\mu}_\beta|0> + <0|\hat{\mu}_\beta|n><n|\hat{\mu}_\alpha|0>}{E_n-E_0} \\ \alpha_{\alpha\beta\gamma} = \Sigma_n' \frac{<0|\hat{\mu}_\alpha|n><n|\hat{\Theta}_{\beta\gamma}|0> + <0|\hat{\Theta}_{\beta\gamma}|n><n|\hat{\mu}_\alpha|0>}{E_n-E_0} \end{cases} . \quad (2.13)$$

These two tensor quantities characterize, respectively, the dipole moment induced by an electric field ($\alpha_{\alpha\beta}$) and the quadrupole moment induced by an electric field ($\alpha_{\alpha\beta\gamma}$) [1,2].

Upon replacing the Cartesian tensors in (2.13) with the related spherical tensors, we can write a generic *polarizability* $\alpha_{lkl'k'}$:

$$\alpha_{lkl'k'} = \Sigma_n' \frac{<0|\hat{Q}_{lk}|n><n|\hat{Q}_{l'k'}|0> + <0|\hat{Q}_{l'k'}|n><n|\hat{Q}_{lk}|0>}{E_n-E_0} \quad (2.14)$$

Thus we define $\alpha_{1k1k'} = \alpha_1$ the *dipole polarizability*, corresponding to the Cartesian $\alpha_{\alpha\beta}$, whereas $\alpha_{1k2k'} = \alpha_2$ is defined the *quadrupole polarizability*, corresponding to the Cartesian $\alpha_{\alpha\beta\gamma}$. Given the initial conditions, these polarizabilities are the system's responses to a non-oscillating electric field: for this reason, they will be called hereinafter the *static polarizabilities*.

As mentioned above, polarizability is a tensor, whose components account for the anisotropy in the charge distribution of the species interacting with an external electric field. In fact, for many molecules, clusters and some open-shell atoms, the redistribution of charge under application of an external electric field depends on the direction of the electric field vector itself. Anisotropy in the charge rearrangement, therefore, implies the representation of polarizability as a tensor. This, in turn, can be decomposed into a scalar contribution and an anisotropic contribution [2], where the scalar part is defined as the trace of the polarizability tensor, whereas the anisotropic contribution is

proportional to the difference between the triple product of the squared trace of the polarizability tensor and the trace of the squared polarizability tensor [2]. However, some molecules and most atoms (e.g. closed-shell species) have isotropic charge distributions. This means that, for those systems, there is no anisotropic contribution to the polarizability, and the polarizability tensors reduces to the scalar part. This Thesis will mostly discuss systems where charge distribution is isotropic or, at least, where anisotropy is negligible. For this reason, scalar polarizability and isotropic interactions will be discussed more in detail throughout this work, compared to the anisotropic case.

2.1.4. Dynamic Polarizabilities

When an atom interacts with an oscillating field, then the interaction energy should be investigated with the Time-dependent Perturbation Theory. Before applying it, some assumptions should be made:

- The total Hamiltonian $\widehat{\mathcal{H}}$ of the interacting system can be written as an unperturbed time-independent contribution $\widehat{\mathcal{H}}_0$ and a small time-dependent perturbation due to the interaction with the field, $\widehat{\mathcal{H}}' = \hat{V} f(t)$, where $\hat{V}$ is a time-independent operator, while $f(t)$ is a function of time. The total Hamiltonian is then such that $\widehat{\mathcal{H}} = \widehat{\mathcal{H}}_0 + \widehat{\mathcal{H}}'$;
- The wave function for $\widehat{\mathcal{H}}$ should be $\Psi = \Sigma_k a_k(t)\psi_k \exp(-i\omega_k t)$, where ψ_k stands for the *k*-th unperturbed eigenstate, whereas ω_k corresponds to the related angular frequency. As the perturbation is small and the system resides in the initial state $|n>$, the coefficient $a_k(t)$ should satisfy the equation

  $$\partial_t a_k(t) = -\frac{i}{\hbar} V_{kn} f(t) \exp(i\omega_{kn} t)\,, k \neq n; \tag{2.15}$$

  where $\omega_{kn} = \omega_k - \omega_n$.
- The frequency ω is high enough to make the field gradient and the higher derivatives negligible. According to such conditions, one can start integrating eq. (2.15),

$$a_k(t) = -\frac{i}{\hbar} \hat{V}_{kn} \int_0^t d\tau\, f(\tau) \exp(i\omega_{kn}\tau) \tag{2.16}$$

We can now specify the time factor: if the field is supposed to have been turned on in a distant past, the interaction can be written as $\widehat{\mathcal{H}}'(t) = 2\hat{V}\,(\exp[(\epsilon + i\omega t)] + \exp[(\epsilon - i\omega t)])$, where the factor

ϵ is small and tends to zero when the oscillating field has been on for a long time (steady state approximation) [1].

Upon replacing this new formulation of the interaction into eq. (2.16), one gets

$$a_k(t) = -\frac{i}{\hbar}\hat{V}_{kn}\left(\int_{-\infty}^{t} d\tau\ \exp[(\epsilon + i\omega t)] + \exp[(\epsilon - i\omega t)]\right) =$$

$$= -\frac{\hat{V}_{kn}}{\hbar}\left(\frac{\exp[(\epsilon+i\omega_{kn}+i\omega)t]}{\omega_{kn}+\omega-i\epsilon} + \frac{\exp[(\epsilon+i\omega_{kn}-i\omega)t]}{\omega_{kn}-\omega-i\epsilon}\right) \quad (2.17)$$

Upon letting ϵ tend to zero, eq. (2.17) becomes

$$a_k(t) = -\frac{\hat{V}_{kn}}{\hbar}\left(\frac{\exp[(i\omega_{kn}+i\omega)t]}{\omega_{kn}+\omega} + \frac{\exp[(i\omega_{kn}-i\omega)t]}{\omega_{kn}-\omega}\right) \quad (2.18)$$

We now specify the time-independent function V for an electric field polarized along the β direction, $V(t) = -F_\beta \mu_\beta \cos(\omega t)$. The α-component of the system's dipole moment is then the sum of a time-independent intrinsic contribution and a time-dependent contribution induced by the applied oscillating field:

$$\mu_\alpha = <0|\hat{\mu}_\alpha|0> + \Sigma'_k a_k(t) <0|\hat{\mu}_\alpha|k> \exp(i\omega_{0k}t) + c.c., \quad (2.19)$$

where "*c.c.*" means the complex conjugate of μ_α. $a_k(t)$ is known from (2.18), thus (2.19) becomes

$$\mu_\alpha = <0|\hat{\mu}_\alpha|0> + \Sigma'_k (V_{k0}/\hbar)\ [<0|\hat{\mu}_\alpha|k> (\frac{\exp(i\omega t)}{\omega_{k0}+\omega} + \frac{\exp(-i\omega t)}{\omega_{k0}-\omega} + c.c.)]$$

$$= <0|\hat{\mu}_\alpha|0> + F_\beta \cos(\omega t)\, \Sigma'_k \frac{\omega_{k0}(<0|\hat{\mu}_\alpha|k><k|\widehat{\mu_\beta}|0>+<0|\hat{\mu}_\beta|k><k|\hat{\mu}_\alpha|0>)}{\hbar(\omega_{k0}^2-\omega^2)} -$$

$$iF_\beta \sin(\omega t)\, \Sigma'_k \frac{\omega(<0|\hat{\mu}_\alpha|k><k|\widehat{\mu_\beta}|0>-<0|\widehat{\mu_\beta}|k><k|\hat{\mu}_\alpha|0>)}{\hbar(\omega_{k0}^2-\omega^2)} \quad (2.20)$$

If the system resides in a non-degenerate state, then the products within brackets are real and the out-of-phase term vanishes. Eq. (2.20) then becomes

$$\mu_\alpha = <0|\hat{\mu}_\alpha|0> + \alpha_1(\omega) F_\beta \cos(\omega t) \quad (2.21)$$

The term $\alpha_1(\omega)$, that is defined as

$$\alpha_1(\omega) = \Sigma'_k \frac{\omega_{k0}(<0|\widehat{\mu_\alpha}|k><k|\hat{\mu}_\beta|0>+<0|\hat{\mu}_\beta|k><k|\hat{\mu}_\alpha|0>)}{\hbar(\omega_{k0}^2-\omega^2)}, \quad (2.22)$$

and is called the *dipole dynamic polarizability of the system at the frequency ω*. ω_{k0} is the angular frequency for the transition from the state $|0>$ to the state $|k>$.

It is evident that (2.22) has a pole for $\omega = \omega_{k0}$. To circumvent such a problem, one can define the frequency of the field to be complex, as $= iu$, where *u* is real. In this way the pole is removed,

$$\alpha_1(iu) = \Sigma'_k \frac{\omega_{k0}(<0|\widehat{\mu_\alpha}|k><k|\widehat{\mu}_\beta|0>+<0|\widehat{\mu}_\beta|k><k|\widehat{\mu_\alpha}|0>)}{\hbar(\omega_{k0}^2+u^2)} \tag{2.23}$$

Eq. (2.23) can also be more simply expressed as [3]:

$$\alpha_1(iu) = 2Re\ \Sigma'_k \frac{<0|\widehat{\mu}|k><k|\widehat{\mu}|0>}{(E_k-E_0)+iu} \tag{2.24}$$

Similar approaches can be used to derive higher-order polarizabilities, such as *quadrupole* polarizability, $\alpha_2(iu)$, *octupole* polarizability, $\alpha_3(iu)$, and so forth. In general, given the *n*-pole moment operator, $\hat{Q}^{(n)}$, the related n-pole polarizability reads as [3]

$$\alpha_n(iu) = 2Re\ \Sigma'_k \frac{(<0\left|\widehat{Q^{(n)}}\right|k><k\left|\widehat{Q_n^{(n)}}\right|0>}{(E_k-E_0)+iu} \tag{2.25}$$

2.1.5. Intermolecular forces at long range

As intermolecular forces are relatively weak, it is natural to describe them by means of perturbation theory. The simplest case corresponds to the situation where the interacting species, A and B, are far enough, that the overlap can be ignored. In fact, let us consider the interaction of two species A and B. Their respective wave functions are $\Psi^{\mathrm{A}}(1,2,\ldots,n_{\mathrm{A}})$ and $\Psi^{\mathrm{B}}(1',2',\ldots,n'_{\mathrm{B}})$, each one, in turn, function of the positions of the electrons localized at the respective species. By hypothesis, there exists a region of space associated with Ψ^{A} such that Ψ^{A} is non-zero only when all its electrons are in this region. Likewise, there exists a region of space associated with Ψ^{B}, and the two regions do not overlap. The wavefunction for the combined system is expressed as the antisymmetrized product $\hat{\mathcal{A}}\Psi^{\mathrm{A}}\Psi^{\mathrm{B}}$, where $\hat{\mathcal{A}}$ is the antisymmetrization operator. However, the antisymmetrized product contains terms like $\Psi^{\mathrm{A}}(1',2,\ldots,n_{\mathrm{A}})\Psi^{\mathrm{B}}(1,2',\ldots,n'_{\mathrm{B}})$, where electron 1 of A has been exchanged with electron 1' of B. The overlap between this and the original product function,

$$<\Psi^{\mathrm{A}}(1,2,\ldots n_{\mathrm{A}})\Psi^{\mathrm{B}}(1',2',\ldots,n'_{\mathrm{B}})|\Psi^{\mathrm{A}}(1',2,\ldots,n_{\mathrm{A}})\Psi^{\mathrm{B}}(1,2',\ldots,n'_{\mathrm{B}})>$$

is then zero, because Ψ^{A} and Ψ^{B} are non-zero in different regions of space. This means that the two wavefunctions do not mix and, as a consequence, the calculations may be done without antisymmetrization [1]. Of course, this is an approximation, as the overlap is never exactly zero, but the error made by ignoring it decreases exponentially as the distance between A and B increases [1]. However, at the same time, this also means that such an approximation no longer holds when A and B are close enough and overlap becomes significant.

Given these premises, one can associate a set of n_{A} electrons with the species A and define a Hamiltonian $\widehat{\mathcal{H}}^{\mathrm{A}}$in terms of these electrons. Analogously, one can associate a set of n_{B} electrons with the species B and define a corresponding Hamiltonian $\widehat{\mathcal{H}}^{\mathrm{B}}$in terms of these electrons. Thence, the unperturbed Hamiltonian is expressed as the sum of the separate Hamiltonians of A and B,

$$\widehat{\mathcal{H}}^{0} = \widehat{\mathcal{H}}^{\mathrm{A}} + \widehat{\mathcal{H}}^{\mathrm{B}}, \tag{2.26}$$

whereas the perturbation, $\widehat{\mathcal{H}}'$, consists of the electrostatic interaction between the particles of A and those of B [4]:

$$\widehat{\mathcal{H}}' = \int d^3\boldsymbol{r}\, d^3\boldsymbol{r}' \frac{\hat{\rho}^{\mathrm{A}}(\boldsymbol{r})\hat{\rho}^{\mathrm{B}}(\boldsymbol{r}')}{4\pi\epsilon_0|\boldsymbol{r}-\boldsymbol{r}'|} \tag{2.27}$$

Here the terms $\hat{\rho}^{k}(\boldsymbol{r}) = \Sigma_{k\in K} e_k \delta(r-k)$ define the localized charge density of each atom, while $\boldsymbol{r}$ and $\boldsymbol{r}'$ stand for the positions of the electrons of the species A and B, respectively.

It is also very useful to notice that the potential that A feels at $\boldsymbol{r}$ because of B is

$$\hat{V}^{\mathrm{B}}(\boldsymbol{r}) = \int d^3\boldsymbol{r}' \left(\frac{\hat{\rho}^{B}(\boldsymbol{r}')}{4\pi\epsilon_0|\boldsymbol{r}-\boldsymbol{r}'|}\right), \tag{2.28}$$

so that the perturbation $\widehat{\mathcal{H}}'$ can be represented as the energy due to the interaction of the charges of A with the potential of B:

$$\widehat{\mathcal{H}}' = \int d^3\boldsymbol{r}\, \hat{V}^{\mathrm{B}}(\boldsymbol{r})\hat{\rho}^{\mathrm{A}}(\boldsymbol{r}) \tag{2.29}$$

As the premises allow for neglecting antisymmetrization, the unperturbed states of the system are simply the product functions $\Psi = \Psi^{\mathrm{A}}\Psi^{\mathrm{B}}$, that, for brevity, are to be written as $|mn>$. Precisely, here, *m* and *n* identify the energy states of A and B when they do not interact, therefore, when both A and B are in the ground state, then one has $|00>$, when A resides in the first excited state, while

B is still in the ground state, then one has $|10>$ and so forth. All the $|mn>$ states are eigenfunctions of the unperturbed Hamiltonian $\hat{\mathcal{H}}^0$, so that for each state of the pair mn, The Schrödinger equation for the unperturbed Hamiltonian reads as follows:

$$\hat{\mathcal{H}}^0\big|mn> = \left(\hat{\mathcal{H}}^{\mathrm{A}} + \hat{\mathcal{H}}^{\mathrm{B}}\right)\big|mn> = (E_m^{\mathrm{A}} + E_n^{\mathrm{B}})|mn> = E_{mn}^0|mn> \tag{2.30}$$

For closed-shell atoms the non-degenerate Rayleigh-Schrödinger Perturbation Theory yields the perturbed energies to second order of the ground state ($m = n = 0$) [1],

$$E_{00} = E_{00}^0 + E'_{00} + E''_{00} + \cdots, \tag{2.31}$$

with

$$E_{00}^0 = E_0^{\mathrm{A}} + E_0^{\mathrm{B}} \tag{2.32}$$

$$E'_{00} = <00\big|\hat{\mathcal{H}}'\big|00> \tag{2.33}$$

$$E''_{00} = -\Sigma'_{mn} \frac{<00|\hat{\mathcal{H}}'|mn><mn|\hat{\mathcal{H}}'|00>}{E_{mn}^0 - E_{00}^0} \tag{2.34}$$

This is called the *long-range approximation* to the interaction energy [1]: upon writing the first-order term (2.33) in the form (2.27), it yields

$$E'_{00} = \int d^3\boldsymbol{r}\, d^3\boldsymbol{r}' \frac{\rho^{\mathrm{A}}(\boldsymbol{r})\rho^{\mathrm{B}}(\boldsymbol{r}')}{4\pi\epsilon_0|\boldsymbol{r}-\boldsymbol{r}'|}, \tag{2.35}$$

where the integration over the coordinates of the particles in species A and B replaces the charge density operators $\hat{\rho}^{\mathrm{A}}(\boldsymbol{r}), \hat{\rho}^{\mathrm{B}}(\boldsymbol{r})$ with their expectation values at the ground state $\rho^{\mathrm{A}}(\boldsymbol{r}), \rho^{\mathrm{B}}(\boldsymbol{r})$, respectively. Eq. (2.35) corresponds to the classical electrostatic interaction according to Coulomb's law. Thus, the first-order term (2.33) yields the expectation energy for the electrostatic interaction of A and B in the ground state $|00>$.

The second-order term (2.34) accounts for the induction and dispersion energies. To understand this term, it is instructive to split it into three contributions:

$$E''_{00} = U_{ind}^{\mathrm{A}} + U_{ind}^{\mathrm{B}} + U_{disp} \tag{2.36}$$

Here, the first contribution refers to the case when A is excited, while B is in its ground state; the second contribution to the case when A is in its ground state, while B is excited; the third contribution

to the case when both A and B are excited. According to this depiction, each contribution can be explicitly written as

$$U_{ind}^{\mathrm{A}} = -\Sigma_{m\neq 0} \frac{<00|\hat{\mathcal{H}}'|m0><m0|\hat{\mathcal{H}}'|00>}{E_m^{\mathrm{A}}-E_0^{\mathrm{A}}} \tag{2.37}$$

$$U_{ind}^{\mathrm{B}} = -\Sigma_{n\neq 0} \frac{<00|\hat{\mathcal{H}}'|0n><0n|\hat{\mathcal{H}}'|00>}{E_n^{\mathrm{B}}-E_0^{\mathrm{B}}} \tag{2.38}$$

$$U_{disp} = -\Sigma_{m\neq 0;n\neq 0} \frac{<00|\hat{\mathcal{H}}'|mn><mn|\hat{\mathcal{H}}'|00>}{(E_m^{\mathrm{A}}+E_n^{\mathrm{B}})-(E_0^{\mathrm{A}}+E_0^{\mathrm{B}})} \tag{2.39}$$

2.1.6. Induction energy

In the long-range limit, the most natural way to develop the induction energy relies on using the multipole expansion [5]. In particular, eq. (2.9) can be substituted in the interaction Hamiltonian $\hat{\mathcal{H}}'$ in the expression (2.38). Subsequent integration over the coordinates of species A yields the expectation values of the multipole moment operators and, thence, the related multipole static polarizabilities. The induction energy (2.38) can then be rewritten as

$$U_{ind}^{\mathrm{B}} = -\frac{1}{2}F_{\alpha}^{\mathrm{A}}(\mathbf{B})F_{\alpha'}^{\mathrm{A}}(\mathbf{B})\alpha_{1\alpha\alpha'}^{\mathrm{B}} - \frac{1}{3}F_{\alpha}^{\mathrm{A}}(\mathbf{B})F_{\alpha'\beta'}^{\mathrm{A}}(\mathbf{B})\alpha_{2\alpha\alpha'\beta'}^{\mathrm{B}} - \cdots \tag{2.40}$$

When A is a spherical ion placed in the origin (0,0, z), the field in B is $F_z = q/4\pi\epsilon_0 z^2$ and, therefore, the induction energy at the lowest order is $E_{ind}^{\mathrm{B}} = q^2\alpha_{1zz}^{\mathrm{B}}/(4\pi\epsilon_0)^2 z^4$, thus being inversely dependent on the fourth power of the internuclear distance [1]. If both A and B are neutral, the lowest-order induction term vanishes. If, instead, only one of them, such as A, is an ion, induction depends only on the properties of B. Higher-order contributions to the induction energy are present if one of the neutral species bears an electric multipole moment. In this case, induction energy decays faster than R^{-4}. For instance, if A is neutral, but has non-zero dipole moment ($\mu_{\mathrm{A}} \neq 0$), then induction energy is proportional to R^{-6} [1]. For closed-shell atoms, no induction contributions emerge; conversely, for open-shell atoms, the lowest-order induction is associated with the quadrupole moment and is proportional to R^{-7}.

2.1.7. Dispersion energy

Unlike the induction interaction, the dispersion interaction is a fully non-classical effect. The first attempts to give a formulation of it date back to London [6], with a classical model based on the harmonic oscillator (Drude's model).

For a quantum mechanical formulation, it is useful to start from eq. (2.39). For simplicity, we consider only the dipole-dipole term in $\widehat{\mathcal{H}}'$:

$$U_{disp}^{6} = -\Sigma_{m_A\neq 0}\Sigma_{n_A\neq 0}\left(\frac{<0_A 0_B|\hat{\mu}_\alpha^A T_{\alpha\beta}\hat{\mu}_\beta^B|m_A n_B><m_A n_B|\hat{\mu}_\gamma^A T_{\gamma\delta}\hat{\mu}_\delta^B|0_A 0_B>}{(E_m^A+E_n^B)-(E_0^A+E_0^B)}\right) =$$

$$-T_{\alpha\beta}T_{\gamma\delta}\Sigma_{m_A\neq 0}\Sigma_{n_A\neq 0}\frac{<0_A|\hat{\mu}_\alpha^A|m_A><m_A|\hat{\mu}_\gamma^A|0_A><0_B|\hat{\mu}_\beta^B|n_B><n_B|\hat{\mu}_\delta^B|0_B>}{\Delta_0^m E^A+\Delta_0^n E^B}\ , \tag{2.41}$$

where

$$T_{\lambda\nu} = \frac{1}{4\pi\epsilon_0}\nabla_\lambda\nabla_\nu\left(\frac{1}{|\boldsymbol{r}-\boldsymbol{r}'|}\right) \tag{2.42}$$

Eq. (2.41) is not easy to handle, as, unlike the numerator, the denominator cannot be factorized into terms referring solely to A and terms referring solely to B. A way to solve this issue relies on the so called *average-energy approximation* [7]. First, eq. (2.41) is rewritten as

$$U_{disp}^{6} = -T_{\alpha\beta}T_{\gamma\delta}\Sigma_{m_A\neq 0}\Sigma_{n_A\neq 0}\left(\frac{\Delta_0^m E^A\Delta_0^n E^B}{\Delta_0^m E^A+\Delta_0^n E^B}\right)\left(\frac{<0_A|\hat{\mu}_\alpha^A|m_A><m_A|\hat{\mu}_\gamma^A|0_A>}{\Delta_0^m E^A}\right)\left(\frac{<0_A|\hat{\mu}_\beta^B|n_B><n_B|\hat{\mu}_\delta^B|0_A>}{\Delta_0^n E^B}\right). \tag{2.43}$$

Then, the approximation applies to $\frac{\Delta_0^m E^A\Delta_0^n E^B}{\Delta_0^m E^A+\Delta_0^n E^B}$, using average excitations energies U^A and U^B [1]:

$$\frac{\Delta_0^m E^A\Delta_0^n E^B}{\Delta_0^m E^A+\Delta_0^n E^B} = \left(\frac{U_A U_B}{U_A+U_B}\right)(1+\Delta_{mn}), \tag{2.44}$$

with

$$\Delta_{mn} = \frac{(U_A)^{-1}-(\Delta_0^m E^A)^{-1}+(U_B)^{-1}-(\Delta_0^n E^B)^{-1}}{(\Delta_m^0 E^A)^{-1}+(\Delta_n^0 E^B)^{-1}} \tag{2.45}$$

The average energies U^A and U^B should be chosen, so that Δ_{mn} becomes negligible for all m and n. This implies that all the states $|m_A>$ providing important contributions should have excitation

energies close to the average U^{A} and likewise for all the states $|n_{\mathrm{A}}>$. Then, eq. (2.41) yields

$$U_{disp}^{(6)} \approx -\left(\frac{U_{\mathrm{A}}U_{\mathrm{B}}}{4(U_{\mathrm{A}}+U_{\mathrm{B}})}\right) T_{\alpha\beta}T_{\gamma\delta}\alpha_{\alpha\gamma}^{\mathrm{A}}\alpha_{\beta\delta}^{\mathrm{B}} \tag{2.46}$$

If A and B are atoms with isotropic charge distributions, then their polarizabilities are scalar, and, therefore, reduce to $\alpha_{\alpha\gamma}\delta_{\alpha\gamma} = \alpha$. As a consequence of that, $T_{\alpha\beta}$ equals $T_{\gamma\delta}$ and one can exploit the following relation:

$$T_{\alpha\beta}T_{\alpha\beta} = \left(\frac{(3R_\alpha R_\beta - R^2\delta_{\alpha\beta})(3R_\alpha R_\beta - R^2\delta_{\alpha\beta})}{(4\pi\epsilon_0)^2 R^{10}}\right) = \frac{6}{(4\pi\epsilon_0)^2 R^6}\,, \tag{2.47}$$

where $R = |\boldsymbol{r} - \boldsymbol{r}'|$. Eq. (2.46), thus, turns into the simpler form

$$U_{disp}^{(6)} \approx -\frac{3}{2}\left(\frac{U_{\mathrm{A}}U_{\mathrm{B}}}{U_{\mathrm{A}}+U_{\mathrm{B}}}\right)\left(\frac{\alpha_1^{\mathrm{A}}\alpha_1^{\mathrm{B}}}{(4\pi\epsilon_0)^2 R^6}\right) = -\frac{C_6}{R^6} \tag{2.48}$$

C_6 is termed the *dipole-dipole dispersion coefficient.* Eq. (2.48) is called the London formula for dispersion interaction between atoms. However, U^{A} and U^{B} can only be stated empirically.

Casimir and Polder [8] proposed an alternative approach, based on the following identity:

$$\frac{1}{\mathcal{A}+\mathcal{B}} = \frac{2}{\pi}\int_0^\infty \frac{\mathcal{A}\mathcal{B}}{(\mathcal{A}^2+\omega^2)(\mathcal{B}^2+\omega^2)}\,d\omega, \tag{2.49}$$

which is valid for positive $\mathcal{A}$ and $\mathcal{B}$. Applying this formula to the denominator in eq. (2.41), now written as $\hbar(\omega_m^{\mathrm{A}} + \omega_n^{\mathrm{B}})$, one gets

$$U_{disp}^{(6)} = -\frac{2\hbar}{\pi}T_{\alpha\beta}T_{\gamma\delta}\int_0^\infty d\omega\ \Sigma'_{\mathrm{m}}\frac{<0_{\mathrm{A}}|\hat{\mu}_\alpha^{\mathrm{A}}|m_{\mathrm{A}}><m_{\mathrm{A}}|\hat{\mu}_\gamma^{\mathrm{A}}|0_{\mathrm{A}}>\omega_m^{\mathrm{A}}}{\hbar((\omega_m^{\mathrm{A}})^2+\omega^2)}\Sigma'_n\frac{\omega_n^{\mathrm{B}}<0_{\mathrm{B}}|\hat{\mu}_\beta^{\mathrm{B}}|n_{\mathrm{B}}><n_{\mathrm{B}}|\hat{\mu}_\delta^{\mathrm{B}}|0_{\mathrm{B}}>}{\hbar((\omega_n^{\mathrm{B}})^2+\omega^2)} \tag{2.50}$$

where the prime indicates that the summation excludes $m = n = 0$. Eq. (2.50) can be expressed in terms of the polarizabilities of A and B at imaginary frequencies (see eqs. 2.23-24). Here, for simplicity, we set $\omega = u$ and, thence, eq. (2.50) yields:

$$U_{disp}^{(6)} = -\frac{\hbar}{2\pi}T_{\alpha\beta}T_{\gamma\delta}\int_0^\infty d\omega\ \alpha_{\alpha\gamma}^{\mathrm{A}}(i\omega)\alpha_{\beta\delta}^{\mathrm{B}}(i\omega) \tag{2.51}$$

We remind the reader that $\alpha_{\lambda\nu}^{\mathrm{X}}(i\omega)$ refers to the dynamic polarizability tensor of the atom X. For atoms with isotropic charge distributions,

$$U_{disp}^{(6)} = -\left(\frac{3\hbar}{(4\pi\epsilon_0)^2\pi R^6}\right)\int_0^\infty d\omega\alpha_1^{\mathrm{A}}(i\omega)\alpha_1^{\mathrm{B}}(i\omega) \tag{2.52}$$

Using eq. (2.48) and the atomic unit system, one can represent the dipole-dipole dispersion coefficient C_6 as [3]

$$C_6^{AB} = \frac{3}{\pi}\int_0^\infty \alpha_1^A(i\omega)\alpha_1^B(i\omega)d\omega, \tag{2.53}$$

which determines the lowest-order dispersion interaction, coming with the radial dependence on the inverse power of six. As the dipole polarizability is non-vanishing for any system having electrons, the lowest-order dispersion interaction is always present.

Following the same procedure as before, the dispersion coefficients for the dipole-quadrupole interaction, C_8 can be achieved [3]:

$$C_8^{AB} = \frac{15}{\pi}\int_0^\infty [\alpha_1^A(i\omega)\alpha_2^B(i\omega) + \alpha_1^B(i\omega)\alpha_2^A(i\omega)]d\omega \tag{2.54}$$

C_8 coefficient from eq. (2.54) determines the dispersion contribution coming next to the dipole-dipole term, appearing as C_8^{AB}/R^8.

Finally, an analogous derivation permits to determine the coefficient for the dispersion interaction between an atom A with isotropic charge distribution, and an ideally conductive surface with no irregularities, C_3. Derivations of this parameter were reported by several authors, among which Dzyaloshinkii *et al.* [9], Parsegian [10] and Tikochinsky and Spruch [11]. In atomic units, the derivation yields with the integral over the frequency of the dipole polarizability of the atom at imaginary frequencies [12]:

$$C_3 = \frac{1}{4\pi}\int_0^\infty d\omega\, \alpha_1^A(i\omega) \tag{2.55}$$

2.1.8. Retardation effects

When the distance between the interacting species A and B is larger than the wavelength λ_0, corresponding to the characteristic atomic absorption frequency of the perturbed species under study, the correlation between the charge distribution fluctuations in the two species becomes less effective [1,13]. This is due to the finite speed of the interaction, propagating at the speed of light, *c*. As a consequence, the charge distribution fluctuations are no longer in phase and, thus, the response of A to the instantaneous dipole of B cumulates a retardation, and likewise the response of B to that of A. The retardation phenomenon affecting dispersion interaction was studied in detail

by Casimir and Polder [8]. Based on the approach of Ref. [13], Zhang and Dalgarno [12] proposed a particularly relevant consideration of the retardation effect for the lowest dispersion interaction terms in a system of two like closed-shell atoms. For the dipole-dipole and dipole-quadrupole dispersion terms this yields:

$$U_{disp} = -\frac{C_6 f_6(R)}{R^6} - \frac{C_8 f_8(R)}{R^8} \tag{2.56}$$

There, $f_6(R)$ and $f_8(R)$ stand for the dipole-dipole and dipole-quadrupole retardation functions, respectively. Those are, in turn, defined as

$$f_6(R) = 1/(\pi C_6) \int_0^\infty d\omega \exp(-2\alpha_{FS}\omega R)\, \alpha_1^2(i\omega) P_{11}(\omega\alpha_{FS}R); \tag{2.57}$$

$$f_8(R) = 1/(3\pi C_6) \int_0^\infty d\omega \exp(-2\alpha_{FS}\omega R)\, \alpha_1\ (i\omega)\alpha_2(i\omega) P_{12}(\omega\alpha_{FS}R); \tag{2.58}$$

where α_{FS} refers to the fine structure constant, while P_{11} and P_{12} are two polynomials, in turn, defined as [12,13]:

$$P_{11}(x) = x^4 + 2x^3 + 5x^2 + 6x + 3 \tag{2.59}$$

$$P_{12}(x) = \frac{1}{2}x^6 + 3x^5 + \frac{27}{2}x^4 + 42x^3 + 81x^2 + 90x + 45 \tag{2.60}$$

2.2. Computational methods for long-range interactions

Throughout this section, the approaches most widely used to model long-range interactions have been exposed. For the description of these approaches, two important assumptions are made: first, the validity of the Born-Oppenheimer (BO) approximation, according to which electron and nuclear motions do not couple; second, relativistic effects, when required, provide a minor contribution to the interaction energy and, therefore, can be embodied in the non-relativistic Hamiltonian as corrections.

2.2.1. Size-consistency and size-extensivity

Quantum chemical methods used to model systems such as atoms and molecules are often described in term of two properties: *size-consistency* and *size-extensivity*. The definition of the former addresses the capability of a method to describe molecular systems at the dissociation limit: let A and B be two species separated by a distance large enough, that no electron exchange occurs between them. Knowledge of the global potential requires the choice of a molecular approach. In

order for this approach to be size-consistent, the energy calculated for the super-system A + B should equal the sum of the energies calculated for the two isolated systems A, B [1,14,15]. In particular, for long-range interactions size-consistency is a highly desirable property, as it ensures the correct behavior of the potential in the limit where all forces vanish.

On the other hand, size-extensivity is a more mathematically formal feature. First defined by Bartlett [16], size-extensivity refers to the capability by a method of linearly scaling as the number of electrons of the system, i.e. to scale as the exact energy does [15].

With respect to size-consistency, size-extensivity is perhaps a more general property, as it affects not only dimeric calculations, but even monomeric ones: in fact, size-extensivity is a scaling property of the energy [15]. For instance, if a given method is size-extensive, then, for a given system, it is possible to reliably compare the results for an all-electron calculation and a calculation where only the valence shell is correlated.

Size-consistency and size-extensivity are neither mutually exclusive or mutually inclusive properties: some methods can be size-extensive, but not size-consistent or vice versa, or even be both size-consistent and size-extensive.

2.3. Hartree-Fock method

2.3.1. Introduction

The generic Hamiltonian for a *n*-electron atom,

$$\hat{\mathcal{H}}'(\boldsymbol{r_1}, \boldsymbol{r_2}, \dots, \boldsymbol{r_n}) = \frac{\hbar^2}{2m_e}\Sigma_i\hat{\nabla}_i^2 + \Sigma_i\hat{V}_{Ne}(\boldsymbol{r_i}) + \Sigma_{i\neq j}\hat{V}_{ee}(\boldsymbol{r_{ij}}), \tag{2.61}$$

consists of three main terms: a kinetic energy operator, $\hbar/2m_e\Sigma_i\nabla_i^2$, a nuclear-electron potential operator, $\Sigma_i V_{Ne}(\boldsymbol{r_i})$, and an electron-electron potential operator $\Sigma_{i\neq j}V_{ee}(\boldsymbol{r_{ij}})$. To solve the related Schrödinger equation, a wavefunction is needed, which depends, simultaneously, on all the *n* electrons constituting the system, $\Psi(1,2,\dots,n)$. However, the electron-electron interaction term of eq. (2.61) makes the related Schrödinger equation not exactly solvable.

To circumvent such a problem, several methods providing approximate solutions were proposed to numerically solve the Schrödinger equation for atoms consisting of many electrons. One of the

first approximate methods to be developed was the Hartree-Fock (HF) method [17], that marked the birth of ab initio methods.

In the following sections, the principles of the Hartree-Fock method are discussed, together with the self-consistent field solution and the problem of electron correlation.

2.3.2 Fundamentals of the Hartree-Fock method

The Hartree-Fock method approximates the electron-electron potential term in eq. (2.61) by imposing it to depend on the position of one electron. The interactions of all the other electrons is then accounted for in an average way [18]. In other words, this approximation supposes each electron to move throughout the mean field generated by the others. In this way, the wave function Ψ is partitioned into *n* 1-electron wavefunctions (orbitals):

$$\Psi(1,2,\dots,n) \approx \psi_1(1)\psi_2(2)\dots\psi_n(n), \tag{2.62}$$

where each 1-electron wave function is the solution of a related 1-electron Schrödinger equation of the form:

$$-\frac{\hbar^2}{2m}\hat{\nabla}^2\psi_i(\boldsymbol{r}) + \hat{V}(\boldsymbol{r})\psi_i(\boldsymbol{r}) = \epsilon_i\psi_i(\boldsymbol{r}), \tag{2.63}$$

where $\hat{V}(\boldsymbol{r})$ refers to the potential where the electron moves. This consists of the nucleus-electron attraction as written in eq. (2.61) and the potential felt by the electron due to the mean field of the other *n*-1 electrons,

$$V_{ee}(\boldsymbol{r}) = -e\int\frac{d\boldsymbol{r}'\rho(\boldsymbol{r}')}{|\boldsymbol{r}-\boldsymbol{r}'|}, \tag{2.64}$$

with

$$\rho(\boldsymbol{r}') = \Sigma_j^{occupied}\left|\psi_j(\boldsymbol{r}')\right|^2 \quad , \tag{2.65}$$

and the summation running over all the occupied orbitals, except for that of the electron moving in the mean field. In eq. (2.63) the operator terms can be grouped to yield the 1-electron *Fock operator* $\hat{f}_i$.

The HF energy for the *i*-th electron is then the sum of the following contributions [18]:

$$\epsilon_i = < \phi_i \left| -\frac{\hbar^2}{2m}\hat{\nabla}^2 \right| \phi_i > \; + < \phi_i \left| -\frac{Ze^2}{|\boldsymbol{r}-\boldsymbol{R}|} \right| \phi_i > + \Sigma_{i \neq j} < \phi_i(\boldsymbol{r})\phi_j(\boldsymbol{r}') \left| \frac{e^2}{|\boldsymbol{r}-\boldsymbol{r}'|} \right| \phi_i(\boldsymbol{r})\phi_j(\boldsymbol{r}') > \tag{2.66}$$

Here, the functions ϕ_i, ϕ_j, constitute a first approximation (guess) to the *exact* partitioned orbitals ψ_i, ψ_j (trial functions). The first term is the kinetic energy operator, $\hat{T}$; the second term, in turn, corresponds to the nuclear-electron potential operator, $\hat{V}_{Ne}$, depending on the distance between the electron position $\boldsymbol{r}$ and the nucleus position $\boldsymbol{R}$; the third term corresponds to the electron-electron potential operator, $\hat{V}_{ee}$, depending on the distance between the respective positions of the interacting electrons. This latter represents the potential felt by the electron in the mean field of the other *n*-1 electrons.

An equation of the form (2.66) exist for each electron. Solving these equations provides the Hartree-Fock eigenvalues ϵ_i.

Hartree-Fock equations (2.66) are non-linear and should be solved iteratively. The iterative method to solve them is called the *self-consistent field* (SCF) method. The idea is to solve the Schrödinger equation for an electron moving in the potential of the nucleus and of the other electrons [18]. The method consists of the following steps:

1) A first guess (ϕ_i) for the trial 1-electron wavefunction (spin-orbital) is proposed. Usually, for an atomic orbital calculation, the trial spin-orbital is a spin-orbital of the hydrogen-like atom, whose Schrödinger equation can be exactly solved;
2) The trial wave function is used to solve eq. (2.66) and achieve the trial energy;
3) A systematic procedure to guess the wave function is made, until the energy is minimized (for $\phi_i \approx \psi_i$). If the energy is minimized, then the HF calculation has reached the convergence limit. Otherwise, new guesses are tried for a number of iterations set by the user.

2.3.3. Wavefunctions for Hartree-Fock calculations: Slater determinants

Factorization of the *n*-electron wavefunction as defined in eq. (2.62) is too strong an approximation, as it does not account for the antisymmetric nature of the wavefunction itself. To explain antisymmetry, the following example is very instructive: the ground state of He atom has the $1s^2$ electron configuration, with one electron with spin function α and the other with spin function β. According to eq. (2.62), this should be written as

$$\Psi(\boldsymbol{r_1}, \boldsymbol{r_2}) = \psi_{1s\alpha}(\boldsymbol{r_1})\psi_{1s\beta}(\boldsymbol{r_2}) \tag{2.67}$$

However, the configuration (2.67) is arbitrary: the configuration obtained upon permutation of the electrons 1 and 2 is possible as well:

$$\Psi(\boldsymbol{r_1}, \boldsymbol{r_2}) = \psi_{1s\alpha}(\boldsymbol{r_2})\psi_{1s\beta}(\boldsymbol{r_1}) \tag{2.68}$$

Thus, both configurations are possible, but they differ for their spin-orbital functions. It is then clear that a simple product of spin-orbitals does not account for electron indistinguishability. To account for this feature, the wavefunction should be built up as such, that the permutation of its electrons returns the same wavefunction multiplied by -1. A solution to solve this problem relies on a normalized linear combination of (2.67) and (2.68):

$$\Psi(\boldsymbol{r_1}, \boldsymbol{r_2}) = \frac{1}{\sqrt{2}}[\psi_{1s\alpha}(\boldsymbol{r_1})\psi_{1s\beta}(\boldsymbol{r_2}) - \psi_{1s\alpha}(\boldsymbol{r_2})\psi_{1s\beta}(\boldsymbol{r_1})] \tag{2.69}$$

The wavefunction (2.69) may be written in a compact form as a determinant:

$$\Psi(\boldsymbol{r_1}, \boldsymbol{r_2}) = 1/\sqrt{2} \begin{vmatrix} \psi_{1s\alpha}(\boldsymbol{r_1}) & \psi_{1s\beta}(\boldsymbol{r_1}) \\ \psi_{1s\alpha}(\boldsymbol{r_2}) & \psi_{1s\beta}(\boldsymbol{r_2}) \end{vmatrix} \tag{2.70}$$

This determinantal form of the wavefunction is called the *Slater determinant* [18,19] and allows for the description of *n*-electron configurations accounting for the electron indistinguishability and antisymmetric feature of the wavefunction. Configuration (2.70) can thus be generalized for an *n*-electron atom as follows:

$$\Psi(\boldsymbol{r_1}, \boldsymbol{r_2}, \dots, \boldsymbol{r_n}) = 1/\sqrt{n!} \begin{vmatrix} \psi_1(\boldsymbol{r_1}) & \dots & \psi_n(\boldsymbol{r_1}) \\ \vdots & \ddots & \vdots \\ \psi_1(\boldsymbol{r_n}) & \dots & \psi_n(\boldsymbol{r_n}) \end{vmatrix} \tag{2.71}$$

Wavefunctions such as that of ground-state He and all the closed-shell atoms can be accurately described with one Slater determinant. However, for open-shell systems the situation is more complex: in fact, such systems may have several degenerate configurations, each one corresponding to a different Slater determinant. The most accurate way to describe these systems, therefore, relies on representing the related wavefunction as a linear combination of Slater determinants, each one accounting for a different degenerate (or quasi-degenerate) electron configuration. A wavefunction of this kind is termed *multi-determinantal*, whereas wavefunctions needing only one Slater determinant to be accurately represented are termed *single-determinantal*.

HF calculations calculate wavefunctions as single Slater determinants of spin-orbital functions. For the HF method, two kinds of mono-determinantal wavefunctions exist: in one case, a single set of space-orbital functions is used for both α and β spin states: a wavefunction of this kind is called a *spin-restricted* wavefunction and the HF method using it is defined the *restricted* HF (RHF) method; in another case, two distinct sets of space-orbital functions are used, one for α spin states, the other for β spin states: a wavefunction of this kind is termed a *spin-unrestricted* wavefunction and the HF method using it is called the *unrestricted* HF (UHF) method.

2.3.4. Limits of the Hartree-Fock method

Standard HF method makes several approximations that can turn out to be inadequate for the description of several physico-chemical properties. For instance, each eigenfunction is assumed to be describable as a single Slater determinant. This feature makes the HF a *mono-determinantal* method, or *single-reference* method. Indeed, such a depiction is inadequate for the description of many open-shell systems, which, in turn, require multi-determinantal wavefunctions. Moreover, the RHF method is size-extensive, but not generally size-consistent [20]: in fact, it fails in describing the dissociation limit of several species, such as H_2, where the wavefunction should be more accurately described as the interaction of several different configurations. In contrast, the UHF method is both size-extensive and size-consistent [20]. Another too strong approximation is a consequence of the mean field approximation: the assumption of the mean field, in fact, imposes that the instantaneous position of an electron is not influenced by the presence of neighboring electrons and their fluctuations [21]: in reality, the motion of electrons is correlated and their probability density is determined by their interactions. This electron-electron interaction is called the *electron correlation* and its contribution to the total energy of the system may be estimated by subtracting the HF energy from the exact value for it: this energy difference is called the *correlation energy* [22]. Electron correlation plays an important role in determining the physical properties of atoms and molecules: for instance, as it may be noticed from Section 2.1, the dispersion interaction is wholly a correlation effect [1,21]. Electron correlation splits into two contributions, i.e., *static* correlation and *dynamic* correlation. The former is typical of open-shell systems and occurs when the system presents several degenerate or quasi-degenerate electron configurations (i.e. when the related wavefunction is multi-determinantal); the latter, on the other hand, occurs both in open- and closed shell systems and accounts for all electron-electron

couplings that are not involved in static correlation, such as those interactions between non-degenerate configurations [23]; examples of dynamic correlation, therefore, include the interactions between outermost electrons (*valence-valence* correlation), the interactions between innermost electrons (*core-core* correlation) and the interactions between innermost and outermost electrons (*core-valence* correlation). Thus, in order to account for static correlation, an accurate wavefunction should consist of the linear combination of all the degenerate or quasi-degenerate configurations (Slater determinants); in contrast, in order to account for dynamic correlation, an accurate wavefunction should consist of the linear combination of the ground state configuration, having dominant weight, and of several non-degenerate configurations (such as excited configurations).

Thus, in order to encompass these severe limits of HF methods, in particular the description of electron correlation, several ab initio levels of theory have been developed. These levels of theory take the name of *Post-Hartree-Fock* (or correlation) methods. Two examples of Post-HF methods are the Configuration Interaction method and the Coupled Cluster method.

2.4. Configuration Interaction method

2.4.1. Fundamentals of the Configuration Interaction method

The oldest method to solve the issue of electron correlation is the so called *Configuration Interaction* (CI) method [1,14,24]. As its name suggests, the method relies on mixing one or more reference configurations (namely, the *reference wavefunction,* Ψ_0) with other "corrective" configurations accounting for the missing electron correlation. Basing on the reference wavefunction, CI may be *multi-reference* or *single-reference*. In the former case, Ψ_0 is multi-determinantal and consists of a linear combination of configuration determinants, whose weight coefficients are variationally optimized together with the atomic orbitals in each configuration. Thus, the reference wavefunction is said to be constructed with the Multi-Reference Self-Consistent Field (MCSCF) method [25,26]. In turn, the CI wavefunction constructed from the MCSCF reference wavefunction refers to the *Multi-Reference* CI (MRCI) method [27]. In contrast, for single-reference CI a mono-determinantal wavefunction Ψ_0 is used, usually corresponding to the RHF wavefunction. As this Thesis mostly regards systems represented by mono-determinantal wavefunctions, only the single-reference CI method will be considered. In this method, a number

of excited Slater determinants is linearly combined with the mono-determinantal reference wavefunction Ψ_0 [1,14,24]:

$$\Psi = |\Psi_0> + \Sigma_{ia}\, c_i^a |\Psi_i^a> + \frac{1}{4}\Sigma_{ijab} c_{ij}^{ab} \left|\Psi_{ij}^{ab}\right> + \cdots = |\Psi_0> + \Sigma_{ia}\, c_i^a \hat{a}_a^+ \hat{a}_i |\Psi_0> + \Sigma_{ijab}\, c_{ij}^{ab} \hat{a}_a^+ \hat{a}_i \hat{a}_b^+ \hat{a}_j \left|\Psi_0\right>, \quad (2.72)$$

where the summations run over the occupied spin-orbitals *i, j* and the virtual (unoccupied) ones *a, b*. The coefficients c_i^a, c_{ij}^{ab} are weight coefficients, chosen so to minimize the energy [14], whereas $\hat{a}^+$ and $\hat{a}$ stand for the creation and annihilation operators, respectively, from Second Quantization. In particular, in eq. (2.72), the first summation runs over the singly excited Slater determinant, whereas the second one over the doubly excited Slater determinant. In this way, all-order excitations can be summed up to the reference wavefunction. The CI method that accounts for all the *n*-ply excited functions is called the *Full Configuration Interaction* (FCI) method [1,14]. However, the huge number of possible excitations makes FCI practical only for few-electron systems. For this reason, the expansion (2.72) is truncated to the most significant excited configurations [1,14,24]. According to the Brillouin theorem, the sole singly excited configurations do not contribute to electron correlation [1,24], thus, the first approximation to FCI consists in truncating the CI chain (2.72) to the doubly excited determinants (CISD): CISD accounts for most of the correlation energy [24]. Further refinements rely on including the triply excited configurations (CISDT) and the quadruply excited configurations (CISDTQ) [24], but their inclusion is very expensive [1]. Furthermore, in the CI method, only the coefficients of the expansion (2.72) are optimized to minimize the energy of the system; in contrast, the spin-orbitals filling the Slater determinants are generated separately in a preceding HF calculation and are held fixed during the optimization of the configuration expansion [14]. Another limit of CI method is its lack of size-consistency, due to the truncation of the FCI chain, and the lack of compactness of its description of the electronic system: convergence of the CI wavefunction is slow, not only due to the large number of higher-order excitations, but also due to the linear parametrization in the CI model [14]. Furthermore, truncation of the FCI chain suppresses size-extensivity, so that the method no longer scales linearly with the number of electrons of the system [15,16].

2.5. Coupled Cluster method

2.5.1. Introduction

The Coupled Cluster Method (CC) was originally devised by Coester and Kummel in the late 1950s to deal with nuclear physics problems [28,29]. In spite of that, the application of such a theory to quantum chemical problems was formulated only during the subsequent decade, by Čizek and Paldus [29,30]. Nowadays, the Coupled Cluster Method is very popular to treat atoms and small molecules, due to its high accuracy [29], that makes it the golden standard of quantum chemical levels of theory. Electric properties of many atomic and molecular systems, for instance, can be investigated by means of Coupled Cluster Method, in particular, the static [31] and dynamic [32] polarizabilities and the induction [33] and dispersion [31] potentials. In particular, for the description of induction and dispersion energies, a key advantage of this level of theory relies on its size-consistency and size-extensivity [14].

In the next sections the Coupled Cluster Theory will be described in detail, together with three methods derived from this theory: the Coupled Cluster method including the single and double excitations, CCSD, Coupled Cluster method including the single, double and triple excitations, CCSDT, and the Coupled Cluster method including single, double and non-iterative triple excitations, CCSD(T). A further section will be devoted to describe one of the main applications of this theory, i.e. the Coupled Cluster Equation of Motion (CC-EOM) and the derived CCSD-EOM method, and the Coupled-Cluster-based Polarization Propagator, that can be used to calculate the dynamic polarizabilities of atoms and molecules [32]. It should be pointed out that, for the aims of the Thesis, only single-reference restricted Coupled Cluster level of theory built up on RHF reference wavefunctions, will be discussed.

2.5.2. Fundamentals of Coupled Cluster Theory

In CC the related wave function is given by an exponential *ansatz*, consisting of an exponential operator acting on a *zero-order wavefunction* Ψ_0 and converting it into the exact wave function Ψ [34].

$$\Psi = \exp(\hat{T})\,\Psi_0 \tag{2.73}$$

In the non-relativistic restricted frame, the zero-order wavefunction is a single Slater determinant, most often (and for the aims of the Thesis) a Hartree-Fock wavefunction [29], whereas the exponential operator is called the *Cluster Operator* [34]. Upon Taylor series expansion, the Cluster Operator yields the sum of all the possible excitation operators (or, more simply, *excitations*) and their products (coupling):

$$\exp(\hat{T}) = \hat{T}_1 + \hat{T}_2 + \dots \hat{T}_n + \hat{T}_1\hat{T}_2 + \cdots + \hat{T}_m\hat{T}_n + \frac{1}{2}\hat{T}_1^2 + \frac{1}{2}\hat{T}_n^2 + \cdots \tag{2.74}$$

The subscript of each excitation accounts for its order: $\hat{T}_1$ corresponds to a single excitation, $\hat{T}_2$ a double excitation,…, $\hat{T}_m$ and $\hat{T}_n$ the m-tuple and n-tuple excitations, respectively. The exponential operator (2.74) may be written in a more compact way as follows [30]:

$$\exp(\hat{T}) = \Sigma_{i=1}(\hat{T}_i + \hat{Q}_i), \tag{2.75}$$

where the $\hat{Q}_i$ operator is written in terms of the coupled $\hat{T}_i$ excitation operators. For instance,

$$\hat{Q}_1 = 0;\ \hat{Q}_2 = \frac{1}{2}\hat{T}_1^2;\ \hat{Q}_3 = \hat{T}_1\hat{T}_2 + \frac{1}{3!}\hat{T}_1^3;\ \hat{Q}_4 = \hat{T}_1\hat{T}_3 + \frac{1}{2}\hat{T}_1^2\hat{T}_2 + \frac{1}{4!}\hat{T}_1^4 + \frac{1}{2}\hat{T}_2^2; \dots\ . \tag{2.76}$$

Thence, the uncoupled $\hat{T}_i$ operators are termed the *connected terms*; in contrast, the $\hat{Q}_i$ operators are termed the *disconnected terms* [30]. Disconnected terms represents a key advantage of CC over CI method, as those terms ensures size-extensivity and size-consistency [15].

In turn, the excitation operators $\hat{T}_i$ are written in terms of creation and annihilation operators and of *Cluster amplitudes*, *t*, [29]; the first two excitations for instance are defined as follows [34]:

$$\begin{aligned} \hat{T}_1 &= \Sigma_{ia} t_i^a \hat{a}^+ i \\ \hat{T}_2 &= \frac{1}{(2!)^2}\Sigma_{ijab} t_{ij}^{ab} \hat{a}^+ \hat{b}^+ ji \end{aligned} \tag{2.77}$$

The amplitudes, parametrizing the exponential ansatz, are unknown and should be determined in order to achieve the CC wave function and the corresponding energy.

The approach to determine the energy and the amplitudes is called the *coupled-cluster approach* [29]. In this approach one has first to rewrite the Schrödinger Equation by inserting the exponential ansatz:

$$\hat{\mathcal{H}} \exp(\hat{T}) |\Psi_0> = E \exp(\hat{T}) |\Psi_0>\ . \tag{2.78}$$

Then (2.78) is multiplied by $\exp(-\hat{T})$ on the left, to eliminate the exponential operator on the right-hand side. Then the left-hand side should be projected onto the reference wave function and onto all the excited determinants Φ generated by the action of $\hat{T}$ on the reference wave function. We thus obtain two equations:

$$< \Psi_0| \exp\left(-\hat{T}\right) \hat{\mathcal{H}} \exp(\hat{T})|\Psi_0 > = E \tag{2.79}$$

$$< \Phi| \exp\left(-\hat{T}\right) \hat{\mathcal{H}} \exp(\hat{T})|\Psi_0 > = 0, \tag{2.80}$$

where eq. (2.79) returns the energy of the system, while eq. (2.80) returns the Cluster amplitudes. Those two equations are often rewritten as [29]

$$< \Psi_0 \left| \hat{\mathcal{H}}_N \exp\left(\hat{T}\right) \right| \Psi_0 > = \Delta E \tag{2.81}$$

$$< \Phi| \hat{\mathcal{H}}_N \exp(\hat{T})|\Psi_0 > = 0 \tag{2.82}$$

where ΔE refers to the correlation energy,

$$\Delta E = E - < \Psi_0 \left| \hat{\mathcal{H}} \right| \Psi_0 > \tag{2.83}$$

$\hat{\mathcal{H}}_N$ refers to the normal-ordered Hamiltonian (i.e. all the creation operators stand on the right with respect to the related annihilation operators) obtained by subtracting the reference energy $< \Psi_0 \left| \hat{\mathcal{H}} \right| \Psi_0 >$ from $\hat{\mathcal{H}}$. We can thus notice a very important feature of Coupled Cluster theory: it accounts for *dynamic correlation*.

The drawback of this theory relies, again, on the two equations yielding its key-solutions, (2.79) and (2.80): the exponential ansatz makes such equations non-linear and hence remarkably complex to solve. It is then apparent that truncation should be applied to the excitations, as such as to find a compromise between high accuracy of the results and reasonable computational cost.

2.5.3. CCSD

Given the HF wave function to be a good zero-order approximation of the true wave function Ψ (this is usually the case for ground state closed-shell systems), the contribution of double excitations is estimated to amount to 94-96% of the correlation energy [30], while singles and triples contribute roughly 1-2% [35]. Furthermore, the truncation of the excitations solely to the singles yields no significant improvement to the reference wave function, as a consequence of the

Brillouin Theorem [30,34]. These statements lead to consider the inclusion of the interacting singles and doubles in the Cluster operator as the first reasonable approximation of the exact wave function: such a method is called CCSD [35,36]. The truncation of the excitations to the singles and doubles is physically justified, as the sum of those excitations (operators) spans the space of functions interacting with the reference wave function Ψ_0 through the two-body Hamiltonian [37].

In order to achieve the Cluster equations for the CCSD, it is simply necessary to substitute $\hat{T} = \hat{T}_1 + \hat{T}_2$ into the eqs. (2.81-82). This returns the following equations:

$$< \Psi_0 \left| \hat{\mathcal{H}}_N \left(\hat{T}_1 + \hat{T}_2 + \frac{1}{2}\hat{T}_1^2 \right) \right| \Psi_0 > = \Delta E \tag{2.84}$$

$$< \Phi_S \left| \hat{\mathcal{H}}_N \left(1 + \hat{T}_1 + \hat{T}_2 + \frac{1}{2}\hat{T}_1^2 + \hat{T}_1\hat{T}_2 + \frac{1}{3!}\hat{T}_1^3 \right) \right| \Psi_0 > = 0 \tag{2.85}$$

$$< \Phi_D \left| \hat{\mathcal{H}}_N \left(1 + \hat{T}_1 + \hat{T}_2 + \frac{1}{2}\hat{T}_1^2 + \hat{T}_1\hat{T}_2 + \frac{1}{3!}\hat{T}_1^3 + \frac{1}{2}\hat{T}_1^2\hat{T}_2 + \frac{1}{4!}\hat{T}_1^4 + \frac{1}{2}\hat{T}_2^2 \right) \right| \Psi_0 > = 0 \tag{2.86}$$

Notice that the subscripts *S* and *D* mean the singly- and the doubly-excited determinants respectively. In order to easily distinguish them, in eqs. (2.84-86) connected operators were grouped and likewise the disconnected ones. This distinction is useful to notice a key advantage of CCSD, ensuring its accuracy in spite of the truncation of the CC chain to the second-order excitations: through the disconnected terms, in fact, it is possible to partially account for higher-order excitations, such as triples ($\hat{T}_1\hat{T}_2, \hat{T}_1^3$) and quadruples ($\hat{T}_1^2\hat{T}_2, \hat{T}_1^4, \hat{T}_2^2$) [38]. However, it should also be noticed that the higher-order excitation coefficients are simply obtained as products of lower-order excitations coefficients [38]. For quadruple excitations, this does not represent a serious problem, as the disconnected part of these excitations provides a larger contribution to them than the connected part [38]. In contrast, accounting for the disconnected part of the triple excitations is not sufficient to accurately treat them, as, in this latter case, the connected contribution is dominant [30,35,38]. Accurate modelling of triple excitations is particularly crucial when the system under study has strong electron correlations (e.g. many-electron atoms, transition metal elements) or even when highly accurate results are needed (about 350 cm^{-1} "chemical accuracy") [35]. Thus, if high accuracies and adequate treatment of electron correlation are required, the connected triple excitation cannot be neglected in the truncated CC chain.

2.5.4. Higher-order corrections: CCSDT

The most obvious way to account for the important connected $\hat{T}_3$ excitation relies on truncating expansion (2.74) to the correspondingly higher level [35]. Thence, the CCSDT method is obtained. For the former, the equations for the energy and the Cluster amplitudes yield with

$$< \Psi_0 \left| \widehat{\mathcal{H}}_N \left(\hat{T}_1 + \hat{T}_2 + \hat{T}_3 + \frac{1}{2}\widehat{T_1^2} + \hat{T}_1\hat{T}_2 + \frac{1}{3!}\hat{T}_1^3 \right) \right| \Psi_0 > = \Delta E \tag{2.87}$$

$$< \Phi_S \left| \widehat{\mathcal{H}}_N \left(1 + \hat{T}_1 + \hat{T}_2 + \hat{T}_3 + \frac{1}{2}\widehat{T_1^2} + \hat{T}_1\hat{T}_2 + \frac{1}{3!}\hat{T}_1^3 \right) \right| \Psi_0 > = 0 \tag{2.88}$$

$$< \Phi_D \left| \widehat{\mathcal{H}}_N \left(1 + \hat{T}_1 + \hat{T}_2 + \hat{T}_3 + \frac{1}{2}\widehat{T_1^2} + \hat{T}_1\hat{T}_2 + \frac{1}{3!}\hat{T}_1^3 + \hat{T}_1\hat{T}_3 + \frac{1}{2}\hat{T}_1^2\hat{T}_2 + \frac{1}{4}\hat{T}_1^4 + \frac{1}{2}\hat{T}_2^2 \right) \right| \Psi_0 > = 0 \tag{2.89}$$

$$< \Phi_T \left| \widehat{\mathcal{H}}_N \left(\hat{T}_2 + \hat{T}_3 + \hat{T}_1\hat{T}_2 + \hat{T}_1\hat{T}_3 + \frac{1}{2}\hat{T}_1^2\hat{T}_2 + \frac{1}{2}\hat{T}_1\hat{T}_2^2 + \frac{1}{2}\hat{T}_2^2 + \frac{1}{2}\hat{T}_1^2\hat{T}_3 + \frac{1}{3!}\hat{T}_1^3\hat{T}_2 \right) \right| \Psi_0 > = 0 \tag{2.90}$$

Here, the subscript *T* means the triple excitations. As it can be noticed from eqs. (2.87-90), CCSDT includes the triple excitations, both connected and disconnected, and higher-order corrections, by means of their disconnected parts. The inclusion of the connected triples has proven crucial in ensuring highly accurate description of atoms and molecules [30,35,38], however, it has a severe limit: CCSDT is computationally very demanding [29,39]; indeed, while CCSD scales as M^6 (where M refers to the number of occupied and unoccupied orbitals accounted for in the calculation), CCSDT scales as M^8 [35] and this increase in computational costs limits its applicability to small systems.

2.5.5. CCSD(T)

A solution to include the connected contribution to the triples into the CC calculation without the high computational costs of CCSDT relies on treating it in a non-iterative way. CCSD(T) method successfully addresses this issue. First proposed by Raghavachari *et al.* [40] in 1989, CCSD(T) corrects the converged CCSD wave function with the perturbative treatment of the triple excitations [39].

A "friendly" way to devise the CCSD(T) equations was proposed by Stanton [39] and relies on choosing the CCSD energy as the "zero-order" quantity, rather than the HF analog. Then, the

Cluster equations for CCSD, (2.84-86) are used to build up the matrix representation of $\widehat{\mathcal{H}}_N \exp(\hat{T})$, here abbreviated as $\overline{\widehat{\mathcal{H}}}$:

$$\overline{\widehat{\mathcal{H}}} = \begin{bmatrix} E_{CCSD} & \overline{\mathcal{H}}_{0\Phi} & \overline{\mathcal{H}}_{0X} \\ 0 & \overline{\mathcal{H}}_{\Phi\Phi} & \overline{\mathcal{H}}_{\Phi X} \\ \overline{\mathcal{H}}_{0X} & \overline{\mathcal{H}}_{X\Phi} & \overline{\mathcal{H}}_{XX} \end{bmatrix}, \tag{2.91}$$

where

$$\overline{\mathcal{H}}_{0\Phi} = < \Phi | \widehat{\mathcal{H}}_N \exp(\hat{T}_{CCSD}) | \Psi_0 >, \tag{2.92}$$

in turn, corresponding to the equations for the CCSD Cluster amplitudes (2.85-86): in fact, here, Φ ranges the singly and doubly excited wavefunctions, while, analogously to the previous sections, Ψ_0 refers to the reference function (in Stanton's approach called the *zero-order wavefunction* [39]). X ("Chi"), on the other hand, ranges the excited wavefunctions not included in the space g spanned by the reference function and the singles and doubles, i.e. $\{\Psi_0\} \cup \{\Phi\} \equiv g$. In Stanton's approach, all $\overline{\mathcal{H}}_{gg}$ terms are deemed *zero-order terms*; the remaining terms of eq. (2.91) are, thus, classified according to the lowest non-vanishing order of the correlation [39]. Notice that, in this convention, the single excitation $\hat{T}_1$ is considered a second-order perturbation, whereas the double excitation $\hat{T}_2$ is considered a first-order perturbation. The CCSD energy is achieved upon diagonalizing (2.91) in the g basis. As $\overline{\widehat{\mathcal{H}}}$ instead of $\widehat{\mathcal{H}}$ is used, it is convenient to briefly define the Ψ_0 and Φ states simply as zero-order states $|0>$. In this framework, (2.91) can be decomposed into an unperturbed term and several perturbed terms:

$$\overline{\widehat{\mathcal{H}}} = \overline{\widehat{\mathcal{H}}}^{(0)} + \overline{\widehat{\mathcal{H}}}^{(1)} + \overline{\widehat{\mathcal{H}}}^{(2)} + \cdots \tag{2.93}$$

Accordingly, for CCSD(T), the correlation energy can be written as

$$\Delta E = \Delta E^{(3)} + \Delta E^{(4)}, \tag{2.94}$$

where the first non-vanishing term is

$$\Delta E^{(3)} = \frac{\left\langle \mathrm{X}\left|\widehat{\overline{\mathcal{H}}}^{(1)}\right|0\right\rangle\left\langle 0\left|\widehat{\overline{\mathcal{H}}}^{(2)}\right|\mathrm{X}\right\rangle}{<\mathrm{X}|(\widehat{\mathcal{H}}^{(o)}-<0|\widehat{\mathcal{H}}^{(o)}|0>)|\mathrm{X}>} \tag{2.95}$$

Notice that the second-order correction vanishes, as $< \mathrm{X}\left|\widehat{\overline{\mathcal{H}}}\right| 0 >$ requires at least a connected triple excitation and no such terms are present in the first-order bare electronic Hamiltonian [39]. Upon specifying the singly, doubly and triply excited wavefunctions, eq. (2.95) turns into

$$\Delta E^{(3)} = \frac{<\Phi_S|0><\Phi_S|\widehat{\overline{\mathcal{H}}}^{(1)}|\Phi_T><\Phi_T|\widehat{\overline{\mathcal{H}}}^{(2)}|0>}{<\Phi_\mathrm{T}|(\widehat{\mathcal{H}}^{(o)}-<0|\widehat{\mathcal{H}}^{(o)}|0>)|\Phi_\mathrm{T}>} + \frac{<\Phi_D|0><\Phi_D|\widehat{\overline{\mathcal{H}}}^{(1)}|\Phi_T><\Phi_T|\widehat{\overline{\mathcal{H}}}^{(2)}|0>}{<\Phi_\mathrm{T}|(\widehat{\mathcal{H}}^{(o)}-<0|\widehat{\mathcal{H}}^{(o)}|0>)|\Phi_\mathrm{T}>} \tag{2.96}$$

Eq. (2.96) clearly shows that the third-order correction to the correlation energy accounts for the main contribution to the triple excitations, i.e. the connected triples, but, on the other hand, does not include the higher-order disconnected terms where $\hat{T}_3$ couples with the lower-order excitation operators. However, the perturbative treatment of the triple excitation allows for achieving results that are very close to CCSDT analogs [39], but at a smaller computational cost (M^7). This capability by CCSD(T) method to ensure accurate results at a reasonable computational cost, has made this method *the golden standard* of quantum chemistry for small-size systems [41].

2.6. Coupled Cluster method for electric properties

2.6.1. Static properties

The long-range approximation introduced above implies that electrostatic, induction and dispersion interaction components (see eqs. (2.35-39)) can be described in terms of the related properties of the individual species. Thus, ab initio methods for the calculation of molecular properties are an important aspect of the theory of intermolecular forces [1]. In fact, several properties, such as multipole moments, can be expressed not only as expectation values, but also as energy derivatives [1,42]. The link between the expectation value and the energy derivative depiction relies on the Hellmann-Feynman theorem [43,44]. The theorem states that if the Hamiltonian $\widehat{\mathcal{H}}(\lambda)$ depends on some parameter λ, and $\psi(\lambda)$ is a normalized eigenfunction whose eigenvalue is $E(\lambda)$, then

$$\partial_\lambda E = \partial_\lambda < \psi(\lambda)\left|\widehat{\mathcal{H}}\right|\psi(\lambda) > = < \psi\left|\partial_\lambda\widehat{\mathcal{H}}\right|\psi > \tag{2.97}$$

According to the long-range approximation, properties such as polarizabilities arise as the effect of a perturbation of the form $\lambda\hat{Q}$, where λ is a parameter, such as the strength of the external electric field or of its gradient, whereas $\hat{Q}$ is an operator, such as a multipole moment. Thus, according to the Hellmann-Feynman theorem, the derivative of the energy with respect to the given parameter λ can be expressed as

$$\partial_\lambda E = < \psi | \partial_\lambda \hat{\mathcal{H}} | \psi > = < \psi | \hat{Q} | \psi > , \tag{2.98}$$

Provided $\lambda \to 0$ and the property can be expressed either as an expectation value or as an energy derivative.

The Hellmann-Feynman theorem can be used to calculate properties such as polarizability [1]: in fact, the static polarizability tensor $\alpha_{\alpha\beta}$ is defined as the second derivative of energy with respect to the external applied uniform electric field $\boldsymbol{F}$,

$$\frac{\partial^2 E}{\partial F_\alpha \partial F_\beta} |_{F=0} \tag{2.99}$$

The total Hamiltonian of a system interacting with an external electric field may be written as a sum of several perturbations of the kind $\lambda_i \hat{Q}_i$ [1]:

$$\hat{\mathcal{H}} = \hat{\mathcal{H}}^{(0)} + \lambda_1 \hat{Q}_1 + \lambda_2 \hat{Q}_2 + \cdots \tag{2.100}$$

Thus, using the theorem and upon differentiating eq. (2.98), one may get any second derivative of the energy:

$$\frac{\partial^2 E}{\partial \lambda_1 \partial \lambda_2} = \partial_{\lambda_2} < \psi | \partial_{\lambda_1} \hat{\mathcal{H}} | \psi > = \partial_{\lambda_2} < \psi | \hat{Q}_1 | \psi > \tag{2.101}$$

This approach is called the *finite- field* (FF) approach [1,42,45], and provides a practical way to calculate polarizabilities: the wavefunction ψ is computed in the presence of the uniform electric field F_β, while the expectation value for the dipole moment, $< \psi | \hat{\mu}_\alpha | \psi > = \mu_\alpha$, is evaluated through the Hellmann-Feynman theorem. In general, the finite-field approach can be used whenever one wants to calculate a property that can be expressed as a derivative of energy or another expectation value with respect to a small perturbation. Many quantum chemistry programs, such as MOLPRO [46], can use specific tensor fields to define higher-order quadrupole and octupole polarizabilities. In particular, MOLPRO [46] carries out a single numerical differentiation

of the multipole moment $<\psi|\hat{Q}|\psi>$ for several values of the field, in order to achieve the multipole polarizabilities. Moreover, more precise results can be attained by computing the extended field dependence and making a polynomial fit to it.

2.6.2. Polarization Propagator

As seen in Section 2.1, the dispersion interaction depends on the dynamic properties of the system, such as dynamic polarizabilities. Thus, when dispersion interaction terms, such as dispersion coefficients, are needed, the knowledge of static properties is not sufficient, but, in contrast, dynamic response properties such as excitation energies and transition multipole moments (see eq. (2.25)) should be known in order to evaluate dynamic polarizabilities and, in turn, dispersion coefficients through, e.g., Casimir-Polder integrals by eqs. (2.53-54). In the framework of Coupled Cluster method, this can be done by introducing a time-dependent perturbation into the system Hamiltonian [47]. Coupled-Cluster-Equation-of-Motion method [34,47,48] addresses this issue to calculate excitation energies and, more generally, response properties.

In this method, two Schrödinger-equation eigenstates are considered at the same time: an initial state Ψ_i and a target state Ψ_k.

$$\begin{aligned} \widehat{\mathcal{H}}\Psi_i &= E_i\Psi_i \\ \widehat{\mathcal{H}}\Psi_k &= E_k\Psi_k \end{aligned} \tag{2.102}$$

The method is targeted to achieve the energy difference between the two states, $E_{ik} = E_k - E_i$.

Upon using the normal-ordered Hamiltonian $\widehat{\mathcal{H}}_N$, eqs. (2.102) become

$$\widehat{\mathcal{H}}_N\Psi_i = \Delta E_i\Psi_i \tag{2.103}$$

$$\widehat{\mathcal{H}}_N\Psi_k = \Delta E_k\Psi_k, \tag{2.104}$$

where ΔE_i and ΔE_k are respectively the correlation energies for the initial and target states. As both subtract the same quantity, i.e. the reference energy, then the energy difference between the two states corresponds to the difference between the related correlation energies. In this framework, the initial state Ψ_i is given by the Cluster operator acting on the reference state Ψ_0 (eq. (2.73)), while the target state Ψ_k is given by a linear operator $\hat{R}_k$ acting on the initial state Ψ_i. The linear excitation operator $\hat{R}_k$ is, in turn, defined as [34]

$$\hat{R}_k = r_0 + \Sigma_{i,a} r_i^a \{\hat{a}^+ i\} + \Sigma_{i<j,a<b} r_{ij}^{ab} \{\hat{a}^+ i \hat{b}^+ j\} + \cdots \quad (2.105)$$

The most widespread variant of the CC-EOM method is the CCSD-EOM, where the Cluster operator is truncated to the singles and the doubles [49]. The computational cost of CCSD-EOM is comparable to CCSD's [29].

However, the main issue of the CC-EOM approach arises because of the non-hermiticity of the Hamiltonian used. Such a problem paves the way for alternative methods, developed in the frame of the abovementioned approach. An alternative method solving the non-hermiticity problem is the Polarization Propagator approach by Moszinski *et al.* [50]. The Polarization Propagator treats electric properties involving excitations, such as dynamic polarizabilities, as linear response functions [32,50]. The imposition of the hermiticity condition ensures the time reversal symmetry for the electric properties to be respected, together with the consequent constraint for them to be even functions of the frequency [50].

Given a non-degenerate *n*-electron Hamiltonian $\widehat{\mathcal{H}}$, the related Polarization Propagator, $\ll \hat{A}, \hat{B} \gg_\omega$, is defined as [32,50]

$$\ll \hat{A}, \hat{B} \gg_\omega = -<\Psi_i|\hat{B}\left(\frac{\hat{Q}}{\widehat{\mathcal{H}}-E_i+\omega}\right)\hat{A}\Psi_i> -<\Psi_i|\hat{A}\left(\frac{\hat{Q}}{\widehat{\mathcal{H}}-E_i-\omega}\right)\hat{B}\Psi_i> \quad (2.106)$$

For the initial state Ψ_i the ground state has been taken into account, whereas $\hat{Q}$ represents the projection onto the space of all the excited states of the system; E_i is defined as the eigenvalue of the Ground State Ψ_i. Eq. (2.106) thus describes the system's linear response to a perturbation ($\hat{A}$ or $\hat{B}$) that oscillates at a frequency ω. The operators $\hat{A}$ and $\hat{B}$ can be assumed to be Hermitian.

In fact, the propagator exhibits the Hermitian symmetry

$$\ll \hat{A}, \hat{B} \gg_\omega^* = \ll \hat{A}, \hat{B} \gg_{-\omega^*} \quad (2.107)$$

if and only if *A* and *B* are Hermitian. If the frequency is a pure complex quantity, then $\omega^* = -\omega$ and thus the Polarization Propagator is real for each *A* and *B*. This implies that the second term in (2.106) does not need to be separately computed, as it is just the *generalized complex conjugate* (g.c.c.) of the first term.

In addition, if the frequency is real, then the Polarization Propagator has the time-reversal symmetry ($\ll \hat{A}, \hat{B} \gg_{\omega} = \ll \hat{A}, \hat{B} \gg_{-\omega}$) and by Schwartz's Reflection Theorem, such a condition can be extended to the case when the frequency is complex.

For the first-order wave function we consider the function $\Psi^{(1)}(\omega)$ that satisfies the equation [32]:

$$\left(\hat{\mathcal{H}} - E_i + \omega\right)\Psi^{(1)}(\omega) = -\hat{A}\Psi_i \tag{2.108}$$

By means of (2.108) the Polarization Propagator can be expressed as [32,50]

$$\ll \hat{A}, \hat{B} \gg_{\omega} = < \Psi_i | \left(\hat{B} - \widehat{\overline{B}}\right) \Psi^{(1)}(\omega) > + g.c.c., \tag{2.109}$$

with $\widehat{\overline{B}} = < \Psi_i | \hat{B} \Psi_i >$.

We now define the Coupled Cluster Ground State wave function in the renormalized form [50]

$$\Psi_i = \frac{\exp(\hat{T})\Psi_0}{<\exp(\hat{T})\Psi_0 | \exp(\hat{T})\Psi_0>^{\frac{1}{2}}}, \tag{2.110}$$

while the first-order wave function is defined accordingly [32,50],

$$\Psi^{(1)}(\omega) = \frac{\Omega(\omega)\exp(\hat{T})\Psi_0}{<\exp(\hat{T})\Psi_0 | \exp(\hat{T})\Psi_0>^{\frac{1}{2}}} = \left[\Omega_0(\omega) + \widehat{\Omega}(\omega)\right]\Psi_i. \tag{2.111}$$

$\Omega_0(\omega)$ is a number, while $\widehat{\Omega}(\omega)$ is an excitation operator of the same form as $\hat{T}$. By specifying the wave functions in (2.108), one achieves [32]

$$< \delta T | \left[\exp\left(\hat{T}\right) \hat{\mathcal{H}} \exp\left(\hat{T}\right), \widehat{\Omega}(\omega)\right] + \omega\widehat{\Omega} + \exp\left(\hat{T}\right) \hat{A} \exp\left(\hat{T}\right) > = 0, \tag{2.112}$$

with δT meaning an arbitrary variation of the operator; the square-bracketed term constitutes the commutator. In agreement with Refs. [32] and [50] the scalar products have been expressed in (2.112) in the short-hand form

$$< X | Y > = < X\Psi_0 | \Psi_0 Y > \tag{2.113}$$

If the time-dependent perturbation is periodic with a period ωt, then the $\hat{T}$ operator can be written in terms of the $\widehat{\Omega}$ operator and finding them is thus easier. When such operators are known, the Polarization Propagator can be computed from the expression [32,50]

$$\ll \hat{A}; \hat{B} \gg_{\omega} = \frac{<\exp(\hat{T})|\hat{B}\hat{Q}\hat{\Omega}(\omega)\exp(\hat{T})>}{<\exp(\hat{T})|\exp(\hat{T})>} + g.c.c. \tag{2.114}$$

Upon expanding the exponential and the denominator, eq. (2.114) generates several terms that are not *connected* (i.e. cannot be constructed from a finite number of multiple commutators containing the operators in play). However, if $\hat{T}, \hat{B}, \hat{\Omega}$ can be expressed in such a way, then the disconnected terms vanish. Thus, to enforce the constraint on the connectivity of eq. (2.114), the $\hat{S}$ excitation operator is introduced [32,41,50],

$$\exp(\hat{S})\,\Psi_0 = \frac{\exp(\hat{T}^+)\exp(\hat{T})\Psi_0}{<\exp(\hat{T})|\exp(\hat{T})>} \tag{2.115}$$

The main advantage coming from this new *ansatz* relies, in fact, on the connectivity property of the $\hat{S}$ operator: this allows the Polarization Propagator to be size-extensive [41].

When only the single and double excitations are taken into account ($\hat{T} = \hat{T}_1 + \hat{T}_2$), then $\hat{S}$ becomes [50]

$$\hat{S} = \hat{T} + \hat{\hat{P}}_1\left(\left[\hat{T}_1^+, \hat{T}_2\right]\right) + o(\hat{T}^3), \tag{2.116}$$

where the superoperator $\hat{\hat{P}}_n(X)$ appears, projecting the *n*-tuple excitation part of the operator *X* [32].

By means of eq. (2.115), eq. (2.116) can be rewritten in a form where all the terms are explicitly expressed as commutator products of operators [32,50]:

$$\ll \hat{A}; \hat{B} \gg_{\omega} = < \exp(-\hat{S})\exp(\hat{T}^+)\,\hat{B}\exp(-\hat{T}^+)\exp(\hat{S})|\hat{\hat{P}}(\left(\exp(\hat{S}^+)\,\hat{\Omega}(\omega)\exp(-\hat{S}^+)\right) > + g.c.c. \tag{2.117}$$

It should be noted that the expansion of eq. (2.117) is finite, but yields multiple commutators up to quite high order: for instance, the CCSD polarization propagator may contain up to seven excitation operators ($\hat{T}$ or $\hat{S}$). The situation gets even more complicated when higher cluster excitations are included (e.g. CCSDT) [32]. This makes CCSD polarization propagator the most reasonable compromise between accuracy and computational cost and for this reason we will focus on it.

At the CCSD level, the *n*-tuple excitation operator $\hat{S}_n$ yields the following solution:

$$\hat{S}_n = \hat{T}_n - \frac{1}{n}\Sigma_{m=1}^{4}\frac{1}{m!}\hat{\hat{P}}_n\left(\left[\hat{S}_1 + 2\hat{S}_2, \hat{U}\right]_m + \left[\hat{T}_1^+ + 2\hat{T}_2^+, \hat{T}\right]_m\right), \tag{2.118}$$

where $\left[\hat{X}, \hat{Y}\right]_m$ defines a m-times nested commutator (e.g. $\left[\hat{X}, \hat{Y}\right]_{m+1} = [\left[\hat{X}, \hat{Y}\right]_m, \hat{Y}]$], whereas $\hat{U}$ is a similarly-transformed de-excitation operator [50],

$$\hat{U} = \exp(-\hat{T})\,\hat{T}^+\exp(\hat{T}) = \hat{T}^+ + \Sigma_{m=1}^{4}\frac{1}{m!}\left[\hat{T}^+, \hat{T}\right]_m \tag{2.119}$$

Upon solving eq. (2.118) iteratively, we can obtain $\hat{S}_n$ as an expansion in powers of $\hat{T}$. In this case the single and double excitations in $\hat{S}$ read as [32]

$$\begin{aligned}\hat{S}_1 &= \hat{T}_1 + \hat{\hat{P}}_1\left(\left[\hat{T}_1^+, \hat{T}_2\right] + \left[\left[\hat{T}_2^+, \hat{T}_2\right], \hat{T}_1\right] + \frac{1}{2}\left[\left[\hat{T}_1^+, \hat{T}_1\right], \hat{T}_1\right]\right)\\ \hat{S}_2 &= \hat{T}_2 + \hat{\hat{P}}_2\left(\frac{1}{2}\left[\left[\hat{T}_2^+, \hat{T}_2\right], \hat{T}_2\right] + \left[\left[\hat{T}_1^+, \hat{T}_2\right], \hat{T}_1\right]\right)\end{aligned} \tag{2.120}$$

We now have to gauge the importance of the excitation terms $\hat{T}$, $\hat{S}$ and $\hat{\Omega}$ appearing in eq. (2.117). This is actually done by applying a Møller-Plesset expansion to them. Upon expanding the operators up to the third order in the Møller-Plesset operator, eq. (2.117) for the CCSD polarization propagator approximates to [32]

$$\ll \hat{A}, \hat{B} \gg_\omega = < \hat{B}\hat{\Omega}_1(\omega) > + < \hat{S}|\left[\hat{B}, \hat{\Omega}(\omega)\right] > + < \left[\hat{B}, \hat{S}_2\right]|\hat{\Omega}_1(\omega) > + < [\left[\hat{T}^+, \hat{B}\right], \hat{S}]|\hat{\Omega}(\omega) > + g.c.c., \tag{2.121}$$

where

$$\hat{S} = \hat{T} + \hat{\hat{P}}_1\left(\left[\hat{T}_1^+, \hat{T}_2\right]\right) + \frac{1}{2}\widehat{\hat{P}_2}\left(\left[\hat{T}_2^+, \hat{T}_2\right], \hat{T}_2\right]\right) \tag{2.122}$$

This is usually called the CCSD(3) polarization propagator. We may derive higher-order approximations to eq. (2.117), but this would not be very useful: in fact, CCSD theory is correct through the second order in Møller-Plesset operator, therefore higher-order corrections beyond the third one would not provide significant refinements [32].

2.6.3. Alternatives

Among molecular approaches, Coupled Cluster not only offers the most accurate treatment of electron correlation [34], but is also suitable for monomeric calculations of properties usually investigated by means of atomic approaches, such as response properties, with high accuracies. These features make CC the ideal molecular approach to investigate the long-range tail of the

interaction potential and, at the same time, the global interaction potential. Thus, when dealing with long-range interactions by means of molecular approaches, CC, when applicable, is a method of the first choice.

As an example of cheaper but less accurate approach to investigate long-range interactions, we can mention Møller-Plesset perturbation theory [51], MP*n* (where "*n*" means the perturbation order). At this level of theory, the Hartree-Fock Hamiltonian is taken as the zero-order Hamiltonian, while electron correlation is treated as a perturbation. For a closed-shell system, the zero-order wavefunction or reference wavefunction is supplied by the Slater Determinant, while the zero-order energy is the sum of the occupied orbital energies. At the first order, the energy is given by the expectation value of the total Hamiltonian for the HF wavefunction. Electron correlations are treated from the second order. However, MP*n* method presents several drawbacks: first, accounting for higher-order perturbation terms does not ensure a better convergence or more accurate results [52]. By contrast, the computational cost increases as the perturbation order increases [1]. Another general deficiency, which is common to all Many-Body Perturbation Theory (MBPT) implementations, regards the description of valence-valence interactions, which is usually not accurate [53]. Furthermore, MBPT methods to any order are size-extensive, but generally not size-consistent.

The reason why we paid attention to MP*n* above is that it can be considered as the simplest implementation of MBPT, which, in turn, is also widely used as a building block for several more complex atomic approaches (see, for instance, Ref. [54]). In particular, in the specific case of diatomic systems of interest in the Thesis context, monomeric approaches reduce to atomic ones. Techniques for atomic electronic structure calculations are much more diverse and, generally, accurate compared to those available for molecular ones, due to high symmetry.

An atomic approach that accurately describes core-core, core-valence and valence-valence interactions combines the Configuration-Interaction method [24] CI and Many-Body Perturbation theory MBPT (CI-MBPT). The former, in fact, accurately accounts for the valence-valence correlation, while the latter provides a relatively accurate description of core-core and core-valence correlations [53,54]. The method works by dividing the system electrons in two group: core and valence. For the former, the effective Hamiltonian is constructed using the MBPT method for the interaction of the valence electrons with the core, while CI is used to treat the valence electrons

[3,53,54]. Relativistic effects can be explicitly accounted for upon replacing the Hartree-Fock Hamiltonian with the Dirac-Fock Hamiltonian [53,55] (see Section 2.7.1): in this latter case, CI-MBPT has proven to be particularly accurate [3,55]. However, this method presents several limits: first, the convergence of MBPT requires the core and valence states to be well separated in energy [53]; second, it becomes impracticable when the number of valence electrons becomes larger than five [54,55]: in this case, in fact, the CI space becomes too large to saturate the CI part of the method, whereas such a large number of valence electrons makes the effective Hamiltonian no longer accurately represented by a two-electron operator; three-particle MBPT corrections [53] should be included, thus leading to the Hamiltonian that is much less sparse than for the pure CI [54]. On the side of intermolecular interactions, as an atomic approach, CI+MBPT performs with reasonable accuracy on the calculation of response static (e.g. static polarizabilities) and dynamic properties (e.g. dynamic polarizabilities, oscillator strengths) for atoms with a small valence space (see, for instance, Ref. [3]), such as alkaline earth elements and, generally, divalent atoms [3], due to the optimal treatment of electron correlation. However, being a method based on perturbation theory, it is not suitable for evaluations of the global interaction potentials between two species.

A key advantage of CI-MBPT method is its flexibility, as it can embody empirical corrections to increase accuracy: core-core and core-valence correlations can be corrected upon introducing parameters based on experimental data. Such empirical parameters replace the higher-order perturbative corrections at a lower computational cost. Moreover, they ensure an accurate description of the low-energy levels [3]. Corrections to valence-valence correlations can be accounted for by embodying summations of tabulated experimental energy levels [3].

2.7. Coupled Cluster computational strategies

2.7.1. Scalar relativistic corrections

2.7.1.1. Introduction

A plethora of chemical systems do exist which requires a relativistic treatment, for instance transition metals and heavy and super-heavy elements [56-59]. Before starting considering the formalism of relativistic quantum chemistry, it is necessary to understand how relativity affects the electronic structure of such elements.

The relativistic mass increase for a particle is classically expressed as

$$m = m_0/\sqrt{1-(^v/_c)^2}\,, \tag{2.123}$$

where m_0 and $\boldsymbol{v}$ are, respectively, the rest mass and the velocity of the particle. In a relatively heavy atom, where indeed electrons are affected by relativity, the large atomic number *Z* causes the electrons to move faster and the related mass increase leads the Bohr radius of the Hydrogen-like s and $p_{1/2}$ orbitals to decrease with respect to its non-relativistic counterpart, a_{0B}, as [60]

$$a_B = \frac{h^2}{mc^2} = a_{0B}\sqrt{1-(^v/_c)^2} \tag{2.124}$$

This effect is called the *direct* relativistic effect and affects the s and p valence shells and the innermost core electrons [60,61]. The consequence of this effect results in the *contraction* of the related orbitals, as seen from eq. (2.124). As a result of their contraction, the s and p shells *screen* the nucleus more effectively, thus decreasing the Coulombic attraction on the outer d and f shells. These, in turn, expand, as a consequence of the nucleus screening and destabilize energetically [60-61]. This phenomenon, provoked by the direct relativistic effect on the outer s and p electrons, is called the *indirect* relativistic effect [61].

A full relativistic treatment of atomic systems relies on the Dirac Equation [56-58], whose corresponding Hamiltonian, $\hat{\mathcal{H}}_D$, is a *4x4* matrix, accounting for the Coulombic interaction of the electrons with an extended nucleus (*V)* and the interaction of the particles spin and momenta $\hat{\boldsymbol{\sigma}} \cdot \hat{\boldsymbol{p}}$:

$$\hat{\mathcal{H}}_D = \begin{Vmatrix} V & c\hat{\boldsymbol{\sigma}} \cdot \hat{\boldsymbol{p}} \\ c\hat{\boldsymbol{\sigma}} \cdot \hat{\boldsymbol{p}} & V - 2mc^2 \end{Vmatrix} = c\hat{\boldsymbol{\alpha}} \cdot \hat{\boldsymbol{p}} + (\beta - 1)mc^2 + V, \tag{2.125}$$

where β is a *4x4* matrix containing the identity matrix *I* and whose terms are $\begin{Vmatrix} I & 0 \\ 0 & -I \end{Vmatrix}$.

As a consequence, the solutions of Dirac equation are 4-component vectors ϕ accounting for the spin contribution (4-spinor) and taking into account both particles with positive energies (fermions) and particles with negative energies (anti-fermions). Among the four components of a 4-spinor, one can notice two upper components (upper 2-spinor) and two lower components (lower 2-spinor): the former are larger for the fermionic states, whereas the latter are larger for the anti-fermionic states [61]. Specifically, as the electrons are fermions, for atoms and molecules the upper and lower 2-spinors are usually called the *large* component ϕ_L and the *small* component ϕ_S, respectively. In a vast majority of cases (e.g. light atoms, chemical transformations) accounting

for anti-fermions provides negligible correction for the description of systems of chemical interests, therefore it is necessary to decouple Dirac Hamiltonian, so to split its terms into a positive energy term and a negative energy term, where the latter can be neglected. The aim is thus the transformation of the Dirac Hamiltonian (2.125) into a block-diagonal Hamiltonian and such a result is achieved by means of unitary transformations of the form [56-58,62]:

$$\widehat{\mathcal{H}}_{bd} = U\widehat{\mathcal{H}}_D U^+ = \begin{Vmatrix} h_+ & 0 \\ 0 & h_- \end{Vmatrix} \tag{2.126}$$

Attaining the block-diagonal Hamiltonian requires the knowledge of the unitary operator *U*. Two approaches to calculate the unitary operator and decouple Dirac Hamiltonian are the *Douglas-Kroll-Hess Transformation* (DKH) [56,57,62] and the *eXact-2-Component approach* (X2C) [58]. Both approaches assume that spin-orbit coupling provides a minor contribution to the relativistic energy and, therefore, neglect it. This approximation is called the *scalar relativistic approximation* [63,64] and the related corrections refer to the *scalar relativistic effects*.

2.7.1.2. Douglas-Kroll-Hess Transformation

The Dirac Hamiltonian can be written as a sum of even and odd terms; the former are block diagonal and commute with the matrix β, whereas the latter are off-diagonal and anticommute with the matrix β. The DKH transformation applies a sequence of further unitary transformations as that in (2.125) to eliminate the odd terms step by step. The outcome is the final block-diagonal Hamiltonian expressed as a series of even terms in the *k*-th order in *U* [57,62]:

$$\widehat{\mathcal{H}}_{bd} = \cdots U_2 U_1 \widehat{\mathcal{H}}_D U_1^+ U_2^+ \ldots = \Sigma_{k=0}^{\infty} \mathcal{E}_k. \tag{2.127}$$

In the DKH formalism the unitary transformations are obtained by a power series expansion in terms of a set of an anti-Hermitian operator $\widehat{W}$ [57]:

$$U_i = a_{i,0}\mathbf{1} + \Sigma_{k=0}^{\infty} a_{i,k} \widehat{W}_i^k \tag{2.128}$$

Up to the fourth term $\mathcal{E}_k$ does not depend on the parametrization of the unitary transformations, while the higher-order terms are dependent on the $a_{i,k}$ coefficients of the general parametrization [56,57].

The sum of the even terms (2.127) is infinite. Thus it is necessary to approximate the exact block-diagonal Hamiltonian by truncation of (2.127) up to the *k*-th term. This *k*-th term upon which the truncation is carried out gives the order of the approximation to the DKH transformation. This is then called DKH*k*.

$$\widehat{\mathcal{H}}_{DKHk} = \Sigma_{k=0}^{n} \mathcal{E}_k. \tag{2.129}$$

Some of the $\mathcal{E}_k$ terms are reported below [57]:

$$\mathcal{E}_0 = (\beta - 1)mc^2, \tag{2.130a}$$

$$\mathcal{E}_1 = V + \frac{\beta \boldsymbol{p^2}}{2m}, \tag{2.130b}$$

$$\mathcal{E}_2 = -\beta \frac{\boldsymbol{p^2}}{8m^3c^2} + \frac{\hbar}{8(mc)^2}\nabla^2 V + \frac{\hbar^2}{(2mc)^2}\boldsymbol{\Sigma} \cdot [(\nabla \cdot \mathrm{V}) \times \mathbf{p}] \tag{2.130c}$$

In the zeroth term, $\mathcal{E}_0$, we can easily recognize the rest energy, whereas in the second-order term (2.130c) we can recognize the mass-velocity, the Darwin term and the Spin-orbit coupling, where $\boldsymbol{\Sigma}$ refers to the Dirac spin matrix.

The first DKH correction ever implemented was that truncated to the second-order term, DKH2, but nowadays corrections to the third (DKH3) up to the sixth term (DKH6) are also available in many quantum chemistry software [62]. Recent versions of the MOLPRO package [46] implement even higher-order corrections.

2.7.1.3. eXact-2-Component Approach

Large and small components, ϕ_L and ϕ_S, are related by a *2x2* matrix *X*, so that [57,58]

$$\phi_S = X\phi^L \tag{2.131}$$

This matrix can be used to build up the matrix *U* that decouples Dirac Hamiltonian:

$$U(X) = \begin{Vmatrix} \frac{1}{\sqrt{1+X^+X}} & \frac{X^+}{\sqrt{1+X^+X}} \\ -\frac{X^+}{\sqrt{1+X^+X}} & \frac{1}{\sqrt{1+X^+X}} \end{Vmatrix} \tag{2.132}$$

X is an energy-dependent matrix, depending on the energy of the system and on the Coulombic potential [58].

The X2C approach determines X in a non-iterative way and uses it to construct the unitary matrix $U(X)$ [58]: the coefficients of the large and small components, c_L, c_S are determined by solving the Fock-Roothaan equations and thence used to calculate X according to the formula

$$X = c_S(c_L)^{-1} \tag{2.133}$$

Since the exact unitary matrix is directly evaluated from the coefficients c_L, c_S, there is no need for expanding the decoupled Hamiltonian in the series of its even terms as in DKH. Thence, no approximation is imposed to the decoupled Hamiltonian. Furthermore, this approach does not make use of 4-spinors as solutions of Dirac equation, but instead constructs easier handling 2-component spinors [58]. For such reasons, the approach is called the eXact 2-Component correction, or X2C.

2.7.2. Effective Core Potential

In the previous sections, we analyzed the relativistic methods commonly used to treat *all-electron* (AE) problems, i.e. problems where both valence and core electrons are explicitly treated. However, a common intuitive assumption among chemists states that, roughly, the valence shell of atoms is the main responsible for their chemical behavior. From this assumption, the introduction of effective core potentials (ECP) follows. According to this model, the valence electrons move in the field of a suitable ECP [66], *describing* the core electrons, that are thus accounted for separately. In this way, the ECP is supposed to account for much of the relativistic effects due to the core, while the valence electrons are treated non-relativistically [66].

The reason for the popularity of ECPs relies on two advantages: the smaller computational cost compared to the AE treatment [67,68] and the relative ease with which major relativistic effects can be included [68].

Among the wide range of available ECPs, we worked with *energy-consistent* ECPs, i.e. ECPs adjusted to non-relativistic, quasi-relativistic or relativistic energies, such as Hartree-Fock or Dirac-Hartree-Fock [69]. In particular, we chose to expose the following two, that will be used in the next chapters:

1) Quasi-relativistic Wood-Boring ECP (ECPMWB);
2) Relativistic Dirac-Fock ECP (ECPMDF).

1) ECPMWB describes the core potential with the function [67]

$$V(R_i) = -\frac{Q}{R_i} + \Sigma_l A_l \exp(-a_l R_i^2)\, P_l, \tag{2.134}$$

where Q indicates the charge of the core, i subscript runs over the electrons, while P_l is a projector, projecting onto the Hilbert subspace with angular symmetry l. A_l and a_l (l = 0,1,2,3) are empirical parameters, each of them being adjusted to the energy of a valence state of the atom [67]. These reference valence energies are derived from quasi-relativistic HF calculations, relying on solving Dirac-Slater equation approximately. In this approximation, the small component of the 4-spinor wave function is neglected, so that the equation reduces to the second-order Cowan-Griffin equation [70]:

$$\frac{d^2\phi^L}{dR^2} = \left(\hat{g} + \hat{f}\right)\phi^L, \tag{2.135}$$

where ϕ^L denotes the large component of Dirac-Slater solution. The factors $\hat{g}$ and $\hat{f}$ are defined, respectively, as [70]

$$\begin{aligned} \hat{g} &= -\epsilon + \frac{l(l+1)}{R^2} + V \\ \hat{f} &= \widehat{\mathcal{H}}_m(R) + \widehat{\mathcal{H}}_D(R) + \widehat{\mathcal{H}}_{SO} \end{aligned} \tag{2.136}$$

In the definition of those two parameters we can recognize the reference valence energy of the given state (ϵ) and the central-field potential (V) for $\hat{g}$ and the mass-velocity ($\widehat{\mathcal{H}}_m$), Darwin ($\widehat{\mathcal{H}}_D$) and Spin-Orbit ($\widehat{\mathcal{H}}_{SO}$) Hamiltonians. In Wood-Boring approach, this latter Hamiltonian is usually dropped from f and treated as a first-order perturbation [70].

2) ECPMDF differs from ECPMWB as the effective potential describing the core accounts for both large and small components of the 4-spinor wave function. In particular, the empirical coefficients are here adjusted to reference valence energies achieved with the multiconfigurational Dirac-Coulomb-Hartree-Fock (MCDHF) level [68].

2.7.3. Basis set

2.7.3.1. Introduction

In quantum chemical calculations, the accurate description of the atomic orbitals requires the choice of a set of basis functions: larger basis sets ensure a more accurate description of the

orbitals, however, computational cost sharply increases with the size of the basis [1]. In particular, the major contribution to the computational cost of the basis set is provided by the 2-electron integrals, i.e., integrals where two different electron positions $\boldsymbol{r}$ appear. Typically, for M basis functions there are $\frac{1}{8}M^4$ 2-electron integrals [1], therefore the choice of the basis set is usually a compromise between accuracy and computational cost.

Early calculations employed Slater-type orbitals (STO) as basis functions [1,14],

$$\chi = R_{lk}(\boldsymbol{r}) \exp(-\zeta r), \tag{2.137}$$

where R_{lk} is a solid harmonic, whose argument, $\boldsymbol{r} \equiv (r, \theta, \phi)$, stands for the position of the electron relative to the nucleus, while ζ is a parameter. However, nowadays the majority of standard ab initio packages operate with basis sets employing contracted Gaussian functions (GTO) of the form

$$\chi = R_{lk}(\boldsymbol{r}) \, \Sigma_i \, c_i N_i \exp(-\alpha_i r^2) \tag{2.138}$$

Here, c_i are a set of expansion coefficients, usually chosen to optimize the energy of the isolated atom, but fixed for the dimer calculations [1,14]; N_i is a normalization factor. The individual terms $N_i \exp(-\alpha_i r^2)$ are called the *primitive Gaussian functions* (there, α_i is a parameter, called the *contraction*).

For a given atom, a minimal basis set employs one primitive for each orbital. At the next level, a larger number of primitives can be used to describe each orbital: for instance, the minimal 6-31G Gaussian basis set employs one basis function for the core atomic orbitals, given as a linear combination of six Gaussian primitives of the form (2.138). For the valence orbitals, two sets of basis functions are used, one consisting of a linear combination of three primitives, while the other one consists of one primitive [1]. Since a different number of basis functions is used to describe the atomic core and valence, this class of basis sets is called *split-valence* basis sets. In particular, 6-31G is called a *split-valence double-zeta basis set*. On the side of the valence orbitals description, a significant refinement is represented by the TZ (*Triple-Zeta)* basis set, where three basis functions are used for each valence orbital. From there, further improvements may come from adding more basis functions to model the valence orbitals [1]. Generally, the number of basis functions employed to describe the valence orbitals is indicated by the cardinal number n, where

n may be equal to 2 (D), 3 (T), 4 (Q), 5 and so forth. Thus, a basis set with $n = 2$ is called DZ, a basis set with $n = 3$ TZ, with $n = 4$ QZ, with $n = 5$ 5Z and so on. At the next level, the description of the orbital is refined by the addition of *polarization functions*, which, in turn, model polarization of the electron density due to an external perturbation, such as an applied electric field. For instance, description of polarization effects in the hydrogen atom would require the addition of a p-function to the minimal s-function used to describe the 1s orbital. Likewise, polarization of p orbitals is modelled by adding d-functions to the minimal p-function, polarization of d orbitals is modelled by adding f-functions, and so forth.

On the other hand, charge distributions far from the nucleus, such as the case of anions, are described by means of *diffuse functions*. These are additional Gaussian basis functions with a small exponent. Diffuse functions are also used to describe dipole moments and related phenomena, such as intermolecular interactions.

For modern quantum chemistry packages, such as MOLPRO [46], a wide variety of Gaussian basis sets is currently available to compromise accuracy and computational demands [71], depending on the complexity of the system and its desirable properties. In particular, for the Thesis research, a popular branch of so called *correlation-consistent basis set* was used, for their well-known properties, flexibility and systematic extension towards the complete basis set limit. Both concepts are explained in detail in the following sections.

2.7.3.2. Correlation-consistent basis sets: atom- and bond-centered basis functions

It is well known that the accurate description of atomic polarizabilities and, generally, variables depending on electron correlation effects, requires large basis sets [1]. Therefore, the larger the basis set, the more accurate the description of long-range interactions and related variables. To account for the reliable description of such phenomena, Dunning and coworkers [72-76] devised basis sets addressing the accurate calculations of valence-correlated wavefunctions of ground-state neutral systems [14]: such basis sets are called *correlation-consistent basis sets*, usually abbreviated as cc-pV*n*Z, where “cc-p” stands for “correlation-consistent polarized”, while “V” indicates that they are valence-only basis sets. Such basis sets include successively larger polarization functions, such as *d, f, g, h* and so forth. On the other hand, “-*n*Z" stands for the number of basis functions used to describe each valence atomic orbital: if *n* equals 2, then two

basis functions are used to model each valence atomic orbital and the basis set is called *Double-Zeta* (DZ); analogously, one can have *Triple-Zeta* (TZ) basis sets, *Quadruple-Zeta* basis sets and so forth, up to *Sextuple-Zeta* basis sets (6Z) [1]. However, such basis sets do not have the flexibility required both for the investigation of core correlation and for the study of anions and excited states [14]. For such applications, additional diffuse atomic orbitals should be added. This is indicated by the prefix "aug-" [1,14] (standing for "augmented") . Core correlation is taken into account by cc-pCV*n*Z, also called *correlation-consistent polarized core-valence* basis set. Core correlation is modelled upon introducing sets of atomic orbitals having radial maxima close to the nucleus: such functions are introduced in a *correlation-consistent way*, i.e., functions with similar contributions to correlation energy are introduced simultaneously [14]. For the description of core-valence correlation energy *correlation-consistent weighted core-valence polarized* basis set (cc-pWCV*n*Z) [14,77] are used. There, the core functions are optimized with respect to the core and the valence correlation energy. Other additions may account for scalar relativistic corrections, signified by the addition of the suffix –DK (for Douglas-Kroll-Hess correction) or –X2C (for the eXact-2-component correction). Other additions account for the use of effective core potentials to approximate innermost atomic shells (-PP). Table 2.1 shows the basis functions comprising correlation-consistent cc-pV*n*Z, cc-pCV*n*Z and aug-cc-pV*n*Z basis sets (n ranging from D to 5) for the first-row elements of the Periodic Table.

Table 2.1. Basis functions composing the cc-pVnZ, cc-pCV*n*Z and aug-cc-pV*n*Z basis sets for the first-row atoms. For the cc-pCV*n*Z and aug-cc-pV*n*Z basis sets, only the core-correlating and diffuse orbitals are reported, respectively. N_V, N_{CV}, N_{aug} refer to the total number of contracted orbitals in the basis sets [14].

n	cc-pV*n*Z	N_V	cc-pCV*n*Z	N_{CV}	aug-cc-pV*n*Z	N_{aug}
D	[3s2p1d]	14	+ 1s1p	18	+ 1s1p1d	23
T	[4s3p2d1f]	30	+ 2s2p1d	43	+ 1s1p1d1f	46
Q	[5s4p3d2f1g]	55	+ 3s3p2d1f	84	+ 1s1p1d1f1g	80
5	[6s5p4d3f2g1h]	91	+ 4s4p3d2f1g	145	+ 1s1p1d1f1g1h	127

Exponents and contraction coefficients are optimized to fit the benchmark atomic properties, such as the correlation energy. For instance, in the case of the first-row atoms from boron to neon, the (sp) sets of primitive Gaussian functions can be obtained from HF calculations, whereas the polarization (d, f, g…) sets are determined from correlated atomic calculations [72].

Basis sets discussed so far are *atom-centered*, i.e. the related basis functions are centered on the atomic nucleus. When dimer calculations are in need, the atom-centered description may not reproduce the dimer interaction potential with the required accuracy, due to the lack of accurate description of the region between the atomic charge distributions. To solve this issue, it was proposed to add *bond-centered functions*, i.e. basis functions to be placed midway the internuclear distance [78]. Such basis functions are commonly called *bond functions* [1,78,79] (bf). There is not an exact rule about the basis functions to choose in order to accurately saturate dispersion interactions: usually a small set of s- and p-functions may account for about 20% of the dispersion energy [1]. In this regard, Cybulski and Toczylowski [79] reported a set of bond functions of the form 3s3p2d2f1g, with the following exponents: for sp, 0.94, 0.34, 0.12; for df, 0.64, 0.23; for g, 0.35. Placed midway several rare gas (He, Ne, Ar) dimers and matched with atom-centered augmented correlation-consistent basis sets, these functions allowed for a significant accuracy increase for several properties, even reaching for such results a 1% deviation from experimental data [79].

2.7.3.3. Complete basis set limit

As another feature, correlation-consistent basis sets form a hierarchical set, suitable for extrapolating computed properties to the complete basis set limit [1,14] (CBS). CBS limit is the extrapolated estimate of a result using an ideal infinitely large basis set. Several empirical formulae exist to carry out the extrapolation: given a generic property *X*, CBS extrapolation employs correlation-consistent basis sets of successively higher order (e.g. D, T, Q or T, Q, 5 series) to reach the asymptotic convergence of the result. Two examples of three-point (i.e. extrapolating the result from analogs computed at three different cardinal number n of the basis set) CBS extrapolation schemes are listed below:

$$X(n) = X(\infty) + B\exp\big(-(n-1)\big) + C\exp(-(n-1)^2) \tag{2.139}$$

$$X(n) = X(\infty) + \frac{B}{\left(n+\frac{1}{2}\right)^4} + \frac{C}{\left(n+\frac{1}{2}\right)^6} \tag{2.140}$$

There, $X(n)$ refers to a generic quantity as a function of the basis set zeta cardinal number n; $n = \infty$ means the CBS limit. Scheme (2.139) is the three-term mixed exponential CBS formula [80,81], whereas scheme (2.140) is the three-point two-term inverse power function first reported by Martin and Taylor [82,83]. It should be noted that a universal extrapolation rule does not exist: each formula produces different results and this difference is worthy of tracing out. In particular, a good criterion to choose a CBS formula is the property that one wants to extrapolate. In this respect, the choice of eqs. (2.139) and (2.140) is motivated by two considerations: first, they are able to extrapolate non-energetic properties as well as the energy [84]; second, their linear character ensures the convergence of the properties related to correlation energy upon CBS extrapolation [84].

2.7.3.4. Basis set superposition error and counterpoise correction

CBS extrapolation cannot eliminate a spurious consequence of the practical use of incomplete basis sets. Given two species, A and B, for each one, its "own" basis set would be used to calculate the related energies, E_A, E_B. Therefore, when switching to the dimer A-B, it would be natural to calculate the related energy E_{AB}, in the combined basis set of the two monomers. However, in finite basis sets, this approach introduces a systematic error in the interaction energy: the energy of A in the "dimer" basis set would be slightly smaller than the energy of A in the "monomer" basis set,

$$E_A(AB) \leq E_A(A), \tag{2.141}$$

where $E_A(AB)$ stands for the energy of A in the joint basis, whereas $E_A(A)$ stands for the energy of A in the monomer basis set. In other words, in the dimer calculation, the basis function on B improves the description of A and vice versa. This phenomenon has no physical meaning, it is an artifact, and is commonly referred to as the *basis set superposition error* [1,14] (BSSE). This error is due to the finiteness of the basis set employed for the monomer, that is inadequate for a fully accurate description of its properties. As a consequence, the interaction potential is spuriously low if it is calculated as the difference [1]

$$V_{AB} = E_{AB}(AB) - E_A(A) - E_B(B) \tag{2.142}$$

BSSE is particularly high for Van der Waals complexes [14], as, in that case, it strongly depends on the internuclear distance [1].

Boys and Bernardi [85] proposed a scheme to circumvent BSSE, simply consisting of using the dimer basis (AB) for all the calculations [1,14]:

$$V_{AB}^{cp} = E_{\mathrm{AB}}(\mathrm{AB}) - E_{\mathrm{A}}(\mathrm{AB}) - E_{\mathrm{B}}(\mathrm{AB}) \quad (2.143)$$

This solution is called the *counterpoise correction* (CP). CP suppresses the spurious attraction due to BSSE, with a relatively simple principle: in the calculation of the monomer A, the presence of the *ghost basis* for monomer B counterbalances the effect that basis B has on monomer A in the calculation of the dimer AB, and vice versa [14].

In the long-range tail of the interaction potential, accounting for counterpoise correction is crucial: in this region the interaction energy is often smaller than the BSSE [86]. Calculation of the monomer and dimer energies by means of size-consistent methods may also increase the accuracy of the interaction energy, while decreasing the BSSE. However, even when the energies are computed in a consistent manner, CP provides a determinant contribution to the elimination of the spurious attraction stemming from the finiteness of the basis set. For this reason, counterpoise correction was accounted in all calculations presented in the Thesis [86].

2.7.4. MOLPRO implementation

In the thesis all the ab initio calculations are carried out using the MOLPRO quantum chemistry package [46]. MOLPRO is a Schrödinger-only code that deals only with ansätze based on one-component non-relativistic wavefunctions [46]. The package implements different levels of theory, both single- and multi-reference. Among single-reference methods, HF, CCSD and CCSD(T) [37] are worthy of mention for the aims of the Thesis. Also, CC methods for the calculation of excitation energies and response properties like dynamic polarizabilities up to quadrupole are available. On this side, in the Thesis, we used the Polarization-Propagator approach in the frame of the EOM-CCSD approach [48]. On the other hand, multipole static polarizabilities can be calculated with the finite-field approach.

Also, it is possible to correct the non-relativistic Hamiltonian for scalar-relativistic effects: both DKH [56,57,62] and X2C [58] corrections are implemented and can be specified in the input file using related keywords. For DKH, the order of expansion terms should be specified in the input file, otherwise the program set DKH2 by default [46].

In addition, MOLPRO allows for setting several control parameters in the calculation. The convergence energy for threshold is particularly worthwhile for the aims of the Thesis: by default, the program sets it to 10^{-6} a.u [46]. However, our calculations required high accuracy and, therefore, we always chose much smaller energy thresholds (from 10^{-10} up to 10^{-12} a.u.).

All ab initio calculations were performed on the Skoltech Pardus HPC cluster.

References

[1] A. J. Stone, The Theory of Intermolecular Forces (Oxford University Press, Oxford, 2013).

[2] K. D. Bonin, V.V. Kresin, Electric Dipole Polarizabilities of Atoms, Molecules and Clusters (World Scientific Publishing, Singapore, 1997).

[3] S.G. Porsev, A. Derevianko, *High-Accuracy Calculations of Dipole, Quadrupole, and Octupole Electric Dynamic Polarizabilities and van der Waals Coefficients C_6, C_8, and C_{10} for Alkaline-Earth Dimers*, JETP, **102**, 2 (2006); doi: 10.1134/S1063776106020014.

[4] H. C. Longuet-Higgins, *The electronic states of composite systems*, Proc. Roy. Soc. A **235**, 537–543. 57, 58 (1956).

[5] A.D. Buckingham, P.W. Fowler, J.M. Hutson, *Theoretical Studies of van der Waals Molecules and Intermolecular Forces*, Chem. Rev. **88**, 963-988 (1988); doi: 10.1021/cr00088a008

[6] F. London, The general theory of molecular forces, *Trans. Faraday Soc.* **33**, 8–26. 57, 64 (1937).

[7] A. Unsöld, *Quantentheorie des Wasserstoffmolekülions und der Born–Landeschen Abstossunskräfte*, Z. Physik **43**, 563-574, 65 (1927).

[8] H. B. G. Casimir and D. Polder, *The Influence of Retardation on the London-van der Waals Forces*, Phys. Rev. **73**, 360 (1948); doi: 10.1103/PhysRev.73.360.

[9] I.E. Dzyaloshinskii, E.M. Lifshitz, and L.P. Pitaevskii, *The general theory of van der Waals forces*, Adv. Phys., **10**:38, 165-209 (1961); doi: 10.1080/00018736100101281.

[10] V. Adrian Parsegian, *Formulae for the electrodynamic interaction of point particles with a substrate*, Mol. Phys. **27**:6, 1503-1511 (1974); doi: 10.1080/00268977400101271.

[11] Y. Tikochinsky, L. Spruch, *Retarded Casimir interaction in the asymptotic domain of an electron and a dielectric wall*, Phys. Rev. A **48**, 4236 (1993); doi: 10.1103/PhysRevA.48.4236.

[12] P. Zhang, and A. Dalgarno, *Long-range interactions of ytterbium atoms*, Mol. Phys. **106**:12-13, 1525-1529 (2008); doi: 10.1080/00268970802126608.

[13] E. A. Power and T. Thirunamachandran, *Dispersion interactions between atoms involving electric quadrupole polarizabilities*, Phys. Rev. A **53**, 1567 (1996); doi: 10.1103/PhysRevA.53.1567.

[14] T. Helgaker, P. Jørgensen, and J. Olsen, *Molecular Electronic-Structure Theory*, Wiley, Chichester (2000).

[15] P.R. Taylor, *Lecture Notes in Quantum Chemistry: European Summer School* (Springer-Verlag, Berlin), pp. 125-202 (1994).

[16] R.J. Bartlett, *Many-Body Perturbation Theory and Coupled Cluster Theory for Electron Correlation in Molecules*, Ann. Rev. Phys. Chem. **32**: 359-401 (1981); doi: 10.1146/annurev.pc.32.100181.002043.

[17] D.R. Hartree, W. Hartree, *Self-consistent field, with exchange, for beryllium*, Proc. Royal Soc. Lond. A **150**, 869:9 (1935); doi: 10.1098/rspa.1935.0085.

[18] D.A. McQuarrie and J.D. Simon, *Physical Chemistry: a Molecular Approach*, University Science Books, Sausalito, CA (1997).

[19] D. M. Hanson, E. Harvey, R. Sweeney, T. J. Zielinski, *Quantum States of Atoms and Molecules*, *J. Chem. Educ.* **82**, 12, 1880 (2005); doi: 10.1021/ed082p1880.2.

[20] B.O. Roos (Ed.), *Lecture Notes in Chemistry II. European Summer School in Quantum Chemistry*, Springer-Verlag, Berlin, Heidelberg, New York (1994).

[21] A.R. Leach, *Molecular Modelling. Principles and Applications*, Second Edition, Pearson Education, Harlow, England (2001).

[22] P.O. Löwdin, *Quantum Theory of Many-Particle Systems. III. Extension of the Hartree-Fock Scheme to Include Degenerate Systems and Correlation Effects*, Phys. Rev. **97**, 1509 (1955); doi: 10.1103/PhysRev.97.1509.

[23] L. Pjela, *Ideas of Quantum Chemistry*, Second Edition, Elsevier, the Netherlands (2013).

[24] C.D. Sherrill, H.F. Schaefer III, *The Configuration Interaction Method: Advances in Highly Correlated Approaches*, Adv. Quantum Chem. **34**, 143-269; doi: 10.1016/S0065-3276(08)60532-8.

[25] F. Jensen, *Introduction to Computational Chemistry*, Wiley, Chichester (2007), pp. 133-158.

[26] H.-J. Werner and P. J. Knowles, *A second order multiconfiguration SCF procedure with optimum convergence*, J. Chem. Phys. **82**, 5053 (1985); doi: 10.1063/1.448627; *An efficient*

second order MC SCF method for long configuration expansions, Chem. Phys. Lett. **115**, 259 (1985); doi: 10.1016/0009-2614(85)80025-7.

[27] H.-J. Werner and P. J. Knowles, *A comparison of variational and non-variational internally contracted multiconfiguration-reference configuration interaction calculations*, Theor. Chem. Acc. **78**, 175 (1990); doi: 10.1007/BF01112867.

[28] F. Coester, H. Kummel, *Short-range correlations in nuclear wave functions, Nucl. Phys.*, **17**, 477-485 (1960); doi: 10.1016/0029-5582(60)90140-1.

[29] P. von Ragu-Schleyer, Encyclopedia of Computational Chemistry (Wiley, Chichester, 1998).

[30] J. Paldus, J. Čížek, I. Shavitt, *Correlation Problems in Atomic and Molecular Systems. IV. Extended Coupled-Pair Many-Electron Theory and Its Application to the BH3 Molecule,* Phys. Rev. A **5**, 50 (1972); doi: 10.1103/PhysRevA.5.50.

[31] P. Zhang, and A. Dalgarno, *Static Dipole Polarizability of Ytterbium*, J. Phys. Chem. A **111**, 49, 12471–12476 (2007); doi: 10.1021/jp0750856.

[32] T. Korona, M. Przybytek and B. Jeziorski, *Time-independent coupled cluster theory of the polarization propagator. Implementation and application of the singles and doubles model to dynamic polarizabilities and van der Waals constants*, Mol. Phys. **104**, 13-14, 10-20 (2006); doi: 10.1080/00268970600673975.

[33] X.-F. Tong, C.-L. Yang, M.-S. Wang, X.-G. Ma, and D.-H. Wang, *Interactions of M^z–X complexes (M = Cu, Ag, and Au; X = He, Ne, and Ar; and z = ±1)*, J. Chem. Phys. **134**, 024306 (2011); doi: 10.1063/1.3526955.

[34] I. Shavitt, R. J. Bartlett, Many-Body Methods in Chemistry and Physics (Cambridge University Press, Cambridge, 2009).

[35] J. Paldus and X. Li in Advances in Chemical Physics, Vol. 110, edited by I. Prigogine and S.A. Rice, Chapter 1 (John Wiley and sons, 1999).

[36] G. D. Purvis and R. J. Bartlett, *A full coupled-cluster singles and doubles model: The inclusion of disconnected triples*, J. *Chem. Phys.*, **76**. 1910-1918 (1982); doi: 10.1063/1.443164.

[37] P. J. Knowles, C. Hampel, and H.-J. Werner, *Coupled cluster theory for high spin, open shell reference wave functions,* J. Chem. Phys., **99**, 5219 (1993); doi: 10.1063/1.465990; Erratum, **112**, 3106 (2000); doi: 10.1063/1.480886.

[38] J. Noga, and R. J. Bartlett, *The full CCSDT model for molecular electronic structure,* J. Chem. Phys. **86**, 7041 (1987); doi: 10.1063/1.452353.

[39] J. F. Stanton, *Why CCSD(T) works: a different perspective*, Chem. Phys. Lett., **281**, 130–134 (1997); doi: 10.1016/S0009-2614(97)01144-5.

[40] K. Raghavachari, G. W. Trucks, J. A. Pople, M. Head-Gordon, *A Fifth-Order Perturbation Comparison of Electron Correlation Theories*, Chem. Phys. Lett., **157**, 6 (1989); doi: 10.1016/S0009-2614(89)87395-6.

[41] T. Korona, *Coupled cluster singles and doubles polarization propagator accurate through the third order of Møller–Plesset theory*, Mol. Phys., **108**:3-4, 343-357 (2009); doi: 10.1080/00268970903476654.

[42] D.M. Elking, L. Perera, R. Duke, T. Darden, and L.G. Pedersen, *A finite field method for calculating molecular polarizability tensors for arbitrary multipole rank*, J. Comp. Chem. **32** (15), 3283–3295 (2011); doi: 10.1002/jcc.21914.

[43] H. Hellmann, *Einführung in die Quantenchemie*, Deuticke, Leipzig. **83** (1937).

[44] R. Feynman, *Forces in molecules*, Phys. Rev. **56**, 340. 83 (1939).

[45] H.D. Cohen, and C.C.J. Roothaan, *Electric Dipole Polarizability of Atoms by the Hartree—Fock Method. I. Theory for Closed-Shell Systems*, J. Chem. Phys. **43**, S34 (1965); doi: 10.1063/1.1701512.

[46] H.-J. Werner, P. J. Knowles, G. Knizia, F. R. Manby, and M. Schutz, *Molpro: A general-purpose quantum chemistry program package*, Wiley Interdiscip. Rev.: Comput. Mol. Sci. **2**, 242 (2012); doi: 10.1002/wcms.82.

[47] H.J. Monkhorst, *Calculation of properties with the coupled-cluster method,* Int. J. Quantum Chem., **12** (S11), 421–432 (1977); doi: 10.1002/qua.560120850.

[48] T. Korona, H. J. Werner, *Local treatment of electron excitations in the EOM-CCSD method,* J. Chem. Phys. **118**, 3006 (2003); doi: 10.1063/1.1537718.

[49] J. F. Stanton and R. J. Bartlett, *The equation of motion coupled-cluster method. A systematic biorthogonal approach to molecular excitation energies, transition probabilities, and excited state properties,* J. Chem. Phys. **98**, 7029 (1993); doi: 10.1063/1.464746.

[50] R. Moszinski, P.S. Żukovski, B. Jeziorski, *Time-Independent Coupled-Cluster Theory of the Polarization Propagator;* Collect. Czech. Chem. Commun. (Vol.**70**) (2005); doi: 10.1135/cccc20051109.

[51] C. Møller and M. S. Plesset, *Note on an Approximation Treatment for Many-Electron Systems*, Phys. Rev. **46**, 618 (1934); doi: 10.1103/PhysRev.46.618.

[52] M.L. Leininger, W.D. Allen, H.F. Schaefer III, and C. D. Sherrill, *Is Møller-Plesset perturbation theory a convergent ab initio method?*, J. Chem. Phys. **112**, 9213 (2000); doi: 10.1063/1.481764.

[53] V.A. Dzuba, V.V. Flambaum, M.G. Kozlov, *Combination of the many-body perturbation theory with the configuration-interaction method*, Phys. Rev. A **54**, 3948 (1996); doi: 10.1103/PhysRevA.54.3948.

[54] M.G. Kozlov, S.G. Porsev, M.S. Safronova, I.I. Tupitsyn, *CI-MBPT: A package of programs for relativistic atomic calculations based on a method combining configuration interaction and many-body perturbation theory*, Comp. Phys. Comm., **195**, 199–213 (2015); doi: 10.1016/j.cpc.2015.05.007.

[55] I.M. Savukov, *Relativistic configuration-interaction and many-body-perturbation-theory calculations of U I hyperfine constants*, Phys. Rev. A **102**, 042806 (2020); doi: 10.1103/PhysRev A.102.042806.

[56] A. Wolf, M. Reiher, B. A. Hess, *The generalized Douglas–Kroll transformation* J. Chem. Phys. **117**, 9215 (2002); doi: 10.1063/1.1515314.

[57] M. Reiher, A. Wolf, *Exact decoupling of the Dirac Hamiltonian. I. General theory*, J. Chem. Phys., Vol. **121**, No. 5, 1 (2004); doi: 10.1063/1.1768160.

[58] D. Peng, M. Reiher, *Exact decoupling of the relativistic Fock operator,* Theor. Chem. Acc. **131**:1081 (2012); doi: 10.1007/s00214-011-1081-y.

[59] G. Visentin, M. Laatiaoui, L.A. Viehland, and A.A. Buchachenko, *Mobility of the Singly-Charged Lanthanide and Actinide Cations: Trends and Perspectives*, Front. Chem. **8**, 438 (2020); doi: 10.3389/fchem.2020.00438.

[60] D.C. Hoffman, D.M. Lee, and V. Pershina in The Chemistry of Actinide and Transactinide Elements, edited by L.R. Morss, N.M. Edelstein and J. Fuger, 4th Ed. (Springer, Dordrecht, 2010).

[61] M. Dolg, in Relativistic Electronic Structure Theory: Part 1, edited by P. Schwerdtfeger (Elsevier, Amsterdam, 2002).

[62] M. Reiher, A. Wolf, *Exact decoupling of the Dirac Hamiltonian. II. The generalized Douglas–Kroll–Hess transformation up to arbitrary order*, J. Chem. Phys. **121**, 10945 (2004); doi: 10.1063/1.1818681.

[63] H. Gollisch and L. Fritsche, *Relativistic One-Particle Equation for Electron States of Heavy Metals*, Phys. Stat. Sol.(b) **86**, 145 (1978); doi: 10.1002/pssb.2220860116.

[64] T. Takeda, *The Scalar Relativistic Approximation*, Z. Physik B **32**, 43-48 (1978); doi: 10.007/BF01322185

[65] G. Visentin and A.A. Buchachenko, *Polarizabilities, dispersion coefficients and retardation functions at the complete basis set CCSD limit: Be-Ba and Yb*, J. Chem. Phys. **151**, 214302 (2019); doi: 10.1063/1.5129583.

[66] I.P. Grant, Relativistic Quantum Theory of Atoms and Molecules. Theory and Computation, (Ed. Springer, USA, 2007).

[67] M. Dolg, H. Stoll, and H. Preuss, *Energy-adjusted ab initio pseudopotentials for the rare earth elements*, J. Chem. Phys. **90**, 1730–1734 (1989); doi: 10.1063/1.456066.

[68] I.S. Lim, H. Stoll, and P. Schwerdtfeger, *Relativistic small-core energy-consistent pseudopotentials for the alkaline-earth elements from Ca to Ra*, J. Chem. Phys. **124**, 034107 (2006); doi: 10.1063/1.2148945.

[69] P. Schwerdtfeger, *The Pseudopotential Approximation in Electronic Structure Theory*, Chem. Phys. Chem. **12**, 3143-3155 (2011); doi: 10.1002/cphc.201100387.

[70] J.H. Wood, M.A. Boring, *Improved Pauli Hamiltonian for local-potential problems*, Phys. Rev. B, **18**, 6 (1978); doi: 10.1103/PhysRevB.18.2701.

[71] B. P. Pritchard, D. Altarawy, B. Didier, T. D. Gibson, T. L. Windus, *A New Basis Set Exchange: An Open, Up-to-date Resource for the Molecular Sciences Community*, J. Chem. Inf. Model. **59**, 11 (2019), 4814-4820; doi: 10.1021/acs.jcim.9b00725.

[72] T.H. Dunning, Jr., *Gaussian basis sets for use in correlated molecular calculations. I. The atoms boron through neon and hydrogen*, J. Chem. Phys. **90**, 1007 (1989); doi: 10.1063/1.456153.

[73] D.E. Woon, and T.H. Dunning, Jr., *Gaussian basis sets for use in correlated molecular calculations. III. The atoms aluminum through argon*, J. Chem. Phys. **98**, 1358 (1993); doi: 10.1063/1.464303.

[74] A.K. Wilson, T. van Mourik, T.H. Dunning, Jr., *Gaussian basis sets for use in correlated molecular calculations. VI. Sextuple zeta correlation consistent basis sets for boron through neon*, J. Mol. Struct. THEOCHEM **388**, 339-349 (1996); doi: 10.1016/S0166-1280(96)80048-0.

[75] T. van Mourik, T.H. Dunning, Jr., *Gaussian basis sets for use in correlated molecular calculations. VIII. Standard and augmented sextuple zeta correlation consistent basis sets for*

aluminum through argon, Int. J. Quantum Chem. **76**, 205 (2000); doi: 10.1002/(SICI)1097-461X(2000)76:2<205::AID-QUA10>3.0.CO;2-C.

[76] N. B. Balabanov and K. A. Peterson, *Systematically convergent basis sets for transition metals. I. All-electron correlation consistent basis sets for the 3d elements Sc–Zn*, J. Chem. Phys. **123**, 064107 (2005); doi: 10.1063/1.1998907.

[77] K. A. Peterson and T. H. Dunning, *Accurate correlation consistent basis sets for molecular core–valence correlation effects: The second row atoms Al–Ar, and the first row atoms B–Ne revisited*, J. Chem. Phys. **117**, 10548 (2002); doi: 10.1063/1.1520138.

[78] F.-M. Tao, and Y.-K. Pan, *Møller-Plesset perturbation investigation of the He_2 potential and the role of midbond basis functions*, J. Chem. Phys. **97**, 4989 (1992); doi: 10.1063/1.463852.

[79] S.M. Cybulski, and R.R. Toczyłowski, *Ground state potential energy curves for He2, Ne2, Ar2, He–Ne, He–Ar, and Ne–Ar: A coupled-cluster study*, J. Chem. Phys. **111**, 10520–10528 (1999); doi: 10.1063/1.480430.

[80] K. A. Peterson, D. E. Woon, and T. H. Dunning, Jr., *Benchmark calculations with correlated molecular wave functions. IV. The classical barrier height of the $H+H_2 \rightarrow H_2+H$ reaction*, J. Chem. Phys. **100**, 7410 (1994); doi: 10.1063/1.466884.

[81] D. Feller and J. A. Sordo, *A CCSDT study of the effects of higher order correlation on spectroscopic constants. I. First row diatomic hydrides*, J. Chem. Phys. **112**, 5604 (2000); doi: 10.1063/1.481135.

[82] J. M. L. Martin, *The total atomization energy and heat of formation of HCN(g)*, Chem. Phys. Lett. **259**, 679 (1996); doi: 10.1016/0009-2614(96)00899-8.

[83] J. M. L. Martin and P. R. Taylor, *Benchmark quality total atomization energies of small polyatomic molecules*, J. Chem. Phys. **106**, 8620 (1997); doi: 10.1063/1.473918.

[84] M.P. de Lara-Castells, R.V. Krems, A.A. Buchachenko, G. Delgado-Barrio, and P. Villareal, *Complete basis set extrapolation limit for electronic structure calculations: Energetic and nonenergetic properties of HeBr and $HeBr_2$ van der Waals dimers*, J. Chem. Phys. **115**, 10438 (2001); doi: 10.1063/1.1415078.

[85] S. Boys and F. Bernardi, *The calculation of small molecular interactions by the differences of separate total energies. Some procedures with reduced errors*, Mol. Phys. **19**, 553 (1970); doi: 10.1080/00268977000101561.

[86] M. Lesiuk and B. Jeziorski, *Size-consistency and counterpoise correction in explicitly correlated calculations of interaction energies and interaction-induced properties*, Phys. Rev. A **99**, 032712 (2019); doi: 10.1103/PhysRevA.99.032712.

3. Modeling dispersion interaction: polarizabilities, dispersion coefficients and retardation functions at the complete basis set CCSD limit: Be-Ba and Yb

The present exposition is based on the paper **G. Visentin** and A.A. Buchachenko*, Polarizabilities, dispersion coefficients, and retardation functions at the complete basis set CCSD limit: From Be to Ba plus Yb,* J. Chem. Phys. **151**, 214302 (2019); doi: 10.1063/1.5129583, partially reproduced with the permission of AIP Publishing.

The related project was funded by the Russian Science Foundation under Project No. 17-13-01466.

Summary

A systematic test on the atomic approach for alkaline earth atoms and Yb is presented. For the static polarizabilities, finite field CCSD(T) method matched with correlation-consistent basis sets saturated for diffuse augmentation, inner-shell electron correlation and scalar-relativistic effects ensure 1-2% accuracy with respect to special state-of-the-art atomic methods. Dynamic polarizabilities, computed by the CCSD(3) polarization propagator method are less accurate, but are still capable of reproducing the lowest-order dispersion coefficients within the 3% accuracy for alkaline earth dimers and, as a worst case, within the 7% accuracy for Yb dimer. Overall, the Chapter demonstrates that atomic long-range calculations with CCSD and CCSD(T) methods should serve as a very informative test for designing ab initio schemes for molecular calculations. On the other hand, detailed analysis of the long-range interactions for alkaline earth and Yb dimers suggests that direct matching of the global potential with its long-range expansion is possible only at internuclear distances as long as 40-50 Å, where the interaction energy plunges to 10^{-3}-10^{-4} wavenumbers. These strict requirements justify the use of synthetic potential functions bridging monomeric and dimeric approaches for reasonably heavy atoms.

3.1. Introduction

Experimental techniques nowadays used in ultracold atomic physics allow one to probe long-range interatomic interactions with unprecedented precision. In quantum condensates [1-3], atoms are held at long distances and any dynamical process is sensitive to interatomic forces at distances of tens to hundreds of Ångstroms. Measurements of collision properties, such as effective scattering lengths [4], Feshbach resonance positions [5] and ultracold reaction rate constants [6], and near-threshold bound energy levels (investigable by means of photoassociation experiments [4]) mostly

sense the long-range interaction tail, which, for a ground-state closed-shell atom, is represented by the inverse power series (See Chapter 2). Moreover, on the side of theoretical methods, asymptotic theories exist, that permit a full description of the ultracold collision dynamics without knowledge of the global potential (see, for instance, Ref. [7]).

However, knowledge of the interaction energy at short and medium ranges often provides improvements with respect to asymptotic theories, allowing one to calculate energy levels and phase shifts with remarkable accuracy.

As was shown in Introductory Chapter 1, the molecular approach is the only one capable of producing the global interaction potentials. However, it lacks accuracy at the relevant interatomic distances where interaction energy goes down to thousandths of wavenumber and less. Moreover, at this energy scale, high-order relativistic and QED effects may not be neglected. At present, they can only be accounted with the atomic approach. This dichotomy was recognized long ago, in the times when ab initio methods were underdeveloped, while long-range interactions were described empirically on a base of scattering, transport or thermochemical measurements. Model concepts and potential functions that combine the long-range asymptotic representation with the theoretical or empirical description of the short-range were devised and advocated, some of them now in use, see e.g. Refs. [8-10].

The great advance of the ab initio methods and availability of precise data from ultracold collision experiments call for further research in combining molecular and atomic approaches (i.e. the combination of dimeric and monomeric approaches for a diatom). Establishing a connection between them at a new level of accuracy is in need for future developments. First, it is important to gain a better understanding on the performance of molecular approaches at long range. As was mentioned, accuracy assessment of molecular potentials is masked by convergence and fitting uncertainties. One possibility to circumvent them is to apply atomic approaches closely emulating the molecular one. Second, the capability of atomic approaches is rapidly exhausted if one needs to describe the higher-order interactions, say, dispersion coefficients of an order above ten. Testing molecular approaches for the lowest order coefficient provides the hints on how accurately it handles higher components. Third, the consistency of the data combined in synthetic potentials always requires careful analysis.

One way to implement such benchmarking is to employ the molecular approach as an atomic one, or, better to say, align atomic calculations as close as possible to molecular ones. Though it cannot be done precisely, as the response properties that govern dispersion interaction may not be reduced to calculations of energies, useful comparisons are still possible with the calibration data of specially designed atomic calculations. What accuracy can one get employing accurate molecular approaches and tricks developed to improve molecular quantum chemistry calculations? How should molecular calculations be arranged to cover longer interatomic distances?

In this Chapter, we address these general questions by systematically applying the methods of the Coupled Cluster family to static and dynamic polarizabilities, dispersion coefficients and retardation corrections. Representing atomic mainstream, these calculations use standard approaches to the basis set augmentation and extrapolation, choice of the correlation constraints and scalar-relativistic corrections (e.g., those discussed in Chapter 2). As the test systems, the alkaline-earth atoms from Be to Ba, and Yb are chosen. Extensive studies of the long-range interactions of these atoms do exist, both theoretical and experimental. In fact, such systems are relatively easy to investigate by means of experimental ultracold physics techniques, due to their electron distribution isotropy at the ground state (for all of them, the ground state is ^{1}S). Among the experimental data, one may mention the stimulated emission pumping experiments for Be [11], while the alkaline earth elements from Mg to Ba and the lanthanide Yb atoms were investigated by means of laser-induced fluorescence spectroscopy [12], laser-excitation spectroscopy [13,14], photoassociation spectroscopy [15-18] and Fourier-transform fluorescence spectroscopy [19]. From the theoretical side, a wide literature of accurate atomic approaches for these atoms is available to benchmark molecular approaches at the long-range: methods such as CI-MBPT [20-22], CI matched with Coupled Cluster method (CI+ all order) [22-26] or evaluations of accurate atomic oscillator strengths (OS) [27] have provided results for the long-range coefficients that are nowadays considered the state-of-the-art of atomic physics calculations. Such an abundance of accurate experimental and theoretical data for the long-range properties of alkaline earth and Yb atoms provided us with a valid benchmark for our molecular results.

3.2. Computational details

All calculations were performed with the MOLPRO quantum chemistry package [28], using the restricted Coupled Cluster method with singles and doubles (CCSD) and with non-iterative triples

CCSD(T) [29] implemented for the restricted Hartree-Fock reference. The energy convergence threshold was always set to 10^{-12} a.u.

For the basis set, all-electron calculations employed the series of the augmented correlation-consistent polarized weighted-core *n*-zeta basis set aug-cc-pwCV*n*Z [30,31] contracted for the X2C scalar relativistic correction [32]. The non-relativistic (NR) calculations for Ca and Sr were performed using the same basis set; the correct NR RHF solution could not be attained for Ba. For the X2C and NR calculations of Be and Mg atoms, analogous basis sets optimized without scalar relativistic correction were used [30-31]. For Yb, the all-electron calculations employed the cc-pwCV*n*Z-X2C basis series [33]. One diffuse primitive of each orbital type with the exponent continuing the two lowest exponents of the standard basis as an even-tempered sequence was added to compensate for the lack of optimized diffuse augmentation. Different core choices were used in the CC calculations, abbreviated in Table 3.1 as the number of core electrons N_c. By inner shells, $N_c = 2$ refers to the $1s^2$ core, 10 to $1s^22s^22p^6$, 18 to $1s^22s^22p^63s^23p^6$, 28 to $1s^22s^22p^63s^23p^63d^{10}$, 36 to $1s^22s^22p^63s^23p^63d^{10}4s^24p^6$, 46 to $1s^22s^22p^63s^23p^63d^{10}4s^24p^64d^{10}$, and $N_c = 0$ means that all electrons were correlated. All abbreviations for the different core descriptions will be abbreviated according to Table 3.1.

Also the small-core effective core potentials of the Dirac-Fock level [31,34,35] were used, ECP10MDF for Ca, ECP28MDF for Sr and ECP46MDF for Ba [35], together with the aug-cc-pWCV*n*Z basis sets [31]. All the explicit electrons were always correlated; therefore, the acronym ECP-N_c in Table 3.1 and hereinafter means that N_c electrons are considered part of the pseudopotentials (or, more informally, let us say that N_c electrons are *absorbed* by the pseudopotentials). No systematically converging basis sets are available for ECP28MWB [36] or ECP28MDF [37] pseudopotentials for Yb atom to carry out the extrapolation to the CBS limit.

The results of each series calculations with increasing basis set cardinal number n were extrapolated to the CBS limit by means of the three-point mixed exponential-Gaussian formula (2.139) [38,39]. This empirical formula was chosen for its linear character, flexibility and ability to extrapolate non-energetic properties [40].

In addition to the above calculations, featured in Ref. [41], the following ab initio approaches were explored: for the scalar relativistic effects, on the atoms from Mg to Ba the Douglas-Kroll-Hess

correction was used [42,43] with the DKH Hamiltonian truncation order *k* depending on the atomic number (for Mg k = 2, for Ca k = 3, for Sr k = 4, for Ba k = 5) and the basis set optimized accordingly. The related results were extrapolated to the CBS limit by means either of formula (2.139) or of the empirical three-point two-term inverse power function reported by Martin and Taylor [44,45] (2.140). Also for these additional options, relativistic corrections, core choices and basis sets with the related cardinal number n are reported in Table 3.1.

Table 3.1. Summary of the options used in the *ab initio* calculations. The CBS entry specifies the basis set cardinal numbers used in the CBS extrapolations.

Atom	Types	N_c	Basis	CBS
Be	NR, X2C	0	aug-cc-pwCV*n*Z	T, Q, 5
Mg	NR, X2C, DKH2	0, 2	aug-cc-pwCV*n*Z	T, Q, 5
Ca	NR, X2C, DKH3	0, 2,10	aug-cc-pwCV*n*Z-X2C	T, Q, 5
			aug-cc-pwCV*n*Z	
	ECP	10	aug-cc-pwCV*n*Z-PP	T, Q, 5
Sr	NR, X2C, DKH4	2, 10, 28	aug-cc-pwCV*n*Z-X2C	D, T, Q
			aug-cc-pwCV*n*Z	
	ECP	28	aug-cc-pwCV*n*Z-PP	T, Q, 5
Ba	X2C, DKH5	10, 28,46	aug-cc-pwCV*n*Z-X2C	D, T, Q
			aug-cc-pwCV*n*Z	
	ECP	46	aug-cc-pwCV*n*Z-PP	T, Q, 5
Yb	X2C	18, 28, 36	cc-pwCV*n*Z-X2C + aug	D, T, Q

3.3. Static polarizabilities

Static dipole, quadrupole and octupole polarizabilities, respectively α_1, α_2, α_3, were computed by the finite-field (FF) method [46,47] (see Section 2.6.1). For the dipole and quadrupole fields standard MOLPRO settings were used; the octupole field was set as the $2F_{zzz} - 3F_{xxz} - 3F_{yyz}$ combination of the Cartesian components, equal to the (3,0) component of the third-rank spherical tensor operator [47], except for a normalization factor. The settings for other components returned

the same results up to normalization factors. The non-uniform symmetric field grids were tested in the CCSD(T) calculations with the basis sets having the highest cardinal number. For the dipole field a grid of 23 values was constructed, ranging the $\pm 10^{-3}$ a.u. field strength interval, with 10^{-5} a.u. as the minimum step. For the quadrupole field a grid of the same size was constructed, ranging the $\pm 3 \cdot 10^{-3}$ a.u., with $3 \cdot 10^{-6}$ a.u. as the minimum step. In contrast, the octupole field was represented by a field grid of 13 points within $\pm 5 \cdot 10^{-5}$ a.u., with the minimum step of 10^{-6} a.u. Polynomial fits up to the sixth order were used to extract the static polarizabilities. The grid sizes and intervals and the order of the fitting polynomial ensured the precision of dipole, quadrupole and octupole polarizability values up to 3, 2 and 1 significant digits, respectively. Figure 3.1 illustrates the convergence of the static polarizabilities to the CBS limit. The latter is taken as zero and the percentage deviations $|\alpha_i[n] - \alpha_i[\infty]|/\alpha_i[\infty]$ (where "n" and "∞" within square brackets refer to the basis set cardinal number and the CBS extrapolation, respectively) are shown for consecutive cardinal numbers *n*. We noticed that the higher is the order of the static polarizability *i*, the slower is the convergence in *n*. This trend is reflected also by the different axis scales. This is due to the saturation of the basis with polarization functions of the angular momenta higher than the polarizability order. Octupole polarizabilities always increase with n; quadrupole ones show a similar behavior (except for Mg and Yb), while the dipole polarizabilities always decrease upon expanding the basis set. The same trends hold for X2C and NR calculations with other core choices.

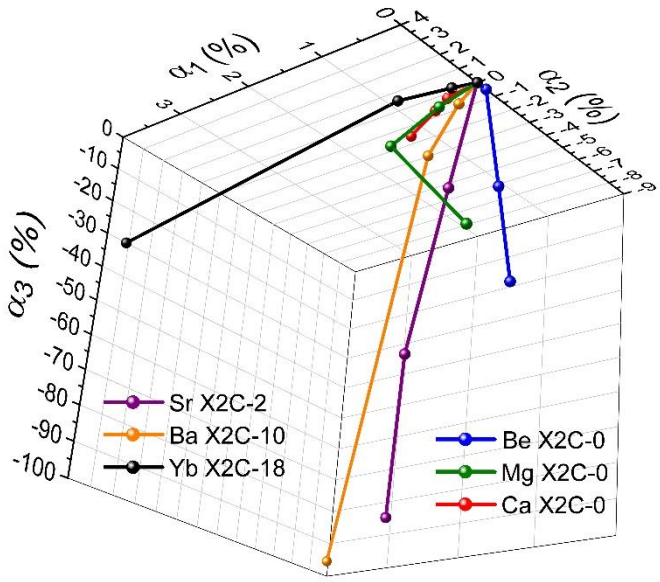

Figure 3.1. CBS limit (2.139) convergence patterns for X2C n = T, Q, 5 (Be-Ca) and n = D, T, Q (Sr, Ba, Yb) calculations. Percentage deviations from the CBS value in the static dipole, quadrupole and octupole polarizabilities are shown along the corresponding axes (reproduced from G. Visentin, and A.A. Buchachenko, J. Chem. Phys. **151**, 214302 (2019), with the permission of AIP Publishing).

Slower convergence in n, typical of quadrupole and octupole polarizabilities, make their limiting CBS values less certain, especially in the case of Sr, Ba and Yb, where the sequence n = D, T, Q is used.

In Table 3.2 the static polarizabilities values of alkaline-earth atoms at the CBS limits (2.139) and (2.140) are reported, the latter being indicated within parentheses. Our results are compared to selected literature data, among which the results of the CI+MBPT calculations by Porsev and Derevianko (PD, Ref. [20]) are included. These ones, together with the results from Ref. [48], provide our main reference for alkaline-earth atoms. In particular, for PD two result sets are shown: the "final" results from their best calculations and the "recommended" ones, in turn corresponding to the final results with the empirical corrections from experimentally known contributions from the lowest dipole-allowed $s^2\ {}^1S_0 \rightarrow sp\ {}^1P_1$ transition; details can be found in Ref. [20]. Besides these "main" reference results, we also quote the results from the compilation [27], which gives polarizability values obtained by accurate oscillator strengths (OS) evaluations.

Table 3.3 reports the static polarizabilities calculated for Yb. There final CI+MBPT results are taken from Refs. [49] and [50]. Several other theoretical data have been recently reviewed [27,51,52].

Table 3.2. Static dipole, quadrupole and octupole polarizabilities of Be-Ba atoms (a.u.). Values in parentheses among the reference data indicate the uncertainties of the last significant digit(s). For our results, values out of parentheses indicate the results achieved with CBS formula (2.139), while values in parentheses indicate the results achieved with CBS formula (2.140).

	Method	α_1	α_2	α_3
Be	X2C-0/NR-0	37.69/37.71	301.3/301.7	3740/3754
	CI-MBPT final/recommended [20]	37.76/37.76(22)	300.6(3)/-	3781/-
	OS [27]	37.73	300.4	3955
	Other theoretical results	37.73 [53]; 37.80 [54]		
Mg	X2C-2/NR-2	71.02 (71.07)/71.01	807.5 (802.869)/813.4	12461 (12864)/12561
	X2C-0/NR-0	71.15/71.63 (71.71)	807.9/814.1 (809.8)	12471/12571 (12989)
	DKH2-2	71.14 (71.08)	807.5 (802.9)	12396 (12685)
	DKH2-0	71.03 (71.00)	806.9 (803.7)	12472 (12876)
	CI-MBPT final/recommended [20]	71.33/71.3(7)	812(6)/-	13510/-
	OS [27]	71.37	811.4	14010
	Experiment	59(16) [55]; 71.5(3.1) [56]		
	Other theoretical results	71.22 [57]; 73.41 [54]	814(3) [58]	
Ca	ECP-10	156.10 (156.14)	3002.1 (3006.0)	66052 (72358)
	X2C-10/NR-10	157.61 (157.79)/	3060.8(3070.1)/	63498(63199)/
		159.81 (159.94)	3134.7 (3145.3)	64911 (64507)
	X2C-2/NR-2	157.54/159.76	3060.8/3133.8	63353/64838
	X2C-0/NR-0	156.92/159.78	3060.2/3134.8	63339/65008

Table 3.2 ***(continued)***

	Method	α_1	α_2	α_3
	DKH3-10	157.66 (157.84)	3062.2 (3071.5)	63489 (63137)
	DKH3-2	157.59 (157.77)	3059.9 (3067.9)	63388 (63037)
	CI-MBPT final/recommended [20]	159.0/157.1(1.3)	3081(23)/-	61620/-
	OS [27]	159.4	3082	65240
	Experiment	169(17) [59]		
	Other theoretical results	157.9 [57]; 158.00 [60];		
		154.58 [54]; 155.3/157.7 [61]		
Sr	ECP-28	198.62 (198.92)	4582.6 (4595.9)	112062 (120662)
	X2C-28	198.93 (197.99)	4600.2 (4603.3)	118682 (128377)
	X2C-10/NR-10	198.36(197.74) /	4601.6 (4604.2) /	118149(148254) /
		209.81 (208.04)	5137.1(4983.8)	134638 (172353)
	X2C-2/NR-2	198.36(197.74) /	4599.5 (4603.3) /	118155(147631) /
		210.09 (204.70)	5120.2(4986.3)	131371 (164836)
	DKH4-10	197.05 (196.36)	4601.2 (4603.0)	145158 (165288)
	DKH4-2	198.39 (196.90)	4600.7 (4604.7)	118180 (147631)
	CI-MBPT final/recommended [20]	202.0/197.2(2)	4630(8)/-	106400/-
	OS [27]	197.9	4643	108700

Table 3.2 ***(continued)***

	Method	α_1	α_2	α_3
	Experiment	186(15) [62]		
	Other theoretical results	198.85 [60]; 199.7 [63]; 199.71 [54]; 197.14(20) [64]	4688 [63]; 4545(120) [65]	
Ba	ECP-46	273.90 (273.73)	8579.3 (8634.3)	190047 (197224)
	X2C-46	276.98 (276.73)	8772.8 (8781.8)	188621 (181443)
	X2C-28	273.34 (260.42)	8548.9 (8560.2)	184403 (179156)
	X2C-10	273.34 (273.73)	8541.9 (8552.8)	184306 (179054)
	X2C-2	273.38 (272.98)	8531.0 (8562.2)	184302 (160669)
	DKH5-10	273.38 (272.93)	8541.5 (8551.9)	184259 (178970)
	CI-MBPT final/recommended [20]	272.1/273.5(2.0)	8900(650)/-	206000/-
	OS [27]	278.1	8789	207600
	Experiment	268(22) [59]		
	Other theoretical results	273.85 [60]; 274.92 [66]; 268.19 [54]	9100 [66]	

The results for different choices of the core demonstrate that the correlation of the inner shells generally decreases atomic polarizabilities (except for Mg, the lightest atom for which such a test is feasible, and the heaviest, Yb). However, the basis set saturation towards the CBS limit plays a more important role compared to the core correlation. Accuracy far below 1% is attained for Ca and Sr at the same core choices as accepted for the corresponding ECPs, N_c = 10 and N_c = 28 respectively. In contrast, the convergence for the Ba results at N_c = 46 reaches 1%-3%. The correlation of the innermost 28 electrons is required, in analogy with the case of Yb. All ECPs perform quite accurately on the dipole and quadrupole polarizabilities, which agree better with the converged X2C results than with the X2C results obtained with the same core choice. On one hand, this reflects the ECP adjustment, while, on the other, it indicates that the scalar relativistic corrections provided by the two approaches are comparable.

Comparison with the CI-MBPT calculations [20,49,50] shows that our dipole polarizabilities for Be-Sr underestimates the final CI-MBPT results by less than 2% and are even closer to the recommended CI-MBPT results, empirically corrected to the dominant dipole-allowed contribution [20]. The case of Ba, where our result bounds the final CI-MPBT value from above, demonstrates that such an agreement is not fortuitous.

The results for the higher-order polarizabilities are also in reasonable agreement with the final CI-MBPT values: our quadrupole polarizabilities for Be-Sr deviate from the CI-MBPT analogs by ca. 1%, while the error for Ba amounts to 4%. Deviations for octupole polarizabilities approach 11% for Sr and Ba.

Our results are also corroborated by previous calculations on the alkaline-earth metals within the CC framework: deviations of our dipole polarizability values from the analogs reported for CCSD(T) calculations with the DKH scalar relativistic correction for Mg, Ca, Sr and Ba in Refs. [57,60] fall well below 1%. Such a deviation should be mostly attributed to the CBS extrapolation. A similar reasonable agreement is achieved with the relativistic CCSD calculations by Sahoo and Das corrected to triples [54], though the latter may not be highly accurate. For Sr atom, an extensive study was carried out by Yu *et al.* [63], who recommended dipole and quadrupole polarizability values based on the error balance of the basis set saturation, core contributions and cluster expansion in the relativistic CC calculations up to the CCSDT level. Our dipole polarizability values deviate from this benchmark by -0.7%, while a larger deviation, amounting to -1.8%, occurs for the quadrupole polarizability and may indicate the increasing importance of the higher-order cluster corrections.

Correlation of the inner shells has little effect on the DKH values for the polarizabilities, regardless of the CBS extrapolation used to achieve them. These results are always less accurate compared to X2C ones, albeit the deviation decreases for the atoms with larger polarizabilities: in the case of the dipole polarizability of Sr, for instance, DKH4-2 agrees with X2C-2 and X2C-10 up to the first digit; the same is valid for the comparison between DKH5-10 and X2C-10 and X2C-28 for Ba. In this latter case, the DKH result is in better agreement with X2C-2, as those results for dipole polarizability coincide up to the second decimal digit.

The comparison of the performances of the CBS extrapolations (2.139) and (2.140) is usually in favor of the former: in fact, the latter shows a poorer and less regular convergence pattern and does not keep a uniform trend in bounding the results achieved with formula (2.139). In particular, for lighter atoms (Mg, Ca) and X2C correction, the result is generally slightly overestimated compared to analogs extrapolated with the mixed-exponential formula (2.139), whereas the trend is reversed when DKH correction is in play (though for Ca such reversal does not occur). For the Sr and Ba atoms such a trend is generally reversed, though even here formula (2.140) bounds DKH5-10 achieved with (2.139) from above, except for the octupole polarizability value.

Our estimation of the Yb dipole polarizability falls within the error bars of the conservative evaluation by Beloy [52] and the CI-MBPT calculations [49,50]. A good agreement also does exist with the all-electron CCSD(T) calculations by Thierfelder and Schwerdtfeger [67]: with the DKH scalar relativistic correction they found α_1 = 141.52 a.u., whereas with the four-component Dirac-Coulomb calculations the dipole polarizability value decreased to 140.44 a.u.; the authors thus recommended 140.7 a.u., accounting for the Gaunt correction. An extensive study of the Yb dipole polarizability was carried out by Zhang and Dalgarno [68,69] at the CCSD and CCSD(T) levels: with respect to their result for the highly saturated basis set, N_c = 18 and DKH relativistic correction, ours is 2% underestimated. A like accuracy is provided by the results available from Ref. [37], where CCSD calculations within the propagator approaches exploited the Dirac-Fock effective potential ECP28MDF, while the Wood-Boring parametrization ECP28MWB [36] tends to overestimate α_1, as also followed from Refs. [70,71].

Overall, present CCSD(T) CBS results for static dipole polarizabilities are in very good agreement with the best previous estimates and, in particular, with the results from empirically-corrected CI-MBPT calculations. The Sr atom represents the only case where the error is larger

than 0.1% (0.6%). Static quadrupole polarizabilities are generally slightly lower than those available from alternative high-level calculations.

In the best cases, DKH results slightly deviate from the related X2C results and in one case (Ba) the deviation is zero up to the second decimal digit.

On the side of CBS extrapolations, the comparison of the two result sets showed that the three-point two-term inverse power rule (2.140) performs less accurately compared to the three-point mixed exponential rule (2.139), while its convergence trend is less regular. For this reason, rule (2.139) was chosen to achieve all the subsequent results.

Table 3.3. Static dipole, quadrupole, and octupole polarizabilities of the Yb atom (a.u.). Values in parentheses indicate the uncertainties of the last significant digit(s).

	Method	α_1	α_2	α_3
Yb	X2C-36	140.54	2644.4	55209
	X2C-28	140.80	2653.3	55239
	X2C-18	140.74	2656.5	55174
	CI-MBPT final [49,50]	141(2)	2560(80)	
	Experiment	139.3(5.9) [52]; 147(20) [55]		
	Other theoretical results	151.0 [70], 142.6 [71], 143.1 [68], 140.44 [67], 144.59 [54]	2680 [69]	

3.4. Dynamic polarizabilities

The dipole and quadrupole dynamic polarizabilities as functions of imaginary frequency were computed using the CCSD polarization propagator approach [72-76] implemented in the MOLPRO package within the CCSD equation-of-motion procedure [77]. In particular, the CCSD(3) model evaluating the expansion terms of the Møller-Plesset perturbation operator up to the third order (see Chapter 2, Section 2.6.2) was employed. The calculations were performed with the basis sets introduced in Table 3.1 and with the optimal core choices. The static polarizabilities achieved with each basis set were extrapolated to the CBS limit by means of eq.

(2.139) at each point of the large non-uniform imaginary frequency $i\omega$ grid. The full tabulation of the dynamic polarizabilities computed for each imaginary frequency of the grid can be found as the supplementary material of our paper on this topic (Ref. [41]). It is worthy of mention that the X2C calculations for Yb were characterized by severe convergence problems upon solving the system of linear equations for the excitation operator. In order to address this issue, different MOLPRO options were tried for all the imaginary frequencies of the grid, except zero. The zero-frequency dynamic polarizability was thus evaluated by cubic extrapolation of the polarizabilities at the two smallest frequencies.

Figure 3.2 illustrates the percentage deviations of the CCSD-FF and CCSD(3) static dipole and quadrupole polarizabilities from the CCSD(T)-FF values. The contribution of the non-iterative triple excitations is always positive and increases with the atomic number *Z*. In contrast, CCSD(3) method always underestimates the corresponding CCSD-FF values.

Figure 3.3 exemplifies the $\alpha_1(i\omega)$ dependencies for Sr: extension of the basis towards the CBS limit decreases the dynamic polarizabilities at low imaginary frequency, but increases them at high frequencies. In both cases, present results are smaller compared to the recommended CI-MBPT [48] and OS [27] data. However, in the interval between 0.05 and 1 a.u. this trend reverses. This behavior persists in the majority of the calculations on the other atoms.

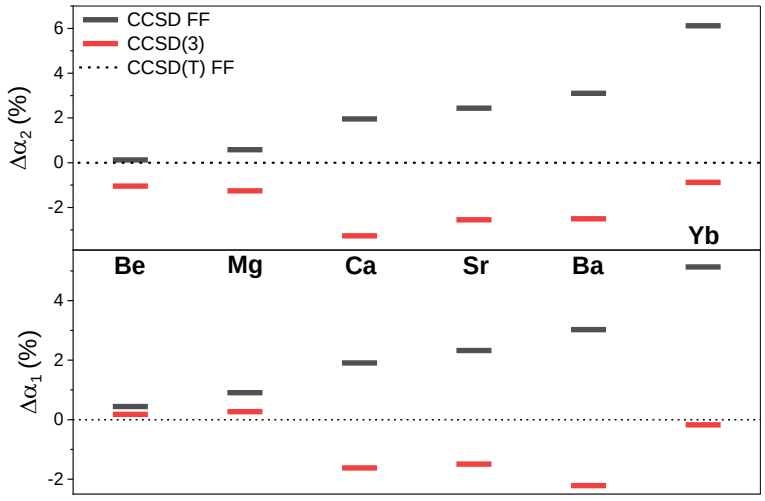

Figure 3.2. Percentage deviations of the CCSD static dipole (bottom panel) and quadrupole (top panel) polarizabilities from their CCSD(T) finite field values. The CBS extrapolations are shown for the X2C-0 (Be, Mg, and Ca), X2C-10 (Sr), and X2C-28 (Ba, Yb) calculations

(reproduced from G. Visentin, and A.A. Buchachenko, J. Chem. Phys. **151**, 214302 (2019), with the permission of AIP Publishing).

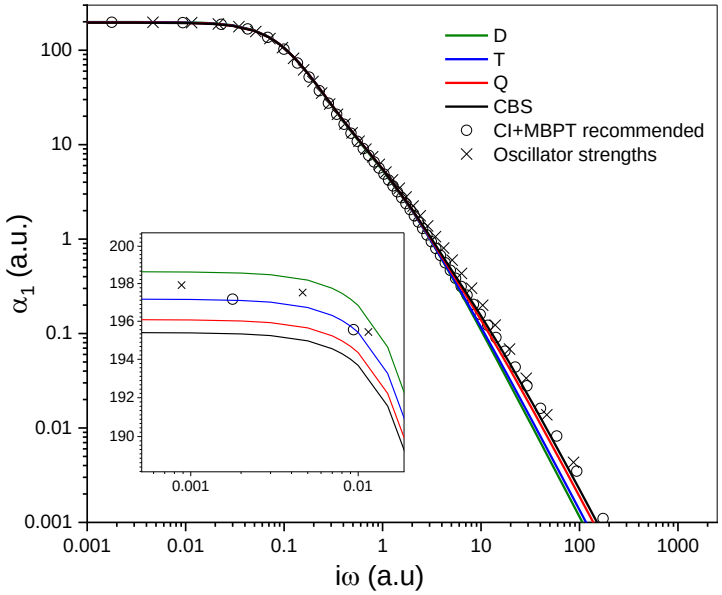

Figure 3.3. Double-logarithmic plot of the dynamic dipole polarizability α_1 ($i\omega$) for Sr. Lines show the present X2C-10 calculations and symbols—recommended CI+MBPT [48] and OS [27] data. The inset gives an expanded view of the $i\omega \to 0$ region (reproduced from G. Visentin, and A.A. Buchachenko, J. Chem. Phys. **151**, 214302 (2019), with the permission of AIP Publishing).

3.5. Dispersion coefficients

3.5.1. Introduction

For all atoms we calculated the atom-wall C_3 and the dipole-dipole and dipole-quadrupole dispersion coefficients, C_6 and C_8, respectively, both for the homonuclear and the heteronuclear case, according to eqs. (2.53-55).

For all imaginary frequency integrals we used cubic spline interpolation of the computed polarizabilities and the classical Simpson formula for a uniform mesh, allowing for a better convergence analysis. The results were checked against the Gauss-Legendre quadrature integration suggested by Amos *et al.* [78]: negligible difference in the dispersion coefficients were found, whereas the results for the atom-wall coefficient showed inconsistency up to a few percent. The integration made use of the dynamic polarizabilities extrapolated according to the CBS formula (2.139) and no extrapolation of the coefficients themselves was attempted.

3.5.2. Homonuclear case

Table 3.4 shows the results for the homonuclear interactions. The coefficients obtained with the best basis set available and those at the CBS limit (2.139) are presented together, to illustrate the effect of the basis set saturation. As before, our main reference for alkaline-earth metal atoms are the CI-MBPT calculations by Porsev and Derevianko (PD) from Refs. [20,48] and the OS results [27]. In particular, the atom-wall coefficient C_3 and the dipole-dipole dispersion coefficient C_6 are compared to the recommended results, whereas the dipole-quadrupole one C_8 takes the corresponding "final" result as its reference term. Besides these reference results, other recent theoretical data are provided [65,79,80]. Under the label "experimental" we refer to the available data coming from photoassociation spectroscopy probing the rovibrational states near the dissociation limit or from the scattering length determination in ultracold samples [11-14,16,17,19].

Figure 3.4 illustrates the percentage deviations of the selected C_6 coefficients from the recommended PD reference values [20]. Our CBS results fall within the error bars for lighter members of the series, but are out by 3% for Sr and Ba. demonstrating the level of accuracy similar to the oscillator strength summation [27].

In order to have a better comparison of the theoretical methods, we used dynamic polarizabilities tabulated in Ref. [48] and parameters of the lowest dipole-allowed $s^2\ ^1S_0 \rightarrow sp\ ^1P_1$ transitions listed in Ref. [20], to recalculate back the analogs of the final PD data (also shown in Fig.3.4). Ba atom represents the only case where the current CBS approach deviates from the "final" CI-MBPT results by more than 1%. On the other hand, available results for Sr indicate that the error bars suggested by Porsev and Derevianko basing on experimental uncertainty in the transition dipole moment are likely too narrow. In addition, with the CCSD-EOM approach [77] we computed the excitation energies and the transition dipole moments of the lowest allowed $s^2\ ^1S_0 \rightarrow sp\ ^1P_1$ transitions and their best values from Ref. [20]; then we applied this same correction to our dynamic polarizabilities: in contrast to the CI-MBPT case, our results for the C_6 coefficients worsen when such a correction is applied.

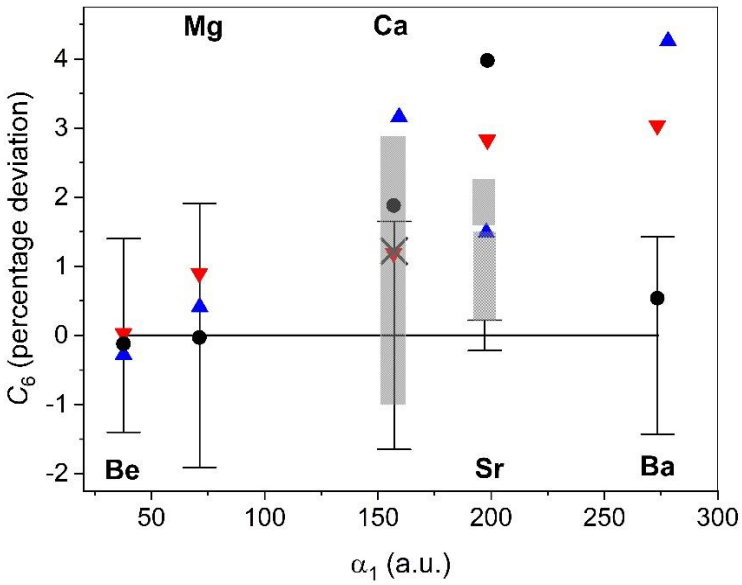

Figure 3.4. Percentage deviations of the C_6 coefficients for homonuclear dimers of the alkaline-earth metal atoms represented by their respective static dipole polarizabilities (see Table 3.2) from the reference recommended results by Porsev and Derevianko [20]. Down triangles represent CBS results (X2C-0 for Be, Mg, and Ca, X2C-10 for Sr, and X2C-28 for Ba), up triangles—the results of Ref. [27]. Circles correspond to the analogs of the final PD results recalculated here. Gray bars show experimental data from Ref. [14] for Ca and Refs. [17] and [19] for Sr. The cross marks another experimental result for Ca [16]. Absolute C_6 values are given in Table 3.4 (reproduced from G. Visentin, and A.A. Buchachenko, J. Chem. Phys. **151**, 214302 (2019), with the permission of AIP Publishing).

Table 3.4 also assesses the performance of the ECP calculations for Ca, Sr and Ba as very reasonable: resulting C_6 coefficients fortuitously turn out to be closer to the reference.

It is noteworthy that in the majority of the previous dimer calculations the long-range behavior is not quantified. However, for light alkaline-metal atoms it was analyzed in the frame of symmetry-adapted perturbation theory (SAPT) [79,80]. Resulting C_6 coefficients are systematically larger than both present and reference data. Better results were obtained by applying the coupled Kohn-Sham method for response properties [79].

Table 3.4. Dispersion coefficients for the homonuclear dimers of the alkaline-earth atoms (a.u.). In addition to the CBS data, the results for the highest *n* available (5 for Be-Ca and Q for Sr, Ba) are given in italics. Values in round parentheses indicate the uncertainties of the last significant digit(s).

	Method	C_3	C_6	C_8 (10^4)
Be	X2C-0	1.01	214.07	1.01
		1.01	*214.02*	*1.01*
	CI-MBPT [20,48]	1.01	214(3)	1.023(6)
	OS [27]	1.01	213.41	1.021
	Other theoretical results		279 [79]	
	Experiment		214 [11]	1.023 [11]
Mg	X2C-0	1.68	632.65	4.12 *4.13*
		1.68	*633.34*	
	CI-MBPT [20,48]	1.666	627(12)	4.15(5)
	OS [27]	1.704	629.59	4.1514
	Other theoretical results		721 [79]	
Ca	ECP-10	2.75	2111.6	21.33
		2.75	*2113.1*	*21.36*
	X2C-10	2.78	2144.1	21.79
		2.78	*2144.2*	*21.83*
	X2C-2	2.82	2147.7	21.79
		2.82	*2148.6*	*21.83*
	X2C-0	2.83	2146.3	21.79
		2.82	*2149.6*	*21.83*
	CI-MBPT [20,48]	2.744	2121(35)	22.3(3)
	OS [27]	2.881	2188.2	22.674
	Other theoretical results		2237 [80]; 2318 [79]; 2151 [61]	23.8433 [80]

Table 3.4 ***(continued)***

	Method	C_3	C_6	C_8 (10^4)
	Experiment		2179 [12]	28.5(5.0) [13]
			2080(7) [13]	22.21 [16]
			2141(41) [14]	
			2147 [16]	
Sr	ECP-28	3.36	3174.3	37.32
		3.36	*3175.0*	*37.32*
	X2C-28	3.36	3186.6	37.75
		3.36	*3200.2*	*37.77*
	X2C-10	3.48	3190.8	37.63
		3.45	*3205.1*	*37.71*
	CI-MBPT [20,48]	3.382	3103(7)	37.92(8)
	OS [27]	3.643	3149.3	38.352
	Other theoretical results		3142 [81]	37(1) [65]
	Experiment		3164(10) [19]	38.23 [19]
			3130(20) [17]	
Ba	ECP-46	4.21	5302.5	75.71
		4.21	*5309.5*	*76.00*
	X2C-46	4.21	5393.4	77.88
		4.22	*5421.6*	*78.30*
	X2C-28	4.47	5317.1	75.71
		4.47	*5348.5*	*76.27*
	X2C-10	4.50	5319.6	75.72
		4.49	*5350.4*	*76.27*
	CI-MBPT [20,48]	4.294	5160(74)	77.2(4.6)
	OS [27]	4.554	5379.6	78.975

Results for Yb are shown in Table 3.5. Two accurate experimental results [15,18] are in full agreement with the uncorrected CI-MBPT C_6 coefficients [49,50]. Our best calculation deviates from these reference values by almost 7%. There is more favorable agreement with experimental derivations for the C_8 coefficients. The results attained with the CCSD-based methods employing effective core potentials [69,82] logically indicate that the energy-

consistent pseudopotentials based on Dirac-Fock adjustment (ECPMDF) perform better than those based on Wood-Boring parametrization (ECPMWB).

Table 3.5. Dispersion coefficients for the Yb dimer (a.u.). In addition to the present CBS data, the results for the augmented cc-pwCVQZ basis are given in italics. Values in round parentheses indicate the uncertainties of the last significant digit(s).

	Method	C_3	C_6	C_8 (10^4)
Yb	X2C-36	3.41 *3.41*	2048.1 *2056.0*	19.75 *19.79*
	X2C-28	3.60 *3.60*	2065.4 *2069.4*	19.82 *19.85*
	X2C-18	3.52 *3.52*	2060.1 *2065.1*	19.78 *19.81*
	CI+MBPT final [49,50]		1929(39)	18.8(6)
	Other theoretical results	3.4 [69]	2085 [69]	20.23 [69]
			2568 [82]	
	Experiment		1933.5(2.2) [15],	21.72(65) [15],
			1932(30) [18]	19(5) [18]

3.5.3. Heteronuclear case

Table 3.6 reports the results for the heteronuclear dispersion coefficients. Comparison with the CI-MBPT data for the heteronuclear dipole-dipole dispersion coefficients (recommended for alkaline-earth dimers [48], original for the dimers of Yb [49]) is in line with the above analysis, with the increase of the dipole dispersion interaction as the atomic number Z increases. The heteronuclear dipole-quadrupole dispersion coefficients present an opposite trend (see Table 3.6).

Table 3.6. Dispersion coefficients for the heteronuclear dimers of the Be-Ba and Yb atoms (a.u.). The present CBS data for C_6 and C_8 coefficients are given in the upper-right and lower-left triangles, respectively. The recommended CI-MBPT results from Refs. [48] and [49] (final, for dimers involving Yb) are shown in italic with values in round parentheses indicating the uncertainties of the last significant digit(s).

C_6 / C_8 (10^4)	Be X2C0	Mg X2C0	Ca X2C2	Sr X2C10	Ba X2C28	Yb X2C28
Be X2C0	…	366	654	798	1018	656
		364(4)	*652(7)*	*782(6)*	*992(9)*	
Mg X2C0	1.20	…	1145	1395	1789	1138
			1138(14)	*1369(13)*	*1742(21)*	*1092*
Ca X2C2	3.36	5.91	…	2600	3346	2077
				2564(21)	*3294(36)*	*2024*
Sr X2C10	4.75	8.31	15.38	…	4114	2549
					3994(29)	*2435*
Ba X2C28	7.21	12.71	23.93	29.36	…	3272
Yb X2C28	1.52	3.67	10.68	15.07	23.24	…

3.6. Retardation functions

Retardation functions for the homonuclear dispersion interaction were calculated for the dipole-dipole ((see eq. (2.57)) and the dipole-quadrupole interaction (see eq. (2.58)) [69]. The results, computed with the selected sets of dynamic polarizabilities are shown in Figure 3.5. The complete tabulations of these functions are available as a supplementary material of our paper (Ref. [41]). The larger is the static polarizability, the softer is the crossover to the retarded asymptotic behavior. The figure also compares the present results for the Yb dimer with the calculations by Zhang and Dalgarno [69]. Up to 10^4 a_0 the deviations of the former from the latter is smaller than 1%. Conversely, at longer distances the divergence reaches 20%. The retardation effect on the dipole-dipole dispersion interaction in the Ca dimer was also considered in the frame of the Cowan-Griffin correction [61,80]. Our results perfectly agree with these calculations: the mismatch increases with the distance up to 0.5% at 1000 a_0.

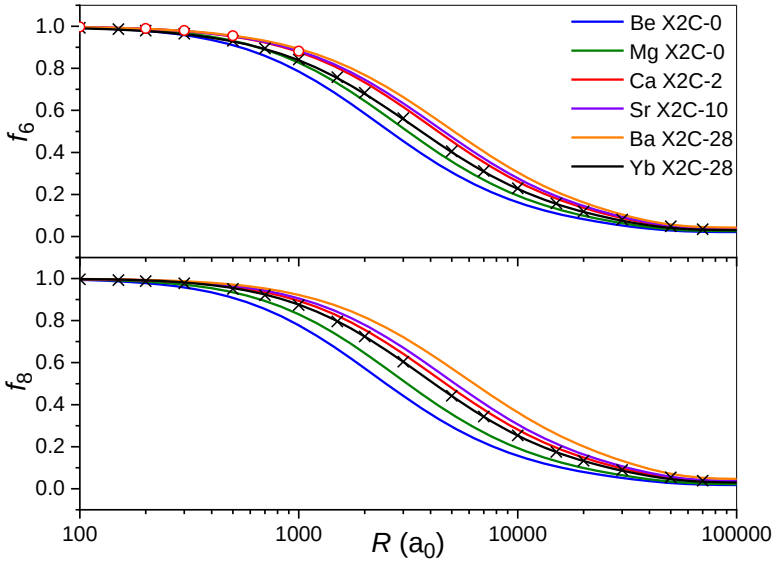

Figure 3.5. Retardation functions for dipole (top panel) and quadrupole (bottom panel) dispersion interactions. Lines correspond to the present calculations, circles and crosses – to the results of Moszynski et al. [61] for Ca_2 and Zhang and Dalgarno [69] for Yb_2, respectively (reproduced from G. Visentin, and A.A. Buchachenko, J. Chem. Phys. **151**, 214302 (2019), with the permission of AIP Publishing).

Given the non-retarded long-range interaction potential truncated to the dipole-quadrupole term,

$$U_{LR} \approx -\frac{C_6}{R^6} - \frac{C_8}{R^8}, \tag{3.1}$$

and its retarded analog from eq, (2.56),

$$U_{LR} \approx -\frac{C_6 f_6(R)}{R^6} - \frac{C_8 f_8(R)}{R^8}, \tag{3.2}$$

the ratios of the latter to the leading term of the former, $-C_6/R^6$, are plotted as functions of the internuclear distance in Figure 3.6. Two approximations to the long-range interaction are close to each other in a relatively narrow range of distances, 80-140 a_0. At shorter internuclear separations the effect of the dipole-quadrupole dispersion term may not be neglected; by contrast, at longer distances the retardation of the dipole-dipole interaction is preponderant. The inset in Figure 3.6 provides an enlarged view of the region of apparent validity of the pure dipole dispersion approximation. Evidently the characteristic dispersion interaction lengths $(2mC_6)^{1/4}$ (the standard atomic weights were taken into account here to evaluate the reduced mass m) marked by the vertical lines quite accurately (better than 3%) define the separations

where the simple C_6/R^6 representation of the long-range potential (the "molecular approach" representation) works well.

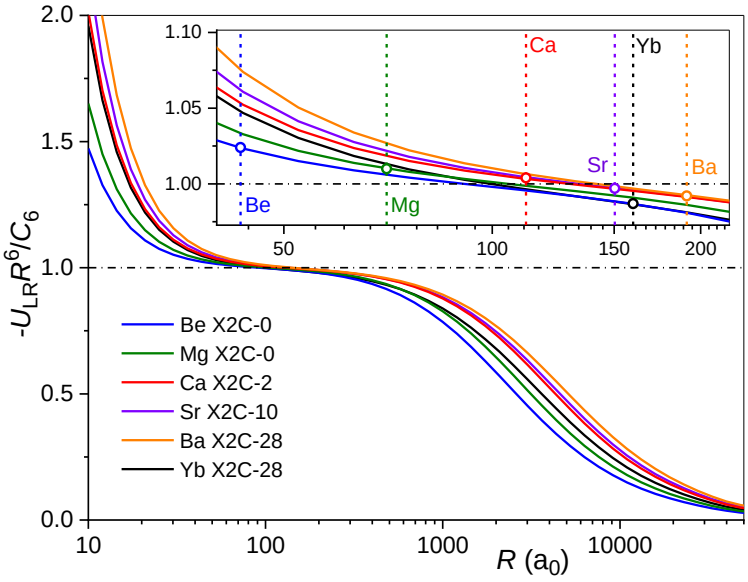

Figure 3.6. The ratios of retarded long-range interaction to the leading nonretarded C_6/R^6 term as functions of the internuclear distance. The inset expands the region of close similarity between the two long-range expansions (reproduced from G. Visentin, and A.A. Buchachenko, J. Chem. Phys. **151**, 214302 (2019), with the permission of AIP Publishing).

3.7. Conclusions

A systematic study of the electric properties controlling the long-range interactions within conventional restricted Coupled Cluster framework, namely, CCSD, CCSD(T) and related polarization propagator CCSD(3) methods, is performed for the first time at the limit of the saturated basis set, converged core correlation and exact two-component approximation for relativistic effects. Comparison between different computational schemes, as well as with special methods for atomic calculations, provides useful conclusions and recommendations.

Static polarizabilities computed by the finite-field method provide a rigorous test on the validity of the CCSD(T) method. Our best results for the dipole polarizability lie between the original and the empirically corrected CI-MBPT results and are in excellent agreement with the oscillator strength summations and critical evaluations of experimental data. A 1% deviation is likely due to higher-order cluster contributions, X2C approximation for the relativistic effects and uncertainty of the complete basis set extrapolation. Static polarizability calculations indicate that, at zero frequency, the CCSD(3) polarization propagator approach

overcompensates the correction to triple excitations, thus underestimating not only CCSD, but also CCSD(T)-FF results. Comparisons with the literature data demonstrate that this same relation does not hold uniformly for finite imaginary frequencies. As a consequence, the lowest-order dimer dispersion coefficients C_6 derived from the CCSD(3) dynamic polarizabilities turn out to be larger compared to the reference CI-MBPT values [20]. The deviation increases along the Be-Ba sequence up to 3%, although experimental estimations available for Ca [14,16] and Sr [17,19] are in better accord with our results. In particular, the lightest members of the series (Be-Ca) fall within the error bars of the recommended state-of-the-art atomic calculations; conversely, for Sr and Ba the percentage deviation is larger than 3% and approaches 7% for Yb. The trend reverses for the C_8 coefficients, with the underestimation of the same reference by up to 2% (Ba). For Yb, the present C_8 coefficient is in better agreement with respect to the experimental derivations.

It is worthy of mention that the present results for the heaviest atoms, Sr, Ba and Yb, are subjected to an extra uncertainty in the CBS extrapolations, that cover the cardinal numbers from 2 to 4. In addition, the results for Yb may be affected by non-optimal diffuse augmentation. Usually, the basis set cardinal numbers n = 4 or 5 are enough to converge dipole and quadrupole polarizabilities within 2% and 1%, respectively, while the octupole polarizability is characterized by worse convergence.

The comparison between extrapolations (2.139) and (2.140) for the static polarizabilities, shows that the two CBS formulae provides similar deviations from the "final" atomic results [20]. Usually, for the lighter elements of the series, eq. (2.140) provides a slightly smaller deviation compared to eq. (2.139). However, the trend is reversed when the comparison is carried out with respect to the recommended results. For the heaviest alkaline-earth atoms Sr and Ba, eq. (2.139) performs better both with respect to the "final" and the recommended atomic values, not only with regard to the percentage deviation, but even for the convergence pattern. Regarding the former, the case of Ba is particularly striking: there, for the X2C-28 dipole static polarizability (see Table 3.2), the result achieved with eq. (2.139) is affected by ca. 0.5% deviation with respect to the reference "final" results [20], while for the analog achieved with eq. (2.140) the percentage deviation amounts to ca. 4.3%. With respect to the "recommended" reference results [20], percentage deviation due to eq. (2.139) decreases to ca. 0.1%, whereas deviation due to eq. (2.140) grows to ca. 4.8%.

Assessment of the inner-shell correlation of the $(m-1)$ and m shells (where m stands for the principal quantum number of the outer s^2 shell) provides good accuracy, with the exception of

Ba, where also the $(m-2)$ should be correlated. The same level is recommended for atomic Yb, albeit keeping the $4s^2 4p^6$ orbitals in the core space is tolerable. The small-core Dirac-Fock based ECPs (ECPMDF) perform accurately even in the case of Ba if all explicit electrons are correlated. These conclusions are generally confirmed by the calculations of other properties.

Estimates of the percentage deviation on the C_6 and C_8 values for the finite basis set at n = 5 show that, for the former, these are usually close to the CBS analogs up to the first significant digit, though larger. This proves the crucial role of basis set saturation in ensuring the accurate performance of the molecular approach on the long-range coefficients of these atomic systems.

The level of accuracy for retardation functions computed with the CCSD(3) dynamic polarizabilities should be more or less the same as for dispersion coefficients. At least, comparison with the literature data available for Ca_2 and Yb_2 confirms such a supposition. Our analysis of the retarded dispersion interactions shows that the pure non-retarded dipole dispersion approximation, C_6/R^6, holds in a quite narrow range of internuclear distances, that becomes as narrower as the atomic number Z increases. Extraction of the C_6 coefficient from the dimer calculations makes sense at the distances close to the characteristic length of $(2mC_6)^{1/4}$.

In summary, the overall accuracy of the ab initio approaches tested here for the long-range interactions of alkaline-earth metals can be estimated at no better than 5%, from a very conservative viewpoint. At this level our results could be useful as an extra reference for the evaluation of experimental and theoretical data. From a theoretical point of view, they are also useful for selecting improved ab initio schemes for molecular calculations aiming to cover long-range regions of the global potential or potential energy surface.

References

[1] N.J. van Druten, C.G. Townsend, M.R. Andrews, D.S. Durfce, D.M. Kurn, M. –O. Mewes, and W. Ketterle, *Bose-Einstein condensates- a new form of quantum matter,* Czech. J. Phys. **46**, 3077-3088 (1996); doi: 10.1007/BF02548113.

[2] B. DeMarco, J. Bohn, E. Cornell, *Deborah S. Jin 1968–2016. Nature* **538,** 318 (2016); doi: 10.1038/538318a.

[3] C.A. Regal, M. Greiner, and D.S. Jin, *Observation of Resonance Condensation of Fermionic Atom Pairs*, Phys. Rev. Lett. **92**, 040403 (2004); doi: 10.1103/PhysRevLett.92.040403.

[4] M. Borkowski, A. A. Buchachenko, R. Ciuryło, P. S. Julienne, H. Yamada, Y. Kikuchi, K. Takahashi, Y. Takasu, and Y. Takahashi, *Beyond-Born-Oppenheimer effects in sub-kHz-*

precision photoassociation spectroscopy of ytterbium atoms, Phys. Rev. A **96**, 063405 (2017); doi: 10.1103/PhysRevA.96.063405.

[5] C. Chin, R. Grimm, P. Julienne, and E. Tiesinga, *Feshbach resonances in ultracold gases*, Rev. Mod. Phys. **82**, 1225; doi: 10.1103/RevModPhys.82.1225.

[6] T. V. Tscherbul, J. Kłos, A. Dalgarno, B. Zygelman, Z. Pavlovic, M. T. Hummon, H.-I. Lu, E. Tsikata, and J. M. Doyle, *Collisional properties of cold spin-polarized nitrogen gas: Theory, experiment, and prospects as a sympathetic coolant for trapped atoms and molecules,* Phys. Rev. A **82**, 042718 (2010); doi: 10.1103/PhysRevA.82.042718.

[7] G. F. Gribakin and V. V. Flambaum, *Calculation of the scattering length in atomic collisions using the semiclassical approximation,* Phys. Rev. A **48**, 546 (1993); doi: 10.1103/PhysRevA.48.546.

[8] C. Douketis, G. Scoles, S. Marchetti, M. Zen, and A. J. Thakkar, *Intermolecular forces via hybrid Hartree–Fock–SCF plus damped dispersion (HFD) energy calculations. An improved spherical model*, J. Chem. Phys. **76**, 3057 (1982); doi: 10.1063/1.443345

[9] K. T. Tang and P. Toennies, *An improved simple model for the van der Waals potential based on universal damping functions for the dispersion coefficients*, J. Chem. Phys. **80**, 3726 (1984); doi: 10.1063/1.447150.

[10] R. J. LeRoy, *dPotFit: A computer program to fit diatomic molecule spectral data to potential energy functions*, J. Quant. Spectrosc. Radiat. Transfer **186**, 179 (2017); doi: 0.1016/j.jqsrt.2016.06.002.

[11] V. V. Meshkov, A. V. Stolyarov, M. C. Heaven, C. Haugen, and R. J. LeRoy, *Direct-potential-fit analyses yield improved empirical potentials for the ground $X^1\,\Sigma_g^+$ state of Be_2,* J. Chem. Phys. **140**, 064315 (2014); doi: 10.1063/1.4864355.

[12] C. R. Vidal, *The molecular constants and potential energy curves of the Ca_2 $A\,^1\Sigma^+_u$–$X\,^1\Sigma^+_g$ system from laser induced fluorescence,* J. Chem. Phys. **72**, 1864 (1980); doi: 10.1063/1.439331.

[13] O. Allard, C. Samuelis, A. Pashov, H. Knockel, and E. Tiemann, *Experimental study of the Ca_2 $^1S+^1S$ asymptote,* Eur. Phys. J. D **26**, 155 (2003); doi: 10.1140/epjd/e2003-00208-4.

[14] R. J. LeRoy and R. D. E. Henderson, *A new potential function form incorporating extended long-range behaviour: application to ground-state Ca_2,* Mol. Phys. **105**, 663 (2007); doi: 10.1080/00268970701241656.

[15] M. Borkowski, A. A. Buchachenko, R. Ciuryło, P. S. Julienne, H. Yamada, Y. Kikuchi, K. Takahashi, Y. Takasu, and Y. Takahashi, *Beyond-Born-Oppenheimer effects in sub-kHz-*

precision photoassociation spectroscopy of ytterbium atoms, Phys. Rev. A **96**, 063405 (2017); doi: 10.1103/PhysRevA.96.063405.

[16] E. Pachomow, V. P. Dahlke, E. Tiemann, F. Riehle, and U. Sterr, *Ground-state properties of Ca2 from narrow-line two-color photoassociation,* Phys. Rev. A **95**, 043422 (2017); doi: 10.1103/PhysRevA.95.043422.

[17] Y. N. Martinez de Escobar, P. G. Mickelson, P. Pellegrini, S. B. Nagel, A. Traverso, M. Yan, R. Cote, and T. C. Killian, *Two-photon photoassociative spectroscopy of ultracold* ^{88}Sr, Phys. Rev. A **78**, 062708 (2008); doi: 10.1103/PhysRevA.78.062708.

[18] M. Kitagawa, K. Enomoto, K. Kasa, Y. Takahashi, R. Ciuryło, P. Naidon, and P. S. Julienne, *Two-color photoassociation spectroscopy of ytterbium atoms and the precise determinations of s-wave scattering lengths,* Phys. Rev. A **77**, 012719 (2008); doi: 10.1103/PhysRevA.77.012719.

[19] A. Stein, H. Knockel, and E. Tiemann, *The* $^1S+^1S$ *asymptote of* Sr_2 *studied by Fourier-transform spectroscopy*, Eur. Phys. J. D **57**, 171 (2010); doi: 10.1140/epjd/e2010-00058-y.

[20] S.G. Porsev, A. Derevianko, *High-Accuracy Calculations of Dipole, Quadrupole, and Octupole Electric Dynamic Polarizabilities and van der Waals Coefficients* C_6, C_8, *and* C_{10} *for Alkaline-Earth Dimers,* JETP,**102**, 2 (2006); doi: 10.1134/S1063776106020014.

[21] V. A. Dzuba, V. V. Flambaum, and M. G. Kozlov, *Combination of the many-body perturbation theory with the configuration-interaction method,* Phys. Rev. A **54**, 3948 (1996); doi: 10.1103/PhysRevA.54.3948.

[22] M. S. Safronova and W. R. Johnson, *All-Order Methods for Relativistic Atomic Structure Calculations,* Adv. At., Mol., Opt. Phys. **55**, 191 (2008); doi: 10.1016/S1049-250X(07)55004-4.

[23] M. G. Kozlov, *Precision calculations of atoms with few valence electrons,* Int. J. Quantum Chem. **100**, 336 (2004); doi: 10.1002/qua.20127.

[24] M. S. Safronova, M. G. Kozlov, W. R. Johnson, and D. Jiang, *Development of a configuration-interaction plus all-order method for atomic calculations,* Phys. Rev. A **80**, 012516 (2009); doi: 10.1103/PhysRevA.80.012516.

[25] M. S. Safronova, M. G. Kozlov, and C. W. Clark, *Precision Calculation of Blackbody Radiation Shifts for Optical Frequency Metrology,* Phys. Rev. Lett. **107**, 143006 (2011); doi: 10.1103/PhysRevLett.107.143006.

[26] M. S. Safronova, S. G. Porsev, M. G. Kozlov, and C. W. Clark, *Polarizabilities of* Si_2^+*: A benchmark test of theory and experiment,* Phys. Rev. A **85**, 052506 (2012); doi: 10.1103/PhysRevA.85.052506.

[27] J. Jiang, J. Mitroy, Y. Cheng, and M. W. J. Bromley, *Effective oscillator strength distributions of spherically symmetric atoms for calculating polarizabilities and long-range atom–atom interactions*, At. Data Nucl. Data Tables **101**, 158 (2015); doi: 10.1016/j.adt.2014.10.001.

[28] H.-J. Werner, P. J. Knowles, G. Knizia, F. R. Manby, and M. Schutz, "Molpro: A general-purpose quantum chemistry program package," Wiley Interdiscip. Rev.: Comput. Mol. Sci. **2**, 242 (2012).

[29] P. J. Knowles, C. Hampel, and H.-J. Werner, *Coupled cluster theory for high spin, open shell reference wave functions,* J. Chem. Phys. **99**, 5219 (1993); doi: 10.1063/1.465990; Erratum, **112**, 3106 (2000); doi: 10.1063/1.480886.

[30] J. G. Hill and K. A. Peterson, *Correlation consistent basis sets for explicitly correlated wavefunctions: valence and core–valence basis sets for Li, Be, Na, and Mg*, Phys. Chem. Chem. Phys. **12**, 10460 (2010); doi: 10.1039/C0CP00020E.

[31] J. G. Hill and K. A. Peterson, *Gaussian basis sets for use in correlated molecular calculations. XI. Pseudopotential-based and all-electron relativistic basis sets for alkali metal (K–Fr) and alkaline earth (Ca–Ra) elements*, J. Chem. Phys. **147**, 244106 (2017); doi: 10.1063/1.5010587.

[32] D. Peng, M. Reiher, *Exact decoupling of the relativistic Fock operator,* Theor.Chem.Acc. **131**:1081 (2012); doi: 10.1007/s00214-011-1081-y.

[33] Q. Lu and K. A. Peterson, *Correlation consistent basis sets for lanthanides: The atoms La–Lu,* J. Chem. Phys. **145**, 054111 (2016); doi: 10.1063/1.4959280.

[34] M. Dolg, in Relativistic Electronic Structure Theory: Part 1, edited by P. Schwerdtfeger (Elsevier, Amsterdam, 2002), p. 793.

[35] I. S. Lim, H. Stoll, and P. Schwerdtfeger, *Relativistic small-core energy-consistent pseudopotentials for the alkaline-earth elements from Ca to Ra*, J. Chem. Phys. **124**, 034107 (2006); doi: 10.1063/1.2148945.

[36] M. Doll, H. Stoll, and H. Preuss, *Energy-adjusted ab initio pseudopotentials for the rare earth elements,* J. Chem. Phys. **90**, 1730 (1989); doi: 10.1063/1.456066.

[37] Y. Wang and M. Dolg, *Pseudopotential study of the ground and excited states of* Yb_2, Theor. Chem. Acc., **100**, 124 (1998); doi: 10.1007/s002140050373.

[38] K. A. Peterson, D. E. Woon, and T. H. Dunning, Jr., *Benchmark calculations with correlated molecular wave functions. IV. The classical barrier height of the* $H+H_2 \rightarrow H_2+H$ *reaction,* J. Chem. Phys. **100**, 7410 (1994); doi: 10.1063/1.466884.

[39] D. Feller and J. A. Sordo, *A CCSDT study of the effects of higher order correlation on spectroscopic constants. I. First row diatomic hydrides,* J. Chem. Phys. **112**, 5604 (2000); doi: 10.1063/1.481135.

[40] M. P. de Lara-Castells, R. V. Krems, A. A. Buchachenko, G. Delgado-Barrio, and P. Villareal, *Complete basis set extrapolation limit for electronic structure calculations: Energetic and nonenergetic properties of HeBr and $HeBr_2$ van der Waals dimers,* J. Chem. Phys. **115**, 10438 (2001); doi: 10.1063/1.1415078.

[41] G. Visentin and A.A. Buchachenko, *Polarizabilities, dispersion coefficients, and retardation functions at the complete basis set CCSD limit: From Be to Ba plus Yb,* J. Chem. Phys. **151**, 214302 (2019); doi: 10.1063/1.5129583.

[42] M. Reiher, A. Wolf, *Exact decoupling of the Dirac Hamiltonian. I. General theory,* J. Chem. Phys., Vol. 121, No. 5, 1 (2004); doi: 10.1063/1.1768160.

[43] M. Reiher, A. Wolf, *Exact decoupling of the Dirac Hamiltonian. II. The generalized Douglas–Kroll–Hess transformation up to arbitrary order*, J. Chem. Phys. **121**, 10945 (2004); doi: 10.1063/1.1818681.

[44] J. M. L. Martin, *The total atomization energy and heat of formation of HCN(g),* Chem. Phys. Lett. **259**, 679 (1996); doi: 10.1016/0009-2614(96)00899-8.

[45] J. M. L. Martin and P. R. Taylor, *Benchmark quality total atomization energies of small polyatomic molecules,* J. Chem. Phys. **106**, 8620 (1997); doi: 10.1063/1.473918.

[46] H. D. Cohen and C. C. J. Roothaan, *Electric Dipole Polarizability of Atoms by the Hartree—Fock Method. I. Theory for Closed-Shell Systems,* J. Chem. Phys. **43**, S34 (1965); doi: 10.1063/1.1701512.

[47] D. M. Elking, L. Perera, R. Duke, T. Darden, and L. G. Pedersen, *A finite field method for calculating molecular polarizability tensors for arbitrary multipole rank,* Comput. Chem. **32**, 3283 (2011); doi: 10.1002/jcc.21914.

[48] A. Derevianko, S. G. Porsev, and J. F. Babb, *Electric dipole polarizabilities at imaginary frequencies for hydrogen, the alkali–metal, alkaline–earth, and noble gas atoms*, At. Data Nucl. Data Tables **96**, 323 (2010); doi: 10.1016/j.adt.2009.12.002.

[49] M. S. Safronova, S. G. Porsev, and C. W. Clark, *Ytterbium in Quantum Gases and Atomic Clocks: van der Waals Interactions and Blackbody Shifts,* Phys. Rev. Lett. **109**, 230802. (2012); doi: 10.1103/PhysRevLett.109.230802.

[50] S. G. Porsev, M. S. Safronova, A. Derevianko, and C. W. Clark, *Long-range interaction coefficients for ytterbium dimers,* Phys. Rev. A **89**, 012711 (2014); doi: 10.1103/PhysRevA.89.012711.

[51] P. Schwerdtfeger and J. K. Nagle, *2018 Table of static dipole polarizabilities of the neutral elements in the periodic table*, Mol. Phys. **117**, 1200 (2019); doi: 10.1080/00268976.2018.1535143.

[52] K. Beloy, *Experimental constraints on the polarizabilities of the 6s2 $^1S0$ and 6s6p $^3P^o_0$ states of Yb*, Phys. Rev. A **86**, 022521 (2012); doi: 10.1103/PhysRevA.86.022521.

[53] D. Tunega, J. Noga, and W. Klopper, *Basis set limit value for the static dipole polarizability of beryllium,* Chem. Phys. Lett. **269**, 435 (1997); doi: 10.1016/S0009-2614(97)00301-1.

[54] B. K. Sahoo and B. P. Das, *Relativistic coupled-cluster studies of dipole polarizabilities in closed-shell atoms*, Phys. Rev. A **77**, 062516 (2008); doi: 10.1103/PhysRevA.77.062516.

[55] L. Ma, J. Indergaard, B. Zhang, I. Larkin, R. Moro, and W. A. de Heer, *Measured atomic ground-state polarizabilities of 35 metallic elements*, Phys. Rev. A **91**, 010501 (2015); doi: 10.1103/PhysRevA.91.010501.

[56] L. Lundin, B. Engman, J. Hilke, and I. Martinson, *Lifetime Measurements in Mg I-Mg IV*, Phys. Scr. **8**, 274 (1973); doi: 10.1088/0031-8949/8/6/009.

[57] A. J. Thakkar and C. Lupinetti, in Theoretical Approaches to the Calculation of Electric Polarizability: Atoms, Molecules and Clusters in Electric Fields, edited by G. Maroulis (Imperial College Press, London, 2006), p. 505.

[58] S. G. Porsev, M. S. Safronova, and M. G. Kozlov, *Calculation of quadrupole polarizabilities with combined configuration interaction and coupled-cluster method*, Phys. Rev. A **85**, 062517 (2012); doi: 10.1103/PhysRevA.85.062517.

[59] H. L. Schwartz, T. M. Miller, and B. Bederson, *Measurement of the static electric dipole polarizabilities of barium and strontium*, Phys. Rev. A **10**, 1924 (1974); doi: 10.1103/PhysRevA.10.1924.

[60] I. Lim and P. Schwerdtfeger, *Four-component and scalar relativistic Douglas-Kroll calculations for static dipole polarizabilities of the alkaline-earth-metal elements and their ions from Ca^n to Ra^n (n=0,+1,+2)*, Phys. Rev. A **70**, 062501 (2004); doi: 10.1103/PhysRevA.70.062501.

[61] R. Moszynski, G. Łach, M. Jaszunski, and B. Bussery-Honvault, *Long-range relativistic interactions in the Cowan-Griffin approximation and their QED retardation: Application to helium, calcium, and cadmium dimers*, Phys. Rev. A **68**, 052706 (2003); doi: 10.1103/PhysRevA.68.052706.

[62] T. M. Miller and B. Bederson, *Atomic and Molecular Polarizabilities-A Review of Recent Advances*, Adv. At. Mol. Phys. **13**, 1 (1978); doi: 10.1016/S0065-2199(08)60054-8.

[63] Y.-M. Yu, B.-B. Suo, H.-H. Feng, H. Fan, and W.-M. Liu, *Finite-field calculation of static polarizabilities and hyperpolarizabilities of In^+ and Sr,* Phys. Rev. A **92**, 052515 (2015); doi: 10.1103/PhysRevA.92.052515.

[64] M. S. Safronova, S. G. Porsev, U. I. Safronova, M. G. Kozlov, and C. W. Clark, *Blackbody-radiation shift in the Sr optical atomic clock,* Phys. Rev. A **87**, 012509 (2013); doi: 10.1103/PhysRevA.87.012509.

[65] S. G. Porsev, M. S. Safronova, and C. W. Clark, *Relativistic calculations of C6 and C8 coefficients for strontium dimers,* Phys. Rev. A **90**, 052715 (2014); doi: 10.1103/PhysRevA.90.052715.

[66] A. A. Buchachenko and L. A. Viehland, *Interaction potentials and transport properties of Ba, Ba^+, and Ba^{2+} in rare gases from He to Xe,* J. Chem. Phys. **148**, 154304 (2018); doi: 10.1063/1.5025861.

[67] C. Thierfelder and P. Schwerdtfeger, *Effect of relativity and electron correlation in static dipole polarizabilities of ytterbium and nobelium,* Phys. Rev. A **79**, 032512 (2009); doi: 10.1103/PhysRevA.79.032512.

[68] P. Zhang and A. Dalgarno, *Static Dipole Polarizability of Ytterbium,* J. Phys. Chem. A **111**, 12471 (2007); doi: 10.1021/jp0750856.

[69] P. Zhang and A. Dalgarno, *Long-range interactions of ytterbium atoms,* Mol. Phys. **106**, 1525 (2008); doi: 10.1080/00268970802126608.

[70] A. A. Buchachenko, G. Chałasinski, and M. M. Szczesniak, *Diffuse basis functions for small-core relativistic pseudopotential basis sets and static dipole polarizabilities of selected lanthanides La, Sm, Eu, Tm and Yb,* Struct. Chem. **18**, 769 (2007); doi: 10.1007/s11224-007-9243-1.

[71] A. A. Buchachenko, *Ab initio dipole polarizabilities and quadrupole moments of the lowest excited states of atomic Yb,* Eur. J. Phys. D **61**, 291 (2011); doi: 10.1140/epjd/e2010-10413-7.

[72] T. Korona, M. Przybytek, and B. Jeziorski, *Time-independent coupled cluster theory of the polarization propagator. Implementation and application of the singles and doubles model to dynamic polarizabilities and van der Waals constants,*Mol. Phys. **104**, 2303 (2006); doi: 10.1080/00268970600673975.

[73] B. Jeziorski and R. Moszynski, *Explicitly connected expansion for the average value of an observable in the coupled-cluster theory,* Int. J. Quantum Chem. **48**, 161 (1993); doi: 10.1002/qua.560480303.

[74] T. Korona and B. Jeziorski, *One-electron properties and electrostatic interaction energies from the expectation value expression and wave function of singles and doubles coupled cluster theory*, J. Chem. Phys. **125**, 184109 (2006); doi: 10.1063/1.2364489.

[75] R. Moszinski, P.S. Żukovski, B. Jeziorski, *Time-Independent Coupled-Cluster Theory of the Polarization Propagator;* Collect. Czech. Chem. Commun. (Vol.70) (2005); doi: 10.1135/cccc20051109.

[76] T. Korona, *The effect of local approximations on first-order properties from expectation-value coupled cluster theory*, Theor. Chem. Acc. **129**, 15 (2011); doi: 10.1007/s00214-010-0872-x.

[77] T. Korona, H. J. Werner, *Local treatment of electron excitations in the EOM-CCSD method*, J. Chem. Phys. **118**, 3006 (2003); doi: 10.1063/1.1537718.

[78] R. D. Amos, N. C. Handy, P. J. Knowles, J. E. Rice, and A. J. Stone, *AB-initio prediction of properties of carbon dioxide, ammonia, and carbon dioxide...ammonia*, J. Phys. Chem. **89**, 2186 (1985); doi: 10.1021/j100257a010.

[79] K. Patkowski, R. Podeszwa, and K. Szalewicz, *Interactions in Diatomic Dimers Involving Closed-Shell Metals*, J. Phys. Chem. A **111**, 12822 (2007); doi: 10.1021/jp076412c.

[80] B. Bussery-Honvault, J. M. Launay, and R. Moszynski, *Cold collisions of ground-state calcium atoms in a laser field: A theoretical study*, Phys. Rev. A **68**, 032718 (2003); doi: 10.1103/PhysRevA.68.032718.

[81] W. Skomorowski, F. Pawlowski, C. P. Koch, and R. Moszynski, *Rovibrational dynamics of the strontium molecule in the* $A^1\,\Sigma_u^+$, $c^3\Pi_u$, *and* $a^3\,\Sigma_u^+$ *manifold from state-of-the-art ab initio calculations*, J. Chem. Phys. **136**, 194306 (2012); doi: 10.1063/1.4713939.

[82] A. A. Buchachenko, G. Chałasinski, and M. M. Szczesniak, *Interactions of lanthanide atoms: Comparative ab initio study of YbHe,* Yb_2 *and TmHe, TmYb potentials*, Eur. Phys. J. D **45**, 147 (2007); doi: 10.1140/epjd/e2006-00263-3.

4. Global interaction potential for dispersion-bound systems: Yb dimer

The present exposition is based on the manuscript **G. Visentin**, A.A. Buchachenko and Paweł Tecmer, *Ab intio Yb_2 ground state potential revisited* (submitted to Phys. Rev. A, arXiv:2107.10353 preprint available at https://arxiv.org/abs/2107.10353).

The related project was funded by the Russian Science Foundation under prolonged Project No. 17-13-01466.

Summary

The methods assessed in Chapter 3 for long-range atomic calculations are used for molecular calculations of Yb dimer. Extrapolation to the complete basis set limit and exploration of atom- and bond-centered diffuse function augmentations ensure basis set saturation, whereas convergence with respect to core correlation is imposed and X2C correction is used to correct for scalar-relativistic effects. The results achieved represent the state-of-the-art of CCSD(T) calculations, stressing the importance of the diffuse basis component and insufficient accuracy of the standard large-core effective core potential. In accordance with the conclusions from the previous Chapter, accuracy loss of molecular approaches beyond 25 Å makes direct matching of atomic and molecular approaches not feasible. Thus, reconciliation of two approaches is achieved by means of a semi-analytical function, scaling the global potential semiclassically to the known number of vibrational bound states. Scaling the potential to the known number of bound vibrational levels with ab initio data from slightly different molecular calculations bounds the dimer binding energy within the narrow 758 ± 4 cm^{-1} range. The difference between original and scaled binding energies exceeds 10%, showing that for a heavy dispersion-bound dimer the state-of-the-art ab initio potentials are still far from accuracy required in ultracold atomic physics, and, therefore, need further empirical adjustment.

4.1. Introduction

In the previous chapter, we showed that standard ab initio methods for molecular approaches are competitive with the state-of-the-art atomic approaches for the long-range dispersion interactions, providing that special care is taken on the basis set and correlation saturation and proper account of the scalar relativistic effects. This conclusion suggests to use the same methods to characterize global interaction potential at short and medium internuclear range and at long range, through

dispersion coefficients. The ground state Yb dimer, Yb_2, provides an ideal system for such a benchmark: it consists of two closed-shell atoms, for which the performance of accurate ab initio scheme has already been assessed in Chapter 3, exhibits non-negligible relativistic effects and has attracted significant research attention in the past.

Indeed, our interest in the global potential of ground state Yb_2 is not solely "technical": recently, weakly bound ytterbium dimer has marked a new frontier for ultracold atomic physics. The energy level scheme of Yb atom convenient for laser confinement, cooling and narrow band excitation were explored in development of the ultraprecise Yb frequency standard [1] for applications to quantum metrology and relativistic geodesy [1]. However, the path is still long for the development of an Yb_2-based atomic clock, which, theoretically, promises further significant improvements of the precision [2]. Related studies of ultracold Yb ensembles stipulated significant progresses in ultracold collision dynamics and photoassociation spectroscopy (PAS) [4-14], which, in turn, provided unique experimental data on atomic states and interatomic interactions (dispersion coefficients derived from these studies have already been quoted in the previous Chapter). Another feature making the Yb dimer a perfect test case for ultracold physics is the natural abundance of a variety of Yb isotopes. This allows one to study mass-dependent non-Born-Oppenheimer effects [11,15]. In recent years, a 500 Hz accuracy of the PAS data on the near-threshold rovibrational levels of the Yb dimer was reported [16]. Such a level of precision, never achieved before, can be used to challenge the constraints on the non-Newtonian gravity forces. It has been shown [16] that the constraint could be improved by two order of magnitude with the refinement of the underlying theoretical spectroscopic model. The model suggested relies on the reference Born-Oppenheimer (BO) and correction terms featuring beyond-BO effects with a few adjustable parameters. One way to improve the model is to accurately assess the non-Born-Oppenheimer effects arising due to non-adiabatic interactions with excited states. Recently, Tecmer *et al.* [17] moved in this direction and improved the ab initio description of the lowest-lying excited states of Yb dimer. However, the better characterization of the reference ground-state $^1\Sigma^+_g$ BO potential is no less important. As follows from Chapter 3, its long-range part is well represented by accurate ab initio calculations [18-21] and can be further improved by fitting to PAS data and scattering length measurements [6,11,22]. In contrast, no experimental data exist for probing the repulsive wall or the well depth of Yb dimer directly. The model can only rely on the ab initio calculations and, therefore, inevitably inherits their inaccuracies.

Up to date, the BO interaction potentials calculated at the CCSD(T) level with small-core effective core potentials [23] have been considered as the best reference. Borkowski *et al.* [11] showed that the ab initio binding energy D_e should only be corrected by 3% to reach the best fit to PAS data. Yet, the sensitivity of the long-range data to the potential well parameters is quite weak. Indeed, other model potentials, completely different from the ab initio ones, were previously tried in similar models [6,22]. Albeit the fits were made for less accurate data, they led to binding energies almost twice as large as the ab initio value. By contrast, all-electron scalar relativistic CCSD(T) calculations [17] gave a 20% smaller binding energy. All these results question the uniqueness of the models developed to fit PAS data and assessing non-Newtonian gravity forces in Refs. [11,16] and call for further refinement of the reference ground-state dimer potential.

The lessons learnt from the dispersion coefficient calculations are used to arrange dimer calculations. In any case, one cannot expect the present level of ab initio theory to match sub-kiloHertz accuracy for such a heavy system as Yb dimer. At best, it should provide the realistic shape of the global interaction potential, leaving only few parameters for refinement by fitting of experimental data. We therefore invoked in this study the semi-analytical potential model from Ref. [11] to combine the data of atomic and molecular calculations and then used the experimentally known number of bound vibrational levels of $^{174}Yb_2$ [6,11] to scale the binding energy value. Trying different modifications of the computational scheme, we were able to constrain this parameter in a range of 0.3%.

4.2. Computational details

As introduced in the previous section, the ab initio approaches used correspond to those successfully assessed in Chapter 3 for Yb polarizabilities and dispersion coefficients. In particular, for the basis set, we implemented the sequence of the correlation-consistent polarized valence cc-pV*n*Z basis set with n = D, T, Q (hereinafter for brevity V*n*Z) contracted for use with the X2C scalar-relativistic approximation [24]. The basis set chosen for the current dimer calculations differs from that used for the monomeric calculations of Yb in Chapter 3. This choice is motivated by the similar atomic results attained by extrapolating these two basis sets at the CBS limit and by the lower computational cost of V*n*Z compared to the weighted core-valence analog. As this basis set lacks the optimized diffuse augmentation, one or two primitives were added for each symmetry type with the exponents continuing the sequence of basis exponents in an even- tempered manner

with the default parameters of the MOLPRO program package [25]. Whenever specifying these options, we will call them e1 or e2 respectively. It should be noted that the e1 option had already been used to supply for the lack of augmentation in the cc-pWCV*n*Z basis set for atomic Yb in Chapter 3. Alternatively, the diffuse component of the basis set was saturated by placing the 3s3p2d2f1g set of of bond-centered functions (bf) [26] at the midpoint of the Yb-Yb separation. Two sets of CCSD(T) calculations were performed, hereinafter indicated in terms of the electrons included into the core, N_c = 46 and 28: for the former, the inner orbitals with principal quantum numbers from 1 to 4 were kept uncorrelated, except for 4f, whereas, for the latter, only the inner orbitals with principal quantum number from 1 to 3 were kept uncorrelated. From the previous chapter and Refs. [17,21] we know that the correlation of deeper shells does not affect the dimer potential well parameters and dispersion coefficients significantly. Energy convergence threshold was set to 10^{-10} hartree in all calculations and counterpoise correction proposed by Boys and Bernardi [27] was used. The restricted HF reference functions were calculated in the D_{2h} symmetry group for the dimer and in the C_{2v} symmetry group for the Yb atom in the full dimer basis set with the X2C correction to molecular integrals.

Consistently with the approach tested in the previous chapter, the CCSD(T) energies computed at the three *n*-levels of the basis set were extrapolated to the CBS limits by use of the two points formulae (2.139) and (2.140). As well as being successfully assessed before, these formulae have also the advantage due to their compatibility with the CP correction [28], in turn, ensured by the linearity of the parameters used.

4.3. Results

The CCSD(T) energies were calculated on a non-uniform grid of 57 internuclear distances *R*, ranging from 2 to 50 Å. At distances larger than 25 Å (interaction energies below 0.05 cm^{-1}), counterpoised potentials show erratic non-smooth variations. This illustrates the difficulties of a molecular approach at long range: even the dominant C_6 dispersion coefficients cannot be determined by fitting. However, the variations are still small in comparison to dissociation energy and do not prevent to tie the potential to the proper dissociation limit. Table 4.1 lists the inflection points at zero kinetic energy, R_0, R_e, D_e, dissociation energy D_0 and the vibrational constants ω_e, $\omega_e x_e$ achieved for the CBS potentials. In particular, R_0 refers to the internuclear distance where the potential is zero, R_e to the equilibrium distance, D_e to the binding energy (i.e. the potential well

depth at R_e) and D_0 to the difference between the binding energy D_e and the energy of the first vibrational level. The vibrational constants were attained from the cubic fits of the ten lowest vibrational level energies computed numerically for the dimer of two ^{174}Yb isotopes. The variations of all parameters agree with the trends found for equilibrium properties: diffuse augmentation is necessary to better retrieve attractive interactions, the effect of 4s4p4d shell correlation on interaction potential is negligible, and uncertainty in the CBS extrapolation falls within a 2% error bar. The table also reports the result for the V*n*Z+e2 N_c = 46 series: this demonstrates that addition of the single atom-centered diffuse function set is sufficient to reach convergence. In addition to that, the same potential parameters achieved for both core and basis set augmentation choices at each V*n*Z basis set (*n* = D, T, Q) are reported in the *Appendix* to the present Chapter.

Table 4.1. Parameters of the CCSD(T) ab initio Yb_2 interaction potentials from the present CBS calculations and literature. Inflection points at zero kinetic energy R_0 and equilibrium distances R_e are expressed in Å; binding energies D_e, dissociation energies D_0 and vibrational constants ω_e, $\omega_e x_e$ are expressed in cm^{-1}. First and second lines for the present results respectively refer to the extrapolations (2.139) and (2.140).

Potential	R_0	R_e	D_e	D_0	ω_e	$\omega_e x_e$	ν	N
VnZ c46	3.916	4.593	617.5	606.5	22.25	0.225	67.97	68
	3.911	4.583	621.2	610.1	22.48	0.230	68.18	68
VnZ+e1 c46	3.907	4.596	646.1	635.0	22.27	0.210	69.15	69
	3.900	4.587	653.8	642.6	22.44	0.212	69.53	69
VnZ+e2 c46	3.907	4.598	646.9	635.8	22.21	0.206	69.20	69
	3.901	4.590	654.1	643.0	22.35	0.207	69.56	69
VnZ+bf c46	3.906	4.594	654.6	643.4	22.45	0.201	69.34	69
	3.905	4.592	655.0	643.9	22.45	0.199	69.45	69
VnZ c28	3.915	4.590	615.0	604.0	22.21	0.226	67.88	67
	3.908	4.578	619.6	608.4	22.46	0.231	68.12	68
VnZ+e1 c28	3.906	4.596	643.6	632.5	22.19	0.205	69.12	69

Table 4.1 ***(continued)***

Potential	R_0	R_e	D_e	D_0	ω_e	$\omega_e x_e$	ν	N
	3.898	4.587	652.0	641.0	22.29	0.206	69.54	69
VnZ+bf c28	3.896	4.585	657.5	646.4	22.20	0.171	69.53	69
	3.893	4.580	659.5	648.4	22.19	0.167	69.71	69
ECP28MWB Refs. [11,23]	3.870	4.522	723.8	711.3	25.26	0.348	71.65	71
ECP28MWB Ref. [29]		4.549	742		25			
28e GRECP+OC Ref. [30]		4.683	642	631	21.5	0.19		
28e GRECP +OC+iTQ Ref. [30]		4.615	767	756	23.5	0.19		
28e GRECP +OC+iTQ+SO Ref. [30]		4.582	787	774	24.1	0.21		
ANO c28 Ref. [17]		4.665	580		21			

The model potential taken from Ref. [11] is a semi-analytical function of a short-range contribution $V_{SR}(R)$ and a long-range contribution $V_{LR}(R)$:

$$V(R) = [1 - f(R)]sV_{SR}(R) + f(R)V_{LR}(R). \tag{4.1}$$

The former denotes the ab initio points interpolated by cubic splines, whereas the latter accounts for the long-range part of the potential, in the standard dispersion series (1.1), suitably truncated to the dipole-quadrupole contribution.

Besides these two contributions, the switching function $f(R)$ appears, defined as follows:

$$f(R) = \begin{cases} 0, & R \le a \\ \frac{1}{2} + \frac{1}{4}\sin\left(\frac{\pi x}{2}\right)[3 - \sin^2(\frac{\pi x}{2})], & a < R < b. \\ 1, & b \le R \end{cases} \tag{4.2}$$

In eq. 4.2 $x = \frac{[(R-a)+(R-b)]}{b-a}$, with a = 10 a_0 (5.292 Å) and b = 19 a_0 (10.054 Å) [11].

Finally, an empirical scaling factor *s* appears in eq. 4.1 and is responsible for the constraint on the number of bound vibrational levels: when *s* is set to one, the model potential describes the interpolation of original ab initio points.

Figure 4.1 depicts the convergence of the equilibrium distance R_e and well depth D_e to the CBS limit for the V*n*Z, V*n*Z+e1 and V*n*Z+bf series. For the two former approaches, dependence on the core choice is weak. The convergence of these is slow but monotonic, thence demonstrating the necessity of the diffuse function augmentation. In contrast, the addition of bond-centered functions for the basis set augmentation (V*n*Z+bf) ensures a faster, though not regular, convergence, which, in addition, is strongly dependent on the core choice. The inset in the figure indicates that the results of two extrapolations are slightly different and bound R_e as 4.59 ± 0.01 Å and D_e as 650 ± 10 cm^{-1}.

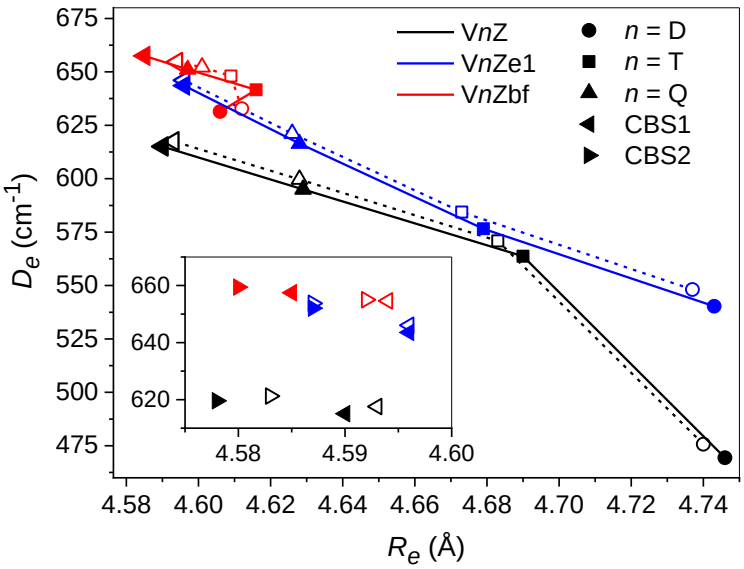

Figure 4.1. Convergence of the equilibrium distance R_e and binding energy D_e to the CBS limit by use of the extrapolation formula (2.139). Colors distinguish basis set augmentation, symbol shapes define basis cardinal numbers n. Solid symbols with solid lines denote N_c = 28 calculation with the small core, open symbols and dashed lines the N_c = 46 calculations with the large core. Inset enlarges the CBS limit region and shows the results of the CBS extrapolation (2.140) as well.

Several other literature results are reported, achieved, as well as ours, within the frame of CCSD(T) method. The potential from Refs. [11,23] derives from the combination of the small-core effective

core potential ECP28MWB [31] with atomic natural orbital (ANO) basis [32] augmented by the specially devised diffuse function set [33] and the bf set [26] simultaneously. Its results describe a more strongly bonded Yb dimer compared to our description: the binding energy is about 11% larger and the equilibrium distance is 1.5% shorter. This overestimated result is a consequence of the deficiency of the effective core potential and the results by Wang and Dolg, whose calculations used the same basis but different diffuse augmentation [29], support this explanation.

Other reference results come from the work by Mosyagin and coworkers [30]: these derive from calculations with the 28-electron generalized relativistic ECP (GRECP) and a series of the supplementary basis sets. Their reference CCSD(T) calculations with the largest basis set correlated only four outer electrons, but, however, correction to outer core correlation (OC, equivalent to the present c46 option) was evaluated with a smaller basis. Contributions of the iterative triple and quadruple cluster excitations (iTQ) and the spin-orbit (SO) coupling were estimated by means of full configuration interaction and relativistic density functional methods. The CCSD(T)+OC and CCSD(T)+OC+iTQ are reported in Table 4.1. The former reasonably approaches our VnZ+e1 c46 CBS results, signifying high accuracy of the GRECP and appreciable saturation of the basis set. The latter estimates the contribution of the higher-order cluster correction as 20%. SO correction applied to the latter approach gives a further contribution to the bonding enhancement in Yb dimer.

Finally, the results from the all-electron calculations by Tecmer *et al.* [17] are reported among the reference data. In this case, the binding energy is 10% smaller, while R_e is overestimated by 0.07 Å. As the difference between scalar relativistic approximations (X2C vs. DKH2) should be very small (See Chapter 3, Section 3.3), this mismatch is due for most part to the deficiency of the relativistic correlation consistent ANO basis: in particular, the lack of diffuse functions in the ANO basis dominates the deviation from our results. The best results are included between the present VTZ+e1 and VQZ results, despite the ANO basis was fully uncontracted.

The only experimental datum available, the estimation of the dissociation energy as 1400 ± 1400 cm^{-1} [34] by mass spectrometry, does not help to assess the ab initio results. As well, the estimations of harmonic frequency, empirical 21 cm^{-1} [35] and upper bound for excited state in inert matrices of 48 cm^{-1} [36], are not useful in this sense. Instead, the fact that ultracold PAS and scattering length data can be fitted reasonably well only with the potential supporting 72 bound

vibrational levels for $^{174}Yb_2$ at zero rotational momentum [6,11] is very helpful. Thus this constraint is explored to bound the true binding energy of Yb dimer with the help of the scaling parameter *s* from the model potential (4.1).

For the newly computed CBS potentials, the long-range contribution to the potential $V_{LR}(R)$ was taken with the compatible ab initio parameters C_6 = 2065.4, C_8 = 198200 a.u. from Ref. [21], while the potential from Ref. [23] was matched with the fitted dispersion coefficients coefficients C_6 = 1937.27, C_8 = 226517 a.u. [11]. We then used the model potential (4.1) with *s* = 1 to evaluate the semiclassical phase at zero kinetic energy [37]

$$\Phi = \frac{1}{\hbar}\int_{R_0}^{\infty}\sqrt{2\mu[-V(R)]}dR\ , \tag{4.3}$$

where μ is the nuclear reduced mass of the ^{174}Yb dimer. As the model potential depends on a short- and a long-range contribution, one can split eq. 4.3 into an integral of the short-range contribution (for $R_0 \le R \le b$) and an integral of the long-range contribution (for $b < R < \infty$). In particular, the long-range contribution to Φ, $\Phi_>$,

$$\Phi_> = \int_b^{\infty}\sqrt{2\mu\left(\frac{C_6}{R^6}+\frac{C_8}{R^8}\right)}\ dR, \tag{4.4}$$

can be analytically integrated, yielding

$$\Phi_> = \sqrt{2\mu}\left[\frac{\left(C_8+b^2C_6\right)^{\frac{3}{2}}}{3b^3C_8}-\frac{C_6^{\frac{3}{2}}}{3C_8}\right] \tag{4.5}$$

This greatly facilitates accurate numerical evaluation of the semiclassical phase. The effective number of the bound vibrational levels is defined as INT $\left(\nu=\frac{\Phi}{\pi}+\frac{3}{8}\right)$ [37]. In Table 4.1 the values of ν thus defined are compared with the number of levels *N* obtained by numerically solving the vibrational Schrödinger equation. In all cases but one semiclassical values agree with the quantum ones. The most accurate present potentials support three states less than needed.

Subsequently, we take the fitted dispersion coefficients C_6 = 1937.27, C_8 = 226517 a.u. for all potentials as the most accurate ones [11] and tune *s* until ν is constrained to be equal or greater than 72. The results for *s* and the binding energies of the scaled potentials are listed in Table 4.2. The table shows that the constraint on the bound levels restricts the error bar of the binding energies

for each potential from 45 cm^{-1} to the much narrower 8 cm^{-1} interval, with a mean value of 758 cm^{-1}, approaching the best estimations obtained with the bond functions. On one hand, this reflects similar shapes of all potentials; on the other hand, it provides quite conservative estimation of the dissociation energy. Notice that this new result is only slightly larger compared to the value fitted to PAS data within BO approximation [11]. Moreover, it falls above the 28e GRECP+OC+iTQ result of 767 cm^{-1} and the same result corrected for SO coupling, 786 cm^{-1} (28e GRECP +OC+iTQ+SO from Ref. [30] in Table 4.1). However, it should also be mentioned that the corrections implemented by Mosyagin *et al.* [30] may be overestimated, as they are not consistent with each other. Moreover, another overestimation factor can derive from the higher-order cluster excitations and SO coupling: these also distort the shape of the CCSD(T) potential and shift its scaling towards larger binding energies. Perhaps, it would be more prudent to consider the present estimate of 758 ± 4 cm^{-1} as an upper bound to the BO binding energy of the $^{174}Yb_2$ dimer.

Table 4.2. Scaling factor *s* and scaled binding energies (cm^{-1}) of the potentials obtained with extrapolation formula (2.139) for $^{174}Yb_2$. Results for the potentials obtained with extrapolation formula (2.140) are written within parentheses.

Potential	*s*	sD_e
VnZ c46	1.233 (1.226)	761.2 (761.8)
VnZ+e1 c46	1.172 (1.157)	757.2 (756.7)
VnZ+e2 c46	1.169 (1.156)	756.5 (755.8)
VnZ+bf c46	1.162 (1.161)	760.7 (760.1)
VnZ c28	1.237 (1.229)	761.0 (761.8)
VnZ+e1 c28	1.173 (1.157)	755.2 (754.3)
VnZ+bf c28	1.153 (1.148)	757.9 (757.0)
Ref. [11]	1.027	743.0±2.4

Unfortunately, the existing data cannot assess the uncertainty on the equilibrium distance. We thus should consider that the best ab initio data suggest a value of 4.59 ± 0.01 Å.

4.4. Conclusions

With the present calculations we set the scalar relativistic CCSD(T) benchmark for interaction potential of the ground state Yb_2 dimer. For the equilibrium distance R_e and the unscaled binding energy D_e the molecular approach successfully assessed in Chapter 3, consisting of all-electron description with the X2C scalar relativistic correction, systematic correlation-consistent basis set of double-, triple- and quadrupole-zeta quality and the CBS extrapolations, two types of the diffuse function augmentation and extensive correlation treatments, respectively bounds them within 4.58-4.60 Å and 640-660 cm^{-1}. This uncertainty is due to the difference between the use of atom- and bond-centered diffuse functions and to the ambiguity of the CBS extrapolations. This result refines previous estimations achieved with the small-core effective core potential [23,29] and all-electron ANO basis set [17]. Corrected scalar- relativistic results by Mosyagin *et al.* [30] are in line with our results.

However, present calculations turned out to be quite demanding, due to the extended basis sets, correlation treatment and strong convergence thresholds. Still, they lack proper convergence at long distances, hindering the direct evaluation of the dispersion coefficients. In the present example, molecular calculations are unreliable beyond 25 Å, while the distance where the dipole-dipole dispersion interaction, $-C_6R^{-6}$, dominates was determined, in the previous chapter, as ca. 75 Å. Thus, direct comparison of molecular and atomic approaches is hardly possible.

The performance of atom-centered and bond-centered basis functions to improve our results was also assessed. From molecular calculations, bond functions turn out to ensure a faster convergence, compared to the case when only atom-centered diffuse functions are in use. However, for V*n*Z and V*n*Z+e1, convergence pattern is more regular, though slower, than for V*n*Z+bf. At CBS limit, within the uncertainty of extrapolation, these two approaches seem to be equivalent in the well region, where, for the equilibrium parameters, they return results with like accuracy. Unfortunately, present results cannot assess the performance at long-range.

A further refinement of the results came from implementing the semi-analytical potential function first proposed by Borkowski *et al.* [11] to fit the data of ultracold photoassociation and scattering experiments and from constraining the number of bound vibrational levels supported by Yb_2

potential. These bound the binding energy within the narrow 758 ± 4 cm^{-1} interval, slightly below the Born-Oppenheimer value of 743.0 ± 2.4 cm^{-1} fitted using the previous potential [11].

The difference between the CCSD(T) and the scaled binding energies is comparable to the estimated corrections to the iterative triple and quadrupole cluster excitations and spin-orbit interaction proposed by Mosyagin and coworkers [30]. The difference amounts to ca. 15%. This relatively large spread reflects, on one hand, the contribution of scalar relativistic corrections, while, on the other, the improvements due to the iterative triples and higher-order cluster corrections. These latter, in particular, are estimated to contribute up to 90% [30].

Future perspectives for the refinement of our present approach and results may come from extending the new Yb_2 potentials to non-Born-Oppenheimer models [11,16], with the aim of improving the description of the mass-dependent effects.

Appendix: summary of ab initio calculations

Table A1. $^{174}Yb_2$ ab initio potential parameters for 46 cc-pVnZ-X2C (n = D, T, Q) potential. R_0 and R_e are expressed in Å, whereas D_e, D_0, ω_e and $\omega_e x_e$ in cm^{-1}. C_6 is expressed in atomic units.

	R_0	R_e	D_e	C_6	D_0	ω_e	$\omega_e x_e$
N_c = 46; cc-pVnZ-X2C no bf no augmentation							
VDZ	4.080	4.740	475.73	1857(65)	465.67	20.23	0.231
VTZ	3.985	4.683	570.87	1946(28)	560.58	20.69	0.199
VQZ	3.943	4.628	599.63	2088(141)	588.89	21.62	0.215
CBS (2.139)	3.916	4.593	617.54	2201(253)	606.44	22.29	0.224
CBS (2.140)	3.911	4.583	621.24		610.10	22.48	0.230
N_c = 46; cc-pVnZ-X2C + e1 no bf single augmentation							
VDZ	4.042	4.737	548.12	2056(14)	537.97	20.40	0.205
VTZ	3.976	4.673	584.36	2056(181)	573.90	21.02	0.201
VQZ	3.934	4.626	621.17	2003(45)	610.33	21.79	0.206
CBS (2.139)	3.907	4.596	646.08	1966(148)	634.97	22.32	0.211
CBS (2.140)	3.907	4.587	653.77		642.6	22.44	0.212

Table A1 ***(continued)***

N_c = 46; cc-pVnZ-X2C + e2 no bf double augmentation							
VDZ	4.042	4.737	548.12	2056(14)	537.97	20.40	0.205
VTZ	3.974	4.670	587.30	1958(38)	576.80	21.09	0.202
VQZ	3.933	4.626	623.01	1952(37)	612.17	21.79	0.206
CBS (2.139)	3.907	4.598	646.88	1950(50)	635.79	22.26	0.207
CBS (2.140)	3.901	4.590	654.09		643.0	22.35	0.207
N_c = 46 cc-pVnZ-X2C + bf no augmentation							
VDZ	3.931	4.612	632.75		621.57	22.47	0.219
VTZ	3.919	4.609	648.06		636.88	22.48	0.213
VQZ	3.911	4.601	652.25		641.05	22.50	0.206
CBS (2.139)	3.906	4.594	654.62		643.41	22.51	0.202
CBS (2.140)	3.905	4.592	655.03		643.9	22.45	0.199

Table A2. $^{174}Yb_2$ ab initio potential parameters for 28 cc-pVnZ-X2C (n = D, T, Q) potential.

	R_0	R_e	D_e	C_6	D_0	ω_e	$\omega_e x_e$
N_c = 28; cc-pVnZ-X2C no bf no augmentation							
VDZ	4.087	4.746	469.35	1859(35)	459.35	20.11	0.231
VTZ	3.992	4.690	563.67	1729(243)	553.43	20.57	0.119
VQZ	3.944	4.629	594.97		584.26	21.54	0.215
CBS (2.139)	3.915	4.590	615.04		603.98	22.26	0.227
CBS (2.140)	3.908	4.578	619.59		608.4	22.46	0.231
N_c = 28; cc-pVnZ-X2C + e1 no bf single augmentation							
VDZ	4.049	4.743	540.31		530.23	20.27	0.205
VTZ	3.982	4.679	576.57		566.17	20.88	0.202
VQZ	3.935	4.628	616.42		605.65	21.64	0.203
CBS (2.139)	3.906	4.596	643.55		632.52	22.17	0.206

Table A2 ***(continued)***

	R_0	R_e	D_e	C_6	D_0	ω_e	$\omega_e x_e$
CBS (2.140)	3.898	4.587	652.04		641.0	22.29	0.206
N_c = 28; cc-pVnZ-X2C + e2 no bf double augmentation							
VDZ	4.030	4.723	551.75		541.54	20.51	0.205
VTZ	3.981	4.677	578.54		568.13	20.93	0.202
VQZ							
CBS (2.139)							
CBS (2.140)							
N_c = 28 cc-pVnZ-X2C + bf no augmentation							
VDZ	3.929	4.606	631.44		620.25	22.50	0.221
VTZ	3.923	4.616	641.62		630.49	22.37	0.208
VQZ	3.907	4.597	651.13		640.03	22.29	0.185
CBS (2.139)	3.896	4.585	657.46		646.37	22.25	0.172
CBS (2.140)	3.893	4.580	659.46		648.4	22.19	0.167

References

[1] A. D. Ludlow, M. M. Boyd, J. Ye, E. Peik, and P. O. Schmidt, *Optical atomic clocks,* Rev. Mod. Phys. **87**, 638 (2015); doi: 10.1103/RevModPhys.87.637.

[2] W. F. McGrew, X. Zhang, R. J. Fasano, S. A. Schäffer, K. Beloy, D. Nicolodi, R. C. Brown, N. Hinkley, G. Milani, M. Schioppo, T. H. Yoon, and A. D. Ludlow, *Atomic clock performance enabling geodesy below the centimetre level,* Nature **564**, 87 (2018); doi: 10.1038/s41586-018-0738-2.

[3] M. Borkowski, *Optical Lattice Clocks with Weakly Bound Molecules*, Phys. Rev. Lett. **120**, 083202 (2018); doi: 10.1103/PhysRevLett.120.083202.

[4] S. Tojo, M. Kitagawa, K. Enomoto, Y. Kato, Y. Takasu, M. Kumakura, and Y. Takahashi, *High-Resolution Photoassociation Spectroscopy of Ultracold Ytterbium Atoms by Using the Intercombination Transition*, Phys. Rev. Lett. **96**, 153201 (2006); doi: 10.1103/PhysRevLett.96.153201.

[5] K. Enomoto, M. Kitagawa, S. Tojo, and Y. Takahashi, *Hyperfine-Structure-Induced Purely Long-Range Molecules,* Phys. Rev. Lett. **100**, 123001 (2008); doi: 10.1103/PhysRevLett.100.123001.

[6] M. Borkowski, R. Ciuryło, P. S. Julienne, S. Tojo, K. Enomoto, and Y. Takahashi, *Line shapes of optical Feshbach resonances near the intercombination transition of bosonic ytterbium*, Phys. Rev. A **80**, 012715 (2009); doi: 10.1103/PhysRevA.80.012715.

[7] Y. Takasu, Y. Saito, Y. Takahashi, M. Borkowski, R. Ciuryło, and P. S. Julienne, *Controlled Production of Subradiant States of a Diatomic Molecule in an Optical Lattice*, Phys. Rev. Lett. **108**, 173002 (2012); doi: 10.1103/PhysRevLett.108.173002.

[8] S. Kato, S. Sugawa, K. Shibata, R. Yamamoto, and Y. Takahashi, *Control of Resonant Interaction between Electronic Ground and Excited States*, Phys. Rev. Lett. **110**, 173201 (2013); doi: 10.1103/PhysRevLett.110.173201.

[9] D. G. Green, C. L. Vaillant, M. D. Frye, M. Morita, and J. M. Hutson, *Quantum chaos in ultracold collisions between Yb($^1S_0$) and Yb($^3P_2$),* Phys. Rev. A **93**, 022703 (2016); doi: 10.1103/PhysRevA.93.022703.

[10] Y. Takasu, Y. Fukushima, Y. Nakamura, and Y. Takahashi, *Magnetoassociation of a Feshbach molecule and spin-orbit interaction between the ground and electronically excited states*, Phys. Rev. A **96**, 023602 (2017); doi: 10.1103/PhysRevA.96.023602.

[11] M. Borkowski, A. A. Buchachenko, R. Ciuryło, P. S. Julienne, H. Yamada, Y. Kikuchi, K. Takahashi, Y. Takasu, and Y. Takahashi, *Beyond-Born-Oppenheimer effects in sub-kHz-precision photoassociation spectroscopy of ytterbium atoms*, Phys. Rev. A **96**, 063405 (2017); doi: 10.1103/PhysRevA.96.063405.

[12] L. Franchi, L. F. Livi, G. Cappellini, G. Binella, M. Inguscio, J. Catani, and L. Fallani, *State-dependent interactions in ultracold ^{174}Yb probed by optical clock spectroscopy,* New J. Phys. **19**, 103037 (2017); doi: 10.1088/1367-2630/aa8fb4.

[13] R. Bouganne, M. B. Aguilera, A. Dareau, E. Soave, J. Beugnon, and F. Gerbier, *Clock spectroscopy of interacting bosons in deep optical lattices,* New J. Phys. **19**, 113006 (2017); doi: 10.1088/1367-2630/aa8c45.

[14] G. Cappellini, L. F. Livi, L. Franchi, D. Tusi, D. Benedicto Orenes, M. Inguscio, J. Catani, and L. Fallani, *Coherent Manipulation of Orbital Feshbach Molecules of Two-Electron Atoms,* Phys. Rev. X **9**, 011028 (2019); doi: 10.1103/PhysRevX.9.011028.

[15] J. J. Lutz and J. M. Hutson, *Deviations from Born-Oppenheimer mass scaling in spectroscopy and ultracold molecular physics,* J. Mol. Spectrosc. **330**, 43 (2016); doi: 10.1016/j.jms.2016.08.007.

[16] M. Borkowski, A. A. Buchachenko, R. Ciuryło, P. S. Julienne, H. Yamada, Y. Kikuchi, Y. Takasu, and Y. Takahashi, *Weakly bound molecules as sensors of new gravitylike forces,* Sci. Rep. **9**, 14807 (2019); doi: 10.1038/s41598-019-51346-y.

[17] P. Tecmer, K. Boguslawski, M. Borkowski, P. S. Żuchowski, and D. Kędziera, *Modeling the electronic structures of the ground and excited states of the ytterbium atom and the ytterbium dimer: A modern quantum chemistry perspective,* Int. J. Quant. Chem. **119**, e25983 (2019); doi: 10.1002/qua.25983.

[18] P. Zhang and A. Dalgarno, *Long-range interactions of ytterbium atoms,* Mol. Phys. **106**, 1525 (2008); doi: 10.1080/00268970802126608.

[19] M. S. Safronova, S. G. Porsev, and C. W. Clark, *Ytterbium in Quantum Gases and Atomic Clocks: van der Waals Interactions and Blackbody Shifts*, Phys. Rev. Lett. **109**, 230802 (2012); doi: 10.1103/PhysRevLett.109.230802.

[20] S. G. Porsev, M. S. Safronova, A. Derevianko, and C. W. Clark, *Long-range interaction coefficients for ytterbium dimers*, Phys. Rev. A **89**, 012711 (2014); doi: 10.1103/PhysRevA.89.012711.

[21] G. Visentin and A.A. Buchachenko, *Polarizabilities, dispersion coefficients, and retardation functions at the complete basis set CCSD limit: From Be to Ba plus Yb,* J. Chem. Phys. **151**, 214302 (2019); doi: 10.1063/1.5129583.

[22] M. Kitagawa, K. Enomoto, K. Kasa, Y. Takahashi, R. Ciuryło, P. Naidon, and P. S. Julienne, *Two-color photoassociation spectroscopy of ytterbium atoms and the precise determinations of s-wave scattering lengths*, Phys. Rev. A **77**, 012719 (2008); doi: 10.1103/PhysRevA.77.012719.

[23] A. A. Buchachenko, G. Chałasinski, and M. M. Szczesniak, *Interactions of lanthanide atoms: Comparative ab initio study of YbHe, Yb_2 and TmHe, TmYb potentials*, Eur. Phys. J. D **45**, 147 (2007); doi: 10.1140/epjd/e2006-00263-3.

[24] Q. Lu and K.A. Peterson, *Correlation consistent basis sets for lanthanides: The atoms La–Lu,* J. Chem. Phys. **145**, 054111 (2016); doi: 10.1063/1.4959280.

[25] H.-J.Werner, P. J. Knowles, G. Knizia, F. R.Manby, and M. Schütz, Molpro: a general-purpose quantum chemistry program package, WIREs Comput. Mol. Sci. **2**, 242 (2012).

[26] S. M. Cybulski and R. R. Toczyłowski, *Ground state potential energy curves for He2,He2, Ne2,Ne2, Ar2,Ar2, He–Ne,He–Ne, He–Ar,He–Ar, and Ne–Ar:Ne–Ar: A coupled-cluster study*, J. Chem. Phys. **111**, 10520 (1999); doi: 10.1063/1.480430.

[27] S. Boys and F. Bernardi, *The calculation of small molecular interactions by the differences of separate total energies. Some procedures with reduced errors,* Mol. Phys. **19**, 553 (1970); doi: 10.1080/00268977000101561.

[28] M. P. de Lara-Castells, R. V. Krems, A. A. Buchachenko, G. Delgado-Barrio, and P. Villarreal, *Complete basis set extrapolation limit for electronic structure calculations: Energetic and nonenergetic properties of HeBr and HeBr2HeBr2 van der Waals dimers,* J. Chem. Phys. **115**, 10438 (2001); doi: 10.1063/1.1415078.

[29] X. Cao and M. Dolg, *Pseudopotential study of lanthanum and lutetium dimers*, Theor. Chem. Acc. **108**, 143 (2002); doi: 10.1007/s00214-002-0372-8.

[30] N. S. Mosyagin, A. N. Petrov, and A. V. Titov, *The effect of the iterative triple and quadruple cluster amplitudes on the adiabatic potential curve in the coupled cluster calculations of the ground electronic state of the Yb dimer*, Int. J. Quant. Chem. **111**, 3793 (2010); doi: 10.1002/qua.22913.

[31] M. Dolg, H. Stroll, and H. Preuss, *Energy-adjusted ab initio pseudopotentials for the rare earth elements***,** J. Chem. Phys. **90**, 1730 (1989); doi: 10.1063/1.456066.

[32] X. Cao and M. Dolg, *Valence basis sets for relativistic energy-consistent small-core lanthanide pseudopotentials***,**J. Chem. Phys. **115**, 7348 (2001); doi: 10.1063/1.1406535.

[33] A. A. Buchachenko, G. Chałasinski, and M. M. Szczesniak, *Diffuse basis functions for small-core relativistic pseudopotential basis sets and static dipole polarizabilities of selected lanthanides La, Sm, Eu, Tm and Yb,* Struct. Chem. **18**, 769 (2007); doi: 10.1007/s11224-007-9243-1.

[34] M. Guido and G. Balducci, *Dissociation Energy of Yb_2,* J. Chem. Phys. **57**, 5611 (1972); doi: 10.1063/1.1678267.

[35] P. Goodfriend, *Estimates of unknown vibrational frequencies of diatomics containing lanthanide atoms,* Spectrochim. Acta A **40**, 283 (1984); doi: 10.1016/0584-8539(84)80050-1.

[36] S. Suzer and L. Andrews, *Optical spectra of Yb atoms and dimers in rare gas matrices,* J. Chem. Phys. **89**, 5514 (1988); doi: 10.1063/1.455576.

[37] G. F. Gribakin and V. V. Flambaum, *Calculation of the scattering length in atomic collisions using the semiclassical approximation*, Phys. Rev. A **48**, 546 (1993); doi: 10.1103/PhysRevA.48.546.

5. Dispersion interaction in Open-Shell systems: extended combination rule for homonuclear dipole dispersion coefficients

The present exposition is based on the paper **G. Visentin,** I.S. Kalinina and A.A. Buchachenko, *Extended combination rule for like-atom dipole dispersion coefficients*, J. Chem. Phys. **153**, 064110 (2020); doi: 10.1063/5.0019010, partially reproduced with the permission of AIP Publishing.
The related project was funded by the Russian Science Foundation under Project No. 17-13-01466.

Summary

Reconciliation of atomic and molecular approaches is assessed for dispersion interactions of open-shell species, for which technical limitations hinder the ab initio calculation of dynamic properties. To explore the transferability of the monomer dynamic polarizabilities, a novel combination rule is devised. The rule defines the dispersion coefficients of the homonuclear dimer through the set of dispersion coefficients between the monomer and auxiliary species and across the same auxiliary species. Discretization of the Casimir-Polder integrals for dispersion coefficients reduces the rule to the straightforward solution of a system of linear equations. The test examples indicate reasonable accuracy of the proposed rule for dispersion coefficients of the target dimers. On the other hand, retrieval of the related dynamic polarizabilities should require larger and more accurate datasets and additional conditions to improve their transferability.

5.1. Introduction

Chapters 3 and 4 demonstrated that ab initio methods, approaches and models in use for achieving accurate description of a dimer can be applied to monomers as well. For the latter, reasonable accuracy is attained even for dispersion coefficients, thus allowing one, in principle, to retrieve consistent global interaction potential upon combining molecular (dimeric) and atomic (monomeric) approaches. Both approaches have their own validity range in internuclear distance, determined by the number of the coefficients retained in the long-range expansion and by numerical limitations for very small energy differences, in the latter and former cases, respectively. In case of the Yb dimer (see Chapter 4), these ranges do not overlap. Furthermore, Figure 3.6 in Chapter 3 hints that overlapping can likely be attained only for light atoms. Therefore, the use of synthetic potential functions that bridge the gap is still necessary. Still, even the fully converged

golden standard Coupled Cluster method has an error by about 12% for dissociation energy and 7% for the leading dispersion coefficient of Yb atom, which, indeed, are neither small or balanced. Yet, this system is heavy, precision of the existing experimental data is unique and there is still room for (expensive) improvements accounting for higher cluster excitations (see Chapter 2, Section 2.5.4) [1-4].

More severe limitations arise when moving to more complex systems. In case of atomic monomers, these mostly concern open-shell systems. If interacting atoms are in states that are degenerate in projections of the orbital or spin electronic angular momenta, the degeneracy is lifted by interatomic interactions and the dimer can be formed in a number of molecular states. In the scalar relativistic frame, atoms in states with non-zero orbital momentum are said to interact anisotropically, as the coupling of molecular axis with non-spherical atomic distribution can be described not only in terms of projections, but also in terms of effective angles [5,6]. For atoms in the states with non-zero spin momentum, one refers to exchange interactions. In contrast to anisotropy, they exhibit exponential decay with distance and, normally, do not contribute to long-range potential. However, if both momenta are non-zero, spin-orbit interaction engages the spin and creates the interaction anisotropy in the total angular momentum.

Theoretical concepts can be straightforwardly extended to the open-shell interactions. Intermolecular perturbation theory presented in Chapter 2 can be reformulated for the tensor polarizabilities and electric moments [7,8], while the symmetry of the dimer states is dictated by the addition of angular momenta and Pauli principles for electron and nuclear permutations implemented in the concept of correlation diagram [9]. It is mostly the technical capability that matters.

Generally, electronic wavefunctions of the dimer states have multi-reference structure. This completely or partially forbids the use of the single-reference Coupled Cluster framework. The same problem, further complicated by the difficulties in realization of the propagator methods, affect the atomic approaches. Of course, alternative ab initio methods can be used to deal with these situations, usually not without losses in generality, consistency and accuracy.

On the other hand, the power of the atomic approach for long-range interaction is rooted in the transferability of atomic parameters. In Chapter 2 it was shown that knowledge of the moments

and polarizabilities of a given atom allows one to evaluate the long-range coefficients for its interaction with any other atom for which the same parameters are available. Thus, conceptually, knowledge of the long-range coefficients for the atom interacting with a series of other atomic partners implies the possibility of retrieving atomic moments and polarizabilities. This statement (somehow oversimplified, due to the presence of resonant long-range terms for excited states of a homonuclear dimer [7,10,11]) is obvious for electrostatic and induction contributions when the long-range coefficients are the products of the properties. It is less trivial for dispersion coefficients that convolute dynamic polarizabilities, see, e.g., eqs. (2.53-54), and was essentially overlooked before in literature.

If the atom of interest has an open-shell structure, one can try to solve a series of simplified problems deducing long-range coefficients for its interactions with the closed-shell partners and restore the same parameters for the open-shell dimer.

In fact, this reasoning is very similar to the concept of combination rules, whose empirical implementations are deeply rooted in the history of intermolecular interaction theory [12] and are currently in use in some modern molecular modeling techniques. It is, therefore, more logical and convenient to present the above reasoning as a foundation of a new generalized combination rule.

5.2. Meaning of "Combination Rule"

In the field of intermolecular interactions, the term *Combination Rule* (CR) defines a relation connecting some potential parameter *a* for a pair of unlike interacting species *i,j* with the same parameter for the interaction of two like species [7,13]:

$$a_{ij} = f(a_{ii}, a_{jj}) \tag{5.1}$$

Originally devised for the Lennard-Jones potential model [7,14-16], the most famous CRs establish the geometric relation

$$a_{ij} = \left(a_{ii} a_{jj}\right)^{1/2}, \tag{5.2}$$

for the interaction energy and the arithmetic mean relation

$$a_{ij} = \frac{1}{2}(a_{ii} + a_{jj}), \tag{5.3}$$

for the equilibrium distance.

Generally, CRs depend on the specific potential parametrization [17-19]. An exception is provided by the long-range interaction, universally represented by the inverse power series (eq. (1.1)). This power series consists of dispersion coefficients, in turn depending on the related dynamic electric properties.

Eq. (2.53) provides a definition for the dispersion coefficient C_6 for two interacting species *A* and *B*. Here, we rather express the C_6 coefficient for the interaction of two partners *i* and *j*. The reason for this change will become evident a little later.

$$C_6^{ij} = \frac{3}{\pi}\int_0^\infty d\omega \alpha^i(i\omega)\alpha^j(i\omega), \tag{5.4}$$

where $\alpha^k(i\omega)$ is the dynamic dipole polarizability of the *k*-th species. Since the dipole polarizability will be the only polarizability treated in this chapter, we set, for simplicity, $\alpha^k(i\omega) \equiv \alpha_1^k(i\omega)$.

We may think of eq. (5.4) as the "fundamental combination rule" [20]. However, simpler approaches are needed when the dynamic polarizability of the dispersion coefficients cannot be evaluated theoretically or empirically. For instance, Hirschfelder [14] describes a geometric mean CR analogous to eq. (5.2),

$$C_6^{ij} = \left(C_6^{ii}C_6^{jj}\right)^{1/2} \tag{5.5}$$

Eq. (5.5) provides the rigorous upper bound to the true dispersion coefficient for unlike species [21,22] and can be regarded as the "pure" combination rule, as it connects dispersion coefficients only without a need of any other information on interacting species. This is the only pure CR previously known for dispersion coefficients.

Another popular CR appears in the classical textbook by Moelwin-Hughes [12]:

$$C_6^{ij} = 2\frac{C_6^{ii}C_6^{jj}}{[(\alpha^j/\alpha^i)C_6^{ii}+(\alpha^i/\alpha^j)C_6^{jj}]} \tag{5.6}$$

Here and hereinafter $\alpha^k \equiv \alpha^k(0)$ stands for the static dipole polarizability.

This CR was then mentioned by Wilson [23] in relation to the Slater-Kirkwood formula and should hold for any kind of London-like approximation (see Chapter 2, Section 2.1.7 and Ref. [24]). The

most popular derivation and first rigorous analysis of eq. (5.6) were exposed by Kramer and Herschbach [25]. Some years later, a family of related combination rules were devised by means of the effective transition frequency expressed in terms of the momenta of the dipole oscillator strength density [26]. Zeiss and Meath [27], and later Thakkar [20], reported that for representative datasets the root-mean-square accuracy of eq. (5.6) falls below 1%. Many authors considered its extensions to higher-order and three-body dispersion coefficients (see e.g. Refs. [18,26,28-31]). Athough eq. (5.6) is not a pure CR, it contains additional parameters, such as the static polarizabilities, which are easily available.

Nowadays, many ambits of Computational Chemistry do exist where CRs for dispersion terms play an important role: first of all, general molecular force fields and dispersion-corrected density functionals. Regarding the former, for instance, the early versions of the CHARMM and GROMOS force fields employ the Slater-Kirkwood formula for dispersion coefficients [32]; conversely, the Merck Molecular Force Field (MMFF) [33] implements the CR (5.6) in order to determine the dipole-dipole dispersion coefficient and even to estimate the strength of unlike species interactions. Regarding the latter, corrections based on the damped inverse power series are derived in order to account for the dispersion interactions in the exchange-correlation density functionals [34-37]: they can be either empirical or computed from scratch and often employ combination rules analogous to (5.6) to determine dispersion coefficients [34,35,37].

Obtaining interaction parameters for unlike species from two like-species ones is a common practice in empirical contexts, as the interaction parameters are easier to deduce experimentally, and, as mentioned above, suit the purpose of molecular mechanics. Yet, in the realm of ab initio calculations, the opposite combination is important as well, in all those cases when the direct calculation of the homonuclear interaction parameter is difficult due to the complex structure of the species of interest (e.g. open-shell systems). However, the prediction of such inverse CRs depends on the choice of the partner and, hence, may be ambiguous.

To solve this ambiguity and thus provide the estimation of the interactions for like species with a solid rule, an extended combination rule for the homonuclear dispersion coefficient C_6 was devised in the form,

$$C_6 = \Sigma_{i=1}^{n} \lambda_i C_6^i, \tag{5.7}$$

where the summation runs over the partner species *i* and the coefficient C_6^i for the interaction of the target and partner species is supposed to be known, while the linear coefficients λ_i are unknowns.

Eq. (5.7) to some extent is inspired by the work by Weinhold [22], who introduced the matrix of C_6 coefficients for a set of species. Proving this matrix to be positive (semi-) definite, Weinhold demonstrated that the geometric mean CR (5.5) is an upper bound to the true C_6^{ij} coefficient and that its inverse formulation represents the lower bound to the true C_6^{ii} or C_6^{jj} coefficient. This concept suggests that considering many partner species, it is possible to make more accurate predictions of the dispersion coefficients.

5.3. Extended combination rule

The combination rule (5.7) can be derived algebraically upon approximating and discretizing the Casimir-Polder integrals (5.4). In devising our CR, we follow Weinhold [22] and thus introduce matrix **C** of the C_6 coefficients describing the interactions between partner species *i*,*j* = 1, 2,…,*n*. We also define the "species vector" $|x>$ of the length *n*, so that for $x = k$, $x_i = \delta_{ik}$. In summary,

$$C_6^{ij} = < i|\boldsymbol{C}|j > \tag{5.8}$$

Let us suppose that the matrix elements can be uniformly represented as the factorized sum

$$C_6^{ij} = \Sigma_{l=1}^{n} \xi_l A_{il} A_{lj}, \tag{5.9}$$

where the two factors *A* refer to the first and second species and the number of terms is equal to the number of partner species. Eq. (5.9) can be considered the discrete representation of Casimir-Polder integral (5.4): in fact, upon a proper choice of ξ coefficients, A_{il} and A_{lj} become equal to the dynamic polarizabilities of the species *i* and *j* respectively, defined on a grid of imaginary frequencies. Eq. (5.9) can be rewritten in the matrix form

$$C_6^{ij} = C_6^{ji} = \Sigma_{l=1}^{n} < j|A_l|j > \xi_l < i|A_l|i > = \boldsymbol{a_j} \Xi \boldsymbol{a_i} \tag{5.10}$$

Here, Ξ is the diagonal matrix of the ξ coefficients, while $\boldsymbol{a_k}$ is the discretized dynamic polarizability of the species *k* represented in the vector form. The interaction between the target and the *i*-th partner species, C_6^i follows a similar expression:

$$C_6^i = \boldsymbol{a}_0 \Xi \boldsymbol{a}_i, \tag{5.11}$$

where the vector $\boldsymbol{a}_0$ refers to the dynamic polarizability of the target species. Upon combining (5.10) and (5.11), one gets

$$C_6^i = \boldsymbol{a}_0 \boldsymbol{a}_j C_6^{ij} \equiv \lambda_j C_6^{ij} \tag{5.12}$$

Eq. (5.12) is a linear system of equations, that should be solved for λ_j provided all dispersion coefficients are known. Applying the same procedure to exclude $\boldsymbol{a}_0$, one arrives to the equation

$$C_6 = \Sigma_{i=1}^{n} \Sigma_{j=1}^{n} \lambda_i \lambda_j C_6^{ij}, \tag{5.13}$$

analogous to eq. (5.7).

Looking at eq. (5.13), one can easily understand that the dispersion coefficient matrix is the only information required in order to implement our extended CR.

To approach the solution of eq. (5.13), one can think of it as the quadrature representation of the integral. Gauss-Legendre (GL) quadrature has found wide applications in the field (see for instance Refs. [38-40]):

$$C_6^{ij} = \frac{3}{\pi} \int_0^{\infty} \alpha^i(i\omega)\alpha^j(i\omega)d\omega = \frac{3}{\pi} \int_{-1}^{1} \alpha^i[i\omega(t)]\alpha^j[i\omega(t)] \left(\frac{d\omega}{dt}\right) dt \approx$$
$$\frac{3}{\pi} \Sigma_{l=1}^{n} w_l \frac{d\omega}{dt}(t_l)\alpha^i[i\omega(t_l)]\alpha^j[i\omega(t_l)] \tag{5.14}$$

The proper transformation $i\omega(t)$ reduces the integration to a finite interval, while w_l indicates the quadrature weight. It is worthy of mention that the accuracy of the CR (5.13) constructed in this way is only limited by the accuracy of GL integration. For a given quadrature type, the latter is limited by the order *n* or by the number of partner species considered.

To evaluate eq. (5.14), three specific types of the GL quadrature were tested:

1) GL1, available from the paper by Amos *et al.* [38] and defined as
$i\omega = 0.3\ (1 - t)/(1 + t)$;
2) GL2, available from the paper by Jiang *et al.* [39] and defined as
$i\omega = t/(1 - t)$;
3) GL3, available from the paper by Derevianko *et al.* [40] and defined as

$i\omega = 2\tan(\frac{\pi t}{2})$

While GL1 is defined within the $-1 \leq t \leq 1$ integration range, GL2 and GL3 are defined for the $0 \leq t \leq 1$ integration range.

Besides the GL quadrature approach, we tested another way to derive eq. (5.13), based on assuming that the dynamic polarizability of the target species can be expanded over the dynamic polarizabilities of the partner species:

$$\alpha(i\omega) = \Sigma_{j=1}^{n} \lambda_j \alpha_j(i\omega) \tag{5.15}$$

Substitution of eq. (5.15) into the C_6^i Casimir-Polder integral immediately leads to the linear system for λ_j (5.12), while the second substitution for C_6 yields eq. (5.13). Hereinafter we refer to this method simply as Expansion, EXP.

5.4. Test cases

5.4.1. First impression: dispersion coefficients of the alkaline ions and the alkaline-earth metals

A preliminary test on the performance of the GL1-3 and EXP implementations was carried out. We took the data for the dynamic polarizabilities from the paper by Jiang *et al.* [39], that tabulates the dynamic polarizabilities of the rare gases, singly charged alkaline cations and alkaline-earth metals, evaluated by the oscillator strength summation, and their dispersion coefficients for the like and unlike interaction, calculated with the 40-point GL2 quadrature. We then considered the rare gases from He to Xe as the partner species and the alkaline ions and the alkaline-earth metals as the target species. The related C_6^{ij}, C_6^i coefficients were computed by Casimir-Polder integration, using either the same quadrature or by classical Simpson rule for the large uniform mesh. The difference between two methods emerges at worst in the third significant digit and is therefore negligible for the present comparison. The coefficients thus achieved were used to evaluate the solution of eq. (5.13) within the GL1-3 and EXP implementations of the rule. The resulting dispersion coefficients for the like interaction of the target species are reported in Tables 5.1-3, together with the percentage deviation *S* from the like-species dispersion coefficients tabulated by Ref. [39]. For GL-based methods we also provide the percentage deviation S_{GL} from the Casimir-Polder integral of the reference target species dynamic polarizabilities evaluated with a specific

quadrature and five points. In addition, a comparison is also made with the inverse CR (5.6), in our notation,

$$C_6 = \frac{(\alpha/\alpha^i)C_6^{ii}C_6^i}{[2C_6^{ii}-(\alpha^i/\alpha)C_6^i]} \tag{5.16}$$

The tables include the arithmetic means of eq. (5.16) over the rare gas partners and the deviations from the reference coefficient for the like interaction of the targets.

Table 5.1. Dispersion coefficients for the like interaction of the alkali atom target species (from Li to Rb), obtained with the combination rules (a.u.). *S* (%) are the deviations from the reference value, S_{GL} (% relevant to the GL methods) are the deviations from Casimir-Polder integration with 5-point quadratures.

	C_6	S_{GL}	S
Li, C_6 = 1395.80, α (0)= 164.30			
EXP	1065.86		23.6
GL1	1165.33	15.2	16.5
GL2	1323.78	11.4	5.2
GL3	321.90	0.1	76.9
Eq. (5.16)	1421.61		1.8
Na, C_6 = 1561.61, α (0)= 162.80			
EXP	1258.30		19.4
GL1	1365.18	11.1	12.6
GL2	1555.41	10.5	0.4
GL3	473.68	0.2	69.7
Eq. (5.16)	1619.39		3.7
K, C_6 = 3906.28, α (0)= 290.00			
EXP	2850.41		27.0
GL1	3118.19	19.7	20.2
GL2	3467.87	11.2	11.2
GL3	766.02	0.1	80.4

Table 5.1 ***(continued)***

	C_6	S_{GL}	S
Eq. (5.16)	4329.14		10.8
Rb, C_6 = 4666.91, α (0)= 317.00			
EXP	3420.00		26.7
GL1	3735.75	19.7	20.0
GL2	4113.24	10.9	11.9
GL3	968.72	0.1	79.2
Eq. (5.16)	5357.36		14.8

Table 5.2. Dispersion coefficients for the like interaction of the alkaline-earth ion target species (from Be^+ to Ba^+), obtained with the combination rules (a.u.). *S* (%) are the deviations from the reference value, S_{GL} (% relevant to the GL methods) are the deviations from Casimir-Polder integration with 5-point quadratures.

	C_6	S_{GL}	S
Be^+, C_6 = 68.79, α (0)= 24.50			
EXP	65.96		7.7
GL1	68.13	1.3	2.9
GL2	68.52	4.8	2.0
GL3	57.04	0.1	17.1
Eq. (5.16)	70.62		2.7
Mg^+, C_6 = 154.59, α (0)= 34.99			
EXP	150.04		2.9
GL1	153.34	1.1	0.8
GL2	152.32	3.8	1.5
GL3	139.60	0.1	9.7
Eq. (5.16)	159.50		3.2

Table 5.2 ***(continued)***

	C_6	S_{GL}	S
Ca^+, C_6 = 541.03, α (0)= 75.46			
EXP	501.12		7.4
GL1	524.63	3.1	3.0
GL2	550.10	6.9	1.7
GL3	355.77	0.1	34.2
Eq. (5.16)	597.62		10.5
Sr^+, C_6 = 775.72, α (0)= 90.19			
EXP	716.11		7.7
GL1	753.37	2.8	2.9
GL2	791.11	6.6	2.0
GL3	505.35	0.1	34.9
Eq. (5.16)	883.27		13.9
Ba+, C_6 = 1293.19, α (0)= 121.25			
EXP	1174.69		9.2
GL1	1239.30	3.7	4.2
GL2	1327.54	6.6	2.7
GL3	764.02	0.1	40.9
Eq. (5.16)	1518.60		17.43

Table 5.3. Dispersion coefficients for the like interaction of the alkaline-earth atom target species (from Be to Ba), obtained with the combination rules (a.u.). *S* (%) are the deviations from the reference value, S_{GL} (% relevant to the GL methods) are the deviations from Casimir-Polder integration with 5-point quadratures.

	C_6	S_{GL}	S
Be, C_6 = 213.40, α (0)= 37.73			
EXP	210.62		1.3
GL1	206.03	4.8	3.5
GL2	207.88	2.2	2.6
GL3	216.06	0.0	1.2
Eq. (5.16)	214.35		0.4
Mg, C_6 = 629.58, α (0)= 71.37			
EXP	610.11		3.1
GL1	626.86	0.7	0.4
GL2	620.04	4.1	1.5
GL3	566.81	0.2	10.0
Eq. (5.16)	638.50		1.4
Ca, C_6 = 2188.19, α (0)= 159.40			
EXP	1989.40		9.1
GL1	2109.59	3.4	3.6
GL2	2236.57	7.7	2.2
GL3	1333.96	2.8	39.0
Eq. (5.16)	2324.65		6.2
Sr, C_6 = 3149.29, α (0)= 197.90			
EXP	2809.06		10.8
GL1	2979.58	4.9	5.4
GL2	3508.50	0.1	11.4
GL3	1691.28	0.1	46.3
Eq. (5.16)	3427.45		8.8

Table 5.3 ***(continued)***

	C_6	S_{GL}	S
Ba, C_6 = 5379.59, α (0)= 278.10			
EXP	4621.82		14.1
GL1	5338.81	0.4	0.8
GL2	5486.66	8.1	2.0
GL3	2347.54	0.1	56.3
Eq. (5.16)	6027.06		12.0

With the five-fold set of the rare gas partners, all the methods tend to perform better for those target atoms having smaller polarizabilities, as demonstrated by the increasing deviation from the alkaline cations and the alkaline-earth metal to the alkaline metal atoms. The small polarizabilities of the rare gases (static values range from 1.4 a.u. to 27 a.u.) fit the alkaline ions and the alkaline-earth metals better than the alkaline metals. Eq. (5.16) also performs better on less polarizable targets and, for the alkaline-earth atoms, retrieves dispersion coefficients more accurately compared to our method. In contrast, generally the expansion and GL1 and GL2 methods exceed eq. (5.16) in accuracy for the alkaline ions and the alkaline-earth atoms.

GL3 method always returns strongly underestimated dispersion coefficients and shows the largest deviation among all the different implementations of eq. (5.13). In agreement with the deviation from the reference data, the deviation of the CR with respect to the results of the five-point integration S_{GL} decreases as target polarizability decreases. As before, this trend is due to the better fitting of the less polarizable atoms by the rare gas small polarizabilities. Only GL3 always shows the same deviation from its crude integration counterpart.

Overall, this preliminary test using a minimal set of partners reveals promising results: the dispersion coefficients of those target having small polarizabilities are quite competitive at this level with respect to both the reference values and the results of eq. (5.13). We can thus suppose that the use of partner species with larger polarizabilities or the extension of the partner set to a larger number of species may further refine the results for the least polarizable targets and make the results for the most polarizable targets competitive.

5.4.2. Interaction of the ground-state Yb atoms

More pristine test was thus considered, with accurately known atomic dynamic polarizabilities. The dynamic polarizabilities of the Yb atom were taken from Ref. [41] (complete basis set limit of the X2C-28 CCSD(3) polarization propagator calculations [42], as it is implemented in the MOLPRO package, see Chapter 2). As in the previous test, the polarizabilities of the partner species were taken from Ref. [39], while the C_6^i and C_6^{ij} coefficients were computed by integrating the Yb polarizabilities from Ref. [41] and the partner polarizabilities from Ref. [39] by the usual classical Simpson rule for the large uniform mesh, with the natural cubic spline interpolation of the polarizabilities.

The EXP and GL1-GL3 methods were checked with the already used set of partner rare gas atoms from He to Xe (Set I), in addition to which Set II, consisting of five alkaline-earth metal atoms from Be to Ba, and Set III, matching the previous two sets, were also employed. The C_6 coefficients for the Yb dimer thus obtained are reported in Table 5.4, together with their percentage deviations S from 2065.40 a.u., the exact value for the given dynamic polarizability [41]. As before, for the GL-based methods the percentage deviation S_{GL} from the Casimir-Polder integral of the reference Yb dynamic polarizability evaluated with a particular quadrature and number of points (5 for sets I and II, 10 for set III) is also given, together with a comparison with the CR (5.16).

Table 5.4. Dispersion coefficients for the Yb dimer obtained using the combination rules (a.u.). S (%) are the deviations from reference value, S_{GL} (%, relevant to GL methods) are the deviations from Casimir-Polder integration with 5- or 10-point quadratures.

CR	Set I			Set II			Set III		
	C_6	S_{GL}	S	C_6	S_{GL}	S	C_6	S_{GL}	S
EXP	1919.1		7.1	2026.2		1.9	2030.8		1.7
GL1	2064.1	1.1	0.1	2086.2	0.0	1.0	2067.8	0.0	0.1
GL2	2063.9	6.5	0.1	2207.3	0.0	6.9	2055.7	0.5	0.5
GL3	1536.0	0.0	25.6	1533.8	0.2	25.7	2134.0	0.0	3.3
Eq.(5.16)	2227.1		7.8	1928.3		6.6	2077.7		0.6

The expansion method works much better for sets II and III, compared to set I. The higher polarizabilities of the alkaline-earth metal atoms fit Yb polarizability better than the polarizabilities of the rare gases. Also Eq. (5.16) improves from set I to set III. In contrast, *S* decreases from set I to set II for all quadrature methods. In fact, for few points Eq. (5.14) better approximates compact integrals for less polarizable partners. Together with *S*, also S_{GL} degrades from set I to set II.

It is noteworthy that, for a given set, different quadrature types perform with different accuracies, due to their distinct convergence with increasing number of points.

In Figure 5.1 the convergence of the C_6 coefficient for three GL quadratures is illustrated; GL1 [38] has the fastest convergence: the related deviation from the reference falls within 1% already at $n = 5$ points. GL2 and GL3 attain the same accuracy only when *n* exceeds 7 and 12 respectively. The slower convergence of GL2 and GL3 explains the larger deviations shown by these methods for the targets treated in the previous section. Albeit the convergence patterns are also partner-dependent, the case of Yb C_6 is quite representative and explains the results of Table 5.4.

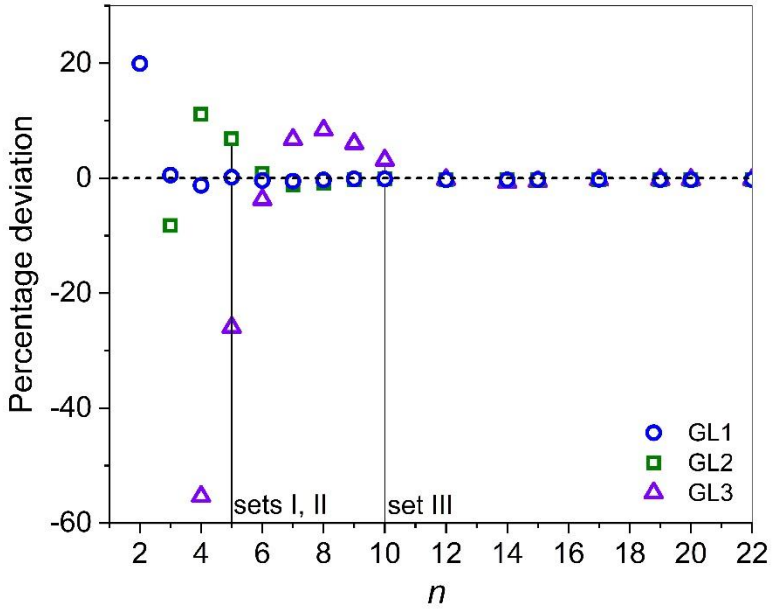

Figure 5.1. Convergence of the Casimir-Polder integration for Yb C_6 coefficient with the number of quadrature points *n* (reproduced from G. Visentin, I.S. Kalinina, and A.A. Buchachenko, J. Chem. Phys. **153**, 064110 (2020), with the permission of AIP Publishing).

According to the derivation of CR (5.13), knowledge of the λ_i coefficients should allow one to retrieve the dynamic polarizability of the target species, beside of the related dispersion coefficients. The extracted Yb dynamic polarizabilities are depicted in Figure 5.2 and compared with the reference ones [41]: the agreement is quite reasonable at imaginary frequencies below 3 a.u. for all methods, except GL3. The limiting zero-frequency values returned by EXP, GL1 and GL2 methods, amounting to 138.2 a.u., 140.4 a.u. and 139.1 a.u. respectively, fall within a 2% deviation from the reference static polarizability (140.6 a.u.). On the other hand, a tendency to break the monotonic behavior together with increasing deviations arises at higher frequencies. From Figure 5.2 the performance of each quadrature formula is also evident: the GL1 transformation provides the widest frequency coverage and the closest approach to zero; GL2 tends to overestimate the dynamic polarizabilities; in contrast, the GL3 points spread within the narrow-medium frequency range. If few points are available, one can take this ranking as an empirical rule. In fact, when a larger number of nodes is taken (from 15-20 nodes) all three quadratures converge more or less to identical accuracies.

In summary, the Yb case suggests that the extended combination rule (5.13) allows the extraction of accurate dispersion coefficients and provides overall reasonable approximations to dynamic polarizability. In particular, for the former a proper choice of the partners, based, for instance, on their static polarizabilities, ensures a 1-2% accuracy with a set of 5-10 partner species.

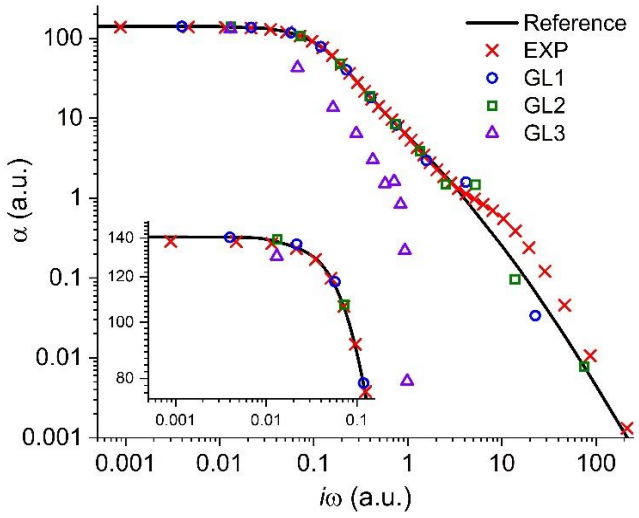

Figure 5.2. Double-logarithmic plot of the Yb dynamic polarizabilities extracted by the combination rule for set III in comparison with the reference. Inset emphasizes the low-frequency region (reproduced from G. Visentin, I.S. Kalinina, and A.A. Buchachenko, J. Chem. Phys. **153**, 064110 (2020), with the permission of AIP Publishing).

5.4.3. Interaction of the ground-state pnictogen atoms

For the third test case, we chose the dispersion coefficients of the atoms belonging to group 15 of the periodic table, the so called pnictogens, from N to Bi, in the electronic ground $^4S^o$ state. In contrast to the previous test, these atoms have non-zero spin. However, the total orbital momentum is zero and, therefore, interaction anisotropy and spin-orbit coupling do not affect these systems. Furthermore, here the dynamic polarizabilities are not known. This situation simulates a practical implementation of the rule (5.13) for extracting the dispersion coefficients C_6 for like interactions from the unlike-partner C_6^i dispersion coefficients computed ab initio.

For the N and P atoms all electrons were explicitly treated; for As, Sb and Bi, instead, small-core relativistic effective core potentials ECP10MDF [43], ECP28MDF and ECP60MDF [44], respectively, were used. For the basis set, the augmented correlation-consistent polarized weighted core valence quintuple-zeta basis set (aug-cc-pwCV5Z) [45,46] was used. For the partner species, we considered set III from the previous test, consisting of the rare gas atoms from He to Xe and of the alkaline-earth metal atoms from Be to Ba. For those atoms we chose a description consistent with that of the target atoms N-Bi: the all-electron augmented correlation-consistent polarized valence quintuple-zeta sets aug-cc-pV5Z was used to describe He [47], the all-electron aug-cc-

pwCV5Z basis set for Ne, Ar [45], Be and Mg [48] and the aug-cc-pwCV5Z basis sets [49] supplementing the ECPs (ECP10MDF for Kr and Ca, ECP28MDF for Xe and Sr, and ECP46MDF Ba [50,51]). The interaction energies were computed by means of the restricted Coupled Cluster method with singles, doubles and non-iterative triples [52] based on the restricted Hartree-Fock reference. The interaction energies for atom-partner atom pairs were corrected with the counterpoise method by Boys and Bernardi [53] and calculated on the irregular grids of 15-25 points ranging the internuclear distances R from 20 to 65 a_0. All non-ECP electrons were correlated. The electronic energies were converged up to 10^{-12} hartree.

We first tested the validity of this scheme by calculating the static polarizabilities at the CCSD(T)-FF level. The results reported in Table 5.5 exhibit a reasonable agreement with the time-dependent density functional (TD-DFT) calculations by Chu and Dalgarno [54] and by Gould and Bučko [55], almost coincide with the similar CCSD(T) calculations from Refs. [56-58] and fit the error bars recommended by Schwerdtfeger and Nagle [59].

Table 5.5. Static dipole polarizabilities of the Group 15 ground-state atoms (a.u.). Uncertainties to the last significant digit are given in parentheses.

Source	N	P	As	Sb	Bi
This work	7.2	25.0	29.6	42.8	48.8
TD-DFT [54]	7.4	25	29	44	
TD-DFT [55]	7.25	24.8	29.6	44.0	43.2
CCSD(T) [56]	7.26	25.1	29.8	42.8	48.8
CCSD(T) [57]	7.26				
CCSD(T) [58]		24.93			
Recommended [59]	7.4(2)	25(1)	30(1)	43(2)	48(4)

For the computed interaction energies, the C_6^i coefficients were determined by the linear least-square fits to the R^{-6} energy dependence after removing the outlier points at largest distances and those at shorter distances. Table 5.6 presents the results thus obtained, which, in turn, provided the input to our combination rule together with the C_6^{ij} coefficients for partner-partner interactions, calculated, as before, by integrating the dynamic polarizabilities tabulated by Jiang *et al.*[39].

Table 5.6. Dispersion coefficients for interactions of the Group 15 atoms (N-Bi) with the rare gases (He-Xe) and the alkaline-earth metal atoms (Be-Ba) (a.u.). Uncertainties to the last significant digit are given in parentheses.

Partners	N	P	As	Sb	Bi
He	5.7(2)	15.2(2)	17.26(4)	24.2(1)	26.7(1)
Ne	11.82(1)	30.3(1)	35.0(1)	47(2)	53.8(1)
Ar	40.0(3)	105.5(2)	122.8(3)	169(1)	190.2(1)
Kr	55.91(5)	154.2(2)	176.5(1)	246.04(4)	278.0(3)
Xe	83.4(1)	233.9(3)	267.2(1)	377(7)	417.6(3)
Be	49.1(2)	185.6(6)	212(1)	303(4)	342.9(4)
Mg	100.4(2)	311.4(6)	361.6(8)	520(2)	569.4(6)
Ca	172.3(3)	542(1)	611.3(7)	904(2)	998(1)
Sr	211.3(5)	663(2)	749.5(7)	1106(2)	1209(1)
Ba	259(1)	844(3)	944.5(8)	1334(6)	1530(9)

The C_6 coefficients for the like interaction of the group 15 atoms obtained from the CRs (5.13) and (5.16) are reported in Table 5.7. All the implementations of eq. (5.13) show a similar trend to the one noticed in the Yb test case. The most accurate quadrature-based method, GL1, aligns in accuracy with the EXP method, whereas GL2 and GL3 returns increasing deviations. The conservative estimates of the CR accuracy do not exceed 15% (excluding the Bi case, where the dispersion coefficient can be underestimated as the static polarizability [55], see Table 5.5).

Table 5.7. Dispersion coefficients for like interactions of Group 15 atoms obtained by combination rules and from literature (a.u.).

Atom	EXP	GL1	GL2	GL3	Eq.(5.16)	Literature
N	26.4	26.4	26.4	20.7	30.1	22.0[a]; 25.7[b]; 24.0[c]
P	186.6	186.6	182.7	195.4	198.9	193[a]; 187[b]
As	252.6	252.6	237.9	215.4	253.8	268[a]; 260[b]
Sb	460.9	460.9	484.6	355.1	514.7	526[a]; 504[b]
Bi	638.0	638.0	633.2	562.4	638.8	513[b]

[a,b] TD-DFT, Refs. [54] and [55], respectively.

[c] CCSDT, Ref. [60].

Figure 5.3 depicts the dynamic polarizabilities of the N and Bi atoms extracted with CR (5.13). From this figure the contrast between the accuracy of the dispersion coefficients and that of the related polarizabilities emerges: in facts, while our CR was able to restore the former reasonably well, it fails in restoring the latter ones as accurately as in the Yb case. The resulting functions of the dynamic polarizabilities can be non-monotonic and not necessarily converge to the static polarizability at the zero-frequency limit. In addition, we noticed that the extracted dynamic polarizabilities are sensitive to the uncertainties of input dispersion coefficients, even when they are as small as those given in Table 5.6.

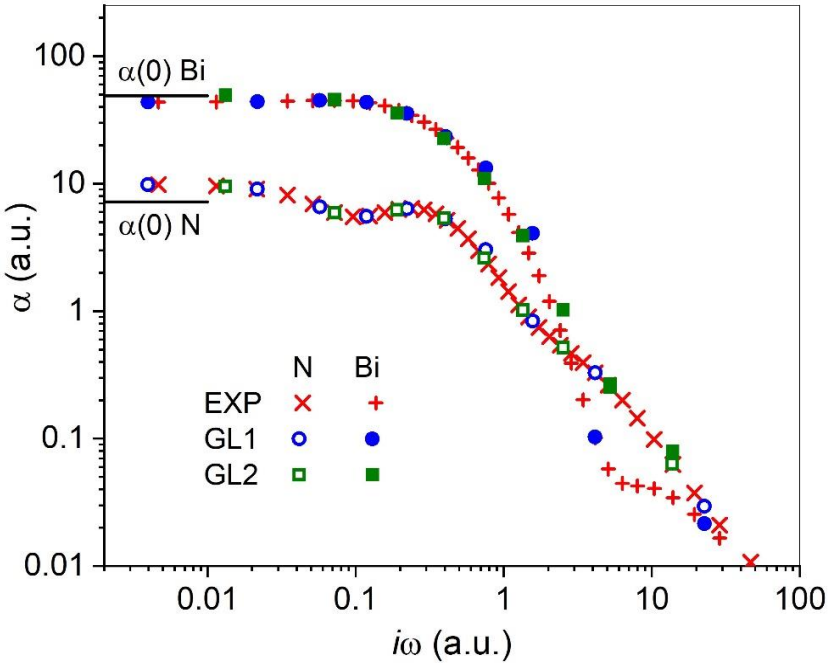

Figure 5.3. Double-logarithmic plot of the N and Bi dynamic polarizabilities extracted by the combination rule (5.13). Horizontal lines mark the respective static polarizabilities (reproduced from G. Visentin, I.S. Kalinina, and A.A. Buchachenko, J. Chem. Phys. **153**, 064110 (2020), with the permission of AIP Publishing).

5.5. Conclusions

An extended pure combination rule (5.13) was proposed. The rule relates the dispersion coefficient for the interaction of the like target species to the same coefficients for interactions between the target and a set of partner species, as well as the interactions of the partners, following the bounding approach described by Weinhold [22]. Our rule can be derived either by expanding the dynamic polarizability of the target species over that of the partners or by uniform discretization of the Casimir-Polder integral over a quadrature, e.g. with the Gauss-Legendre quadrature, and implies the solution of a linear system of equations. Its prediction should be as accurate as the number of partners is increased.

The test cases show that implementations based on the dynamic polarizability expansion (5.15) and the Gauss-Legendre quadrature by Amos *et al.* [38] give very reasonable results for dispersion coefficients when a set of 10 partners is chosen (here, the rare gases from He to Xe and the alkaline-earth metal atoms from Be to Ba). In this way, the rule can be used to retrieve the dispersion

coefficients of complex species dimers, such as open-shell systems and large molecules, when the interactions with closed-shell partners are much easier to attain than the self-interaction or the dynamic polarizabilities. In contrast, CR (5.13) does not ensure the monotonic behavior of the approximated dynamic polarizabilities of the target species. Of course, this does not exclude the possibility to improve the rule: enforcing the correct behavior of the dynamic polarizability [61] may help to achieve more prominent results. Generalization to higher-order long-range coefficients is straightforward. However, a severe limit to our CR is represented by the strong sensitivity of the retrieved dynamic polarizabilities to the accuracy (and transferability) of the atom-partner dispersion coefficients. This limit turned out to be evident when fitted atom-partner coefficients from dimer calculations were used to determine the polarizabilities and demonstrate that the sole knowledge of the former may not be sufficient to retrieve the latter.

References

[1] P. von Ragu-Schleyer, Encyclopedia of Computational Chemistry (Wiley, Chichester, 1998).

[2] J. Paldus and X. Li in Advances in Chemical Physics, Vol. 110, edited by I. Prigogine and S.A. Rice, Chapter 1 (John Wiley and sons, 1999).

[3] J. Noga, and R. J. Bartlett, *The full CCSDT model for molecular electronic structure*, J. Chem. Phys. **86**, 7041 (1987); doi: 10.1063/1.452353.

[4] J. Paldus, J. Čížek, and I. Shavitt, *Correlation Problems in Atomic and Molecular Systems. IV. Extended Coupled-Pair Many-Electron Theory and Its Application to the BH_3 Molecule*, Phys. Rev. A **5**, 50 (1972); doi: 10.1103/PhysRevA.5.50.

[5] V. Aquilanti, and G. Grossi, *Angular momentum coupling schemes in the quantum mechanical treatment of P-state atom collisions*, J. Chem. Phys. **73**, 1165 (1980); doi: 10.1063/1.440270.

[6] R.V. Krems, G. C. Groenenboom, and A. Dalgarno, *Electronic interaction anisotropy between atoms in arbitrary angular momentum states*, J. Phys. Chem. **108**, 8941 (2004); doi: 10.1021/jp0488416.

[7] A. J. Stone, The Theory of Intermolecular Forces (Oxford University Press, Oxford, 2013).

[8] I.G. Kaplan, *Intermolecular interactions: physical picture, computational methods and model potentials*, (John Wiley and Sons, New York, 2006). doi: 10.1002/047086334X.

[9] K.P. Huber, G. Herzberg, *Molecular Spectra and Molecular Structure: Spectra of Diatomic Molecules* (Springer, Boston, MA, 1979); doi: 0.1007/978-1-4757-0961-2.

[10] T. Forster, and K. Kasper, *Ein Konzentrationsumschlag der Fluoreszenz des Pyrens*, Z. Elektrochem. **59**, 976-980, 197 (1955).

[11] P.W. Milonni, and J.H. Eberly, *Lasers*, Wiley eds., New York, **197** (1988).

[12] E. A. Moelwyn-Hughes, Physical Chemistry (Pergamon, New York, 1957), p. 332.

[13] C. L. Kong, *Combining rules for intermolecular potential parameters. I. Rules for the Dymond-Alder potential,*J. Chem. Phys. **59**, 1953 (1973); doi: 10.1063/1.1680281.

[14] J. O. Hirschfelder, C. F. Curtiss, and R. B. Bird, Molecular Theory of Gases and Liquids (John Wiley & Sons, New York, 1954), p. 963.

[15] R. H. Good and Ch. J. Hope, *New Combining Rule for Intermolecular Distances in Intermolecular Potential Functions,* J. Chem. Phys. **53**, 540 (1970); doi: 10.1063/1.1674022.

[16] M. Waldman and A. T. Hagler, *New combining rules for rare gas van der waals parameters,* J. Comput. Chem. **14**, 1077 (1993); doi: 10.1002/jcc.540140909.

[17] H. Pauly and J. P. Toennies, *The Study of Intermolecular Potentials with Molecular Beams at Thermal Energies,* Adv. At. Mol. Phys. **1**, 195 (1965); doi: 10.1016/S0065-2199(08)60283-3.

[18] K. T. Tang and J. P. Toennies, *New Combining Rules for Well Parameters and Shapes of the van der Waals Potential of Mixed Rare Gas Systems,* Z. Phys. D: At., Mol. Clusters **1**, 91 (1986); doi: 10.1007/BF01384663.

[19] G. P. Yin, P. Li, and K. T. Tang, *The ground state van der Waals potentials of the strontium dimer and strontium rare-gas complexes,* J. Chem. Phys. **132**, 074303 (2010); doi: 10.1063/1.3317406.

[20] A. J. Thakkar, *Bounding and estimation of van der Waals coefficients,* J. Chem. Phys. **81**, 1919 (1984); doi: 10.1063/1.447866.

[21] K. T. Tang, *Upper Bounds for van der Waals Interactions of Two and Three Atoms,* J. Chem. Phys. **49**, 4727 (1968); doi: 10.1063/1.1669947.

[22] F. Weinhold, *Upper and lower bounds to the van der Waals interactions between atoms,* J. Phys. B: At. Mol. Phys. **2**, 517 (1969); doi: 10.1088/0022-3700/2/5/301.

[23] J. N. Wilson, *On the London Potential Between Pairs of Rare-Gas Atoms*, J. Chem. Phys. **43**, 2564 (1965); doi: 10.1063/1.1697170.

[24] A. D. Crowell, *Comment on the London Potential between Pairs of Rare-Gas Atoms,* J. Chem. Phys. **49**, 3324 (1968); doi: 10.1063/1.1670594.

[25] H. L. Kramer and D. R. Herschbach, *Combination Rules for van der Waals Force Constants*, J. Chem. Phys. **53**, 2792 (1970); doi: 10.1063/1.1674404.

[26] M. Diaz Pena, C. Pando, and J. A. R. Renuncio, *Combination rules for two-body van der Waals coefficients*, J. Chem. Phys. **72**, 5269 (1980); doi: 10.1063/1.439764.

[27] G. D. Zeiss and W. J. Meath, *Dispersion energy constants C_6(A, B), dipole oscillator strength sums and refractivities for Li, N, O, H_2, N_2, O_2, NH_3, H_2O, NO and N_2O,* Mol. Phys. **33**, 1155 (1977); doi: 10.1080/00268977700100991.

[28] M. Alvarez-Rizzatti and E. A. Mason, *Estimation of dipole-quadrupole dispersion energies*, J. Chem. Phys. **59**, 518 (1973); doi: 10.1063/1.1679837.

[29] J. S. Cohen and R. T. Pack, *Modified statistical method for intermolecular potentials. Combining rules for higher van der Waals coefficients***,** J. Chem. Phys. **61**, 2372 (1974); doi: 10.1063/1.1682318.

[30] W. C. Stwalley, *Higher-order long-range interactions between rare gas and hydrogen atoms,* J. Chem. Phys. **61**, 3840 (1974); doi: 10.1063/1.1682573.

[31] A. D. Koutselos and E. A. Mason, *Correlation and prediction of dispersion coefficients for isoelectronic systems*, J. Chem. Phys. **85**, 2154 (1986); doi: 10.1063/1.451108.

[32] S. Riniker, Fixed-Charge Atomistic Force Fields for Molecular Dynamics Simulations in the Condensed Phase: An Overview, J. Chem. Inf. Model. **58**, 565 (2018); doi: 10.1021/acs.jcim.8b00042.

[33] T. A. Halgren, The representation of van der Waals (vdW) interactions in molecular mechanics force fields: potential form, combination rules, and vdW parameters, J. Am. Chem. Soc. **114**, 7827 (1992); doi: 10.1021/ja00046a032.

[34] Q. Wu and W. Yang, *Empirical correction to density functional theory for van der Waals interactions*, J. Chem. Phys. **116**, 515 (2002); doi: 10.1063/1.1424928.

[35] A. Tkatchenko and M. Scheffler, *Accurate Molecular Van Der Waals Interactions from Ground-State Electron Density and Free-Atom Reference Data*, Phys. Rev. Lett. **102**, 073005 (2009); doi: 10.1103/PhysRevLett.102.073005.

[36] S. Grimme, J. Antony, S. Ehrlich, and H. Krieg, *A consistent and accurate ab initio parametrization of density functional dispersion correction (DFT-D) for the 94 elements H-Pu*, J. Chem. Phys. **132**, 154104 (2010); doi: 10.1063/1.3382344.

[37] C. Deligkaris and J. H. Rodriguez, *Correction to DFT interaction energies by an empirical dispersion term valid for a range of intermolecular distances*, Phys. Chem. Chem. Phys. **14**, 3414 (2012); doi: 10.1039/C2CP23673G.

[38] R. D. Amos, N. C. Handy, P. J. Knowles, J. E. Rice, and A. J. Stone, *AB-initio prediction of properties of carbon dioxide, ammonia, and carbon dioxide...ammonia,* J. Phys. Chem. **89**, 2186 (1985); doi: 10.1021/j100257a010.

[39] J. Jiang, J. Mitroy, Y. Cheng, and M. W. J. Bromley, *Effective oscillator strength distributions of spherically symmetric atoms for calculating polarizabilities and long-range atom–atom interactions*, At. Data Nucl. Data Tables **101**, 158 (2015); doi: 10.1016/j.adt.2014.10.001.

[40] A. Derevianko, S. G. Porsev, and J. F. Babb, *Electric dipole polarizabilities at imaginary frequencies for hydrogen, the alkali-metal, alkaline earth and noble gas atoms*, At. Data Nucl. Data Tables **96**, 323 (2010).

[41] G. Visentin and A.A. Buchachenko, *Polarizabilities, dispersion coefficients and retardation functions at the complete basis set CCSD limit: Be-Ba and Yb*, J. Chem. Phys. **151**, 214302 (2019); doi: 10.1063/1.5129583.

[42] T. Korona and B. Jeziorski, *One-electron properties and electrostatic interaction energies from the expectation value expression and wave function of singles and doubles coupled cluster theory*, J. Chem. Phys. **125**, 184109 (2006); doi: 10.1063/1.2364489.

[43] H. Stoll, B. Metz, and M. Dolg, *Relativistic energy-consistent pseudopotentials—Recent developments*, J. Comput. Chem. **23**, 767 (2002); doi: 10.1002/jcc.10037.

[44] B. Metz, H. Stoll, and M. Dolg, *Small-core multiconfiguration-Dirac–Hartree–Fock-adjusted pseudopotentials for post-d main group elements: Application to PbH and PbO*, J. Chem. Phys. **113**, 2563 (2000); doi: 10.1063/1.1305880.

[45] K. A. Peterson and T. H. Dunning, Jr., *Accurate correlation consistent basis sets for molecular core–valence correlation effects: The second row atoms Al–Ar, and the first row atoms B–Ne revisited*, J. Chem. Phys. **117**, 10548 (2002); doi: 10.1063/1.1520138.

[46] K. A. Peterson and K. E. Yousaf, *Molecular core-valence correlation effects involving the post-d elements Ga–Rn: Benchmarks and new pseudopotential-based correlation consistent basis sets*, J. Chem. Phys. **133**, 174116 (2010); doi: 10.1063/1.3503659.

[47] D. E. Woon and T. H. Dunning, Jr., *Gaussian basis sets for use in correlated molecular calculations. IV. Calculation of static electrical response properties,* J. Chem. Phys. **100**, 2975 (1994); doi: 10.1063/1.466439.

[48] B. P. Prascher, D. E. Woon, K. A. Peterson, T. H. Dunning, Jr., and A. K. Wilson, *Gaussian basis sets for use in correlated molecular calculations. VII. Valence, core-valence, and scalar-relativistic basis sets for Li, Be, Na, and Mg*, Theor. Chem. Acc. **128**, 69 (2011); doi: 10.1007/s00214-010-0764-0.

[49] J. G. Hill and K. A. Peterson, *Gaussian basis sets for use in correlated molecular calculations. XI. Pseudopotential-based and all-electron relativistic basis sets for alkali metal (K–Fr) and alkaline earth (Ca–Ra) elements,* J. Chem. Phys. **147**, 244106 (2017); doi: 10.1063/1.5010587.

[50] K. A. Peterson, D. Figgen, E. Goll, H. Stoll, and M. Dolg, *Systematically convergent basis sets with relativistic pseudopotentials. II. Small-core pseudopotentials and correlation consistent basis sets for the post-d group 16–18 elements,* J. Chem. Phys. **119**, 11113 (2003); doi: 10.1063/1.1622924.

[51] I. S. Lim, H. Stoll, and P. Schwerdtfeger, *Relativistic small-core energy-consistent pseudopotentials for the alkaline-earth elements from Ca to Ra,* J. Chem. Phys. **124**, 034107 (2006); 10.1063/1.2148945.

[52] P. J. Knowles, C. Hampel, and H. J. Werner, *Coupled cluster theory for high spin, open shell reference wave functions,* J. Chem. Phys. **99**, 5219 (1993); doi: 10.1063/1.465990.

[53] S. Boys and F. Bernardi, *The calculation of small molecular interactions by the differences of separate total energies. Some procedures with reduced errors,* Mol. Phys. **19**, 553 (1970); doi: 10.1080/00268977000101561.

[54] X. Chu and A. Dalgarno, *Linear response time-dependent density functional theory for van der Waals coefficients,* J. Chem. Phys. **121**, 4083 (2004); doi: 10.1063/1.1779576.

[55] T. Gould and T. Bucko, *C_6 Coefficients and Dipole Polarizabilities for All Atoms and Many Ions in Rows 1–6 of the Periodic Table,* J. Chem. Theory Comput. **12**, 3603 (2016); doi: 10.1021/acs.jctc.6b00361.

[56] A. A. Buchachenko, *Anisotropy of the static dipole polarizability induced by the spin–orbit interaction: the S-state atoms N–Bi, Cr, Mo and Re,* Proc. R. Soc. A **467**, 1310 (2010); doi: 10.1098/rspa.2010.0440.

[57] A. K. Das and A. J. Thakkar, *Static response properties of second-period atoms: coupled cluster calculations*, J. Phys. B: At., Mol. Opt. Phys. **31**, 2215 (1998); doi: doi.org/10.1088/0953-4075/31/10/011.

[58] C. Lupinetti and A. J. Thakkar, *Polarizabilities and hyperpolarizabilities for the atoms Al, Si, P, S, Cl, and Ar: Coupled cluster calculations*, J. Chem. Phys. **122**, 044301 (2005); doi: doi.org/10.1063/1.1834512.

[59] P. Schwerdtfeger and J. K. Nagle, *2018 Table of static dipole polarizabilities of the neutral elements in the periodic table*, Mol. Phys. **117**, 1200 (2019); doi: 10.1080/00268976.2018.1535143.

[60] T. V. Tscherbul, J. Kłos, A. Dalgarno, B. Zygelman, Z. Pavlovic, M. T. Hummon, H.-I. Lu, E. Tsikata, and J. M. Doyle, *Collisional properties of cold spin-polarized nitrogen gas: Theory, experiment, and prospects as a sympathetic coolant for trapped atoms and molecules*, Phys. Rev. A **82**, 042718 (2010); doi: 10.1103/PhysRevA.82.042718.

[61] K.T. Tang, *Dynamic Polarizabilities and van der Waals Coefficients*, Phys. Rev. **177**, 108 (1969); doi: 10.1103/PhysRev.177.108.

6. Modeling induction interaction in heavy cations: mobility of the singly-charged Lanthanide and Actinide cations

The present exposition is based on the paper **G. Visentin**, M. Laatiaoui, L.A. Viehland, and A.A. Buchachenko, *Mobility of the Singly-Charged Lanthanide and Actinide Cations: Trends and Perspectives,* Front. Chem. **8**, 438 (2020); doi: 10.3389/fchem.2020.00438; under the CC-BY Creative Commons attribution license (CC-BY, version 4.0).

The related project was funded by the Russian Foundation for Basic Research under the project No. 19-03-00144.

Summary

Using the lessons learned in the previous Chapters on accurate customization of ab initio approaches to long-range properties, exploratory scalar-relativistic small-core effective-core potential CCSD(T) calculations are performed on the ground-state interaction potentials of selected singly-charged actinide cations with He and Ar. Special attention is paid to saturation of the atom-centered diffuse basis set component. The calculated interaction potentials are then used to compute the related gas-phase ion mobilities. The results show that the obtained trends for mobility of actinide ions are similar to those found for lanthanides and reveal test cases for exploration of novel experimental techniques, such as Laser Resonance Chromatography. Further improvements of the results would require more sophisticated account of relativistic effects, as it was concluded for ytterbium dimer.

6.1. Introduction

The past century may be considered the era of heavy and superheavy elements: most of them were discovered in that period, with an upsurge between the period immediately preceding the Second World War and the dawn of atomic era (e.g. Fr, $Z = 87$, discovered in 1939 [1]). Since that time, the physics and chemistry of heavy and superheavy elements have received a growing interest from the scientific community. As a peculiar feature of such elements, many of them are synthetic, such as those heavier than $Z = 99$. The way to isolate and characterize the physical and chemical properties of superheavy elements consists of sophisticated techniques of production, isolation and characterization of simple chemical compounds either in gas or in liquid phases [2-7]. However, information on the electronic structure and properties of heavy atoms and ions is also of

great importance. Spectroscopic data, in particular, allow for accurate characterization of the ground state configuration, regardless of the chemical behavior. Moreover, they provide spectral lines that, in turn, can be essential in the search for heavy and superheavy elements in the universe, in particular, in stars [8] and to benchmark data for ab initio methods of atomic and nuclear structure theory [9-14].

Devising a technique for detecting and characterizing heavy elements is indeed challenging, mostly because of the decreasing production yield with increasing atomic number. Standard methods based on fluorescence detection are affected by low sensitivity, making them incompatible with one-atom-at-a-time experiments [15]. For this reason, studies of the gaseous transport properties are currently considered as prospective means for characterizing superheavy ions [16]: in fact, these studies are compatible with in-flight separators that provide recoil ions [17].

First mobility measurements showing that gas-phase ion mobility is sensitive to the electronic configurations of atomic ions date back to the early 1990s [18-24]. In particular, this sensitivity was confirmed for almost all transition metal ions as well as for some main-group ions [25,26].

Gas-phase ion mobility is a fundamental transport property, that defines, macroscopically, steady-state drift velocity of an ion in a neutral buffer gas under the action of a permanent electric field. Steady state, in turn, is defined by the equality of the field-induced dragging force and friction force of the media. The friction reflects interaction. Thus, in some sense, we may consider characterization of an ion by means of its gas-phase interactions with other gaseous species as a kind of chromatographic chemical characterization. The most obvious option relies on choosing monoatomic inert gases, to avoid chemical reactions, suppress energy pooling to internal degrees of freedom of the buffer species and reduce the whole range of interatomic forces to the relatively simple ion-atom interactions.

Theory of Intermolecular forces (see Chapter 2) states that intermolecular interaction potential consists of short- and long-range contributions. In particular, among the latter ones, when one of the interacting partners is an ion, induction contribution arises, scaling with the inverse fourth power of the distance [27-29] and assumes the role of the leading term in the long-range interaction series, followed by the dispersion terms [27,28]. At the lowest order, induction interaction is

sensitive only to the charge of the ion and does not depend on its chemical nature or state (see Chapter 2). Such a dependence emerges only in dispersion forces.

At the macroscopic scale, ion mobility measurements are able to discriminate the ions in the ground state and in a metastable state originating from different electronic configurations [18-24]: the so called *electronic state chromatographic effect* is a direct consequence of the mobility variation with electronic configuration. A recent study [30] has proposed to exploit this effect for spectroscopic characterization of heavy and superheavy ions. According to the proposed method, ions should be collected and pumped from the ground state to the bright state, which, in turn, rapidly relaxes to the metastable state. Then, the prepared ions are released to the drift tube. In other words, ions are first bunched, then drift measurements take place. Detection gives the signal that contains ground-state ions (not pumped or relaxed from the metastable state by collisions) and metastable ions. If metastable ions are detected, then the resonance of the pumping is achieved. This novel technique, called *Laser Resonance Chromatography* (LRC) [30], was initially conceived for the investigation of Lr, the last heavy element not characterized spectroscopically. Indeed, measurements of ion mobility are compatible with the separation and buffer gas trapping techniques, that, in turn, can be controlled by setting external physical conditions, such as operating temperature, pressure and external field strength. These techniques have thus the potentiality to successfully investigate the electronic structure of ions produced in one-atom-at-a-time-mode.

While ion mobility in rare gases has been studied using accurate ab initio potentials for selected lanthanide ions in the ground state [31,32] and for Lu^+ in excited metastable states [30], very little is known on the transport properties of actinide ions, except a few absolute and relative measurements for U^+, Fm^+, Cf^+ and Am^+-Pu^+ ions [33-35] and qualitative calculations for U^+ [36]. In view of the interest in heavy and superheavy ion transport, it is straightforward to explore it using the scalar-relativistic ab initio frame used before for the lanthanide family. Such an exploratory study was performed for the S-state actinide ions Ac^+, Am^+, Cm^+, No^+ and Lr^+ ions, which permit the use of the accurate CCSD(T) method. As almost no experimental data are available to make the quantitative assessment of the new theoretical results, the major emphasis is given to the qualitative trends and their comparison with those observed for lanthanide ions. It should be noted that theoretical results for lanthanides are borrowed from previous works [30-32]

and, thus, do not contribute to the Thesis research. However, their analysis and comparison with the new actinide data do. Also, all the transport calculations presented here were performed by Prof. Larry A. Viehland (Chatham University, Pittsburgh, USA).

Accurate calculations of the ion transport properties imply the knowledge of the global ion-atom interaction potential, thus making the molecular approach the only option to choose. However, designing it, we followed the lessons learned in the previous Chapters. In particular, a common strategy is imparted from the previous cases, relying on three key-points: 1) the choice of saturated atom-centered diffuse basis sets calibrated through the atomic calculations, 2) the accurate description of the electron core and 3) the effectiveness of CCSD(T) method corrected for scalar-relativistic effects. Here, the efficacy of this strategy is checked in the investigation of the relationship of intermolecular interaction and ion-mobility. In fact, due to the interrelationship of these two properties, reliable results for the former necessarily imply reliable results for the latter.

In the next section, ion-mobility theory is briefly outlined. Then, the ab initio approaches used for ion-atom potentials involving lanthanide ions and their accuracy in mobility calculations are presented. The ab initio approaches used for actinide calculations are presented together with the resulting interaction potential and mobility calculations, followed by the comparison with lanthanide results and assessment of the relationship between mobility and effective ionic radii. Concluding remarks follow.

6.2. Ion mobility and interaction potential

The macroscopic definition of the mobility *K* for trace amounts of drifting ions is provided by the equation

$$\boldsymbol{v}_d = K\boldsymbol{E}, \tag{6.1}$$

where the vector quantities $\boldsymbol{v}_d$ and $\boldsymbol{E}$ represent the ion drift velocity and the electric field vector, respectively.

The ion mobility can be deduced in a reasonably accurate way from the measurable arrival time distribution of the ions drifting through the tube of length *l*. The mean drift time t_d is defined as

$$t_d = l/KE \tag{6.2}$$

The standard mobility, K_0, is in turn defined as

$$K_0 = n_0 K / N_0 \tag{6.3}$$

Here, n_0 and $N_0 = 2.6867805 \cdot 10^{25}$ m^{-3} represent the buffer gas number density and the Loschmidts number, respectively. K_0 depends on the reduced electric field strength, F/n_0 and the temperature of the gas T_0.

From the macroscopic viewpoint, the ion mobility is a transport coefficient determined by the solution of the Boltzmann equation. This fundamental equation accounts for anisotropic diffusion and equilibration of the dragging electrostatic force by the forces emerging from the collisions with buffer gas atoms. If equilibrium is achieved, then the velocity of an ion through the buffer gas is constant. The Boltzmann equation is parametrized by collision integrals, in turn expressed through the binary collision cross sections [37,38]. In case of an ion-atom potential, the cross sections are fully determined by the ion-atom interaction potential. Vice versa, from the knowledge of the zero-field mobility over a reasonably wide range of reduced electric field strengths or gas temperature, one can achieve the interaction potential [37,39,40].

The most sophisticated approach to solving the Boltzmann equation for atomic ions drifting in atomic gases is provided by the Gram-Charlier expansion of the ion distribution function [38,41], whose accuracy is limited only by the accuracy of the underlying ion-atom potential [42,43]. This method was used to obtain all mobility results quoted in this Chapter.

The physical situation considered here corresponds to the so called low-field limit: in this frame K_0 depends on the gas temperature very weakly. Nonetheless, this dependence is highlighted by writing the standard mobility as $K_0(T_0)$. When this condition holds, the Gram-Charlier theory reduces to the one temperature theory [37,38] and $K_0(T_0)$ obeys the fundamental low-field ion mobility equation [38]. This equation is expressed as [37,38]

$$K_0(T_0) = \left(\frac{2\pi}{\mu_0 k_B T_0}\right)^{\frac{1}{2}} \frac{3q}{16 N_0} \frac{1+\alpha_c(T_0)}{\bar{\Omega}^{1,1}(T_0)} \tag{6.4}$$

Here, μ_0 is the reduced mass of the ion-atom system, k_B is the Boltzmann constant, q is the ion charge (here always +1 in electron charge units) and $\alpha_c(T_0)$ is the temperature-dependent correction term, small enough to be neglected for heavy ions [38]. $\bar{\Omega}^{1,1}(T_0)$ is referred as the

momentum transfer collision integral and is defined as the temperature average of the energy-dependent momentum transfer cross section [44]. This term is straightforwardly related to the interaction potential. It should be noted that eq. (6.4) permits one to evaluate mobility analytically for simple specific potential models and, therefore, here was used for this sole purpose.

Accurate mobility measurements provide a stringent test on the quality of interaction potentials. Viehland *et al.* [43] made extensive comparisons for ions lighter than Caesium Z = 55, showing that the potentials calculated with an accurate single-reference method, such as CCSD(T), normally provides zero-field mobilities accurate within 0.05%. Previous results achieved for lanthanide ions [30-32] confirmed these conclusions. For actinides, one should recall that this family is characterized by strong relativistic effects, which may limit the accuracy of the proposed scalar-relativistic approach. However, ion-atom interactions are mostly governed by the density of the outermost electrons, thus, relativity may play a less crucial role here than it plays in the energetics of the electronic levels or in chemical bonding.

6.3. Overview of lanthanide results

In previous studies [31,32] lanthanide ions were described with the small-core (28 electrons) effective core potentials obtained at the quasi-relativistic Wood-Boring Hartree-Fock level of theory, ECP28MWB [45]. For the basis set, the supplementary atomic natural orbital basis set with segmented basis contraction [46] was used, with addition of the optimized s2pdfg diffuse functions [47] to supply for the augmentation. Partner He and Ar atoms, on the other hand, were described using the augmented correlation-consistent polarized basis sets aug-cc-pV5Z [48]. The 3s3p2d2f1g bond function set [49] was placed midway the ion-atom distance. The CCSD(T) calculations with the restricted Hartree-Fock references were carried out, treating the $4s^2 4p^6 4d^{10}$ shells of the ion and the $1s^2 2s^2 2p^6$ shells of the Ar atom as core electrons. The CCSD(T) potentials were calculated on fine grids of internuclear distances spanning the 25-40 Å interval and corrected for the basis set superposition error with the counterpoise procedure proposed by Boys and Bernardi [50].

Results for the potential parameters of the lanthanide ions, i.e. potential minima, equilibrium distances R_e and dissociation energies D_e, revealed an overall attractive behavior, with the equilibrium distance generally decreasing with the atomic number Z for ions with the same

electronic configuration. In particular, it was found that the occupancy of the 5d shell plays a significant role in strengthening the interaction energy and reducing the equilibrium distance.

Calculated zero-field mobilities over a wide temperature range turned out to follow well defined trends and to be sensitive to the outer electronic configuration of the ion. In particular, electronic state chromatographic effect [18-24] was well evident for Lu^+, whose mobilities at the ground (^1S) and metastable excited states (^3D) showed significant differences. On the other hand, the trends with atomic number were found to differ for the two distinct cases of the ion mobilities in He and Ar: in the former case, the mobility of the $4f^m6s$ ions generally increases with *Z*, whereas in the latter case it remains overall constant. The two cases also show opposite mobility variations as the electronic configuration changes.

6.4. Interaction potentials of actinide ions

The approach described in Section 6.3 for the lanthanide ions was adapted to the actinide ions. Thus, in this case, the scalar relativistic small core 60-electron ECP60MWB effective core potential [51] replaced the ECP28MWB one, whereas analogous segmented atomic natural basis sets are used [52]. Lack of diffuse augmentation was, here, supplied by adding a spdfg set of the diffuse primitives, whose exponents (0.01, 0.008, 0.03, 0.07 and 0.05 respectively) were optimized for the polarizabilities of neutral Am, No and Lr atoms. The interested reader may find a more detailed description of the procedure used to attain the optimized exponents in the *Appendix* to the present chapter. Analogously to the lanthanide case, He and Ar were described by means of the same CCSD(T) all-electron approach correlating all the electrons for the former, while, for the latter, leaving the $1s^22s^22p^6$ shells uncorrelated. As to the basis set, the augmented core-correlated polarized-valence basis set aug-cc-pV5Z [48] was used. The 3s3p2d2f1g bond function set [49] was placed at the midpoint of the ion-atom distance. All the calculations were performed with the MOLPRO quantum chemistry package (see Chapter 2). Due to the single-reference restriction imposed by CCSD(T), the application of this approach is limited to the ground states of the Ac^+ ($7s^2$, ^1S), Am^+ ($5f^77s$, $^9S^o$), Cm^+ ($5f^77s^2$, $^8S^o$), No^+ ($5f^{14}7s$, ^2S) and Lr^+ ($5f^{14}7s^2$, ^1S) ions.

An alternative single-reference approach for the calculation of those heavy ions was proposed by Lee *et al.* [53] and relies on the use of large-core ECPs [36] to include the 5f shell and the innermost orbitals into the electron core. This approach, called the *5f-in-core* approach, conceals the related momenta and static correlation effects in the ECPs and the ground state of all the ions thence

corresponds to ^{1}S or ^{2}S, the only exception being Th^+ ($6d^27s$). In order to assess the difference with the small-core approach in a systematic way, we also computed the CCSD(T) interaction potentials for the ground state Ac^+, U^+, Cm^+ and Lr^+ ions with He and Ar using the same large-core ECPs. In contrast to Lee *et al.* [53], the supplementary basis sets of aug-cc-pVQZ quality [36] were used without further modification, but augmented by the 3s3p2d2f1g bond function set [49] placed midway the ion-atom distance. Tables 6.1 and 6.2 report the potential parameters, R_e and D_e, obtained for several actinide ions interacting with He and Ar, respectively. Both results achieved with our small-core scalar relativistic approach and the analogs achieved with the large-core 5f-in-core option are showed. In addition, our results are compared to the large-core 5f-in-core potential parameters by Lee *et al.* [53] and to small-core results for selected lanthanide ions [31].

For Ac^+, that has the 5f shell empty, the comparison shows that the large-core description gives slightly stronger ion-atom interactions. In contrast, the trend reverses for Cm^+ and Lr^+ ions, characterized by $5f^7$ and $5f^{14}$ configurations. The binding energies, D_e, differ by 4-5% for He and by 5-6% for Ar, while the difference amounts to 0.03-0.06 Å for the equilibrium distances, R_e. Moreover, the large-core approach exhibits poor accuracy for mobility calculations of U^+ in He, as reported by Lee *et al.* [53], and for Eu^+ in He with analogous "4f-in-core" ECP), as reported by Buchachenko and Viehland [31]. Overall, the large-core approach underestimates the room-temperature zero-field mobilities by 8 and 4% respectively with respect to the experimental data. Therefore, the comparison above validates the small-core approach, that, in turn, will be considered in the following analyses.

Table 6.1. Equilibrium parameters for the ion-He potentials for actinide and lanthanide ions R_e, (Å) and D_e (cm^{-1}).

Ion	He	
	R_e	D_e
$Ac^+ 7s^2\ ^1S$	4.82	30
$Ac^+ 7s^2\ ^1S$ [a]	4.80	30
$U^+ [5f^3]7s^2$ [53]	4.62	33
$U^+ [5f^3]7s^2$ [a]	4.59	34
$Am^+ 5f^7 7s\ ^9S^o$	4.27	39
$Cm^+ 5f^7 7s^2\ ^8S^o$	4.36	42
$Cm^+ [5f^7]7s^2$ [a]	4.39	40
$No^+ 5f^{14} 7s\ ^2S$	4.03	48
$Lr^+ 5f^{14} 7s^2\ ^1S$	4.08	52
$Lr^+ [5f^{14}]7s^2$ [a]	4.11	50
$Eu^+ 4f^7 6s\ ^9S^o$ [31]	4.45	33
$Yb^+ 4f^{14} 6s\ ^2S^o$ [31]	4.23	38
$Lu^+ 4f^{14} 6s^2\ ^1S$ [31]	4.17	47

[a] Large-core calculations, this work.

Table 6.2. Equilibrium parameters for the ion-Ar potentials for actinide and lanthanide ions, R_e (Å) and D_e (cm^{-1}).

Ion	Ar	
	R_e	D_e
$Ac^+ 7s^2\ ^1S$	4.07	426
$Ac^+ 7s^2\ ^1S$ [a]	4.04	434
$U^+ [5f^3]7s^2$ [53]	3.96	454
$U^+ [5f^3]7s^2$ [a]	3.96	470
$Am^+ 5f^7 7s\ ^9S^o$	3.45	698
$Cm^+ 5f^7 7s^2\ ^8S^o$	3.82	538
$Cm^+ [5f^7]7s^2$ [a]	3.88	509
$No^+ 5f^{14} 7s\ ^2S$	3.38	763
$Lr^+ 5f^{14} 7s^2\ ^1S$	3.71	598
$Lr^+ [5f^{14}]7s^2$ [a]	3.78	565
$Eu^+ 4f^7 6s\ ^9S^o$ [31]	3.31	732
$Yb^+ 4f^{14} 6s\ ^2S^o$ [31]	3.25	789
$Lu^+ 4f^{14} 6s^2\ ^1S$ [31]	3.62	620

[a] Large-core calculations, this work.

In order to facilitate the comparison of the different potentials, it is instructive to analyze the *reduced potential functions* $V(\frac{R}{R_e})/D_e$, which are shown in the right column of Figure 6.1. There, it can be noticed that the actinide ion-atom potentials are sensitive to the outermost filled s orbital. This feature is also common to the lanthanide ion-atom potentials [54]. Interactions of the actinide ions with 7s and $7s^2$ outer shells are significantly different from each other. Their bonding is weaker and repulsion is stronger with He, while smoothens with Ar. Actinide ions with the 7s configuration interact with He more strongly than their lanthanide counterparts, as shown by the significant shrinkage of the equilibrium internuclear distance R_e (almost 0.2 Å) and by the increase of the dissociation energy D_e, which exceeds 20%. Also, it is noteworthy that the occupancy of inner f-shell here plays a more important role in the interaction compared to the lanthanide ion case. For the ns^2 ions the trend is almost the opposite: R_e increases when switching from Lu^+ to Lr^+, whereas D_e undergoes a marginal 2% increase. Regardless of the outer configuration, actinide

ions interact more weakly with Ar compared to the lanthanide ones. Overall, the two ion families show impressive similarity in their interaction potentials, as shown in Figure 6.2, which represents the potentials for each analog. The reduced potentials clearly show that the sensitivity of the curve to the occupancy of the outermost ns orbital decreases from the lanthanides to the actinides. A further demonstration of the similarity statement arises from the observation of the reduced potentials for the No^+ and Yb^+ pair, which are indistinguishable from the Am^+ and Eu^+ one.

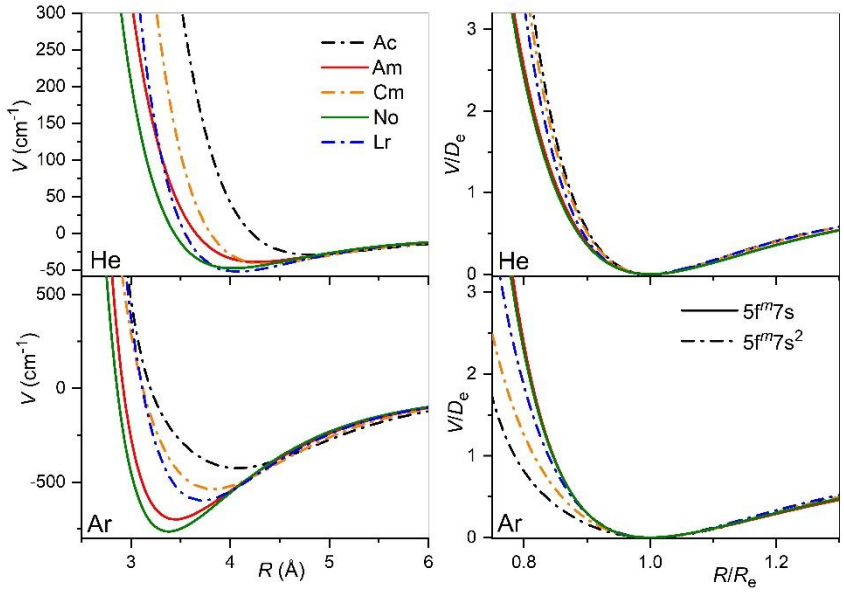

Figure 6.1. Interaction potentials of the actinide ions with He (top panels) and Ar (bottom panels). True and reduced potentials are shown on the left and on the right respectively (reproduced under the CC-BY Creative Commons attribution license).

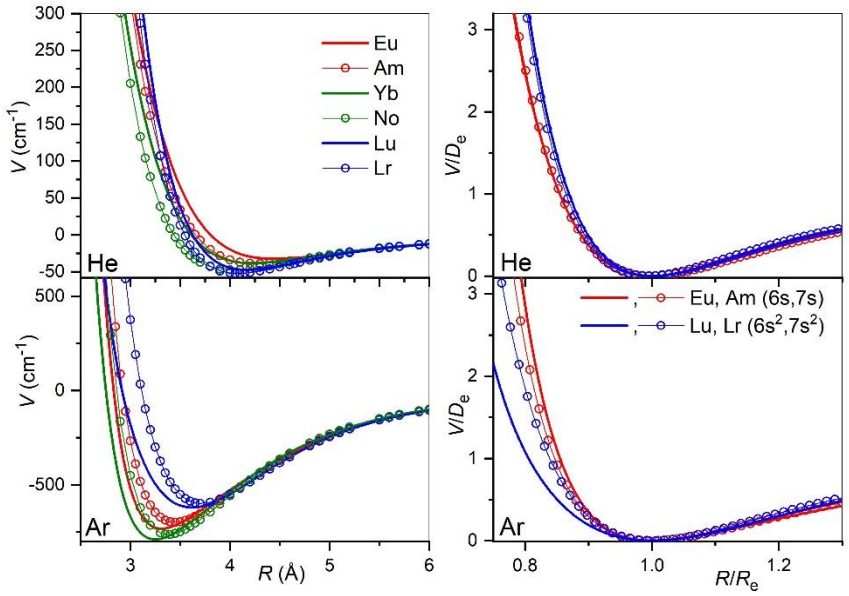

Figure 6.2. Interaction potentials of the analogous actinide and lanthanide ions with He (top panel) and Ar (bottom panel). True and reduced potentials are shown on the left and on the right respectively (reproduced under the CC-BY Creative Commons attribution license).

6.5. Mobility of the actinide ions

Sensitivity of ion mobility to different electronic configurations and atomic number can be checked by means of the ion drift time in eq. (6.2). Given a pair of ions *A*, *B* in different electronic configurations, their absolute drift time can be written as

$$\Delta t_d = t_d^A - t_d^B = \frac{1}{(E/n_0)} \frac{l}{N_0} \frac{K_0^A - K_0^B}{K_0^A K_0^B}, \tag{6.5}$$

while the relative drift time difference can be written as

$$\frac{\Delta t_d}{t_d^B} = \frac{K_0^A - K_0^B}{K_0^A} = -\Delta K_0 / K_0 \tag{6.6}$$

There, K_0 stands for the standard ion mobility for the ion A: in fact, notice that, for brevity, the superscript *A* was omitted. The ratio $\Delta K_0/K_0$ represents the relative deviation of the mobility of the ion *A* from the analog for the ion *B*. This quantity depends on temperature and on (E/n_0) through the individual mobilities.

The interaction potentials reported in the previous section were used to compute the mobilities of Ac^+ ($7s^2$, ^1S), Am^+ ($5f^7 7s$, $^9S^o$), Cm^+ ($5f^7 7s^2$, $^8S^o$), No^+ ($5f^{14} 7s$, ^2S) and Lr^+ ($5f^{14} 7s^2$, ^1S) in He and Ar. Figure 6.3 shows their standard ion mobility over a wide temperature range. As already stated, unfortunately no such measurements have been performed so far, so only theoretical dependences are available. The low-temperature trend towards the polarization limit reflects the dominant interaction term, V^{ind} (see Chapter 2, Section 2.1.6). The mobility minimum is characterized by an intermediate interaction range where attractive Van der Waals forces are also operative, while the maximum mostly reflects the potential well. Finally, the decreasing high-temperature branch signals the repulsive interactions. Standard mobility exhibits a marked sensitivity to ion species: K_0 increases as *Z* increases along the 7s and $7s^2$ ion families. Experimental data by Johnsen and Biondi [33] for the U^+-He interaction, though somewhat uncertain, do not agree with the latter trend, but fits the theoretical results for $7s^2$ family. In Ar the trend for the mobility of the $7s^2$ ions reverses, decreasing as *Z* increases, while the difference in Am^+ and No^+ becomes negligible. This behavior had been previously observed for the lanthanide ions with 6d6s electronic configurations [31,32] and, likewise, reflects the short-range behavior of ion-atom interaction potentials.

In Figure 6.4 the relative mobility differences $\Delta K_0/K_0$ are plotted for the Cm^+-Am^+ and the Lr^+-No^+ ion pairs, differing for their 7s occupancies, and compared to the lanthanide analog Lu^+-Yb^+. In He all three pairs behave similarly, with the room-temperature drift time difference amounting to 10-15%. It should be noted that the difference in the mobility of 7s and $7s^2$ ions in Ar has the opposite sign. It is noteworthy that the deviation due to 5f shell occupancy between Cm^+-Am^+ and Lr^+-No^+ exceeds that between the lanthanide and actinide families. Overall, actinide ion mobilities in both buffer gases are less sensitive to the outer *n*s shell occupancy than the lanthanide ion analogs to the 5d occupancy (see Refs. [31,32]). This consideration is in line with the analysis of the reduced potentials in the previous Section. The ground-state calculations do not allow for estimating the sensitivity of actinide mobility to the 5d configuration responsible for the electronic-state chromatography effect for the metastable states. An investigation of this effect would require interaction potential calculations for the excited metastable states. Experience with the lanthanide ions suggests that the present ab initio methods may be applicable only for Ac^+ and Lr^+ ions in their 6d7s metastable states.

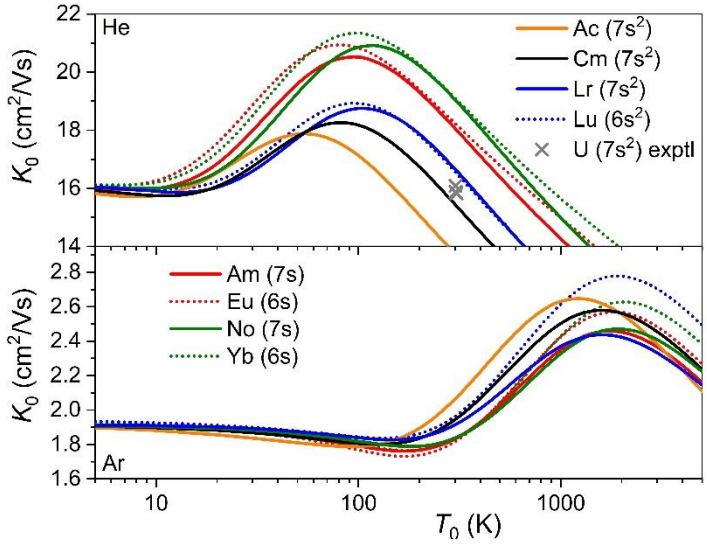

Figure 6.3. Zero-field mobilities of some actinide ions in He (top panel) and Ar (bottom panel) calculated as functions of temperature. For comparison, mobilities of the lanthanide analogs are also reported; crosses indicate experimental data [33] for U^+ in He (reproduced under the CC-BY Creative Commons attribution license).

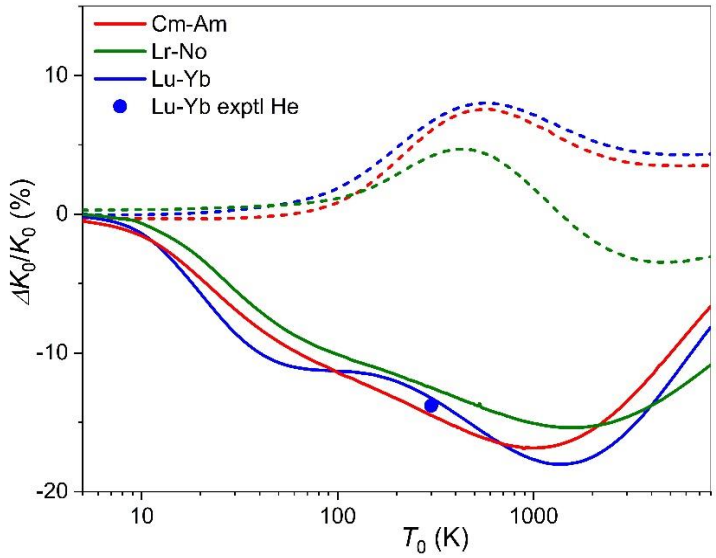

Figure 6.4. Relative changes in the ion mobilities between $7s^2$ and 7s ions Cm^+-Am^+ and Lr^+-No^+. The lanthanide analog of the latter pair, Lu^+-Yb^+, is also reported. Solid and dashed lines refer to He and Ar gases respectively. The experimental room-temperature value is taken from the work by Manard and Kemper (reproduced under the CC-BY Creative Commons attribution license).

6.6. Correlations to the ionic radii

Ionic radii were calculated in order to check their dependence on *Z*. Investigation of this dependence would reveal the effect of relativistic contraction in actinides and, in addition, is important to understand whether the transport measurements can provide a systematic means to probe the ionic radii, accounting for the exploratory experiments for actinides [34,35] and speculating to the superheavy ions.

Here, we use for the ionic radii the empirical definition provided by Wright and Breckenridge [26] (WB):

$$R_{ion}(R) = R_e - R_{RG}, \tag{6.7}$$

where R_e refers to the equilibrium distance of the ion-atom interaction potential, whereas R_{RG} stands for the Van der Waals radius of the atom. Wright and Breckenridge [26] recommended the systematics based on He interactions (with the Van der Waals radius of 1.49 Å) and noticed that eq. (6.7) does not work for Ar (whose Van der Waals radius equals 1.88 Å), because of the distortion exerted on the ion electron density. One may achieve $R_{\rm ion}$ (or, equivalently, R_e) from the zero-field mobility through the momentum transfer collision integral $\overline{\Omega}^{(1,1)}(T_0)$, in the frame of the hard-sphere (HS) model [38]:

$$\overline{\Omega}^{(1,1)}(T_0) = \pi R_e^2 \tag{6.8}$$

Combination of eqs. (6.4) and (6.8) yields with

$$R_e = \left(\frac{2}{\pi\mu_0 k_B T_0}\right)^{\frac{1}{4}} \left(\frac{3q}{16N_0 K_0(T_0)}\right)^{\frac{1}{2}}, \tag{6.9}$$

and, thence, $R_{\rm ion}$ can be obtained from eq. (6.7).

In Figures 6.5, 6.6 the radii thus obtained for the lanthanide [31,32] and actinide ions, respectively, are compared with the parameters of the radial electron distribution calculated by Indelicato *et al.* [55] for bare ions, namely, the mean radii of the outer 7s orbitals, $< r_s >$, and (if any) the 6d orbitals, $< r_d >$, and the maximum of the density of the outermost orbital, r_{max}. Reference parameters of the electron distributions of the bare ions form two parallel trend lines depending on the $7s^2$ (lower line) and 7s (upper line) outer shell configurations. The WB radii for ion-He interactions available from the present calculations follow the opposite order, due to the

enhancement of electron repulsion for the filled outer s-shell. Trends for actinides exhibit qualitative similarities with those achieved for the lanthanide counterparts [31,32], albeit the 7s and $7s^2$ trends are less evident for the parameters derived from interaction potentials and mobilities, except for the radii extracted from the mobility analysis in the frame of the hard-sphere (HS) model. It should be noted that for HS model mobility should not depend on temperature. However, as it is evident from Figure 6.3, it does. Thus, we analyzed two choices, room temperature and the temperature at mobility maximum. The latter results are in good agreement with their lanthanide analogs. However, while HS model provides reliable results for mobilities at their maxima, it returns unphysical results for mobilities close to room temperature. HS results, in fact, make a wrong prediction, showing a general increase in the ionic radii with *Z*. The relative measurements of the drift times for the Pu^+-Am^+ and Cf^+-Fm^+ ion pairs in Ar may serve as a good term of comparison to prove our statement. Furthermore, the results of the HS model are evidently much less informative and consistent in the case of Ar, mirroring the same results for lanthanide-Ar interactions [31,32]. In fact, in analogy with the lanthanide case, the mismatch between the electronic parameters and models based on ion-atom interactions and transport is much more significant compared to the interaction with He. The effective ionic radii achieved from the interaction potentials are too small in comparison to $< r_s >$ and even $r_{\max}$, while the *Z*-dependence is less marked. The inconsistency of eq. (6.7) for Ar is in agreement with the analysis by Wright and Breckenridge [26]. In contrast, the case of He provides a more consistent picture: the WB radii correlate well (within 15%) with the electronic parameters, being 1 and 0.8% larger than $r_{\max}$ and $< r_s >$ respectively, due to the presence of the He atom. Through the HS model, the relative shrinkage of the ionic radii in these pairs is estimated as 3.1 ± 1.3 and 2% respectively. These variations had already been discussed in the work by Indelicato *et al.* [55] in terms of electronic structure parameters of the bare ions. The present analysis indicates that the drift times in Ar at room temperature correspond to the mobility minimum and may not be sensitive to the effective ionic size. Therefore, one should be cautious in interpreting such data within the oversimplified HS model, as already noticed by Backe *et al.* [17].

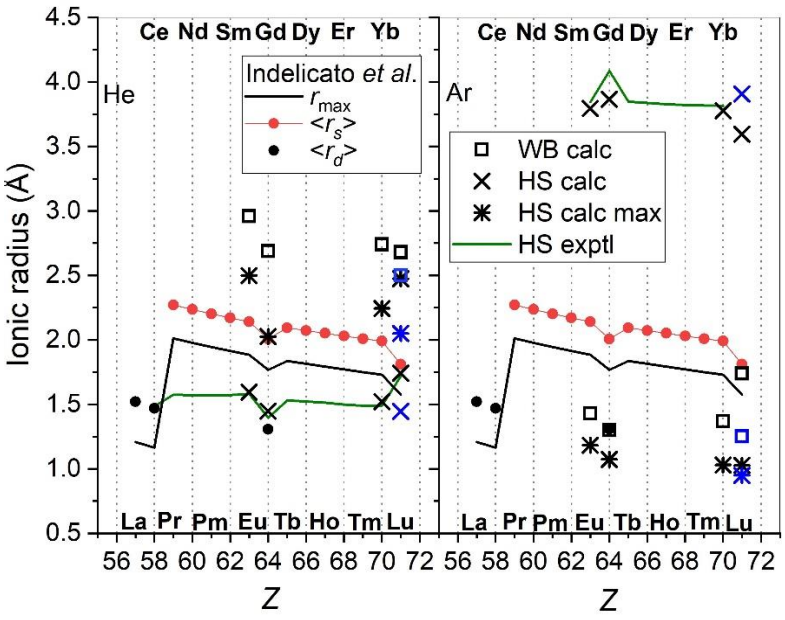

Figure 6.5. The radii of the lanthanide ions determined with He (left panel) and Ar (right panel) data from Refs. [31,32]. The WB radii from ab initio calculations and the results of the HS model applied to experimental and calculated room-temperature mobilities "HS exptl." and "HS calc.", respectively, are presented, together with the results of the HS model applied to the calculated mobility at its maximum ("HS calc. max"). Blue color is used for Lu^+ ($4f^{14}5d6s$). Parameters of the ion electron distribution calculated by Indelicato *et al.* [55] are also reported (see text for explanation). Reproduced under the CC-BY Creative Commons attribution license.

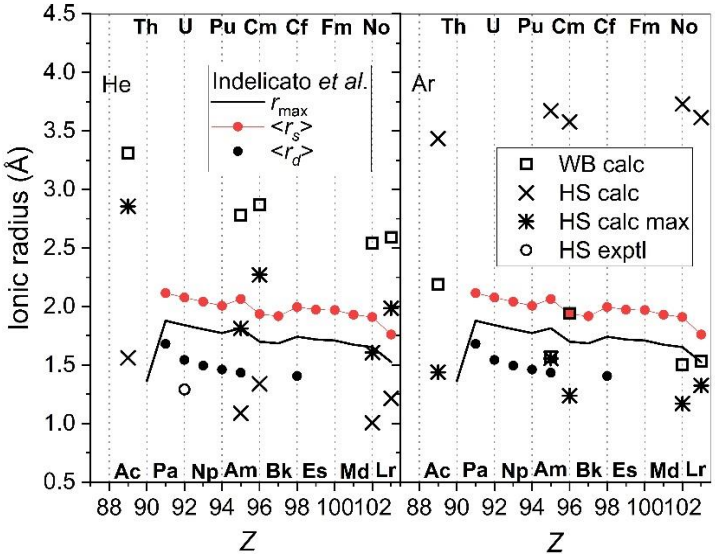

Figure 6.6. The radii of the actinide ions determined from He (left panel) and Ar (right panel). The WB radii from ab initio calculations are presented and compared to the results of the HS model applied to experimental and calculated room-temperature mobilities "HS exptl" and "HS calc.", respectively, and to the calculated mobility at the maximum ("HS calc max"). Parameters of the ion electron distribution calculated by Indelicato *et al.* [55] are also shown (reproduced under the CC-BY Creative Commons attribution license).

6.7. Conclusions

Previous investigations of ion-atom interaction potentials and ion mobilities for lanthanides by means of scalar relativistic small-core CCSD(T) approaches [31,32] indicated that mobility is very sensitive to the electronic configuration of the ion. Both room-temperature measurements and ab initio theoretical calculations for the lanthanide ions showed that the mobilities of the 5d6s and $6s^2$ ions are significantly different from the mobility of the 6s ions and slowly varying changes with the 4f occupancy, or, equivalently, with Z, can occur to determine these mobility differences [31,32]. From the comparison of experiment and theory, it is evident that the latter can presently predict the mobility differences for lanthanide ions in the ground and metastable electronic states and determine the conditions (buffer gas temperature, reduced electric field strength, pressure, etc.) ensuring the best discrimination of the ions by their drift times.

Here, this approach was extended to the actinide ions, for which experimental data are very scarce. For the ion-atom interaction potentials, equilibrium parameters (the equilibrium distance R_e and the dissociation energy D_e) obtained with small-core approaches were compared to their large-core

analogs, either available from literature [53] or calculated for the present comparison. This comparison checked the significant role of the 5f shell in strengthening the interaction (with 4-5% stabilization for He and 5-6% for Ar) and validated the small-core approach over the large-core one for investigation of the actinide ion-atom interaction. Calculation of the reduced potential functions revealed the sensitivity of the actinide ion-atom potentials to the outermost filled s orbital, with significant differences in bonding depending on the 7s or $7s^2$ configurations. Further comparisons with small-core results for lanthanide ions showed that interaction with He is much stronger in the case of actinides with 7s configuration compared to their lanthanide counterparts (with a 20% increase in the dissociation energy) and the more significant role played for the formers by the inner f shell. For the $7s^2$ actinide ions, in contrast, the trend is reversed. For Ar, actinide interaction is weaker compared to lanthanide. However, overall the two ion families show striking similarities in their interaction potentials.

Significant differences in the mobility of the 7s and $7s^2$ ions were found, which are qualitatively confirmed by the spatial electron density distribution of the bare ions [55]. However, actinide ion mobilities were found to be less sensitive to the outer *n*s occupancy than the lanthanide analogs to the 5d occupancy. In contrast, 5f shell occupancy plays a significant role in shaping mobility spreads of actinide ions. Mobility was also observed to be sensitive to the ion atomic number *Z*: in He, it increases as *Z* increases along the 7s and $7s^2$ ion families, whereas the trend reverses in Ar. This behavior, previously observed for the lanthanide ions with 6d6s configurations [31,32], reflects the short-range behavior of ion-atom interaction potentials. Mobility sensitivity to different occupancies of the outer ns shell paves the way to the investigation of the electronic state chromatographic effects, already observed for the $md^n \leftrightarrow md^{n-1}(m+1)s$ electron promotion in transition metal ions [18-24], also for actinides and encourages the extension of these studies to superheavy ions with Z = 104-112. For the former, the present scalar relativistic approach may be applicable only for Ac^+ and Lr^+ ions in their 6d7s metastable states. Another important application relies on the so-called Laser Resonance Chromatography, proposed as a technique for the indirect detection of the spectroscopic transitions by discrimination of the ions in metastable states [30], which is being explored for Lu^+ and Lr^+.

Ionic radii were calculated with the empirical formula proposed by Wright and Breckenridge [26] and in the frame of the HS model, and compared with the parameters of the radial electron

distribution by Indelicato *et al.* [55]. Actinide ions exhibit similar trends to those of their lanthanide counterparts. However, while the HS model provides qualitatively accountable results for mobilities at their maxima, it turns out to be misleading when used to evaluate mobilities around the room temperature.

Appendix: basis set augmentation for actinide ions

In Section 6.4 we illustrated the basis set used to investigate the actinide ions. The segmented atomic natural orbital basis set compatible with the small-core ECP ECP60MWB [52] suffers from the lack of diffuse functions and, thus, is not sufficient to accurately account for the polarizability of actinide ions. It is then necessary to optimize the basis set for augmentation: this optimization process consists in adding diffuse exponents ξ to the s, p, d, f, g primitives, such that ensure the basis set saturation for a calculated property of the given ion. Each primitive is optimized separately starting from s in a step-by-step procedure: first s is optimized, while the other primitives are kept frozen, second p is optimized, while s is set to its optimized value and the other primitives are still frozen, third d is optimized, while s and p are set to their optimized values and the remaining primitives are kept frozen, and so forth.

For our treatment, we chose dipole static polarizability as a property to check the basis set saturation with the basis function types chosen. Polarizability was calculated in the frame of the CCSD(T)-FF approach (see Chapter 2) as the second-order numerical derivative of the ion energy in the applied electric field. Two field steps were chosen for the calculation of the related energies and of the polarizability: $\Delta F_1 = 1 \cdot 10^{-4}$ a.u. and $\Delta F_2 = 2 \cdot 10^{-4}$ a.u. Following the step-by-step procedure for the basis set augmentation, at each step we let the exponent ξ of the given primitive decrease from 1 to a minimum number. These intervals were chosen as follows:

- Step 1: for the s primitive ξ is allowed to vary by 0.020, 0.015, 0.010, 0.005, 0.001, 0.0005 and 0.0001;
- Step 2: the exponent for s is kept at its optimized value; for the p primitive ξ is allowed to vary by 0.015, 0.01, 0.008, 0.005, 0.003, 0.002, 0.001, 0.0008;
- Step 3: the exponents for s and p are kept at their optimized values. For the d primitive ξ is allowed to vary by 0.05, 0.04, 0.02, 0.01, 0.008, 0.005, 0.002, 0.001, 0.0005;

- Step 4: the exponents for s, p and d are kept at their optimized values. For the f primitive ξ is allowed to vary by 0.15, 0.12, 0.11, 0.1, 0.09, 0.07, 0.06, 0.05, 0.04, 0.025, 0.01;
- Step 5: the exponents for s, p, d and f are kept at their optimized values. For the g primitive ξ is allowed to vary by 1.85, 1.8, 1.75, 1.7, 1.65, 1.6, 1.5, 1.45, 1.35, 1.2, 1.1, 1.0, 0.7, 0.45, 0.4, 0.2, 0.15, 0.1, 0.05, 0.02, 0.01.

As an example of this procedure Figure A1 shows the dipole static polarizability of Am atom calculated with two different field steps $(1 \cdot 10^{-4}, 2 \cdot 10^{-4})$ as a function of the increment $\Delta\xi_f$ of the f primitive. The trend line for the polarizability overall does not change with the field step, except for very few points, where usually the polarizability for the second field step is smaller. The increment of ξ increases polarizability along a sigmoidal trend from $\Delta\xi_f = 0$ to $\Delta\xi_f = 0.6$. At 0.7 the curve stabilizes into a plateau and then decreases for higher increments. The decrease of the curve indicates the saturation of the basis set for that primitive and the abscissa corresponding to the plateau is the saturation point of the basis set for the chosen primitive. Thus, in the case of the f primitive the basis set saturates at $\Delta\xi_f = 0.07$, that is then chosen as the diffuse exponent of the optimized augmented primitive.

Table A1 lists the optimized exponents. These are recommended for all actinide ANO basis sets.

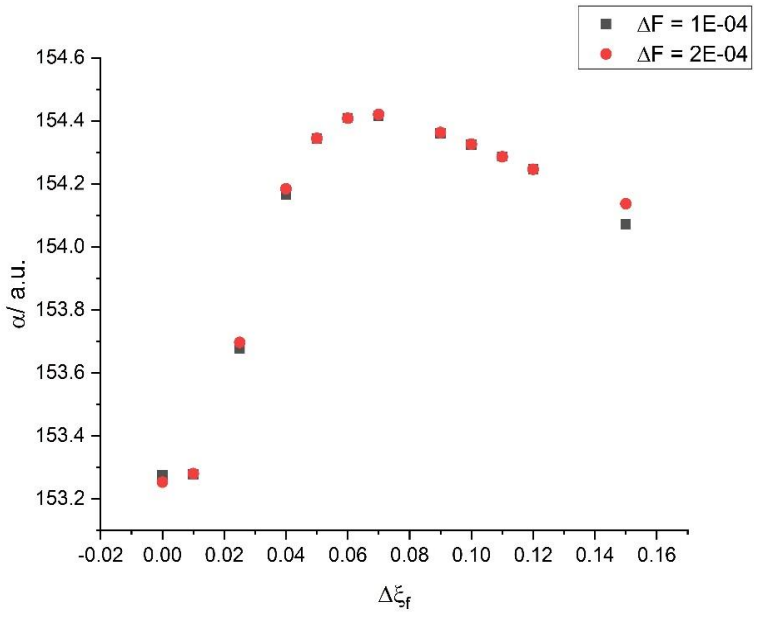

Figure A1. Am dipole static polarizability calculated with two field steps as a function of the increment $\Delta\xi_f$ of the f primitive exponent.

Table A1. Optimized values for the exponents used to augment the primitives of the segmented actinide ANO basis set. In the left-hand column the primitives to be augmented are listed; in the right-hand column the related optimized augmenting exponents are listed.

Primitive	Optimized exponent
s	0.01
p	0.008
d	0.03
f	0.07
g	0.05

References

[1] M. Perey, *L'élément 87: AcK, dérivé de l'actinium,* J. Phys. Radium **10**, 435–438 (1939); doi: 10.1051/jphysrad:019390010010043500.

[2] A. Türler, and V.G. Pershina, *Advances in the production and chemistry of the heaviest elements,* Chem. Rev. **113**, 1237–1312 (2013); doi: 10.1021/cr3002438.

[3] M. Schädel, and D. Shaughnessy, The Chemistry of Superheavy Elements. Berlin; Heidelberg: Springer (Eds.). (2014).

[4] Y. T. Oganessian, and S.N. Dmitriev, *Synthesis and study of properties of superheavy atoms. Factory of superheavy elements,* Russ. Chem. Rev. **85**, 901–916 (2016); doi: 10.1070/RCR4607.

[5] R. Eichler, "Superheavy element chemistry-new experimental results challenge theoretical understanding," in New Horizons in Fundamental Physics, FIAS Interdisciplinary Science Series, eds S. Schramm and M. Schafer (Cham:Springer), 41–53 (2017). doi: 10.1007/978-3-319-44165-8_4.

[6] R. Eichler, *The periodic table–an experimenter's guide to transactinide Chemistry,* Radiochim. Acta **107**, 865–877 (2019); doi: 10.1515/ract-2018-3080.

[7] C. E. Düllmann, *Production and study of chemical properties of superheavy elements,* Radiochim. Acta **107**, 587–602 (2019); doi: 10.1515/ract-2019-0012.

[8] G.M. Ter-Akopian, and S.N. Dmitriev, *Searches for superheavy elements in nature: cosmic-ray nuclei; spontaneous fission*, Nucl. Phys. A **944**, 177–189 (2015); doi: 10.1016/j.nuclphysa.2015.09.004.

[9] V.G. Pershina, *Electronic structure and properties of the transactinides and their compounds*, Chem. Rev. **96**, 1977–2010 (1996); doi: 10.1021/cr941182g.

[10] P. Pyykkö, *The physics behind chemistry and the periodic table*, Chem. Rev.**112**, 371–384 (2012); doi: 10.1021/cr200042e.

[11] P. Pyykkö, *Is the periodic table all right ("PTOK")?*, Eur. Phys. J. Web Conf. **131**:01001 (2016); doi: 10.1051/epjconf/201613101001.

[12] E. Eliav, S. Fritzsche, and U. Kaldor, *Electronic structure theory of the superheavy elements*, Nucl. Phys. A **944**, 518–550 (2015); doi: 10.1016/j.nuclphysa.2015.06.017.

[13] V.A. Dzuba, V.V. Flambaum, and J.K. Webb, *Isotope shift and search for metastable superheavy elements in astrophysical data*, Phys. Rev. A **95**:062515 (2017); doi: 10.1103/PhysRevA.95.062515.

[14] W. Liu and (Ed.), Handbook of Relativistic Quantum Chemistry, Berlin: Springer (2017).

[15] P. Campbell, I. D. Moore, and M. R. Pearson, *Laser spectroscopy for nuclear structure physics*, Progr. Part. Nucl. Phys. **86**, 127–180 (2016); doi: 10.1016/j.ppnp.2015.09.003.

[16] E. Rickert, H. Backe, M. Block, M. Laatiaoui, W. Lauth, J. Schneider, et al, *Ion mobilities for heaviest element identification*, Hyper. Int. **241**:49 (2020); doi: 10.1007/s10751-019-1691-7.

[17] H. Backe, W. Lauth, M. Block, and M. Laatiaoui, Prospects for laser spectroscopy, ion chemistry and mobility measurements of superheavy elements in buffer-gas traps, Nucl. Phys. A **944**, 492–517 (2015); doi: 10.1016/j.nuclphysa.2015.07.002.

[18] P.R. Kemper, and M.T. Bowers, *Electronic-state chromatography: application to first-row transition-metal ions*, J. Phys. Chem. **95**, 5134–5146 (1991); doi: 10.1021/j100166a042.

[19] M.T. Bowers, P.R. Kemper, G. von Helden, and P.A.M. van Koppen, *Gas-phase ion chromatography: transition metal state selection and carbon cluster formation*, Science **260**, 1446–1451 (1993); doi: 10.1126/science.260.5113.1446.

[20] W.S. Taylor, E.M. Spicer, and D.F. Barnas, *Metastable metal ion production in sputtering DC glow discharge plasmas: characterization by electronic state chromatography*, J. Phys. Chem. A **103**, 643–650 (1999); doi: 10.1021/jp983887i.

[21] C. Iceman, C. Rue, R.M. Moision, B.K. Chatterjee, and P.M. Armentrout, *Ion mobility studies of electronically excited states of atomic transition metal cations: development of an ion mobility source for guided ion beam experiments*, J. Am. Soc. Mass Spectrom. **18**, 1196–1205 (2007); doi: 10.1016/j.jasms.2007.02.012.

[22] Y. Ibrahim, E. Alsharaeh, R. Mabrouki, P. Momoh, E. Xie, and M.S. El-Shall, *Ion mobility of ground and excited states of laser-generated transition metal cations*, J. Phys. Chem. A **112**, 1112–1124 (2008); doi: 10.1021/jp077477i.

[23] M.J. Manard, and P.R. Kemper, *An experimental investigation into the reduced mobilities of lanthanide cations using high-resolution ion mobility mass spectrometry*, Int. J. Mass Spectrom. **407**, 69–76 (2016a); doi: 10.1016/j.ijms.2016.07.006.

[24] M.J. Manard, and P.R. Kemper, *Reduced mobilities of lanthanide cations measured using high-resolution ion mobility mass spectrometry with comparisons between experiment and theory*, Int. J. Mass Spectrom. **402**, 1–11 (2016b); doi: 10.1016/j.ijms.2016.02.014.

[25] D. Bellert, and W.H. Breckenridge, *Bonding in ground-state and excitedstate $A^+ \cdot Rg$ van der waals ions (A = atom, Rg = rare-gas atom): a modelpotential analysis*, Chem. Rev. **102**, 1595–1622 (2002); doi: 10.1021/cr980090e.

[26] T.G. Wright, and W.H. Breckenridge, *Radii of atomic ions determined from diatomic ion-He bond lengths*, J. Phys. Chem. A **114**, 3182–3189 (2010); doi: 10.1021/jp9091927.

[27] A. Stone, *The Theory of Intermolecular Forces* (Oxford University Press, Oxford, 2013) Press. doi: 10.1093/acprof:oso/9780199672394.001.0001.

[28] I.G. Kaplan, *Intermolecular interactions: physical picture, computational methods and model potentials*, (John Wiley and Sons, New York, 2006). doi: 10.1002/047086334X.

[29] A.D. Buckingham, P.W. Fowler, J.M. Hutson, *Theoretical Studies of van der Waals Molecules and Intermolecular Forces*, Chem. Rev. **88**, 963-988 (1988); doi: 10.1021/cr00088a008.

[30] M. Laatiaoui, "Laser resonance chromatography (LRC): a new methodology in superheavy element research," in The 13th International Conference on Stopping and Manipulation of Ions and Related Topics (SMI-2019), Book of Abstracts, 8 (Montreal, QC, 2019).

[31] A.A. Buchachenko, and L.A. Viehland, *Mobility of singly-charged lanthanide cations in rare gases: theoretical assessment of the state specificity*, J. Chem. Phys. **140**:114309 (2014); doi: 10.1063/1.4868102.

[32] A.A. Buchachenko, and L.A. Viehland, *Ab initio study of the mobility of Gd+ ions in He and Ar gases*; Int. J. Mass Spectrom. **443**, 86–92 (2019); doi: 10.1016/j.ijms.2019.06.005.

[33] R. Johnsen, and M.A. Biondi, *Mobilities of uranium and mercury ions in Helium*, J. Chem. Phys. **57**, 5292–5294 (1972); doi: 10.1063/1.1678220.

[34] M. Sewtz, H. Backe, A. Dretzke, G. Kube, W. Lauth, P. Schwamb, et al., *First observation of atomic levels for the element fermium (z = 100)*, Phys. Rev. Lett. **90**:163002 (2003); doi: 10.1103/PhysRevLett.90.163002;

[35] H. Backe, A. Dretzke, R. Horn, T. Kolb, W. Lauth, R. Repnow, et al., *Ion mobility measurements and ion chemical reaction studies at heavy elements in a buffer gas cell*, Hyperf. Int. **162**, 77–84 (2005); doi: 10.1007/s10751-005-9210-4.

[36] A. Moritz, X. Cao, and M. Dolg, *Quasirelativistic energy-consistent 5f-in-core pseudopotentials for trivalent actinide elements*, Theor. Chem. Acc. **117**,473–481(2007); doi: 10.1007/s00214-006-0180-7.

[37] E. Mason, and E. McDaniel, *Transport Properties of Ions in Gases*, New York, NY: John Wiley and Sons (1988); doi: 10.1002/3527602852.

[38] L.A. Viehland, Gaseous Ion Mobility, Diffusion, and Reaction. Cham: Springer (2018); doi: 10.1007/978-3-030-04494-7.

[39] L.A. Viehland, M.M Harrington, and E.A. Mason, *Direct determination of ion-neutral molecule interaction potentials from gaseous ion mobility measurements*, Chem. Phys. **17**, 433–441 (1976); doi: 10.1016/S0301-0104(76)80007-9.

[40] L.A. Viehland, *Interaction potentials for Li+-rare gas systems*, Chem. Phys.**78**, 279–294 (1983); doi: 10.1016/0301-0104(83)85114-3.

[41] L.A. Viehland, *Velocity distribution functions and transport coefficients of atomic ions in atomic gases by a Gram-Charlier approach*, Chem. Phys. **179**, 71–92 (1994); doi: 10.1016/0301-0104(93)E0337-U.

[42] L.A. Viehland, *Zero-field mobilities in helium: highly accurate values for use in ion mobility spectrometry*, Int. J. Ion Mobility Spectrom. **15**, 21–29 (2012); doi: 10.1007/s12127-011-0079-4.

[43] L.A. Viehland, T. Skaist, C. Adhikari, and W.F. Siems, *Accurate zero-field mobilities of atomic ions in the rare gases for calibration of ion mobility spectrometers*, Int. J. Ion Mobility Spectrom. **20**, 1–9 (2017); doi: 10.1007/s12127-016-0212-5.

[44] J.O. Hirschfelder, C.F. Curtiss, and R.B. Bird, *Molecular Theory of Gases and Liquids*, New York, NY: John Wiley and Sons (1955).

[45] M. Dolg, H. Stoll, and H. Preuss, *Energy-adjusted ab initio pseudopotentials for the rare earth elements*, J. Chem. Phys. **90**, 1730–1734 (1989); doi: 10.1063/1.456066.

[46] X. Cao, and M. Dolg, *Segmented contraction scheme for small-core lanthanide pseudopotential basis sets*, J. Mol. Struct. **581**, 139–147 (2002); doi: 10.1016/S0166-1280(01)00751-5.

[47] A.A. Buchachenko, G. Chałasinski, and M.M. Szczesniak, *Diffuse basis functions for small-core relativistic pseudopotential basis sets and static dipole polarizabilities of selected lanthanides La, Sm, Eu, Tm and Yb*, Struct. Chem. **18**, 769–772 (2007); doi: 10.1007/s11224-007-9243-1.

[48] D.E. Woon, and T.H. Dunning, *Gaussian basis sets for use in correlated molecular calculations. iv. calculation of static electrical response properties*, J. Chem. Phys**. 100**, 2975–2988 (1994); doi: 10.1063/1.466439.

[49] S.M. Cybulski, and R.R. Toczyłowski, *Ground state potential energy curves for He2, Ne2, Ar2, He − Ne, He − Ar, and Ne − Ar: a coupled-cluster study*, J. Chem. Phys. **111**, 10520–10528 (1999); doi: 10.1063/1.480430.

[50] S. Boys and F. Bernardi, *The calculation of small molecular interactions by the differences of separate total energies. Some procedures with reduced errors,* Mol. Phys. **19**, 553 (1970); doi: 10.1080/00268977000101561.

[51] W. Küchle, M. Dolg, H. Stoll, and H. Preuss, *Energy-adjusted pseudopotentials for the actinides. Parameter sets and test calculations for thorium and thorium monoxide,* J. Chem. Phys. **100**, 7535–7542 (1994); doi: 10.1063/1.466847.

[52] X. Cao, and M. Dolg, *Segmented contraction scheme for small-core actinide pseudopotential basis sets*, J. Mol. Struct. **673**, 203–209 (2004); doi: 10.1016/j.theochem.2003.12.015.

[53] E.P.F. Lee, L.A. Viehland, R. Johnsen, W.H. Breckenridge, and T.G. Wright, *Interaction potentials of uranium cations with rare gases (RG) and transport of U^+ in RG (RG = He, Ne, Ar, Kr, and Xe),* J. Phys. Chem. A **115**,12126–12131 (2011); doi: 10.1021/jp2076879.

[54] G. Visentin, M. Laatiaoui, L.A. Viehland, and A.A. Buchachenko, *Mobility of the Singly-Charged Lanthanide and Actinide Cations: Trends and Perspectives,* Front. Chem. **8**, 438 (2020); doi: 10.3389/fchem.2020.00438.

[55] P. Indelicato, J.P. Santos, S. Boucard, and J.-P. Desclaux, *QED and relativistic corrections in superheavy elements*, Eur. Phys. J. D **45**, 155–170 (2007); doi: 10.1140/epjd/e2007-00229-y.

7. Summary

The main goal of the thesis was to reconcile and assess the dichotomy of the atomic (monomeric) and molecular (dimeric) approaches to the long-range intermolecular (interatomic) interactions within the accurate and practically convenient ab initio methods of the single-reference Coupled Cluster family. Both approaches have their own *pro* and *contra*. Atomic one directly provides the long-range coefficients of different origins up to (in principle) infinite order and connects them to transferrable electric properties of the atoms. On the other hand, it is obviously unable to produce the global interaction potential. Molecular approach, designed for the latter task, is limited at long range by intrinsic convergence tolerances and usually provides only the leading long-range coefficients subjected to fitting errors. Moreover, both suffer from technical limitations inherent to the particular ab initio methodology.

Toward this goal, computational strategies based on the single-reference CCSD and CCSD(T) methods were customized to accurate modeling of dispersion interaction. Customization was achieved by ensuring the convergence with respect to core correlation and basis set saturation, as well as by accounting the scalar-relativistic effects at exact two-component level. The performance of the scalar-relativistic approach was then assessed across four tasks, representing typical cases where accurate description of long-range interatomic interactions is required. The strategies employed for the accomplishment of these tasks yielded with several useful conclusions, that are summarized in the following points:

1) Atomic calculations using scalar-relativistic Coupled Cluster approaches ensure accurate results for the polarizabilities and the dispersion coefficients of alkaline earth atoms and Yb, being always in reasonable agreement with the state-of-the-art atomic calculations. Detailed analysis of the long-range interactions of the dimers indicates that, for reasonably heavy atoms (i.e. those atoms being heavier than Ca), strict accuracy limits hinder direct matching of atomic and molecular approaches to model the global interaction potential and, thus, synthetic potentials implementing *ad hoc* combinations of two approaches are still needed;
2) Atomic and molecular calculations using scalar-relativistic approaches can be reconciled by means of a synthetic potential function, that combine them to build up the global potential of the ground-state Yb dimer. This dodge provides a new state-of-the-art potential, that may be

useful for interpretation of measurements from photoassociation spectroscopy, search for new frequency standards and investigation of non-Newtonian gravity-like forces;

3) Scalar relativistic approaches can be matched with our novel combination rule to explore transferability of dynamic properties, in order to achieve dispersion coefficients and dynamic polarizabilities for open-shell dimers from the known analogs for a set of closed-shell partners. For dispersion coefficients, a set of ten partners is sufficient to ensure transferability, while for dynamic polarizabilities transferability may be ensured by increasing the partner set or improving accuracy of molecular calculations;
4) Scalar-relativistic approaches can predict and interpret trends in ion mobility. In this regard, Chapter 6 shows that such approaches are reliable for modeling the interactions of actinide ions. Customization to accurate description of dispersion interaction is found to be important even for modeling the systems where dispersion plays a minor role compared to other interaction terms, such as induction.

The lessons imparted by these four test cases find a wide range of applications, ranging both refinement of ab initio modeling of intermolecular interactions and support of related experimental results. For instance, in the former ambit, future tasks may target the description of larger systems being of interest in the field of ultracold physics, such as small molecules. In addition, the conclusions collected from our novel combination rule and its limits (see Chapter 5) call for further research in the field of interaction of open-shell species. In this latter regard, these lessons suggest a parallel strategy as well, more focused on modeling the global potential, rather than dynamic properties. This relies on using our scalar-relativistic CC approach to correct the potentials achieved from multi-reference Configuration Interaction (MRCI) calculations (see Chapter 2 for information on this latter level of theory). The most helpful application of this latter approach targets the investigation of the gas-phase mobility of transition metal singly-charged cations and their interrelationship with the interaction potential, following the path delineated in Chapter 6. On the other hand, our results may also be very useful as benchmarks for ultracold physics experiments, such as in the case of the state-of-the-art global potential achieved for Yb dimer (see Chapter 4). Moreover, ion mobility results for actinide ions (see Chapter 6) are fully reliable to support the investigation of novel experimental techniques, such as Laser Resonance Chromatography.

Acknowledgements

I would like to thank first my supervisor, Prof. Alexei A. Buchachenko, not only for his unquestionable scientific value, but also for his equally unquestionable human value: he led me to the discovery of this field of research, always followed my achievements and motivated me in furthering them and helped me in understanding the whole *trait d'union* linking the projects I dealt with. Such qualities are something rare in people and need to be acknowledged and praised. Together with him, I owe my gratitude to Prof. Larry A. Viehland for his calculations of ion mobilities.

In addition, I should also thank Dr. Dmitry S. Bezrukov for his time and suggestions on how to solve specific algebraic problems using Fortan90. Also, my gratitude is to be devoted to my friends too, in particular to Christian Tantardini and Marina Teplyakova (Osipova): I spent very good time with them in scientific conversations and their encouragement helped me in deepening my interest in Quantum Chemistry and always improve myself in this discipline. Furthermore, they helped me to understand Russian culture and mentality, that, previously, I had known just through literature.

I also thank my first supervisor, Prof. Walther Caminati, from Alma Mater Studiorum University of Bologna, who first made me discover physical chemistry, a field where I would like to continue my study and working activity.

I would like to express the last, but not the least, wish of gratitude to my family for their constant support.